

Spring 2006

# Improving estimation of gross primary productivity of terrestrial ecosystems

Qingyuan Zhang

*University of New Hampshire, Durham*

Follow this and additional works at: <https://scholars.unh.edu/dissertation>

---

## Recommended Citation

Zhang, Qingyuan, "Improving estimation of gross primary productivity of terrestrial ecosystems" (2006). *Doctoral Dissertations*. 332.  
<https://scholars.unh.edu/dissertation/332>

This Dissertation is brought to you for free and open access by the Student Scholarship at University of New Hampshire Scholars' Repository. It has been accepted for inclusion in Doctoral Dissertations by an authorized administrator of University of New Hampshire Scholars' Repository. For more information, please contact [nicole.hentz@unh.edu](mailto:nicole.hentz@unh.edu).

**IMPROVING ESTIMATION OF GROSS PRIMARY PRODUCTIVITY OF  
TERRESTRIAL ECOSYSTEMS**

**BY**

**Qingyuan Zhang**

**B.S. ShanDong University, 1994**

**M.S. TsingHua University, 1996**

**DISSERTATION**

**Submitted to the University of New Hampshire**

**In Partial Fulfillment of**

**the Requirements for the Degree of**

**Doctor of Philosophy**

**In**

**Natural Resources and Environmental Studies**

**May, 2006**

UMI Number: 3217445

### INFORMATION TO USERS

The quality of this reproduction is dependent upon the quality of the copy submitted. Broken or indistinct print, colored or poor quality illustrations and photographs, print bleed-through, substandard margins, and improper alignment can adversely affect reproduction.

In the unlikely event that the author did not send a complete manuscript and there are missing pages, these will be noted. Also, if unauthorized copyright material had to be removed, a note will indicate the deletion.

**UMI**<sup>®</sup>

---

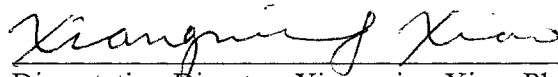
UMI Microform 3217445

Copyright 2006 by ProQuest Information and Learning Company.

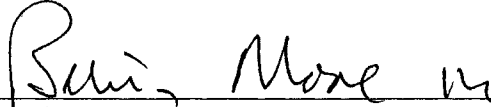
All rights reserved. This microform edition is protected against unauthorized copying under Title 17, United States Code.

ProQuest Information and Learning Company  
300 North Zeeb Road  
P.O. Box 1346  
Ann Arbor, MI 48106-1346

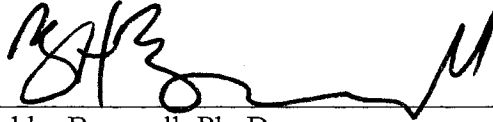
This dissertation has been examined and approved.



\_\_\_\_\_  
Dissertation Director, Xiangming Xiao, Ph. D.  
Research Associate Professor of Earth, Oceans and Space



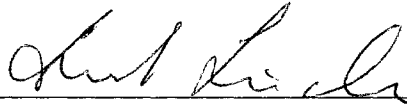
\_\_\_\_\_  
Berrien Moore III, Ph. D.  
Professor of Earth, Oceans and Space



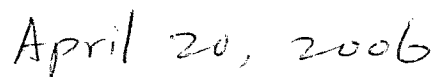
\_\_\_\_\_  
Bobby Braswell, Ph. D.  
Research Assistant Professor of Earth, Oceans and Space



\_\_\_\_\_  
John Aber, Ph. D.  
Professor of Natural Resource and Earth, Oceans and Space



\_\_\_\_\_  
Ernst Linder, Ph. D.  
Professor of Mathematics and Statistics



\_\_\_\_\_  
Date

## ACKNOWLEDGEMENTS

Thanks are extended to the members of my committee, Xiangming Xiao, Berrien Moore III, Bobby (Rob) Braswell, John Aber and Ernst Linder, for their guidance, encouragement and support during the past years at UNH. I sincerely appreciate their generous contribution and patient guidance of this research. I learned very much from countless discussions with them about research and life.

My special gratitude goes to Xiangming Xiao for providing the encouragement, inspiration, support and guidance that have made this work possible. I would like to express my gratitude to Xiao's family for their understanding, help and support when I felt regretful after my father passed away.

I appreciate the Baldwin family for many things Barbara and Dwight have done for my family. They helped my family to be familiar with the around area and the American culture. They offered much suggestion about life, education, study and work in the U.S. I won't forget their spiritual encouragement.

I learned about the Metropolis algorithm from Ernst Linder, Bobby Braswell and George Hurtt. Without their help, the analysis would not have been possible. Bobby Braswell provided me his SAIL-2 code, PROSPECT code and Metropolis algorithm code.

Many thanks to Scott Ollinger, Barry Rock, Steven Boles, Karen Bushold, Faith Sheridan and other members of Complex Systems Research Center: the faculty, staff and fellow graduate students. I lived a happy life for the past several years amongst them.

They are all easygoing and warmhearted. I received a lot of help from them and also learned a lot from interacting with them.

I have been very fortunate to share my life and studies with my wife and my son. Their understanding, patience and love during the past years in Durham have helped me finish the project.

This research was funded in part by NASA Earth System Science Fellowship (NGT5-30477) and NASA Earth Observation System Interdisciplinary Science project (NAG5-10135)

## TABLE OF CONTENTS

ACKNOWLEDGEMENTS.....	iii
TABLE OF CONTENTS .....	v
LIST OF TABLES .....	ix
LIST OF FIGURES.....	x
ABSTRACT .....	xvi

CHAPTER	PAGE
1. INTRODUCTION.....	1
1.1 Benefits of the MODIS for land study.....	1
1.2 Review on FAPAR study.....	2
1.3 Review on radiative transfer theory and the estimation of biophysical/ biochemical parameters by inverting radiative transfer models.....	4
1.3.1 Brief introduction of radiative transfer and radiative transfer equation.....	4
1.3.2 Introduction of leaf radiative transfer models .....	5
1.3.3 Introduction of canopy radiative transfer models.....	7
1.3.4 Introduction of canopy radiative transfer models coupled with leaf RT models .....	9
1.3.5 Review on Applications of Radiative Transfer Theory on estimation of biophysical/biochemical parameters .....	9
1.4 Why should FAPAR by Chlorophyll (FAPAR <sub>chl</sub> ) be proposed.....	10
1.5 How to get FAPAR by chlorophyll (FAPAR <sub>chl</sub> ) .....	12
1.6 Objectives of my dissertation research and structure of my dissertation.....	13
2. IMPROVING MONITORING OF SEASONAL SPECTRAL SIGNAL DYNAMICS OF TYPICAL VEGETATION TYPES FROM MODIS .....	18
2.1 Introduction .....	18
2.2 Methods.....	20
2.2.1 Daily MODIS data and preprocessing .....	20
2.2.2 Sites.....	22
2.2.3 MODIS daily data processing.....	26
2.3 Results.....	31
2.3.1 Seasonal Spectral Reflectance Dynamics of Typical Vegetation Types from MODIS.....	31
2.3.2 Seasonal NDVI, EVI, LSWI and MEVI Dynamics of Typical Vegetation Types from MODIS .....	35

2.4	Discussion and conclusions.....	39
3.	LESSONS LEARNED FROM INVERSION OF PROSAIL WITH MULTIPLE DAILY MODIS DATA.....	89
3.1	Introduction .....	89
3.2	Metropolis algorithm for inversion.....	91
3.3	Results.....	94
	TASK 1: How fast does the Matlab version run? .....	94
	TASK 2: Which daily MODIS observations may be used as inputs to invert the radiative transfer model? .....	94
	TASK 3: Which MODIS bands should be used and should brown pigments be considered?.....	94
	TASK 3.1 inverted results using all seven MODIS bands without consideration of leaf brown pigment (i.e., assume that there is no brown pigment in leaf).....	95
	TASK 3.2 inverted results using all seven MODIS bands with consideration of leaf brown pigment.....	96
	TASK 3.3 inverted results using five MODIS bands excluding blue and SWIR <sub>2</sub> without consideration of leaf brown pigment .....	96
	TASK 3.4 inverted results using five MODIS bands excluding blue and SWIR <sub>2</sub> with consideration of leaf brown pigment .....	97
3.4	Conclusions and summary .....	97
4.	ESTIMATING LIGHT ABSORPTION BY CHLOROPHYLL, LEAF AND CANOPY IN A DECIDUOUS BROADLEAF FOREST USING MODIS DATA AND A RADIATIVE TRANSFER MODEL.....	124
4.1	Introduction .....	124
4.2	Description of the radiative transfer model and the inversion algorithm .....	127
	4.2.1 Brief description of the PROSPECT+SAIL-2 model .....	127
	4.2.2 Description of inversion algorithm -- the Metropolis algorithm .....	129
	4.2.3 Calculation of FAPAR <sub>canopy</sub> , FAPAR <sub>leaf</sub> , and FAPAR <sub>chl</sub> .....	132
	4.2.4 Inversion of the PROSAIL-2 model with simulated data .....	133
4.3	Description of the Harvard Forest site and multiple daily MODIS data collections.....	134
	4.3.1 Brief description of the Harvard Forest site .....	134
	4.3.2 Collection of multiple daily MODIS data over the Harvard Forest site .....	135
	4.3.3 Inversion of the PROSAIL-2 model with MODIS data.....	138
4.4	Results.....	139
	4.4.1 Comparison between retrieved and observed reflectance values .....	139
	4.4.2 Temporal variation of eight variables (PAI, SFRAC, CF, C <sub>ab</sub> , N, C <sub>w</sub> , C <sub>m</sub> , C <sub>brown</sub> ) in the PROSAIL-2 model.....	140
	4.4.3. Temporal variation of FAPAR <sub>canopy</sub> , FAPAR <sub>leaf</sub> , and FAPAR <sub>chl</sub> .....	142
4.5	Discussion .....	144
4.6	Summary .....	148



5. CHARACTERIZATION OF SEASONAL SPECTRAL VARIATION OF FOREST CANOPY IN A TEMPERATE DECIDUOUS BROADLEAF FOREST USING DAILY MODIS DATA .....	165
5.1 Introduction .....	165
5.2 Brief description of the Bartlett Experimental Forest site .....	168
5.3 Method to remove snow- or atmosphere-contaminated MODIS daily observations.....	169
5.4 Description of the radiative transfer model and the inversion algorithm .....	172
5.4.1 Brief description of the PROSPECT+SAIL-2 model .....	172
5.4.2 Description of inversion algorithm -- the Metropolis algorithm .....	173
5.4.3 Calculation of $FAPAR_{canopy}$ , $FAPAR_{leaf}$ , and $FAPAR_{chl}$ .....	175
5.5 Results .....	176
5.5.1 Temporal analyses of MODIS daily reflectance data in 2004.....	176
5.5.2 Comparison between retrieved and observed reflectance values of MODIS daily data collection from DOY 184 to 201 in 2005.....	178
5.5.3 Uncertainty of individual variables from inversion of the PROSAIL-2 model with MODIS daily data collection from DOY 184 to 201 in 2005 .....	179
5.5.4 Distribution of $FAPAR_{canopy}$ , $FAPAR_{leaf}$ , and $FAPAR_{chl}$ using MODIS daily data collection from DOY 184 to 201 in 2005 .....	180
5.6 Discussion .....	181
6. ARE SEASONAL MODIS SPECTRAL VARIATIONS OF TWO TEMPERATE DECIDUOUS BROADLEAF FOREST CANOPIES DURING PLANT GROWING SEASON ONLY DUE TO VEGETATION'S ANISOTROPIC NATURE?.....	200
6.1 Introduction .....	200
6.2 Brief description of two research sites of the Missouri Ozark Forest (MOF)..	203
6.3 Method to get high-quality MODIS daily observations.....	204
6.4 Description of the radiative transfer model, the inversion algorithm and forward simulation .....	206
6.4.1 Brief description of the coupled leaf-canopy radiative transfer model PROSPECT+SAIL-2.....	206
6.4.2 Brief description of the Metropolis algorithm for inversion .....	207
6.4.3 Reproducing bidirectional MODIS five band reflectance with seasonal MODIS observation geometry.....	208
6.5 Results .....	209
6.5.1 Temporal analyses of MODIS daily reflectance data in 2003.....	209
6.5.2 Comparison between retrieved and observed reflectance values of MODIS daily data collections from DOY 193-216 for site 1 and from DOY 201-216 for site 2 in 2003 .....	210
6.5.3 Uncertainty of individual variables from inversion of the PROSAIL-2 model with MODIS daily data collections from DOY 193-216 for site 1 and from DOY 201-216 for site 2 in 2003 .....	211
6.5.4 Distribution of $FAPAR_{canopy}$ , $FAPAR_{leaf}$ , and $FAPAR_{chl}$ using MODIS daily data collections from DOY 193-216 for site 1 and from DOY 201-216 for site 2 in 2003.....	213

6.5.5	Comparison of reflectance, related NDVI, EVI and LSWI in 2003 and reproduced reflectance and related NDVI, EVI and LSWI with the inverted mean variables in PROSPECT-SAIL-2 and with the viewing geometries from MODIS daily data collection .....	214
6.6	Discussion .....	215
7.	SUMMARY AND CONCLUSIONS .....	241
	REFERENCES .....	245

## LIST OF TABLES

Table 1.1	A comparison among Terra/Aqua MODIS, Landsat TM, NOAA AVHRR and SPOT-4 VEGETATION (VGT) optical sensors .....	16
Table 2.1	The latitude and longitude of the six sites for study in this chapter .....	43
Table 3.1	A list of variables in the PROSAIL-2 model and their search ranges .....	99
Table 4.1	A list of variables in the PROSAIL-2 model and their search ranges .....	150
Table 4.2	Posterior means, standard deviations, variable behavior from inversion of the PROSAIL-2 model with the three simulated data sets: no data error, noise standard deviation $\sigma=5\%$ * data, noise standard deviation $\sigma = 10\%$ *data.....	151
Table 4.3	A list of MODIS multiple daily data collections in 2001 through 2003 for inversion of the PROSAIL-2 model. DOY – day of year.....	153
Table 4.4	Variable behavior from inversion of the PROSAIL-2 model with the MODIS data collection from DOY 147 to162 in 2002 .....	154
Table 5.1	A list of variables in the PROSAIL-2 model and their search ranges .....	185
Table 6.1	A list of variables in the PROSAIL-2 model and their search ranges .....	218

## LIST OF FIGURES

Figure 1.1 Spectral Absorption (%) (400nm - 2400nm) of leaf brown pigment (senescence), leaf dry matter, leaf water and leaf chlorophyll of a leaf with chlorophyll=40 $\mu\text{g}/\text{cm}^2$ , leaf water=0.012g/cm <sup>2</sup> , leaf dry matter=0.005g/cm <sup>2</sup> and brown pigment=1 (courtesy of Fred Baret).....	17
Figure 2.1 Mean reflectance of six biome types used by MODIS LAI/FPAR science team (from Wang, 2002) .....	44
Figure 2.2 MODIS daily observations of the Xilingol grassland site in 2002 (reflectance scale=0.0001) .....	45
Figure 2.3 MODIS daily observations (all reflectance $\leq$ 1) of the Xilingol grassland site in 2002 (reflectance scale=0.0001).....	47
Figure 2.4 MODIS daily observations (all reflectance $\leq$ 1) of the Xilingol grassland site in DOY 50 to 270, 2002 (reflectance scale=0.0001).....	49
Figure 2.5 MODIS daily observations (blue reflectance $\leq$ 0.2) of the Xilingol grassland site in DOY 50 to 270, 2002 (reflectance scale=0.0001).....	51
Figure 2.6 MODIS daily observations of the Xilingol grassland site in DOY 50 to 270, 2002 (reflectance scale=0.0001) after discarding the observations with scattering blue reflectance.....	53
Figure 2.7 MODIS daily observations of the Xilingol grassland site in DOY 50 to 270, 2002 (reflectance scale=0.0001) after discarding the observations with scattering too low reflectance of all the seven bands .....	55
Figure 2.8 MODIS daily observations of the Xilingol grassland site in DOY 50 to 270 (reflectance scale=0.0001) in Figure 2.7, observations before DOY 50, observations after DOY 270 and relative annual NDVI, EVI and LSWI in 2002 .....	57
Figure 2.9 MODIS daily observations of the Xilingol grassland site in Figure 2.8 (reflectance scale=0.0001) were partitioned into two parts: the observations with SWIR <sub>2</sub> less than 0.25 (black blue points); the others with SWIR <sub>2</sub> greater than 0.25 (pink points) .....	59
Figure 2.10 (a) NDVI, EVI and LSWI of the observations in Figure 2.9 with SWIR <sub>2</sub> less than 0.25; (b) NDVI, EVI, and LSWI of the others in Figure 2.9 with SWIR <sub>2</sub> greater than 0.25.....	61
Figure 2.11 Subset (SWIR <sub>2</sub> <0.25) of MODIS daily clustering observations of the Xilingol grassland site in 2002 (reflectance scale=0.0001) without snow covered and relative NDVI, EVI, LSWI and snow cover fraction (cfsnow).....	62
Figure 2.12 MODIS daily observations of the Harvard Forest site in 2002 (reflectance scale=0.0001) were collected as atmospheric contamination free observations from DOY 90 to 318 plus observations before and after the period, and were partitioned into two parts: the observations with SWIR <sub>2</sub> less than 0.25 (black blue points); the others with SWIR <sub>2</sub> greater than 0.25 (pink points) .....	64

Figure 2.13 (a) NDVI, EVI and LSWI of the observations with SWIR <sub>2</sub> less than 0.25 in Figure 2.12; (b) NDVI, EVI, and LSWI of the others with SWIR <sub>2</sub> greater than 0.25 in Figure 2.12 .....	66
Figure 2.14 Subset (SWIR <sub>2</sub> <0.25) of MODIS daily observations (reflectance scale=0.0001) of the Harvard Forest site in 2002 in Figure 2.12 without snow covered and relative NDVI, EVI, and LSWI .....	67
Figure 2.15 MODIS daily observations of the Howland Forest site in 2002 (reflectance scale=0.0001) were collected as atmospheric contamination free observations from DOY 115 to 318 plus observations before and after the period, and relative NDVI, EVI and LSWI were calculated.....	69
Figure 2.16 Subset (SWIR <sub>2</sub> <0.25) of MODIS daily observations (reflectance scale=0.0001) of the Howland Forest site in 2002 without snow covered and relative NDVI, EVI, and LSWI .....	71
Figure 2.17 MODIS daily atmospheric contamination free observations of the Walker Branch Watershed Forest site in 2002 (reflectance scale=0.0001) and relative NDVI, EVI and LSWI. Note that all of the observations were snow free .....	73
Figure 2.18 MODIS daily clustering observations of the Soybean site in 2002 (reflectance scale=0.0001) and relative NDVI, EVI and LSWI.....	75
Figure 2.19 Subset (SWIR <sub>2</sub> <0.25) of MODIS daily clustering observations (reflectance scale=0.0001) of the Soybean site in 2002 in Figure 2.18 after discarding the observations that have atmospheric effect and relative NDVI, EVI and LSWI .....	77
Figure 2.20 All MODIS daily observations (reflectance scale =0.0001) of the tropical km67 seasonal moist forest site since 1/1/2001 to 7/10/2004. DOY calculated beginning from 1/1/2001.....	79
Figure 2.21 Comparison of MODIS blue, red and SWIR <sub>2</sub> reflectance of all contamination free observations of the Xilingol grassland site, Harvard Forest site, Howland Forest site, Walker Branch Watershed site and Soybean site in 2002 (reflectance scale=0.0001) .....	81
Figure 2.22 Comparison of MEVI and EVI of all contamination free observations of the Xilingol grassland site, Harvard Forest site, Howland Forest site, Walker Branch Watershed site and Soybean site in 2002 (reflectance scale=0.0001).....	82
Figure 2.23 Comparison of NDVI and NIR <sub>1</sub> of all contamination free observations of the Xilingol grassland site, Harvard Forest site, Howland Forest site, Walker Branch Watershed site and Soybean site in 2002 (reflectance scale=0.0001).....	83
Figure 2.24 Selected MODIS daily observations (reflectance scale =0.0001) of the tropical km67 seasonal moist forest site since 1/1/2001 to 7/10/2004 (DOY calculated beginning from 1/1/2001) that satisfy the following criteria: (1) $0.03 \leq \rho_{SWIR_2} \leq 0.1$ ; (2) $\rho_{blue} \leq 0.3$ ; (3) $NDVI \geq \frac{1}{6}$ ; (4) if $\rho_{NIR_1} \geq 0.45$ , $NDVI \geq \frac{3}{5}$ ; (5) $-0.004 \leq \rho_{blue} - 0.25\rho_{SWIR_2} \leq 0.04$ and (6) $-0.004 \leq \rho_{red} - 0.5\rho_{SWIR_2} \leq 0.04$ .....	84
Figure 2.25 NDVI, LSWI, EVI and MEVI of the selected MODIS daily observations (reflectance scale =0.0001) of the tropical km67 seasonal moist forest site since 1/1/2001 to 7/10/2004 (DOY calculated beginning from 1/1/2001).....	86
Figure 2.26 MODIS daily NIR <sub>1</sub> reflectance from Figure 2.24 and seasonal dynamics of precipitation and leaf litterfall at the km67 site (precipitation and leaf litterfall from Saleska et al., 2003).....	87

Figure 2.27 Standard LAI product in 2002 of: (a) the Harvard Forest site; (b) the Howland Forest site; (c) the Walker Branch Watershed Forest site and (d) the km67 site.....	88
Figure 3.1 Retrieved results using seven MODIS bands without consideration of brown pigments for the Harvard Forest for MODIS data collection from day of year (DOY) 201 to 214 in 2001: retrieved histograms: (a) plant area index (PAI), (b) stem fraction, and (c) cover fraction.....	100
Figure 3.2 Retrieved results using seven MODIS bands with consideration of brown pigments for the Harvard Forest for MODIS data collection from day of year (DOY) 201 to 214 in 2001: retrieved histograms: (a) plant area index (PAI), (b) stem fraction, and (c) cover fraction.....	106
Figure 3.3 Retrieved results using MODIS bands except blue and SWIR <sub>2</sub> without consideration of brown pigment for the Harvard Forest for MODIS data collection from day of year (DOY) 201 to 214 in 2001: retrieved histograms: (a) plant area index (PAI), (b) stem fraction, and (c) cover fraction.....	112
Figure 3.4 Retrieved results using MODIS bands except blue and SWIR <sub>2</sub> with consideration of brown pigments for the Harvard Forest for MODIS data collection from day of year (DOY) 201 to 214 in 2001: retrieved histograms: (a) plant area index (PAI), (b) stem fraction, and (c) cover fraction.....	118
Figure 4.1 Viewing geometries of data collection from DOY 201 to 214 in 2001(17 observations) .....	155
Figure 4.2 A comparison between the observed reflectance and PROSAIL-2-reproduced reflectance for five MODIS spectral bands (red, green, NIR <sub>1</sub> , NIR <sub>2</sub> and SWIR <sub>1</sub> ). Surface reflectance were reproduced with the mean values of inverted variables from the PROSAIL-2 model in 2001, 2002 and 2003.(a) MODIS red and green bands and (b) MODIS NIR <sub>1</sub> , NIR <sub>2</sub> , and SWIR <sub>1</sub> spectral bands.....	156
Figure 4.3 Histogram of leaf chlorophyll content ( $C_{ab}$ , $\mu\text{g}/\text{cm}^2$ ) for MODIS data collection from DOY 147 to 162 in 2002 .....	157
Figure 4.4 Histogram of stem fraction for MODIS data collection from DOY 147 to 162 in 2002 .....	158
Figure 4.5 Histogram of cover fraction for MODIS data collection from DOY 147 to 162 in 2002 .....	159
Figure 4.6 Histogram of one soil parameter in SAIL-2 ( $\text{SOIL}_A$ ) for MODIS data collection from DOY 147 to 162 in 2002.....	160
Figure 4.7 Histogram of leaf area index (LAI) for MODIS data collection from DOY 147 to 162 in 2002.....	161
Figure 4.8 Temporal variation of canopy-level variables from inversion of PROSAIL-2 model and LAI at Harvard Forest in 2001, 2002 and 2003. (a) Plant Area Index (PAI); (b) Stem Fraction; (c) Cover Fraction; and (d) leaf area index (LAI) .....	162
Figure 4.9 Temporal variation of leaf-level variables from inversion of PROSAIL-2 model at Harvard Forest in 2001, 2002 and 2003:(a) leaf chlorophyll content ( $C_{ab}$ , $\mu\text{g}/\text{cm}^2$ ) (b) leaf brown pigment ( $C_{\text{brown}}$ ); (c) leaf dry matter ( $C_m$ , $\text{g}/\text{cm}^2$ ); (d) N (structural parameter of leaf); and (e) leaf equivalent water thickness ( $C_w$ , cm)....	163
Figure 4.10 Temporal variations of the fraction of photosynthetically active radiation absorbed by chlorophyll, leaf and canopy, and vegetation indices at Harvard Forest in 2001, 2002, 2003. (a) A comparison of estimated $\text{FAPAR}_{\text{canopy}}$ , $\text{FAPAR}_{\text{leaf}}$ and	

FAPAR <sub>chl</sub> ; (b) a comparison between estimated FAPAR <sub>leaf</sub> and NDVI; and (c) a comparison between estimated FAPAR <sub>chl</sub> and EVI .....	164
Figure 5.1 Reflectance of (a) blue and (b) SWIR <sub>2</sub> of MODIS daily observations of the Bartlett Experimental Forest tower site in 2004 (reflectance scale=0.0001) with blue less than 0.2 and SWIR <sub>2</sub> less than 0.15; reflectance of (c) blue and (d) SWIR <sub>2</sub> of MODIS daily observations in 2004 (reflectance scale=0.0001) with blue less than 0.1 and SWIR <sub>2</sub> less than 0.15.....	186
Figure 5.2 Clustering MODIS daily observations of the Bartlett Experimental Forest tower site in 2004 (reflectance scale=0.0001) and related NDVI, EVI and LSWI.	187
Figure 5.3 Snow cover fraction calculated with clustering MODIS daily observations of the Bartlett Experimental Forest tower site in 2004.....	189
Figure 5.4 Contamination free MODIS daily observations of the Bartlett Experimental Forest tower site in 2004 (reflectance scale=0.0001) and related NDVI, EVI and LSWI.....	190
Figure 5.5 A comparison between the observed reflectance and PROSAIL-2-reproduced reflectance for five MODIS spectral bands (red, green, NIR <sub>1</sub> , NIR <sub>2</sub> and SWIR <sub>1</sub> ). Surface reflectances were reproduced with the mean values of inverted variables from the PROSAIL-2 model using MODIS from DOY 184 to 201 in 2005.....	192
Figure 5.6 (a) Histogram of plant area index (PAI) for MODIS data collection of the Bartlett Experimental Forest tower site from DOY 184 to 201 in 2005; (b) Histogram of leaf area index (LAI) for MODIS data collection of the Bartlett Experimental Forest tower site from DOY 184 to 201 in 2005 .....	193
Figure 5.7 (a) Histogram of stem fraction for MODIS data collection of the Bartlett Experimental Forest tower site from DOY 184 to 201 in 2005; (b) Histogram of cover fraction for MODIS data collection of the Bartlett Experimental Forest tower site from DOY 184 to 201 in 2005 .....	194
Figure 5.8 Histograms of leaf variables for MODIS data collection of the Bartlett Experimental Forest tower site from DOY 184 to 201 in 2005.....	195
Figure 5.9 Histograms of (a) average leaf inclination angle (degree);(b) average stem inclination angle(degree); (c) leaf BRDF effect variable (d) stem BRDF effect variable for MODIS data collection of the Bartlett Experimental Forest tower site from DOY 184 to 201 in 2005 .....	197
Figure 5.10 Histograms of (a) one stem variable in SAIL-2 (STEM <sub>A</sub> ); (b) one stem variable in SAIL-2 (STEM <sub>B</sub> ); (c) one soil variable in SAIL-2 (SOIL <sub>A</sub> ); (d) one soil variable in SAIL-2 (SOIL <sub>B</sub> ) for MODIS data collection of the Bartlett Experimental Forest tower site from DOY 184 to 201 in 2005.....	198
Figure 5.11 Histograms of fraction of photosynthetically active radiation absorbed by (a) canopy (FAPAR <sub>canopy</sub> ); (b) by leaf (FAPAR <sub>leaf</sub> ) ; (c) by chlorophyll (FAPAR <sub>chl</sub> ) for MODIS data collection of the Bartlett Experimental Forest tower site from DOY 184 to 201 in 2005 .....	199
Figure 6.1 Reflectance of (a) blue and (b) SWIR <sub>2</sub> of MODIS daily observations of the Missouri Ozark Forest (MOF) site 1 in 2003 (reflectance scale=0.0001) with blue less than 0.2 and SWIR <sub>2</sub> less than 0.15; reflectance of (c) blue and (d) SWIR <sub>2</sub> of MODIS daily observations in 2003 with blue less than 0.065 and SWIR <sub>2</sub> less than 0.15 .....	219

Figure 6.2 Reflectance of clustering MODIS daily observations of the MO Forest site 1 in 2003 (reflectance scale=0.0001) and related NDVI, EVI and LSWI.....	220
Figure 6.3 A comparison between the observed reflectance and PROSAIL-2 reproduced reflectance for five MODIS spectral bands (red, green, NIR <sub>1</sub> , NIR <sub>2</sub> and SWIR <sub>1</sub> ). Surface reflectance were reproduced with the mean values of inverted variables from the PROSAIL-2 model using MODIS over the MO forest site 1 from DOY 193 to 216 in 2003.....	222
Figure 6.4 (a) Histogram of plant area index (PAI) for MODIS data collection of the MO forest site 1 from DOY 193 to 216 in 2003; (b) Histogram of leaf area index (LAI) for MODIS data collection of the MO forest site 1 from DOY 193 to 216 in 2003 .....	223
Figure 6.5 (a) Histogram of stem fraction for MODIS data collection of the MO forest site 1 from DOY 193 to 216 in 2003; (b) Histogram of cover fraction for MODIS data collection of the MO forest site 1 from DOY 193 to 216 in 2003.....	224
Figure 6.6 Histograms of leaf variables for MODIS data collection of the MO forest site 1 from DOY 193 to 216 in 2003 .....	225
Figure 6.7 Histograms of fraction of photosynthetically active radiation absorbed by (a) canopy (FAPAR <sub>canopy</sub> ); (b) by leaf (FAPAR <sub>leaf</sub> ) ; (c) by chlorophyll (FAPAR <sub>chl</sub> ) for MODIS data collection of the MO forest site 1 from DOY 193 to 216 in 2003 ....	227
Figure 6.8 A comparison of reflectance, related NDVI, EVI and LSWI of MODIS clustering daily observations of the MO Forest site 1 in 2003 (reflectance scale=0.0001) and reproduced reflectance and related NDVI, EVI and LSWI with the inverted mean variables in PROSPECT-SAIL-2 of data collection from DOY 196 – 216 in 2003 and with the same viewing geometries. ....	228
Figure 6.9 Reflectance of (a) blue and (b) SWIR <sub>2</sub> of MODIS daily observations of the Missouri Ozark Forest (MOF) site 2 in 2003 (reflectance scale=0.0001) with blue less than 0.2 and SWIR <sub>2</sub> less than 0.15; reflectance of (c) blue and (d) SWIR <sub>2</sub> of MODIS daily observations in 2003 with blue less than 0.051 and SWIR <sub>2</sub> less than 0.15 .....	230
Figure 6.10 Reflectance of clustering MODIS daily observations of the MO Forest site 2 in 2003 (reflectance scale=0.0001) and related NDVI, EVI and LSWI.....	231
Figure 6.11 A comparison between the observed reflectance and PROSAIL-2 reproduced reflectance for five MODIS spectral bands (red, green, NIR <sub>1</sub> , NIR <sub>2</sub> and SWIR <sub>1</sub> ). Surface reflectance were reproduced with the mean values of inverted variables from the PROSAIL-2 model using MODIS over the MO forest site 2 from DOY 201 to 216 in 2003.....	233
Figure 6.12 (a) Histogram of plant area index (PAI) for MODIS data collection of the MO forest site 2 from DOY 201 to 216 in 2003; (b) Histogram of leaf area index (LAI) for MODIS data collection of the MO forest site 2 from DOY 201 to 216 in 2003 .....	234
Figure 6.13 (a) Histogram of stem fraction for MODIS data collection of the MO forest site 2 from DOY 201 to 216 in 2003; (b) Histogram of cover fraction for MODIS data collection of the MO forest site 2 from DOY 201 to 216 in 2003.....	235
Figure 6.14 Histograms of leaf variables for MODIS data collection of the MO forest site 2 from DOY 201 to 216 in 2003 .....	236



- Figure 6.15 Histograms of fraction of photosynthetically active radiation absorbed by (a) canopy ( $FAPAR_{canopy}$ ); (b) by leaf ( $FAPAR_{leaf}$ ); (c) by chlorophyll ( $FAPAR_{chl}$ ) for MODIS data collection of the MO forest site 2 from DOY 201 to 216 in 2003 .... 238
- Figure 6.16 A comparison of reflectance, related NDVI, EVI and LSWI of MODIS clustering daily observations of the MO Forest site 2 in 2003 (reflectance scale=0.0001) and reproduced reflectance and related NDVI, EVI and LSWI with the inverted mean variables in PROSPECT-SAIL-2 of data collection from DOY 201 – 216 in 2003 and with the same viewing geometries. .... 239

## ABSTRACT

### IMPROVING ESTIMATION OF GROSS PRIMARY PRODUCTIVITY OF TERRESTRIAL ECOSYSTEMS

BY

Qingyuan Zhang

University of New Hampshire, May, 2006

The MODerate Resolution Imaging Spectroradiometer (MODIS) provides an unprecedented opportunity to monitor and quantify seasonal changes of vegetation and phenology. MODIS has the potential to improve the estimation, which is based on the algorithms for the NOAA Advanced Very High Resolution Radiometer (AVHRR), of biophysical/ biochemical variables of vegetation. My doctoral study improves estimation of gross primary productivity (GPP) through two aspects: first, my study improved the detection of vegetation phenology by distinguishing MODIS contaminated observations and contamination-free observations, and secondly, I inverted the fraction of absorbed photosynthetically active radiation (PAR) by chlorophyll using radiative transfer models and daily MODIS data.

My dissertation has five aspects: (1) to develop a procedure to distinguish atmospherically contaminated observations, snow contaminated observations and contamination-free observations; (2) to monitor vegetation phenology using reflectance of the seven MODIS spectral bands for land and relative vegetation indices; (3) to clarify the concepts of fractions of PAR absorbed by canopy, leaf and chlorophyll; (4) to explore

the potential of estimating the fractions of PAR absorbed at different scales; and (5) to check if vegetation seasonal MODIS spectral variations during plant growing season are only due to vegetation's anisotropic nature.

A procedure to extract contamination-free daily MODIS observations is proposed and developed. It has been employed for the Harvard Forest site, the Howland Forest site, the Walker Branch Watershed Forest site, the km67 Forest site in tropic, a soybean site in Nebraska, the Xilingol grassland site in China, the Bartlett Experimental Forest site, and two broadleaf deciduous forest sites in Missouri. The extracted MODIS signals (reflectance and vegetation indices) provide rich information for interpretation. The richness of information from the results goes beyond the widely used normalized difference vegetation index (NDVI) and leaf area index (LAI). The more precise phenology information can be used for seasonal GPP estimation.

The concepts of fractions of PAR absorbed by canopy, leaf and chlorophyll are described. I extracted fraction of PAR absorbed by chlorophyll for the Harvard Forest site, the Bartlett Experimental Forest site and the two deciduous broadleaf forest sites in Missouri using a coupled canopy-leaf radiative transfer model and daily MODIS data. Metropolis algorithm is used to invert the variables in the radiative transfer model. It provides posterior distributions for individual variables. Some of the inverted variables have been partly evaluated though validation for all variables is extremely expensive. Using the values of inverted variables of the two forest sites in Missouri, I calculated reflectance for the seven MODIS spectral ranges with real MODIS viewing geometries through whole growing season. I found that there should be other factors, except

vegetation's anisotropic nature, due to seasonal MODIS spectral variations of the forests during the plant growing season.

My study suggests that in addition to measurements of canopy-level variables (e.g., LAI), field measurements of leaf-level variables (e.g., chlorophyll, other pigments, leaf dry matter, and leaf water content) will be useful for both remote sensing and ecological research.

## CHAPTER 1

### INTRODUCTION

#### **1.1 Benefits of the MODIS for land study**

The MODerate Resolution Imaging Spectroradiometer (MODIS), combining some of the characteristics of the two widely used satellite sensors - the National Oceanic and Atmospheric Administration (NOAA) Advanced Very High Resolution Radiometer (AVHRR) and the Landsat Thematic Mapper (TM) - and offering products with spatial resolution of 250m, 500m and 1000m respectively, provided improved monitoring for land. The MODIS has seven atmospheric corrected spectral bands reflectance mainly for land study, centered at 648, 858, 470, 555, 1240, 1640 and 2130 nm, for land study. They are hereafter called red, NIR<sub>1</sub>, blue, green, NIR<sub>2</sub>, SWIR<sub>1</sub> and SWIR<sub>2</sub> of MODIS (Table 1.1) (Justice et al., 1998; Xiao et al., 2004a).

The MODIS has more spectral bands than AVHRR, and MODIS red and NIR<sub>1</sub> are narrower than AVHRR CH1 (channel 1) and CH2 (channel 2) respectively. MODIS red and NIR<sub>1</sub> have finer spatial resolution of 250 m while AVHRR CH1 and CH2 have the spatial resolution of 1000 m. MODIS blue can be used in atmospheric correction (King et al., 1999) and help in determining if an observation of dark vegetation pixel is affected by clouds (please see chapter 4 of the dissertation). MODIS green, NIR<sub>2</sub>, SWIR<sub>1</sub>, and SWIR<sub>2</sub> can be useful in monitoring and distinguishing land vegetation. Gitelson and others (Gitelson et al., 1996, 1997) have reported that the green spectral band could still

be sensitive when vegetation chlorophyll content is high, even the red band could be saturated then. Short-wave infrared (SWIR) spectral band could be used to detect water status of land surface (Tucker, 1980; Gao, 1996; Xiao et al., 2002a, 2002b; Xiao et al., 2003; Zarco-Tejada et al., 2003; Xiao et al., 2004b; Xiao et al., 2004c; Xiao et al., 2005a; Xiao et al., 2005c). King et al. (1999) reported that MODIS SWIR<sub>2</sub> was even more sensitive to a subpixel water body.

MODIS has coarser spatial resolution than TM (30 m). However, MODIS has a shorter revisit time and so has more observations than TM. During a connective 16-day period, MODIS can possibly have observations with different observation geometries. So it is possible to consider the bi-directional distribution function (BRDF) effect with MODIS observations (Strahler, 1999). In a brief summary, TM may provide more detailed spatial information than MODIS, and MODIS may provide more detailed seasonal information and more detailed BRDF effect information than TM.

## **1.2 Review on FAPAR study**

Net ecosystem exchange (NEE) of CO<sub>2</sub> between terrestrial ecosystems and the atmosphere, indicating a carbon sink or source, is the difference between gross primary production (GPP) and ecosystem respiration. Plant photosynthesis requires photosynthetically active radiation (PAR), water, nutrients and CO<sub>2</sub>. The fraction of PAR absorbed by vegetation canopy (FAPAR<sub>canopy</sub>) is an important biophysical variable. Two pioneering studies (Goward et al., 1992 and Myneni et al., 1992) studied the relationship between FAPAR<sub>canopy</sub> and normalized difference vegetation index (NDVI) (Tucker, 1979; equation 1.1, where  $\rho_{\text{nir}}$ ,  $\rho_{\text{red}}$  are reflectance values of near infrared (NIR)

and red bands respectively) using canopy radiative transfer models. The latter one is one of the fundamental papers for the MODIS standard FAPAR product.  $FAPAR_{canopy}$  is usually estimated as a linear or non-linear function (e.g., Prince et al., 1995; Diner et al., 1999) of NDVI. The study for Multi-angle Imaging Spectro-Radiometer (MISR) (Diner et al., 1999) reported a linear relationship between them.

$$NDVI = \frac{\rho_{nir} - \rho_{red}}{\rho_{nir} + \rho_{red}} \quad (1.1)$$

$FAPAR_{canopy}$  is also related to leaf area index (LAI), and usually estimated as a function of LAI and light extinction coefficient ( $k$ ) in a number of process-based biogeochemical models (e.g., Ruimy et al., 1999). MODIS (Myneni et al., 1997) and MISR (Diner et al., 1999) used the NDVI –  $FAPAR_{canopy}$  and LAI –  $FAPAR_{canopy}$  relationships as their back-up algorithms respectively. The NDVI –  $FAPAR_{canopy}$  and LAI –  $FAPAR_{canopy}$  relationships have been the paradigm that dominates the literature for estimating GPP and net primary production (NPP) of terrestrial vegetation at various spatial scales (e.g. Field et al., 1995; Running et al., 2004). Many remote-sensing-based Production Efficiency Models (e.g., Potter et al., 1993; Prince et al., 1995; Ruimy et al., 1996; Running et al., 2004) have applied the relationships to estimate GPP or NPP:

$$GPP = \varepsilon_g \times FAPAR_{canopy} \times PAR \quad (1.2)$$

$$NPP = \varepsilon_n \times FAPAR_{canopy} \times PAR \quad (1.3)$$

where  $\varepsilon_g$  and  $\varepsilon_n$  is the radiation use efficiency.

Some European researchers (Gobron et al., 2000b; Gobron et al., 2002; Taberner et al., 2002) developed unique procedures for producing  $FAPAR_{canopy}$  for GLobal Imager (GLI, on ADEOS-II), SPOT VEGETATION (VGT) (Table 1.1), Sea Wide Field-of-view

Sensor (SeaWiFS on ORBVVIEW-II), and MEdium Resolution Imaging Spectrometer Instrument (MERIS, on ENVISAT). They did BRDF correction with the Rahman, Pinty, Verstraete (RPV) model (Rahman et al., 1993a; Rahman et al., 1993b). They considered the atmospheric and soil background effect (Gobron et al., 1997) by combining sensor blue band with red and near infrared (NIR) bands.  $FAPAR_{canopy}$  was optimized as a ratio of polynomials of corrected NIR and red reflectance. The technique is more complex than the simple linear or non-linear NDVI –  $FAPAR_{canopy}$  and LAI –  $FAPAR_{canopy}$  relation functions. Moreover, the technique was more physically based and more factors were considered. However, one limit of the technique is that its input reflectance should be the reflectance before atmospheric correction.

### **1.3 Review on radiative transfer theory and the estimation of biophysical/biochemical parameters by inverting radiative transfer models**

#### **1.3.1 Brief introduction of radiative transfer and radiative transfer equation**

The radiative transfer (RT) theory was first formulated for stellar atmospheres and has been extensively studied (e.g., Chandrasekhar, 1960) and widely applied in many disciplines including high energy astrophysics, biomedical applications, atmosphere remote sensing (e.g., cloud, aerosols), land remote sensing (e.g., canopy, leaf, soil), ocean remote sensing, climate study and ice and snow remote sensing (e.g., Ishimaru, 1978a, 1978b; Verhoef, 1998). The radiative transfer equation (RTE) is known as the core of the RT theory. Reflected, transmitted and absorbed radiation can be calculated with RTE from the object's properties (e.g., leaf reflectance is determined partly by pigments content, dry matter content, water thickness; canopy reflectance is determined partly by



leaf area index, leaf angle distribution etc.), the incident radiation and observation geometry. All canopy-level and leaf-level RT reflectance models are based on the RT theory. The RTE describes the differential change of the radiance in one direction due to absorption and scattering. There is no generally analytic solution to RTE, so RT models specify the scattering phase function in terms of the properties of the medium and solve the RTE for given boundary conditions (Goel et al., 1984a; Goel et al., 1984c, 1984d, 1984b; Goel et al., 1985; Goel, 1988; Verhoef, 1998).

### 1.3.2 Introduction of leaf radiative transfer models

As early as in 1913, some scientists were trying to develop a leaf reflectance model (e.g., Willstatter et al., 1913). It is a relatively long history of the development of leaf reflectance models. Beginning from 1913, there have been many papers reporting their efforts to describe their RT based leaf models, (e.g., Willstatter et al., 1913; Allen et al., 1968; Allen et al., 1969; Allen et al., 1970; Gausman et al., 1970; Breece et al., 1971; Yamada et al., 1988; Jacquemoud et al., 1990; Baret et al., 1997; Dawson et al., 1998; Ganapol et al., 1998; Zarco-Tejada et al., 2000a; Zarco-Tejada et al., 2000b; Verhoef et al., 2003; Di Bella et al., 2004).

I used the five-variable PROSPECT model - leaf internal structure variable ( $N$ ), leaf chlorophyll content ( $C_{ab}$ ), leaf dry matter content ( $C_m$ ), leaf water thickness ( $C_w$ ) and leaf brown pigment ( $C_{brown}$ ) (Baret et al., 1997; Verhoef et al., 2003; Di Bella et al., 2004) for my doctorate study. The five-variable PROSPECT model was developed from previous studies (Kubelka et al., 1931; Allen et al., 1968; Allen et al., 1969; Allen et al., 1970; Gausman et al., 1970; Jacquemoud et al., 1990; Hosgood et al., 1995; Jacquemoud

et al., 1996). Within these efforts, some scientists extended one single compact leaf layer to N spaces (Allen et al., 1970; Gausman et al., 1970) by introducing the VAI index (Void Area Index, a leaf internal structure parameter) where  $VAI = N - 1$  (N means the number of spaces or “plates”), and with subsequent improvements and development by discretization of the medium (PROSPECT, Jacquemoud et al., 1990). For a non-senescent monocotyledons leaf grown in a greenhouse, N ranges between 1 and 1.5; for a non-senescent dicotyledonous leaf grown in a greenhouse, N ranges between 1.5 and 2.5; leaves with N values greater than 2.5 are senescent (Jacquemoud et al., 1990). For natural grown plants, the discrimination disappears (Jacquemoud et al., 1996).

LIBERTY (Dawson et al., 1998) and LEAFMOD (Ganapol et al., 1998; Ganapol et al., 1999) were recently presented. LIBERTY was a conifer needle (pine needle) reflectance model. No report on extensions of LIBERTY to other species presented. Both LIBERTY and LEAFMOD use leaf thickness, a field-measurable indicator, as a leaf variable, rather than N in PROSPECT. Both LIBERTY and LEAFMOD models lack extensive validation of PROSPECT (e.g., Jacquemoud et al., 1990; Hosgood et al., 1995; Jacquemoud et al., 1996; Demarez et al., 1999; Newnham et al., 2001). Zarco-Tejada (Zarco-Tejada et al., 2000a; Zarco-Tejada et al., 2000b) added the consideration of chlorophyll fluorescence effect to the PROSPECT model for hyper-spectral data simulation and inversion.

The earliest bi-directional reflectance distribution function (BRDF) consideration for leaf optical characteristics in literature is presented in October, 2005 (Bousquet et al., 2005). The efforts are useful even though the results are preliminary. I expect their

continuing studies will be coupled to the PROSPECT model or other leaf models in the future.

### 1.3.3 Introduction of canopy radiative transfer models

Different vegetations have different canopy structure characteristics, hence different anisotropic natures. Turbid medium canopy reflectance models, geometric canopy reflectance models, and computer-based simulation canopy models are three major types according to the different assumptions and model complexity of canopy radiative transfer reflectance models. There are also some hybrid canopy models which combine two of the types.

In turbid medium radiative transfer canopy models, the elements of canopy are randomly distributed except leaf area index (LAI) and leaf angle distribution function (LAD). For instance, the SAIL (Scattering by Arbitrarily Inclined Leaves) model (Verhoef, 1984) assumes that leaf azimuths are randomly distributed. It can compute the absorption and scattering coefficients for any leaf inclination. Kusk (Kusk, 1985) added a hotspot effect for SAIL. The SAIL model has been validated over soybeans, orchards, maize, sugar beet, etc (Goel et al., 1984c, 1984d; Badhwar et al., 1985; Goel et al., 1985; Major et al., 1992; Andrieu et al., 1997; Jacquemoud et al., 2000). Braswell and others (Braswell et al., 1996) developed the SAIL model. It decomposes a canopy into stems and leaves. Stems and leaves have different spectral characteristics. Inclination angles and hot spot effect of both leaves and stems were considered. The turbid RT models do not care about some canopy architecture variables. For example, the SAIL model does

not use canopy height as an input parameter, but it does use leaf hotspot (leaf length: canopy height) and stem hotspot (stem length: canopy height) as input parameters.

Geometric models represent the canopy reflectance as a linear combination of the reflectance spectra from sunlit and shaded objects within the field of view of the sensor (observer): sunlit crown, sunlit background, shadowed crown and shadowed background. Some models apply principles of random set overlap. The fractions of all elements viewed by the sensor are modeled as functions of canopy characteristics: for example, canopy LAI, canopy height, crown geometry, leaf angle distribution, and crown horizontal area and so on. Their component's spectra are often from field measurements (e.g., Jahnke et al., 1965; Terjung et al., 1972; Jackson et al., 1979; Li et al., 1986; Strahler et al., 1990; Li et al., 1992).

Computer-based simulation canopy models often use the Monte Carlo method, three-dimensional photo transport and simulation with radiosity to calculate reflectance, transmittance and absorption at both leaf level and canopy level (e.g., Govaerts et al., 1996; North, 1996; Govaerts et al., 1998; Chelle et al., 1999; Garcia-Haro et al., 1999; Ustin et al., 2001; Combal et al., 2002). These models simulate photo activities within leaf and canopy based on the explicit representation of position, shape, orientation, and optical properties of all relevant scatters in the canopy. A great need of computer time is expected.

There are some models that combine radiative transfer models from different categories. For instance, some hybrid models represent a canopy by combining the large-scale structure (geometric considering) with a radiative transfer approximation for crown internal microstructure and multiple scattering within and between crowns, trunk and

ground. Li et al. (Li et al., 1995) was one example of the hybrid models and is used by the MODIS scientific team to do terrestrial reflectance BRDF correction (Justice et al., 1998; Strahler, 1999). Lacaze and Roujean (Lacaze et al., 2001) and Garcia-Haro and Sommer (Garcia-Haro et al., 2002) are two other examples.

#### 1.3.4 Introduction of canopy radiative transfer models coupled with leaf RT models

Canopy models can be coupled with leaf RT models to account for vegetation chemistry. There are some studies that coupled canopy models with leaf RT models. For example, Jacquemoud and others (Jacquemoud, 1993; Jacquemoud et al., 1995; Jacquemoud et al., 2000) coupled SAIL with PROSPECT (called PROSAIL). They (Jacquemoud et al., 2000) also coupled PROSPECT with Gobron et al. (1997), Kuusk (1998) and another canopy RT model. Among the four models coupled, the authors concluded that PROSAIL was the best one based on their simulation data. LIBERTY and LEAFMOD have also been coupled with other canopy models (e.g. Ganapol et al., 1999). But LIBERTY, LEAFMOD, and the other canopy models lack wide validation. And PROSAIL has been shown to be a good level of compromise between simplicity and accuracy (Jacquemoud et al., 1996; 1995; 1993; Andrieu et al., 1997).

#### 1.3.5 Review on Applications of Radiative Transfer Theory on estimation of biophysical/biochemical parameters

The canopy/leaf radiative transfer model inversion is complicated. Iteration algorithm (e.g., quasi-Newton optimization algorithm) is one of the methods to invert canopy/leaf radiative transfer models (Jacquemoud et al., 2000; Bacour et al., 2001;

Bacour et al., 2002a; Bacour et al., 2002b). Iteration algorithm is easy to describe and to code. Recently, look-up table approaches (Knyazikhin et al., 1998a; Knyazikhin et al., 1998b; Gobron et al., 2000a; Weiss et al., 2000) and neural network methods (Baret et al., 1995; Weiss et al., 1999; Fang et al., 2003) are studied. The iterative optimization procedures are local optimization techniques and they have limited potential to search 'global' optimal solutions. For instance, if there are a few minimum points within a search space, the iterative procedures could offer a local extreme-point solution and might fail to provide a global extreme-point solution given an initial guessed value.

#### **1.4 Why should FAPAR by Chlorophyll (FAPAR<sub>chl</sub>) be proposed**

Photosynthesis occurs in the chloroplasts of plant (forest, grass, and crop) leaves and is composed of (1) a light reaction in which chlorophyll absorbs photosynthetically active radiation (PAR) from sunlight; and (2) a dark reaction (the carbon fixation process) in which the absorbed energy is then used to combine water and CO<sub>2</sub> to produce sugar. To estimate GPP is to estimate plant photosynthesis. Chloroplasts of mesophyll cells, in which photosynthesis occurs, contain photosynthetic pigments. For fresh green leaves during the summer, chlorophylls in chloroplasts dominate, resulting in leaves of plants being green; therefore PAR by chlorophylls is the most important part used for leaf photosynthesis. When a senescent season begins, chlorophyll content in chloroplasts of deciduous plants decreases. This results in the bright red and orange colors of fall foliage. The capability of a single leaf to convert solar energy to photosynthesis is mainly determined by its chlorophylls (see Figure 1.1).

From the perspective of canopy,  $FAPAR_{canopy}$  can be partitioned into two parts:  $FAPAR$  by leaf and  $FAPAR$  by stem. The presence of stem has a significant effect on  $FAPAR_{canopy}$ . For example, in forests with a leaf area index of  $<3.0$ , stem increased canopy  $FAPAR$  by 10-40% (Asner et al., 1998b). Furthermore, a leaf is composed of chlorophyll and some proportions of non-photosynthetic components (e.g., non-photosynthetic pigments in the leaf, primary, secondary, tertiary veins, and cell walls), dependent upon leaf type and leaf age. Non-photosynthetic absorption can vary in magnitude (e.g., 20-50%) among different species, leaf morphology, leaf age and growth history (Hanan et al., 1998; Lambers et al., 1998; Hanan et al., 2002).  $FAPAR_{canopy}$  should be partitioned into the fraction of PAR absorbed by chlorophyll ( $FAPAR_{chl}$ ) in leaf and by non-photosynthetic vegetation, i.e., NPV ( $FAPAR_{NPV}$ , including non-photosynthetic pigments in leaf, stems, branches, cell walls and veins).

$$FAPAR_{canopy} = FAPAR_{chl} + FAPAR_{NPV} \quad (1.4)$$

Figure 1.1 also shows that it is necessary to partition  $FAPAR_{leaf}$  hence  $FAPAR_{canopy}$ . Hence, a  $FAPAR_{chl}$ -centered vegetation photosynthesis model (VPM) was proposed

$$GPP = \varepsilon_g \times FAPAR_{chl} \times PAR \quad (1.5)$$

$$\varepsilon_g = \varepsilon_0 \times T_{scalar} \times W_{scalar} \times P_{scalar} \quad (1.6)$$

where light use efficiency ( $\varepsilon_g$ ) is affected by temperature, water and phenology of leaf,  $\varepsilon_0$  is the apparent quantum yield or maximum light use efficiency ( $\mu\text{mol CO}_2/\mu\text{mol PAR}$ ),  $T_{scalar}$ ,  $W_{scalar}$  and  $P_{scalar}$  are the downward regulation scalars for the effect of temperature, water and leaf phenology (leaf age) on light use efficiency of vegetation, respectively (Xiao et al., 2004b; Xiao et al., 2004c; Xiao et al., 2005b; Xiao et al., 2005c).

## 1.5 How to get FAPAR by chlorophyll (FAPAR<sub>chl</sub>)

How to quantify seasonal FAPAR<sub>chl</sub> of a terrestrial ecosystem poses a great challenge to remote sensing and ecology researchers, as it is an extremely difficult task to measure FAPAR<sub>chl</sub> and FAPAR<sub>NPV</sub> at the leaf and canopy levels on large scales over plant growing seasons. Canopy NPV parts confound optical methods. Some studies (Demarez et al., 1999; Rock et al., unpublished data) have shown there exist seasonal variations of leaf/canopy reflectance for deciduous leaves and needle leaves. So canopy leaves may vary their photosynthetic capacity and PAR absorption through the growing season. Until now, no field and laboratory experiments to measure FAPAR<sub>chl</sub> at the leaf and canopy levels over plant growing seasons have been reported, and there has been no literature reported efforts to calculate FAPAR<sub>chl</sub> with physics-based radiative transfer models.

Eddy flux approach has been used to measure CO<sub>2</sub>, H<sub>2</sub>O and energy at Harvard Forest site since 1991 and the records of Harvard Forest represent the longest available records in the world (Wofsy et al., 1993; Goulden et al., 1996; Barford et al., 2001). A pioneering study (Hanan et al., 2002) using CO<sub>2</sub> measurements of a native tallgrass prairie site and a wheat site in Oklahoma described a brand new way to estimate FAPAR<sub>chl</sub>, hence the study reported some interesting results. They did regression analysis with the net ecosystem exchange (NEE<sub>CO2</sub> μmol m<sup>-2</sup> s<sup>-1</sup>) at low PAR intensity:

$$PAR \cdot FAPAR_{chl} \cdot \alpha_a = NEE_{CO_2} + R_{eco} \quad (1.5)$$

where  $\alpha_a$  is the 'actual quantum yield' (i.e., the amount of moles of CO<sub>2</sub> fixed per mole of PAR by chlorophylls in the canopy, unit: mol mol<sup>-1</sup>) and  $R_{eco}$  (μmol m<sup>-2</sup> s<sup>-1</sup>) is



ecosystem respiration. When  $PAR$ ,  $\alpha_a$ ,  $NEE_{CO_2}$ , and  $R_{eco}$  are available by measurements, observations or estimations from other ways,  $FAPAR_{chl}$  can be estimated. Their results showed that  $FAPAR_{chl}$  of tall grass is around 0.63 – 0.65 times of  $FAPAR$  by ‘green’ tall grass leaves, and  $FAPAR_{chl}$  of wheat is around 0.5 – 0.54 times of  $FAPAR$  by ‘green’ wheat leaves (see Figure 5 of Hanan et al., 2002). Their results hint that the  $PAR$  absorbed by green leaves is not totally used for photosynthesis.

Another way to estimate  $FAPAR_{chl}$  is to use canopy/leaf radiative transfer models (Asner et al., 1998b; Hanan et al., 2002), i.e., to calculate  $FAPAR_{chl}$  by radiative transfer models. Canopy/leaf radiative transfer models have many variables. To estimate  $FAPAR_{chl}$  by radiative transfer models, one needs to know the values of the variables. Some of the values can be measured and some cannot. However, if there are enough observations, some of all of the variables can be first inverted with canopy/leaf radiative transfer models. Then  $FAPAR_{chl}$  can be calculated with the estimated variables.

## **1.6 Objectives of my dissertation research and structure of my dissertation**

The PROSPECT+SAIL model was used in my research to estimate  $FAPARs$  ( $FAPAR_{chl}$ ,  $FAPAR_{leaf}$  and  $FAPAR_{canopy}$ ). The objectives of this research are six-fold: (1) to develop a procedure to distinguish atmospherically contaminated MODIS observations, snow contaminated observations and contamination-free observations; (2) to monitor vegetation phenology using daily MODIS; (3) to check if the PROSAIL model can predict the MODIS reflectance well; (4) to clarify the concepts of  $FAPAR_{chl}$ ,  $FAPAR_{leaf}$  and  $FAPAR_{canopy}$ ; (5) to explore the potential of estimating  $FAPAR_{canopy}$ ,  $FAPAR_{leaf}$  and  $FAPAR_{chl}$  using PROSAIL with daily images from MODIS onboard NASA Terra/Aqua

satellite; and (6) to check if seasonal MODIS spectral variations of vegetation during plant growing season are only due to vegetation's anisotropic nature. The National Oceanic and Atmospheric Administration (NOAA) Advanced Very High Resolution Radiometer (AVHRR), particularly Normalized Difference Vegetation Index (NDVI, Tucker, 1979) of AVHRR, was the most widely used sensor in all sensors for land remote sensing while its inherent data and sensor problems and other noises limited its utility in change analyses in detail for short-terms (Goward et al., 1995; Prince et al., 1996; Lovell et al., 2001; Pettorelli et al., 2005), e.g., for each day, for ten days, for a month. The algorithms and practical operations to produce NDVI, LAI, and FAPAR<sub>canopy</sub> of MODIS are based on the experiences of usage of NDVI AVHRR/NOAA. The AVHRR NDVI series don't provide atmospheric-contamination or snow-cover information through themselves (Justice et al, 1998). Phenology study based only on NDVI is questionable (Xiao et al., 2004b, 2004c, 2005a, 2005b, 2005c). There isn't a report about the relationship between NDVI and FAPAR<sub>chl</sub> in literature. My study is to explore the potential to extract phenology information, leaf level information and FAPAR<sub>chl</sub> based on real MODIS observations. This study of radiative transfer models will help us to address an important scaling issue – light absorption from chlorophyll to leaf and to canopy; and may provide guidance for designing and conducting field measurement and observations of forest canopies in the near future. Chapter 2 describes the procedure to distinguish contamination observations and contamination-free observations and the application of the procedure in various sites. Chapter 3 documents the lessons about what MODIS observations and what PROSPECT leaf variables should be included in the radiative transfer model inversion procedure. Based on experiences from Chapter 3, Chapter 4

reports the radiative transfer model inversion results for the Harvard Forest. Chapter 5 depicts the seasonal spectral dynamics of the Bartlett Experimental Forest using the application of the procedure of Chapter 2 and the application of the radiative transfer model inversion method from Chapter 4. Chapter 6 tries to answer the question: Are seasonal MODIS spectral variations of vegetation during plant growing season only due to vegetation's anisotropic nature? Chapter 7 summarizes the findings and results of my doctoral study.

Table 1.1 A comparison among Terra/Aqua MODIS, Landsat TM, NOAA AVHRR and SPOT-4 VEGETATION (VGT) optical sensors

Characteristics	MODIS (nm)	Landsat TM (nm)	AVHRR (nm)	VGT (nm)
red	red (620-670)*	TM3 (630-690)	CH1 (580-680)	B2 (610-680)
NIR	NIR <sub>1</sub> (841-876)*	TM4 (760-900)	CH2 (725-1100)	B3 (780-890)
	NIR <sub>2</sub> (1230-1250)			
blue	blue (459-479)	TM1 (450-520)		B0 (430-470)
green	green (545-565)	TM2 (520-600)		
SWIR	SWIR <sub>1</sub> (1628-1652)	TM5 (1550-1750)		SWIR (1580-1750)
	SWIR <sub>2</sub> (2105-2155)	TM7 (2080-2350)		
spatial resolution	250 m <sup>*</sup> , 500 m	30 m	1 km	1 km
revisit time	daily	16 days	daily	daily
*Spectral bands with 250 m spatial resolution				

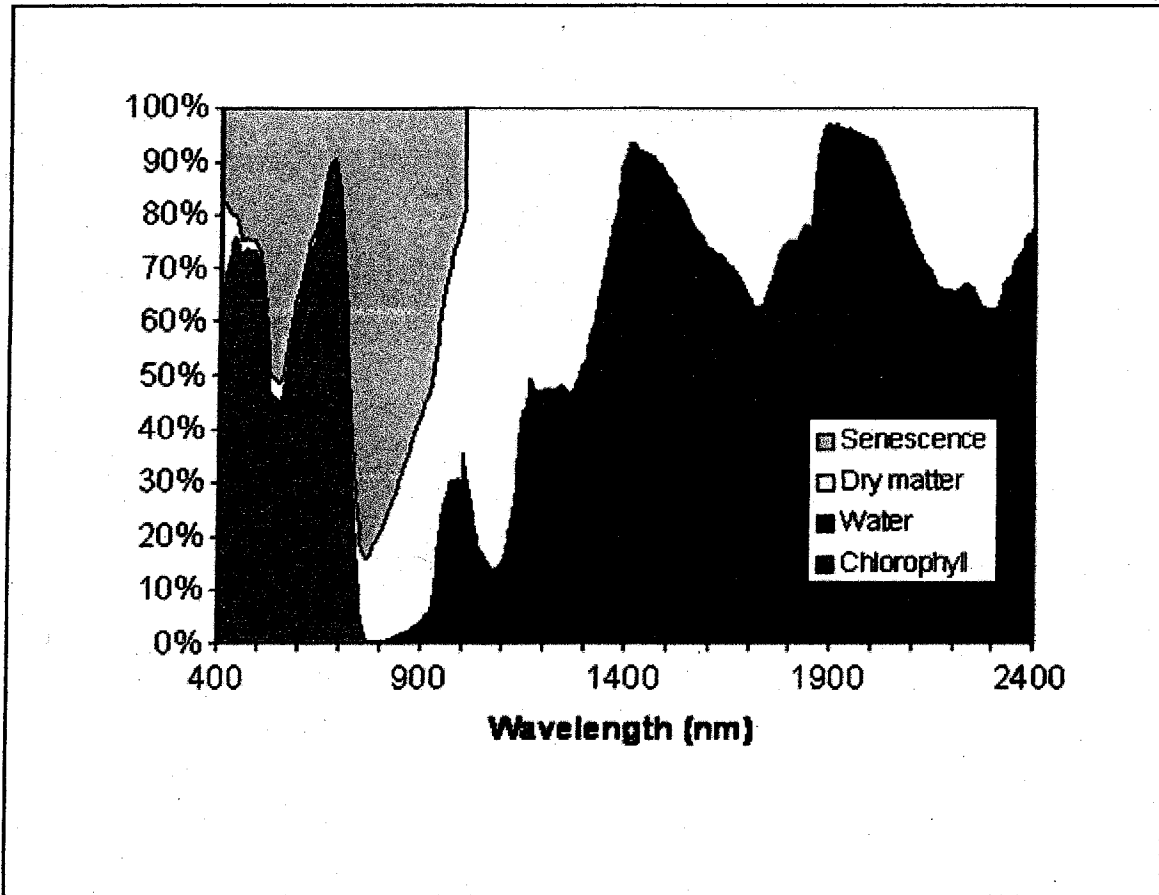


Figure 1.1 Spectral Absorption (%) (400nm - 2400nm) of leaf brown pigment (senescence), leaf dry matter, leaf water and leaf chlorophyll of a leaf with chlorophyll=40  $\mu\text{g}/\text{cm}^2$ , leaf water=0.012g/cm<sup>2</sup>, leaf dry matter=0.005g/cm<sup>2</sup> and brown pigment=1 (courtesy of Fred Baret)

## CHAPTER 2

# IMPROVING MONITORING OF SEASONAL SPECTRAL SIGNAL DYNAMICS OF TYPICAL VEGETATION TYPES FROM MODIS

### 2.1 Introduction

The MODIS leaf area index / fraction of PAR absorbed by canopy (MODIS LAI/FPAR) science team assumes a constant standard leaf spectral property for each biome type (Myneni et al., 2002; Wang, 2002; Figure 2.1) when they do estimation of LAI/FPAR. The European researchers (Gobron et al., 2000b; Gobron et al., 2002; Taberner et al., 2002) assume a single spectra profile for all leaves when they retrieve FPAR. Both the MODIS LAI/FPAR science team and the European researchers did not considerate seasonal leaf spectral variation. However, both experiments and theories show that vegetation leaves have seasonal spectral variation. Some experiments (Demarez et al., 1999; Kodani et al., 2002) showed that the chlorophyll concentration of leaves changed during the growing season. Another experiment (Gond et al., 1999) also showed the variations of leaf water thickness and dry matter during the growing season. In theory, Xanthophyll pigment cycle should also be considered when photon flux density (PFD) over canopy is very high. Xanthophyll pigment cycle is commonly referred as the inter-conversion of antheraxanthin, zeaxanthin and violaxanthin. The violaxanthin of the leaf decreases and the zeaxanthin content of the leaf increases via

antheraxanthin when a green healthy leaf is exposed to a PFD that is in excess of capability of photosynthetic tissues to utilize. The role of zeaxanthin and antheraxanthin is to dissipate the excessive light and to protect the photosynthetic tissues and the leaf (Gamon et al., 1997; Young et al., 1997; Gamon et al., 1999; Stylinski et al., 2002). During leaf senescence stage, chlorophyll content decreases while proportion of carotenoid content in total leaf pigment content increases (Waring et al., 1995; Merzlyak et al., 1997; Demarez et al., 1999; Cavender-Bares et al., 2000; Gitelson et al., 2002b). If the proportion of leaf pigments and/or leaf internal structure changes, the leaf spectra may also change. Other vegetation stress factors can also cause leaf spectra to change (Ceccato et al., 2001).

Some researchers reported that their spectral measurements of leaves changed over the growing season (e.g., Demarez et al., 1999; Rock et al., unpublished data; Gitelson et al., 2002a; Stylinski et al., 2002). Ustin, Duan and Hart documented the canopy reflectance of the grass vegetation, deciduous vegetation and evergreen vegetation in June, September and October of 1992 (Ustin et al., 1994). Kodani et al. documented the seasonal reflectance of Japanese beech in April – November of 1999 (Kodani et al., 2002). Richardson and Berlyn reported their measurements of leaf reflectance of paper beech at different elevation level on a mountain (Richardson et al., 2002). Remer, Wald and Kaufman collected the spectra of various ground surface targets, including some forests, while flying on March 12, 1997, April 22, 1996, May 22, 1996, July 30, 1997 and October 16, 1996 (Remer et al., 2001).

MODIS has seven spectral bands for land study (Table 1.1). Both MODIS/Terra and MODIS/Aqua can revisit daily. MODIS has daily, 8-day, 16-day, and monthly

products, including the daily reflectance products, 8-day reflectance products. The daily MODIS products provide the opportunities to record the seasonal spectral reflectance of the MODIS seven bands for typical vegetation biome types. However, the opportunities have not been utilized extensively by remote sensing researchers and other users.

It can be concluded from the above investigation that the seasonal spectral variation of a MODIS pixel is not only possibly because of canopy LAI variation but also possibly because of the seasonal spectral variation of leaves. Both of the factors should be considered when we interpret seasonal canopy spectral signal. A study (Stylinski et al., 2002) reported that both the canopy reflectance and leaf reflectance of two evergreen chaparral species changed during the growing season. In this chapter, the MODIS spectral signal dynamics of some forests, grassland, and crop in 2002 were collected and analyzed. The yearly collection of MODIS daily reflectance data can be used to check if the MODIS spectral signals of the biome types change during the growing season of 2002.

## **2.2 Methods**

### **2.2.1 Daily MODIS data and preprocessing**

Three MODIS standard products are used in this study: the MODIS daily surface reflectance (MOD09GHK of MODIS/Terra and MYD09GHK of MODIS/Aqua, v004), the MODIS daily observation viewing geometry (MODMGGAD of MODIS/Terra and MYDMGGAD of MODIS/Aqua, v004), and the MODIS daily observation pointers (MODPTHKM of MODIS/Terra and MYDPHKM of MODIS/Aqua, v004). The MOD09GHK/MYD09GHK product has surface reflectance values of seven spectral bands (500m spatial resolution) that are primarily designed for study of vegetation and



land surface: red (620-670 nm), near infrared (NIR<sub>1</sub>, 841-875 nm and NIR<sub>2</sub>, 1230 – 1250 nm), blue (459 – 479 nm), green (545-565 nm), short-wave infrared (SWIR<sub>1</sub>, 1628 – 1652 nm, and SWIR<sub>2</sub>, 2105-2155 nm) (Table 1.1). The MODMGGAD/ MYDMGGAD has information of observation sun-sensor-target geometry (view zenith angle, view azimuth angle, sun zenith angle and sun azimuth angle) and information related to the row and column numbers of location in the tile (see details in equations (2.1) and (2.2) below) at nominal 1-km scale. The MODPTHKM/MYDPPTHKM has pointers, at 500 m scale, to observations that intersect each pixel of MOD09GHK/MYD09GHK in MODMGGAD/MYDMGGAD (see details in equations (2.1) and (2.2) below) (personal communication with Dr. Robert Wolfe). All these three MODIS data products are freely available at USGS EROS Data Center (<http://www.edc.usgs.gov/>).

MOD09GHK/MYD09GHK, MODMGGAD/MYDMGGAD, and MODPTHKM/MYDPPTHKM have spatial resolutions of 500-m, 1-km and 500-m, respectively. The MOD09GHK/ MYD09GHK data are provided in a tile fashion, and each tile has 2400 pixels by 2400 pixels, covering approximately an area of 10° (latitude) by 10° (longitude). To get an observation including reflectance and its observation sun-sensor-target geometry, we utilized the pointer file (MODPTHKM/ MYDPPTHKM) to extract the reflectance of seven MODIS bands from MOD09GHK/MYD09GHK and to extract the relative observation angles from MODMGGAD/ MYDMGGAD. The steps to extract the observation are as follows:

$$r_{1km} = (r_{500m} / 2) - r_{offset} \quad (2.1)$$

$$c_{1km} = (c_{500m} / 2) - c_{offset} \quad (2.2)$$

r\_500m and c\_500m are the row and column numbers of a location in 500-m product (MOD09GHK/MYD09GHK), r\_1km and c\_1km are the row and column numbers of the location that are needed to be determined in 1-km product (MODMGGAD/MYDMGGAD), r\_offset and c\_offset are decoded from pointer file (MODPTHKM/MYDPHKM). Then iobs\_res value from MODPTHKM/MYDPHKM is used to pick up the observation layer of one day in MODMGGAD /MYDMGGAD at this location (personal communication with Dr. Robert Wolfe).

The quality control (QC) value from MOD09GHK/MYD09GHK includes conclusions of quality assessment of total MOD09GHK/MYD09GHK product, quality assessment of each of the seven MODIS bands, information about if atmospheric correction is performed, and information if adjacency correction performed. If the QC value indicates any quality problem, the observation is not used in the analysis.

### 2.2.2 Sites

In this study, six sites were selected: a seasonally moist tropical evergreen forest in Brazil (thereafter called km67 site), the Walker Branch Watershed Forest site (thereafter called Walker site), the Harvard Forest site, the Howland Forest site, one soybean site and one grassland site (Table 2.1). For each site except km67 site, the MODIS Terra and Aqua observations in 2002 covering the site were collected (one pixel). Because it is not easy to collect cloud-free MODIS observations for the seasonally wet tropical area, the MODIS Terra and Aqua observations in 2001-2004 covering the km67 site were collected (one pixel).

The seasonally wet tropical evergreen forest site is located in the Tapajós National Forest near km67 of the Santarém-Cuiabá highway, south of Santarém, Pará, Brazil. An eddy covariance flux tower has been operating nearly continuously at the site to measure CO<sub>2</sub>, H<sub>2</sub>O and energy fluxes since April 2001. This site is dominated by old-growth forests. Soils in the site are primarily nutrient-poor clay oxisols with some sandy utisols (Silver et al., 2000). It has an annual mean temperature of 25<sup>0</sup>C, annual mean humidity of 85%, and an annual precipitation of about 1920 mm with strong seasonal dynamics (Rice et al., 2004). The 7-month wet season is usually from December through June, and the dry season is from July to November (Xiao et al., 2005c). A recent study (Saleska et al., 2003) reported that the forest site acted as a carbon source in the wet season and a carbon sink in the dry season, largely attributed to more ecosystem respiration (including soil respiration) in the wet season than in the dry season. High daytime net ecosystem exchange (NEE) flux and H<sub>2</sub>O flux in the dry season were observed, and high GPP in the dry season were inferred. The spectral signal from MODIS during 2001-2004 over the site are collected, analyzed and compared with the flux results (Saleska et al., 2003).

The Walker site is located on the United States Department of Energy reservation near Oak Ridge, Tennessee (335m elevation). Its vegetation is primarily a mixed-species, eastern North American broad-leaved deciduous forest, dominated by oak (*Quercus alba* L., *Q. prinus* L.), hickory (*Carya ovata* (Mill.) K. Koch), maple (*Acer rubrum* L.), tulip poplar (*Liriodendron tulipifera* L.) and loblolly pine (*Pinus taeda* L.). The canopy height was about 26 m, a little bit higher than the canopy height of the Harvard Forest site. The peak leaf area index of the canopy typically occurs by day of year (DOY) 140 and reaches about 6.0. The annual mean precipitation is about 137.2 cm and the annual mean

air temperature is 13.9<sup>0</sup> C. The soil is an infertile cherty silt-loam. The mean leaf inclination angle is about 40<sup>0</sup> above crown closure and 10<sup>0</sup> below crown closure. The forest has been growing since agricultural abandonment in 1940 (Baldocchi et al., 2001). It is part of the AmeriFlux network (<http://public.ornl.gov/ameriflux/Data/index.cfm>).

The Harvard Forest site (180 - 490 m elevation) is located in Massachusetts, USA. Vegetation is primarily a deciduous broadleaf forest, dominated by red oak (*Quercus rubra*), red maple (*Acer rubrum*), black birch (*Betula lenta*) and white pine (*Pinus strobus*). There are also some evergreen needleleaf species within the forest, for example, eastern hemlock (*Tsuga canadensis*) (Waring et al., 1995). Totally, deciduous broadleaf forest occupied 56% of the land, conifer forest occupied 12%, and mixed forest occupied 20% (Turner et al., 2003). Canopy height is approximately 20 –24m. Soils are mainly sandy loam glacial till with some alluvial and colluvial deposits. The climate is cool, moist temperate with July mean temperature 20°C. Annual mean precipitation is about 110 cm and precipitation is distributed evenly throughout the year. Most areas are drained from moderately to well. Eddy flux measurements of CO<sub>2</sub>, H<sub>2</sub>O and energy at Harvard Forest site have been collected since 1991 and represent the longest available records in the world (Wofsy et al., 1993; Goulden et al., 1996; Barford et al., 2001). It is part of the AmeriFlux network (<http://public.ornl.gov/ameriflux/Data/index.cfm>).

The evergreen coniferous Howland Forest site (60 m elevation) is located in Maine, USA. The vegetation of this 90-year-old evergreen needleleaf forest is about 41% red spruce (*Pinus rubens* Sarg), 25% eastern hemlock (*Tsuga canadensis* (L.) Carr.), 23% other conifers and 11% hardwoods (Hollinger et al., 1999). Canopy height is about 19.5 m. The leaf area index (LAI) of the forest stand is about 5.3. Plant growing season

usually starts around mid-April (~ day of year (DOY) 100) and lasts about 180-days. Soils throughout the forest are glacial tills, acid in reaction, with low fertility and high organic composition. Eddy flux measurements of CO<sub>2</sub>, H<sub>2</sub>O and energy at the site have been conducted since 1996 (Hollinger et al., 1999). It is part of the AmeriFlux network (<http://public.ornl.gov/ameriflux/Data/index.cfm>).

The soybean field site is a University of Nebraska-Lincoln research facility, located 58 km northeast of Lincoln Nebraska, U.S.A. Its area is about 65-ha (806m x 806m). The field was uniformly tilled prior to the initiation of the research program, and has not been further tilled. The field is equipped with center pivot irrigation systems. Water application was to maintain a minimum soil moisture availability of 50% within the root depth zone by using predicted crop water use and daily monitoring of rainfall, irrigation, soil evaporation, and soil moisture (Vina et al., 2004 and personal communication with Dr. Anatoly Gitelson).

The Xilingol site, established for long-term ecological research by the Inner Mongolia Grassland Ecosystem Research Station (IMGERS) of Chinese Academy of Sciences in 1979, is located in the Xilin river basin, middle Inner Mongolia, China, about 60 km south-east of Xilinhot. It is representative of about 210,000 km<sup>2</sup> of "typical steppe" (i.e., *L. chinense* steppe and *S. grandis* steppe) grasslands, out of a total grassland area of about 800,000 km<sup>2</sup> in Inner Mongolia. With a warm, wet growing season from the end of April to early October, these typical steppe grasslands provide good quality forage for livestock and are used primarily for grazing. Its winter is cold and dry. Dominant soils are chestnut and chernozem. The study site has been fenced since 1980 and was lightly grazed before that time (Xiao et al., 1995).

### 2.2.3 MODIS daily data processing

Observations of vegetation can be affected by cloud, covering snow, water/rainfall over soil and vegetation, and other soil factors, etc. I used the Xilingol grassland site as the first and km67 site in tropical area as the last to describe the processing procedure for the MODIS daily data.

If one observation over vegetation and/or soil is only contaminated by cloud, the MODIS blue and SWIR<sub>2</sub> reflectance will increase. If the observation is only contaminated by snow, the MODIS blue will increase; meanwhile, if the soil in the pixel is wet, the SWIR<sub>2</sub> reflectance will be less than 0.25 (Kaufman et al., 2002).

Reflectance of ground target should not be greater than 100%. Figure 2.2 showed all the observations of the Xilingol grassland site that have no any quality problems showed by QC in 2002. Some of the observations have reflectance values of the MODIS blue, green, red, and/or NIR<sub>1</sub> greater than 100%. One possible reason for why reflectance value is greater than 1.0 is that atmospheric correction is not perfect. The observations with reflectance value greater than 1.0 were discarded (please see Figure 2.3).

The annual observation distribution pattern of the Xilingol grassland site has the following characteristics: there are observations with the MODIS blue reflectance less than 20% from day of year (DOY) 50 to DOY 270 which show an clustering pattern, and the MODIS blue reflectance patterns of observations before DOY 50 or after DOY 270 are different from the one from DOY 50-270 (Figure 2.3). First, the observations from DOY 50-270 will be processed (Figure 2.4); secondly, the observations before DOY 50 or after 270 will be processed.

The observations with MODIS blue reflectance greater than 20% from DOY 50-270 were discarded (Figure 2.5). The observations have blue reflectance value greater than 0.2 possibly because they were contaminated by clouds or snow. The observations with scattering blue reflectance values were also discarded (Figure 2.6). There were some observations with very low reflectance values for all the seven MODIS spectral bands in Figure 2.6. Maybe the reason is that MODIS “observed” some standing rain water or some soil with water. The observations with SWIR<sub>1</sub> less than 0.2 or SWIR<sub>2</sub> less than 0.1 were discarded (Figure 2.7).

The observations in Figure 2.7 and the observations from before DOY 50 or after DOY 270 were put together to get Figure 2.8. I calculated NDVI (equation 1.1), enhanced vegetation index (EVI; Huete et al., 1997), and land surface water index (LSWI; Xiao et al., 2004b; Xiao et al., 2004c; Xiao et al., 2005a; Xiao et al., 2005c):

$$EVI = 2.5 \times \frac{\rho_{NIR_1} - \rho_{RED}}{\rho_{NIR_1} + (6 \times \rho_{RED} - 7.5 \times \rho_{BLUE}) + 1} \quad (2.3)$$

$$LSWI = \frac{\rho_{NIR_1} - \rho_{SWIR_1}}{\rho_{NIR_1} + \rho_{SWIR_1}} \quad (2.4)$$

where  $\rho$  is reflectance.

Reflectance of green vegetation (cover fraction > 0.6) and snow at 2.1  $\mu\text{m}$  is less than 0.25 (Tucker, 1979; Karnieli et al., 2001; Xiao et al., 2004a). Reflectance of sparse vegetation (cover fraction < 0.4) and bare dry soil at 2.1  $\mu\text{m}$  is greater than 0.25 (Tucker, 1979; Karnieli et al., 2001). I partitioned the observations into two parts: the observations with MODIS SWIR<sub>2</sub> less than 0.25; the others with MODIS SWIR<sub>2</sub> greater than 0.25 (Figure 2.9). The relative NDVI, EVI and LSWI of the two parts were calculated (Figure 2.10). The relative period of the observations with MODIS SWIR<sub>2</sub> greater than 0.25

matched the non-growing season period of the grassland (Xiao et al., 1995). These observations were composed with two parts: the observations with reflectance at blue less than 0.2 which signals were mainly contributed by bright soils, standing litter/debris or the mixtures of soil/litter/debris/frost, and the observations with reflectance at blue greater than 0.2 which signals were possibly due to bright bare soil.

To detect how much fraction of the observations with MODIS SWIR<sub>2</sub> less than 0.25 were covered by snow, the algorithm from Kaufman et al. (Kaufman et al., 2002) was utilized. The fraction of snow cover ( $f_{snow}$ ) is defined as:

$$f_{snow} = \frac{\frac{\rho_{red} - 0.5\rho_{SWIR_2}}{0.6}}{0.51 + 0.07 \times \frac{\rho_{red} - 0.5\rho_{SWIR_2}}{0.6}} \quad (2.5)$$

Figure 2.11 showed the observations (SWIR<sub>2</sub> less than 0.25) without snow contamination.

Following the above procedure, I got relative results of the Harvard Forest site. Figure 2.12 partitioned the observations of the Harvard Forest site into two parts: one part with SWIR<sub>2</sub> less than 0.25 and another part with SWIR<sub>2</sub> greater than 0.25. Figure 2.13 showed related NDVI, EVI and LSWI of the two parts. Figure 2.14 showed the observations (SWIR<sub>2</sub> less than 0.25) of the Harvard Forest site without snow contamination.

Also with the same procedure, I got relative results of the Howland Forest site. Figure 2.15 showed the observations with SWIR<sub>2</sub> less than 0.25 of the Howland Forest site. Figure 2.16 showed the observations (SWIR<sub>2</sub> less than 0.25) of the Howland Forest site without snow contamination.



The case for the Walker site in 2002 was simpler. All the clustering observations had SWIR<sub>2</sub> reflectance less than 0.25 and no snow covered. Figure 2.17 showed all the clustering observations of the Walker site in 2002.

For agriculture areas, there is possible aerosol in the air. The formula  $\rho_{red} - 0.5\rho_{SWIR_2}$  in equation 2.5 can also be used to detect if there is significant contribution from aerosol to the MODIS observed reflectance. For an observation, if absolute value of the difference is less than  $0.025 * \rho_{SWIR_2}$ , then the observation can be treated as no significant aerosol/other atmospheric effect; otherwise the observation can be treated as atmospherically contaminated. Using the criteria in place of equation 2.5 for the soybean crop site, I got the subset observations from the clustering observations (SWIR<sub>2</sub> less than 0.25) without atmospheric effect (Figure 2.19). All clustering observations of the Soybean site in 2002 were showed in Figure 2.18.

For the tropical km67 forest site, I downloaded MODIS daily reflectance from 1/1/2001 – 7/10/2004. Figure 2.20 showed all the reflectance data. The reflectance patterns of the MODIS seven bands of the km67 site are very different from the Xilingol grassland site, the Harvard Forest site, the Howland Forest site, the Walker Branch Watershed, and the Soybean site I have done in the above description. The MODIS blue, red and green had much noise and had no clear or obvious clustering patterns (Figure 2.20). The plant area index (PAI) at the Tapajós National Forest varies between 5 -7 over space and green vegetation cover is over 90% (Huete et al., 2002). Note that the canopy of seasonally moist tropical evergreen forests has little change in leaf area index over seasons. The vegetation of km67 is dense and dark over the whole year (Karnieli et al., 2001). MODIS SWIR<sub>2</sub> band can be less influenced by atmospheric gases and the most

common types of aerosols even if there is much high possibility of atmospheric contamination over the km67 site than other sites I have described. So I tried to use the MODIS SWIR<sub>2</sub> band to extract seasonal spectral signals of the km67 site through the following steps. I collected together all the contamination free observations of the Xilingol grassland site, the Harvard Forest site, the Howland Forest site, the Walker Branch Watershed, and the Soybean site without atmospheric effects and/or snow effect, and compared their blue, red and SWIR<sub>2</sub> reflectance (Figure 2.21). The MODOS red, blue and SWIR<sub>2</sub> are highly correlated and I got the following formula:

$$\rho_{red} = 0.5212\rho_{SWIR_2} \quad (2.6)$$

$$\rho_{blue} = 0.2653\rho_{SWIR_2} \quad (2.7)$$

The SWIR<sub>2</sub> can be used to replace red and blue when SWIR<sub>2</sub> can penetrates the atmospheric column and a modified EVI (MEVI) is defined as:

$$MEVI = 2.5 \times \frac{\rho_{NIR_1} - 0.5212 \times \rho_{SWIR_2}}{\rho_{NIR_1} + (6 \times 0.5212 \times \rho_{SWIR_2} - 7.5 \times 0.2653 \times \rho_{SWIR_2}) + 1} \quad (2.8)$$

All the contamination free observations I collected in Figure 2.21 were used to calculated EVI and MEVI (Figure 2.22). I also compared NIR<sub>1</sub> reflectance and NDVI (Figure 2.23) for all the contamination free observations I collected in Figure 2.21. EVI and MEVI are highly correlated when there is no atmospheric effect or snow effect. Figure 2.20 showed that there were observations of the km67 site with SWIR<sub>2</sub> reflectance between 0.03 and 0.1. I used the following criteria to select the observations for analysis of the km67 site:

- (1)  $0.03 \leq \rho_{SWIR_2} \leq 0.1$ ; (2)  $\rho_{blue} \leq 0.3$ ; (3)  $NDVI \geq \frac{1}{6}$ ; (4) if  $\rho_{NIR_1} \geq 0.45$ ,  $NDVI \geq \frac{3}{5}$ ; (5)  $-0.004 \leq \rho_{blue} - 0.25\rho_{SWIR_2} \leq 0.04$  and (6)  $-0.004 \leq \rho_{red} - 0.5\rho_{SWIR_2} \leq 0.04$ . The red

reflectance without atmospheric or snow effect of the Harvard Forest site, and the Walker Branch Watershed site during the growing season from after leaf full expansion to before leaf senescence, and the one of the Howland Forest site have a range between 0.015 – 0.05. The relative SWIR<sub>2</sub> range is 0.03 – 0.1. This is the reason for criteria (1). Criteria (2) and (3) were from a past European study (Taberner et al., 2002). I used criteria (4) according to Figure 2.23. The selected observations of the km67 site following the above criteria (1) – (5) were shown in Figure 2.24. The relative NDVI, LSWI, EVI and MEVI were in Figure 2.25.

## **2.3 Results**

### **2.3.1 Seasonal Spectral Reflectance Dynamics of Typical Vegetation Types from MODIS**

The spectral reflectance time series of MODIS seven bands (SWIR<sub>2</sub> reflectance <0.25) without snow covered or atmospheric effects at the Xilingol grassland site in 2002 are in Figure 2.11. Reflectance of all the seven MODIS spectral bands has distinct seasonal cycles. Blue, red, green, SWIR<sub>1</sub> and SWIR<sub>2</sub> began to decrease in middle to late June and reached their minimum in early to middle August in 2002. Then they increased. NIR<sub>1</sub> and NIR<sub>2</sub> had inverse tendency. NIR<sub>1</sub> and NIR<sub>2</sub> began to increase in middle to late June and reached their peaks in early to middle August. After they reached their peaks, they decreased rapidly. Only from day of year (DOY) 168 to 282 (about 115 days) in 2002 had the kind of observations (SWIR<sub>2</sub> reflectance <0.25) without snow covered or atmospheric effects at the Xilingol grassland site (Figure 2.11). The pink points in Figure 2.9 are observations with SWIR<sub>2</sub> reflectance  $\geq 0.25$  which could be partitioned into two

parts: the ones with blue reflectance  $>0.2$  and the ones with blue reflectance  $\leq 0.2$ . The black blue points in Figure 2.9 minus the observations in Figure 2.11 were the observations contaminated by snow with low NDVI, low EVI and high LSWI (Figure 2.10). To analyze vegetation activity at the grassland site, one may just use the observations in Figure 2.11.

The spectral reflectance time series of MODIS seven bands (SWIR<sub>2</sub> reflectance  $<0.25$ ) without snow covered or atmospheric effects at the Harvard Forest in 2002 were in Figure 2.14. The MODIS blue, red, green, NIR<sub>1</sub>, NIR<sub>2</sub> and SWIR<sub>2</sub> reflectance series in 2002 had a distinct seasonal cycle while SWIR<sub>1</sub> did not. The SWIR<sub>1</sub> reflectance curve had a plateau. There were rare observations without snow covered or atmospheric effects during the winter season (January, February and December). The available observations without snow covered or atmospheric effects during the winter season had NIR<sub>1</sub> and NIR<sub>2</sub> reflectance around 0.2. The NIR<sub>1</sub> and NIR<sub>2</sub> reflectance began to increase in late March and reached their peaks in June to July. The NIR<sub>1</sub> and NIR<sub>2</sub> reflectance declined after their peaks. The blue, red and SWIR<sub>2</sub> had inversely tendency. The blue, red and SWIR<sub>2</sub> reflectance began to decrease in late March and reached their minimum in June to July. The blue, red and SWIR<sub>2</sub> reflectance increased after their minimum. The green had a different seasonal cycle from all others. The green reflectance began to increase in late March and reached its peak in late May to early June. The green declined after its peak. The MODIS reflectance of all the seven bands of snow contaminated observations (Figure 2.12 and Figure 2.14) at the Harvard Forest site was different from snow uncontaminated observations. With the different spectral characteristics between snow and

vegetation/soil, the snow contaminated observations could be kicked off and the snow contamination free observations could be kept for vegetation phenology analysis in detail.

The spectral reflectance time series of the MODIS seven bands (SWIR<sub>2</sub> reflectance <0.25) without snow covered or atmospheric effects at the Howland Forest in 2002 were in Figure 2.16. The observations covered period from DOY 115 to DOY 318 in 2002. The MODIS blue, red and SWIR<sub>2</sub> reflectance series in 2002 had a distinct and similar seasonal cycle. They decreased from DOY 115 to DOY 318. The MODIS green, NIR<sub>1</sub>, NIR<sub>2</sub> and SWIR<sub>1</sub> reflectance series in 2002 had a distinct and similar seasonal cycle, but different from the cycle of the blue, red and SWIR<sub>2</sub> reflectance. The MODIS green, NIR<sub>1</sub>, NIR<sub>2</sub> and SWIR<sub>1</sub> reflectance increased from DOY 115, reached their peaks around DOY 191, and then decreased until DOY 318. The observations in Figure 2.15 minus the observations in Figure 2.16 were the observations contaminated by snow. The snow contaminated observations at the Howland Forest site had similar spectral characteristics as the snow contaminated observations at the Harvard Forest site.

The spectral reflectance time series of the MODIS seven bands (SWIR<sub>2</sub> reflectance <0.25) without snow covered or atmospheric effects at the Walker Branch Watershed Forest site in 2002 were in Figure 2.17. The observations covered the whole year of 2002. All the clustering observations were snow free. The MODIS blue, red, SWIR<sub>1</sub> and SWIR<sub>2</sub> reflectance series in 2002 had a distinct and similar seasonal cycle. They decreased from January, reached their minimum, continued their minimum from May to September, and then increased until end of year 2002. The MODIS green reflectance series were almost flat otherwise decreased very slightly through the year.

The spectral reflectance time series of the MODIS seven bands (SWIR<sub>2</sub> reflectance <0.25) without snow covered or atmospheric effects at the Soybean site in 2002 were in Figure 2.19. The observations covered the whole year of 2002. The MODIS blue, red, green, SWIR<sub>1</sub> and SWIR<sub>2</sub> reflectance series in 2002 had a distinct and similar seasonal cycle. They increased in January and February, reached their maximum values in end of February to early March, then decreased, continued their minimum from May to September, and then increased until end of year 2002. The MODIS NIR<sub>2</sub> reflectance series were almost flat otherwise decreased very slightly through the year. The MODIS NIR<sub>1</sub> reflectance series began to increase in March, reached its peak in July, and then decreased. By comparing Figures 2.18 and 2.19, one can see some observations (the ones in Figure 2.18 minus the ones in Figure 2.19) had significant contributions from atmosphere.

The spectral reflectance time series of MODIS seven bands of all observations at the km67 Forest site in 2002 were in Figure 2.20. One cannot visually distinguish which ones are clustering observations without atmospheric effect, especially when keeping in mind that the evergreen forest should have low reflectance in blue, red, green and SWIR<sub>2</sub> bands (see peak growing seasons in Figures 2.14, 2.16 and 2.17). When using the monthly precipitation threshold of <100 mm/month for definition of dry season (Saleska et al., 2003), the dry-wet season change was clearly showed in Figures 2.24 and 2.26. Figure 2.24 showed that there were a few atmospheric clear observations (red reflectance  $\leq 0.04$ ) during dry seasons. One has difficulties to interpret the tendency of the MODIS blue, red and green reflectance with the atmospheric clear observations. However, the MODIS NIR<sub>1</sub> and NIR<sub>2</sub> had obvious increasing tendency during the dry seasons. The

SWIR<sub>1</sub> reflectance range was 0.03 – 0.1 which was as similar as the range of peak growing seasons in Figures 2.14, 2.16 and 2.17.

### 2.3.2 Seasonal NDVI, EVI, LSWI and MEVI Dynamics of Typical Vegetation Types from MODIS

The MODIS NDVI, EVI and LSWI time series without snow covered or atmospheric effects at the Xilingol grassland in 2002 were in Figure 2.11. The time series of the three indices had distinct and almost same seasonal cycle with almost same spring troughs and fall troughs. Following the change of NIR<sub>1</sub> reflectance curve, the three indices began to increase in middle to late June and reached their peaks in early to middle August. After they reached their peaks, they decreased rapidly. Figure 2.10 (a) showed the NDVI, EVI and LSWI pattern of snow contaminated ground (January, November and December). Figure 2.10 (b) showed the NDVI, EVI and LSWI pattern of dry bare ground (February-middle June and late October).

The MODIS NDVI, EVI and LSWI time series without snow covered or atmospheric effects at the Harvard Forest site in 2002 were in Figure 2.14. The time series of NDVI and LSWI had distinct and similar seasonal cycle with similar spring troughs and similar fall troughs. The reason of why NDVI was flat from June to September is that the red reflectance during this period was much less than NIR<sub>1</sub> reflectance and had no significant effect in calculation of NDVI. LSWI was also flat during peak growing season because SWIR<sub>1</sub> reflectance was flat during peak growing season. However, EVI had a different tendency from NDVI and LSWI. EVI began to increase in late March and reach its peak in late June to early July. EVI decreased after its

peak. EVI had the greatest variation in a short time range (e.g. in one day or a few days) among the three indices during June to September. That is to say, EVI kept more of the bi-directional distribution function (BRDF) effect than LSWI and NDVI. Snow contaminated observations (Figure 2.13 and Figure 2.14) at the Harvard Forest site had NDVI, EVI and LSWI as high as the ones of clear peak growing season observations. To analyze vegetation activity, one needs to screen the snow contaminated observations. Function 2.5 from Kaufman et al. (2002) offers one approach to do it.

The MODIS NDVI, EVI and LSWI time series without snow covered or atmospheric effects at the Howland Forest site in 2002 were in Figure 2.16. The time series of NDVI had least variation from DOY 115 to DOY 318 among the three indices. Most of the NDVI curve had values greater than 0.8. LSWI and EVI time series had a distinct and almost same seasonal cycle with almost same spring troughs and fall troughs. Following the change of  $NIR_1$  and  $SWIR_1$  reflectance curves, LSWI and EVI increased from DOY 115, reached their peaks around DOY 191, then decreased until DOY 318. The snow contaminated observations (the ones in Figure 2.15 minus the ones in Figure 2.16) had similar NDVI, EVI and LSWI as the snow contaminated observations at the Harvard Forest site.

The MODIS NDVI, EVI and LSWI time series without snow covered or atmospheric effects at the Walker Branch Watershed Forest in 2002 were in Figure 2.17. The time series of the three indices had a distinct and almost same seasonal cycle with almost same spring troughs and fall troughs. LSWI during January-March and December were negative. NDVI from late May to middle October were flat and greater than 0.8. LSWI from late May to middle October were a little slightly decreasing. EVI from June



to October were most strongly decreasing among the three indices. EVI had the greatest variation in a short time range (e.g. in one day or a few days) among the three indices during May to October. That is to say, EVI kept more of the BRDF effect than LSWI and NDVI. The site could get snow free observations for the whole year.

The MODIS NDVI, EVI and LSWI time series without snow covered or atmospheric effects at the Soybean site in 2002 were in Figure 2.19. The time series of the three indices had a distinct and almost same seasonal cycle with almost same spring troughs and fall troughs. They began to increase in April, reached their peaks in July-August, and then decreased. The site could get snow free observations for the whole year.

The LSWI of the km67 forest site in Figure 2.25 showed the increasing tendency during the dry seasons because of the same tendency of  $NIR_1$  reflectance. EVI and MEVI in Figure 2.25 also had increasing tendency during the dry seasons. It is difficult to say NDVI had this kind of tendency. The leaf litterfall in Figure 2.26 was measured for every two weeks. There were more litter-fall in the dry seasons than in wet seasons. Figure 2.26 showed that, during a dry season, the more cumulative litterfall, the higher  $NIR_1$  reflectance, hence the greater LSWI, EVI and MEVI (Figure 2.25). Note that the evergreen forest canopy is composed of mixed-age leaves.  $NIR_1$  increasing during dry seasons may be attributed to both leaf fall of old leaves and emergence of new leaves, resulting in dynamic changes in proportions of young and old leaves within a vegetation canopy over seasons. Leaf fall of old leaves reduces self-shading, resulting in more sunlight penetrating into the canopy to the remaining younger leaves, in other words, a higher proportion of young leaves within the canopy are observed by the satellite. In general, old leaves have less chlorophyll and water content but more structural materials

(e.g., lignin, cellulose), in comparison to young leaves, which could lead to significant changes in absorbance, transmittance, and reflectance of leaves as the aging processes of leaves progresses. In a field study that conducted leaf optical measurements of a number of tropical evergreen species near Manaus in the Amazon basin (Roberts et al., 1998), the NIR absorbance showed significant change, increasing from near zero for young leaves to 10% for old leaves. Canopy reflectance is largely determined by light absorption of leaf pigments, liquid water and leaf dry matter and light scattering of non-photosynthetic vegetation (NPV). The NPV proportion at the leaf scale increases as (1) the leaf ages and (2) the leaf responds to various environmental stresses (e.g., drought, O<sub>3</sub>, fungi). Increased NIR absorbance at the leaf scale may have a larger impact at the canopy scale by dampening NIR scattering within a canopy and thereby reducing canopy reflectance. Thus, removal of old leaves from the canopy (leaf litter-fall) is likely to result in an increase of NIR reflectance at the canopy level. NIR<sub>1</sub> continued to increase after leaf litter-fall peaked in the middle of the dry season at the km67 site (Figure 2.26), which may be attributed to continuing removal of old leaves throughout the dry season, followed by emergence (flushing) of new leaves in the late dry season. The peak NIR<sub>1</sub> values had a time lag of one to 2 months after the peak leaf litter-fall. Although no seasonal field data of leaf emergence at the km67 site are available, however, field observations from other seasonal tropical forest sites suggested that many drought-tolerant species with deep roots tended to produce new leaves in the late dry season (Van Schaik et al., 1993; Wright et al., 1994). Field data at the Tapajós 's National Forest showed a pulse of stem growth prior to the initiation of the wet season; and increments of aboveground woody biomass (stem growth) were larger in the wet season than in the dry

season (Saleska et al., 2003), which suggest that construction of new leaves may be largely done during the late part of the dry season. For the field site in Manaus, Roberts et al. (1998) reported that new leaf flush occurred mostly within the dry season. Field observations also recorded that epiphylls (fungi, lichens, algae, and bacteria) colonized the mature leaves, which affected light transmittance and absorption (Roberts et al., 1998). Young leaves have a higher photosynthetic capacity than older leaves (Field, 1987), and therefore, it is essential to track changes of the age-structure of leaves in the canopy, which could substantially improve modeling of the seasonal dynamics of photosynthesis. In summary, during the dry seasons, LSWI, EVI and MEVI followed the increasing tendency of NIR<sub>1</sub>.

## **2.4 Discussion and conclusions**

In this chapter, I described an approach to acquire contamination-free observations of MODIS daily image, i.e. the observations without snow cover and/or atmospheric contamination (Figures 2.11, 2.14, 2.16, 2.17 and 2.19). The contamination-free observations of the Xilingol grassland site with SWIR<sub>2</sub> greater than 0.25 (Figures 2.9 and 2.10), which suggested that the observed target was very dry and had no vegetation covered, were also distinguished from other contamination-free observations. The procedure screened the snow or cloud contaminated observations out and kept the observations that held information of vegetation and /or background soil. The previous analysis about the Harvard Forest, the Howland Forest and the km67 tropical seasonal moist forest (Xiao et al., 2004b; Xiao et al., 2004c; Xiao et al., 2005b; Xiao et al., 2005c) can be updated with the results of this chapter.

The MODIS red, blue and SWIR<sub>2</sub> of the clustering observations in Figures 2.11, 2.14, 2.16, 2.17 and 2.19 have very good linear relationships (Figure 2.21) that fall in the estimated relationship functions by a previous study (Kaufman et al., 1997). Functions 2.6 and 2.7 can be reasonably used as criteria to check if the observations are contaminated by aerosols/snow. If so, left sides of equations 2.6 and 2.7 would be greater than their right sides. The criteria can be used in the processing of MODIS to select the best observations for 8-day composite reflectance data (e.g. MOD09A1) or 16-day products (MOD13).

The MODIS NIR<sub>1</sub> reflectance series of the clustering observations in Figures 2.11, 2.14, 2.16, 2.17 and 2.19 had the strongest seasonal variations among the seven spectral bands reflectance series. They had obvious peak signals: before the period, NIR<sub>1</sub> increased; after the period, NIR<sub>1</sub> decreased. The peak NIR<sub>1</sub> reflectance values ranged 0.4 – 0.5. The minimum NIR<sub>1</sub> reflectance values ranged 0.15 – 0.2. However, the maximum blue, green and red reflectance values of the clustering observations in Figures 2.11, 2.14, 2.16, and 2.17 were less than 0.15, and the maximum one in Figure 2.19 were less than 0.17. In a summary, the seasonal variation range of NIR<sub>1</sub> and NIR<sub>2</sub> reflectance in Figures 2.11, 2.14, 2.16, 2.17 and 2.19 was greater than the ones of SWIR and visible reflectance, and the seasonal variation range of SWIR reflectance was greater than the one of visible reflectance.

The MODIS NIR<sub>1</sub> reflectance series of the clustering observations in Figures 2.11, 2.14, 2.16, 2.17 and 2.19 increased before they reached peaks. The increasing tendency was accompanied with the increasing younger leaves proportion in pixels, i.e., decreasing average leaf age at pixel scale. The MODIS NIR<sub>1</sub> reflectance series at the km67 site

(Figure 2.26) showed that  $NIR_1$  reflectance increased during dry seasons in 2001-2004. Both the falling of old leaves and emergence of new leaves could possibly decrease the average leaf age at pixel scale. The  $SWIR_1$  reflectance of the Xilingol grassland site and the Soybean site during peak growing season in 2002 was 0.2 - 0.3, the  $SWIR_1$  reflectance of the Harvard Forest, and the Howland Forest was 0.1 - 0.2, and the  $SWIR_1$  reflectance of the Walker Branch Watershed site was 0.1 - 0.25 (Figures 2.11, 2.14, 2.16, 2.17 and 2.19). Most observations of the km67 site in Figure 2.26 had  $SWIR_1$  reflectance 0.1 - 0.2, a few others had  $SWIR_1$  reflectance 0.2 - 0.25. So there was no  $SWIR_1$  signal that showed any drought signal or less water content in leaf at the km67 site during dry seasons.

All MODIS seven bands reflectance values changed with varying sun-target-satellite geometry (Figures 2.11, 2.14, 2.16, 2.17, 2.19 and 2.24). NDVI, EVI and LSWI were also affected by the BRDF effects.  $NIR_1$  was the most strongly BRDF affected among the seven bands. The difference between maximum reflectance and minimum reflectance of  $NIR_1$  on same day can be as high as absolute 0.2. EVI was the most strongly BRDF affected among the three indices. The difference between maximum EVI and minimum EVI on same day can be as great as absolute 0.2. Note that the greatest EVI at the five non-tropical sites of this chapter was less than 0.75. When EVI is used for quantitative calculation or estimation, the BRDF effect should be considered because BRDF can possibly change EVI by relative more than 25% ( $0.2/0.75 > 25\%$ ).

Another concern about reflectance and indices is that it is somehow difficult to compare them because of the worry of BRDF effect on them. The concern is somehow reasonable. However, if one looks at the signal of reflectance and indices at whole

seasonal scale (Figures 2.11, 2.14, 2.16, 2.17, 2.19, 2.25 and 2.26), one can find that seasonal variation tendency can not be changed by BRDF effect even BRDF effect can make confusion if the temporal scale is less than a whole growing season. For example, Figure 2.17 clearly showed the seasonal variation tendency of spectral reflectance of the MODIS seven bands and NDVI, EVI and LSWI even though  $NIR_1$ ,  $SWIR_1$  reflectance and EVI had obviously strong BRDF effects. In a short summary, one does not need to concern about the BRDF effect if he/she only wants to check seasonal tendency or phenology with seasonal reflectance or NDVI, EVI or LSWI; one needs to consider BRDF effect if he/she wants to use reflectance or EVI in quantitative analysis or estimation.

If the assumption that the leaf spectral property of each biome type is constant (Myneni et al., 2002; Wang, 2002) is correct, leaf area index (LAI) should follow the  $NIR_1$  reflectance seasonal pattern, i.e. LAI should follow the  $NIR_1$  reflectance seasonal patterns in Figures 2.11, 2.14, 2.16, 2.17, 2.19 and 2.26. However, the standard MODIS LAI products at the Harvard Forest site, the Howland Forest site, the Walker Branch Watershed Forest site and the km67 site (see Figure 2.27) did not follow the  $NIR_1$  reflectance seasonal patterns in Figures 2.14, 2.16, 2.17 and 2.26. The inconsistency between the assumption by the MODIS LAI/FPAR standard product team and standard MODIS LAI product suggests that the assumption is not correct, or the LAI product is not correct, or both.

Table 2.1 The latitude and longitude of the six sites for study in this chapter

site	Land cover	Latitude	Longitude
km67	tropical evergreen forest	2.85694 <sup>0</sup> S	54.95903 <sup>0</sup> W
Walker Branch Watershed	deciduous forest	35.95877 <sup>0</sup> N	84.28743 <sup>0</sup> W
Harvard Forest	deciduous forest	42.53572 <sup>0</sup> N	72.17200 <sup>0</sup> W
Howland	evergreen needle forest	45.20407 <sup>0</sup> N	68.7402 <sup>0</sup> W
Soybean	crop	41.16494 <sup>0</sup> N	96.46861 <sup>0</sup> W
Xilingol	grassland	43.63222 <sup>0</sup> N	116.70497 <sup>0</sup> E

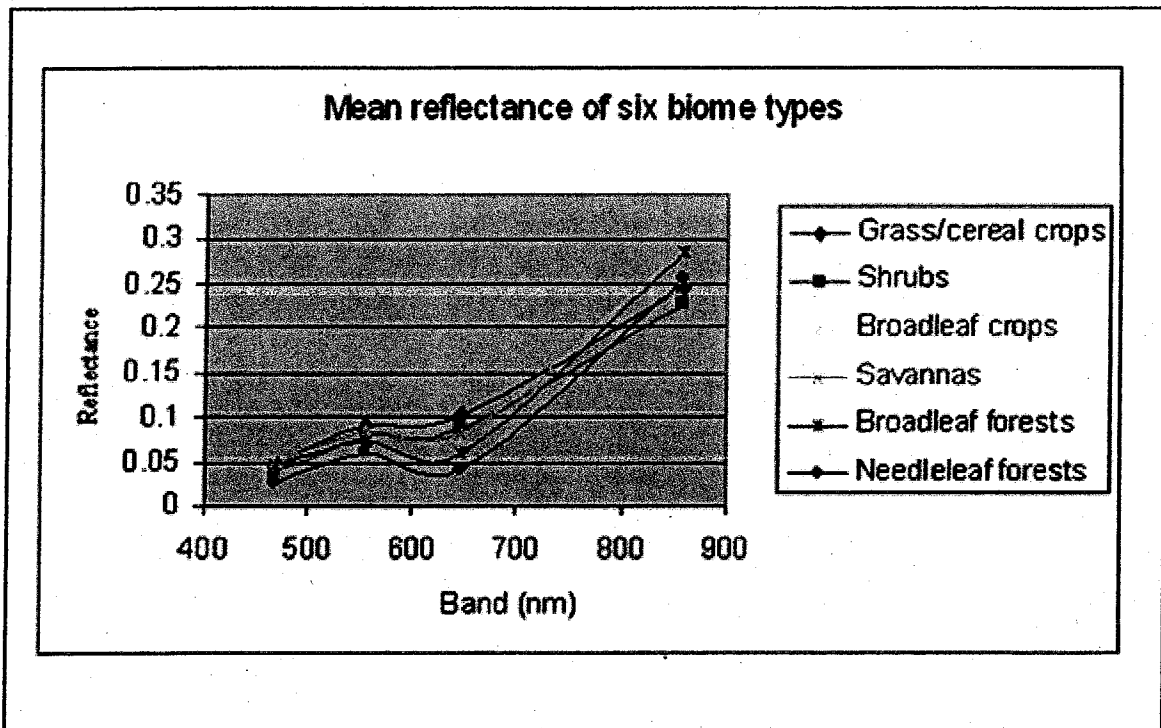


Figure 2.1 Mean reflectance of six biome types used by MODIS LAI/FPAR science team (from Wang, 2002)



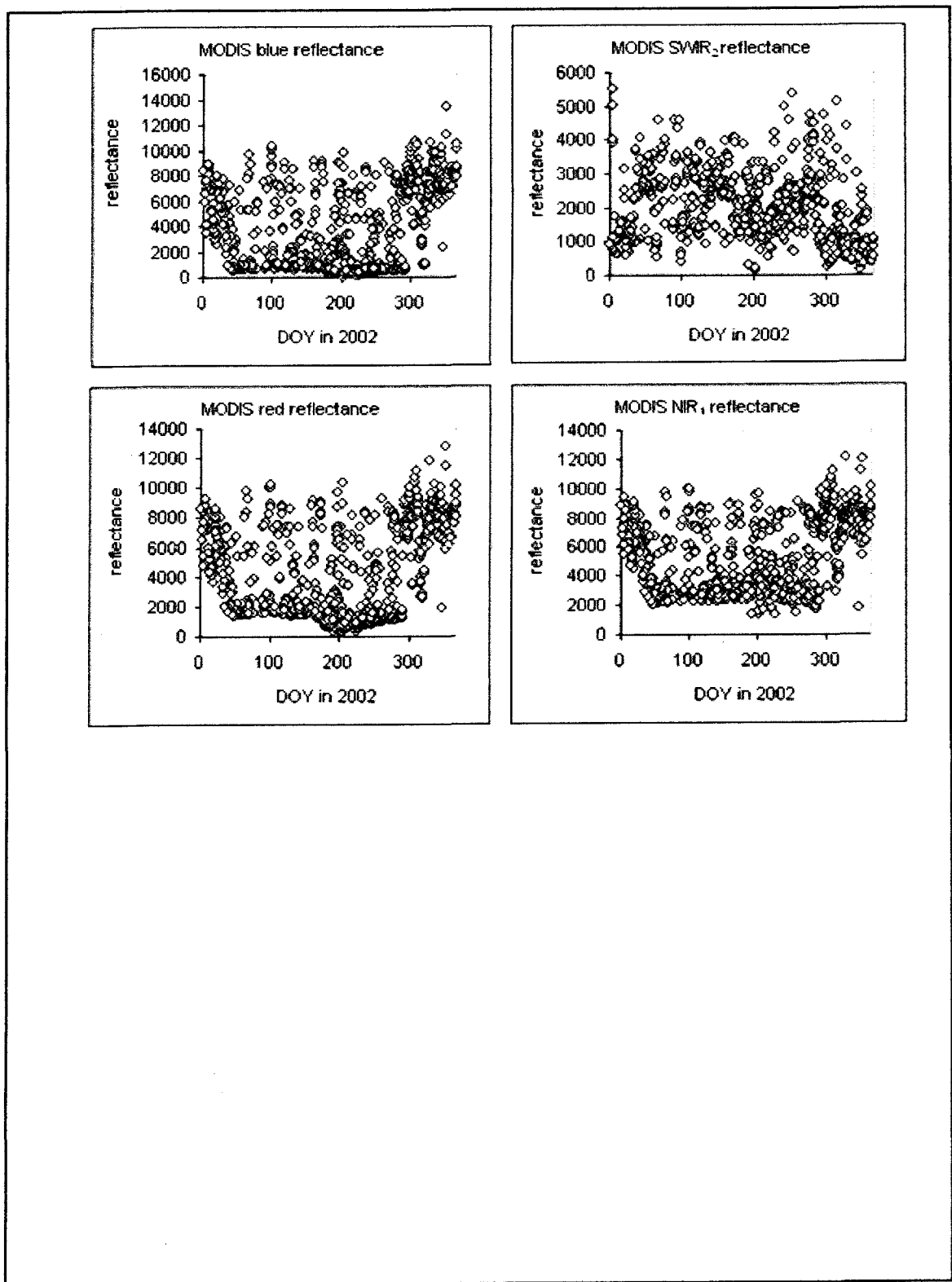


Figure 2.2 MODIS daily observations of the Xilingol grassland site in 2002 (reflectance scale=0.0001)

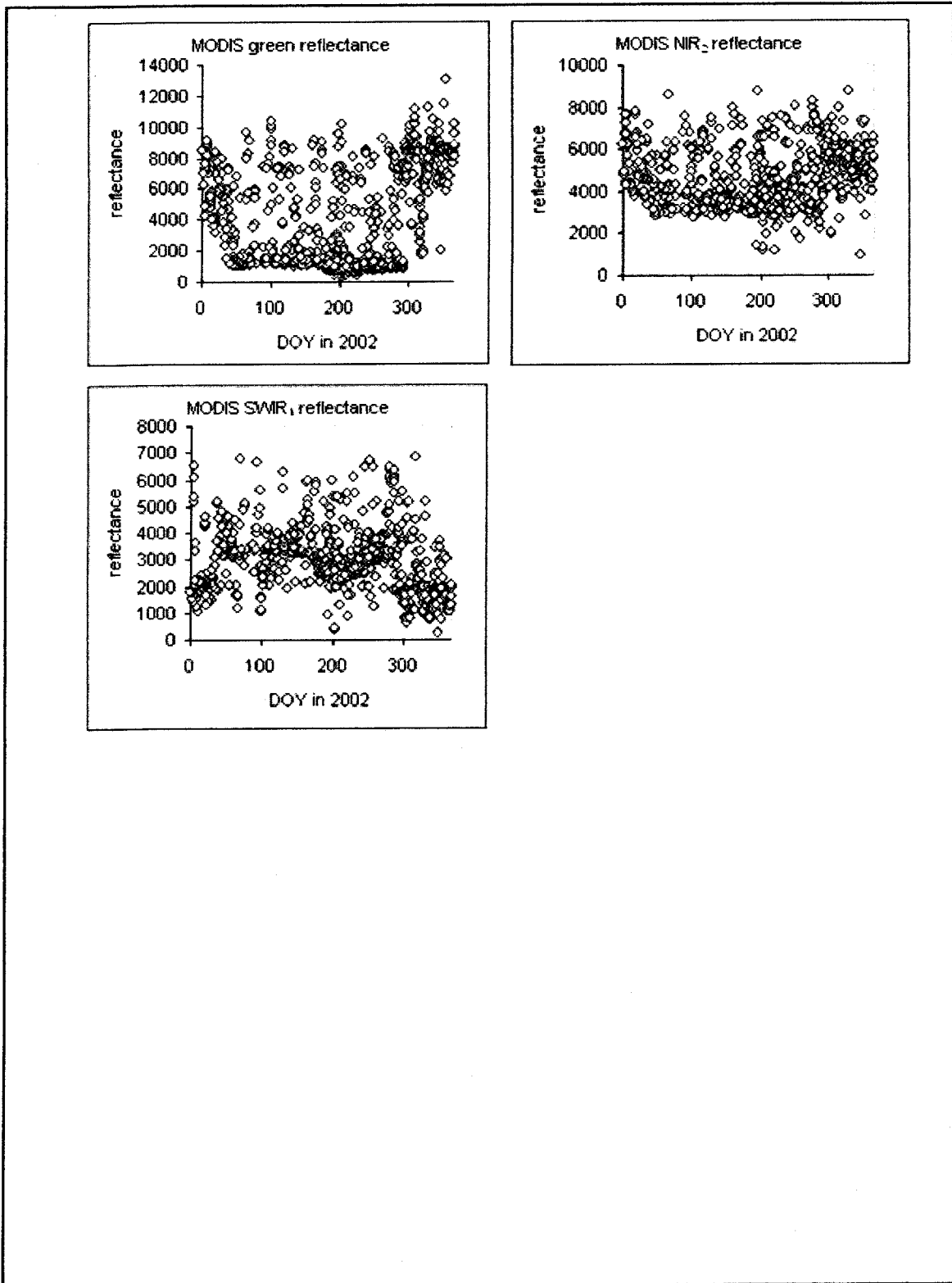


Figure 2.2 (continued) MODIS daily observations of the Xilingol grassland site in 2002 (reflectance scale=0.0001)

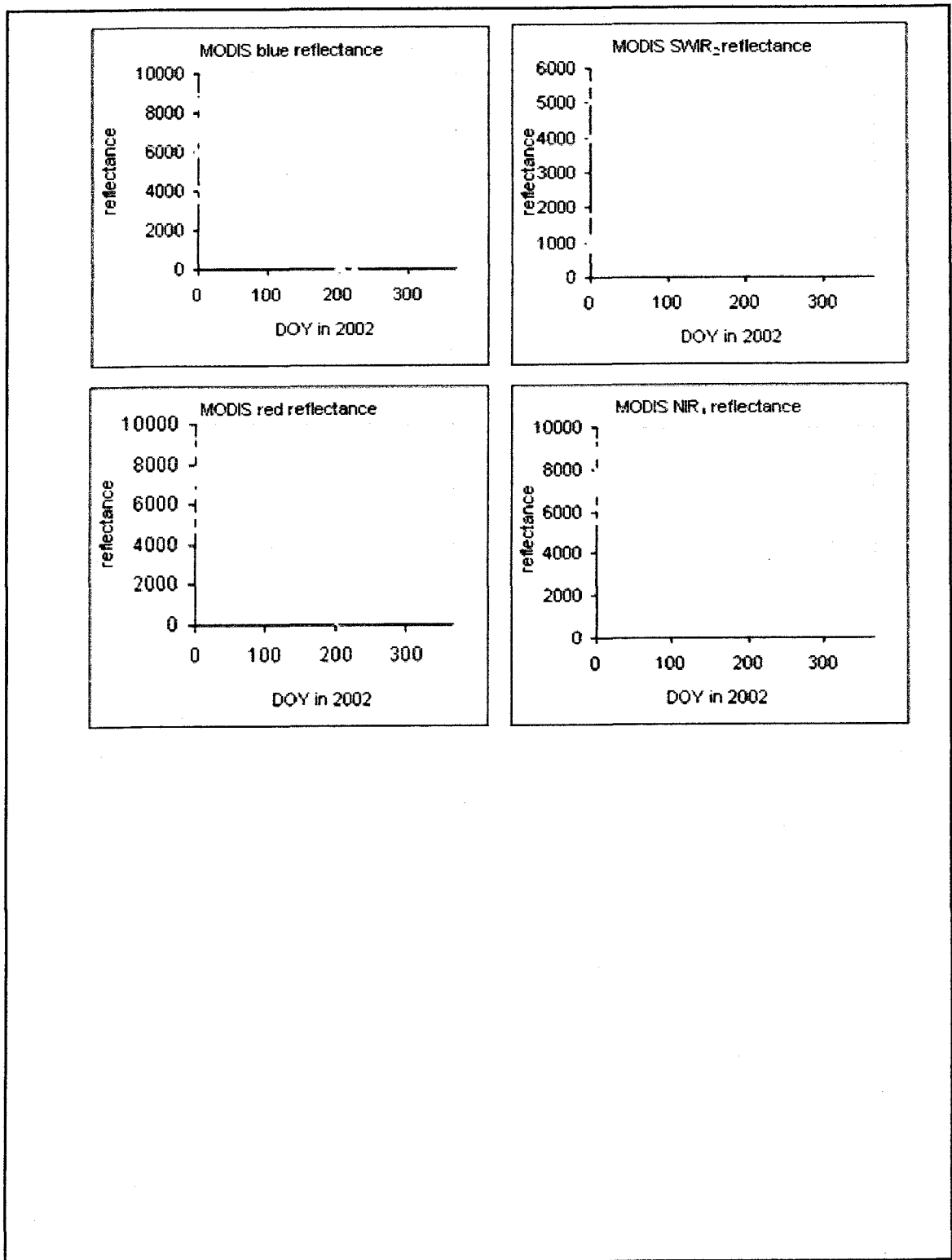


Figure 2.3 MODIS daily observations (all reflectance $\leq 1$ ) of the Xilingol grassland site in 2002 (reflectance scale=0.0001)

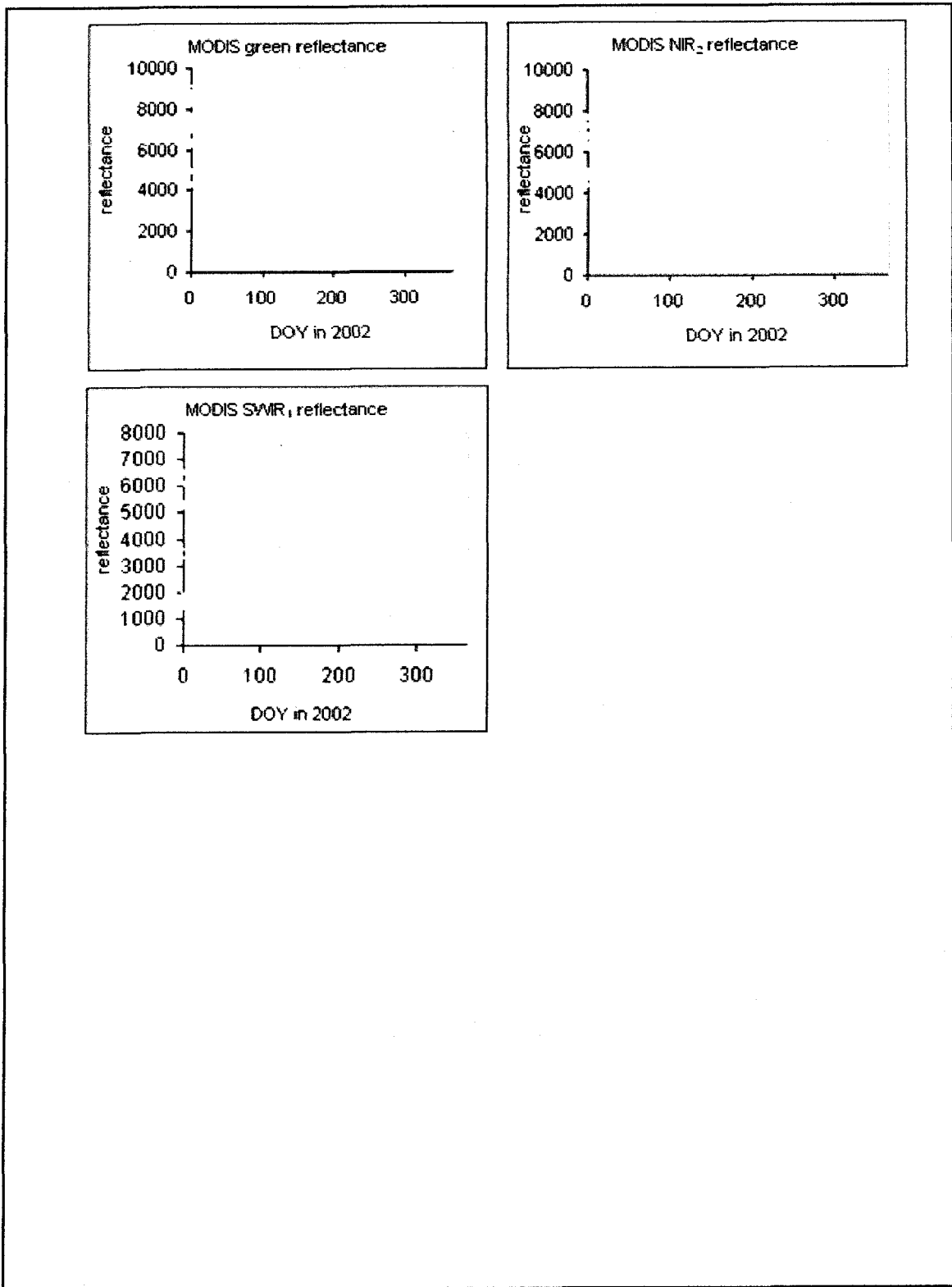


Figure 2.3 (continued) MODIS daily observations (all reflectance $\leq$ 1) of the Xilingol grassland site in 2002 (reflectance scale=0.0001)

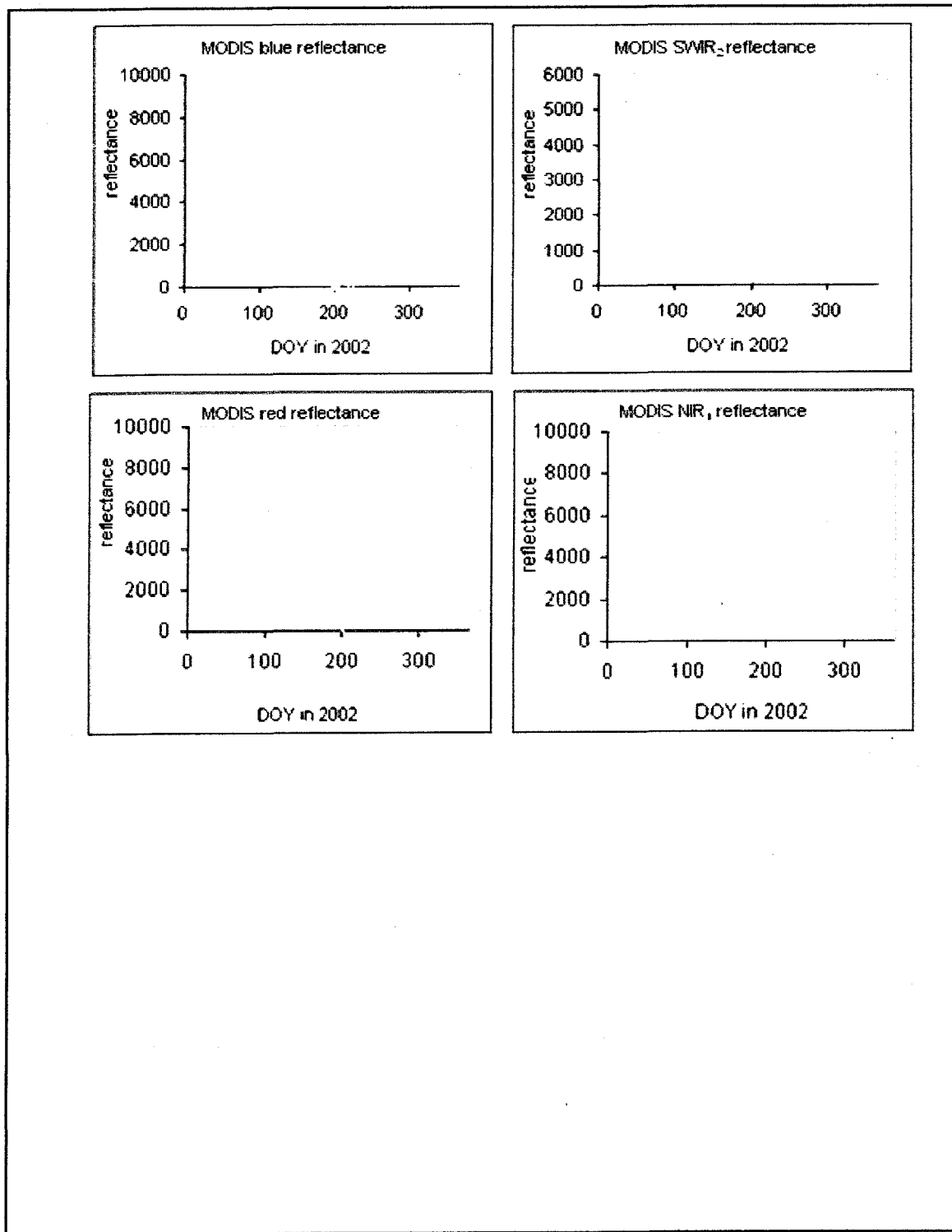


Figure 2.4 MODIS daily observations (all reflectance $\leq$ 1) of the Xilingol grassland site in DOY 50 to 270, 2002 (reflectance scale=0.0001)

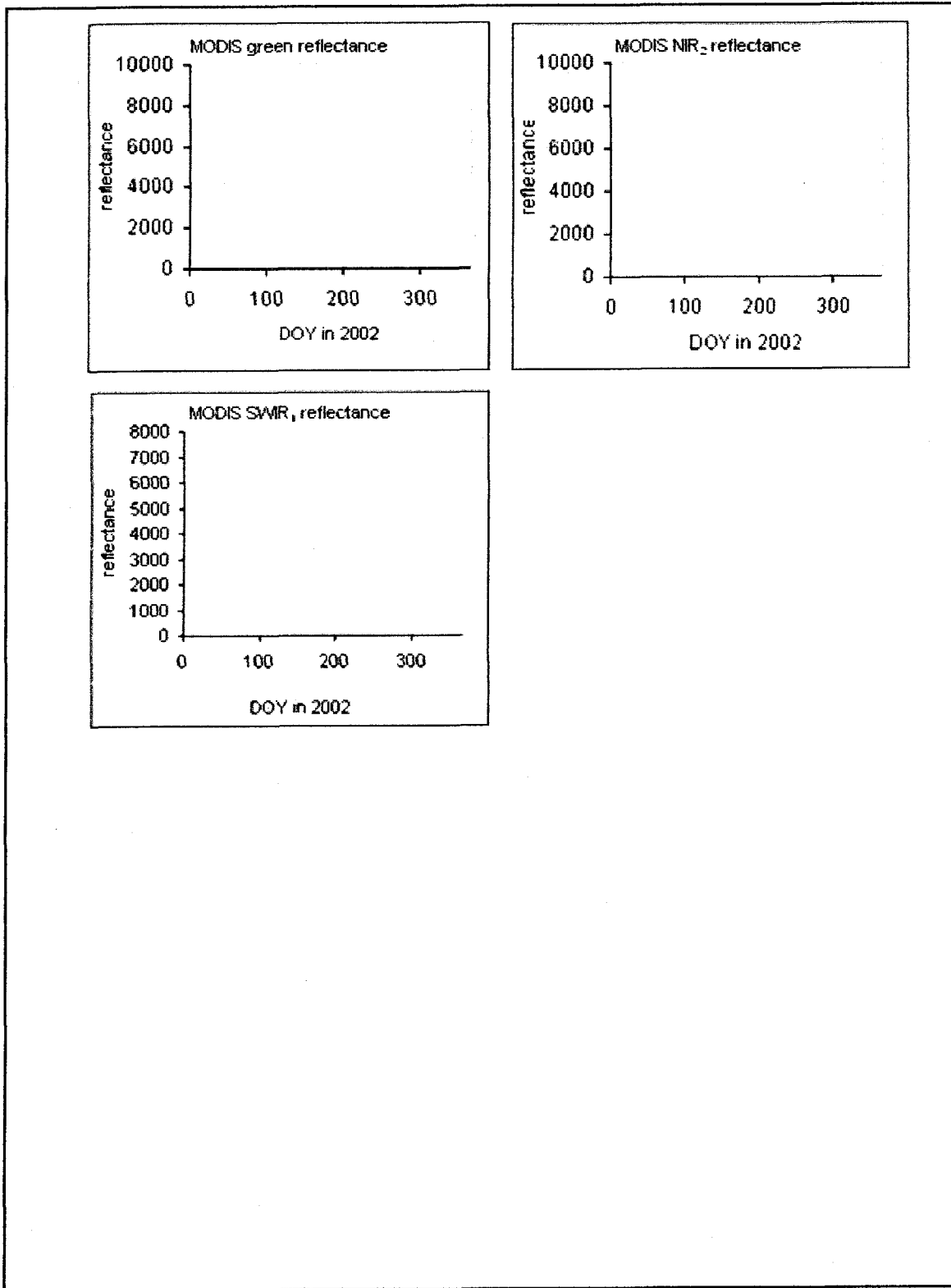


Figure 2.4 (continued) MODIS daily observations (all reflectance $\leq$ 1) of the Xilingol grassland site in DOY 50 to 270, 2002 (reflectance scale=0.0001)

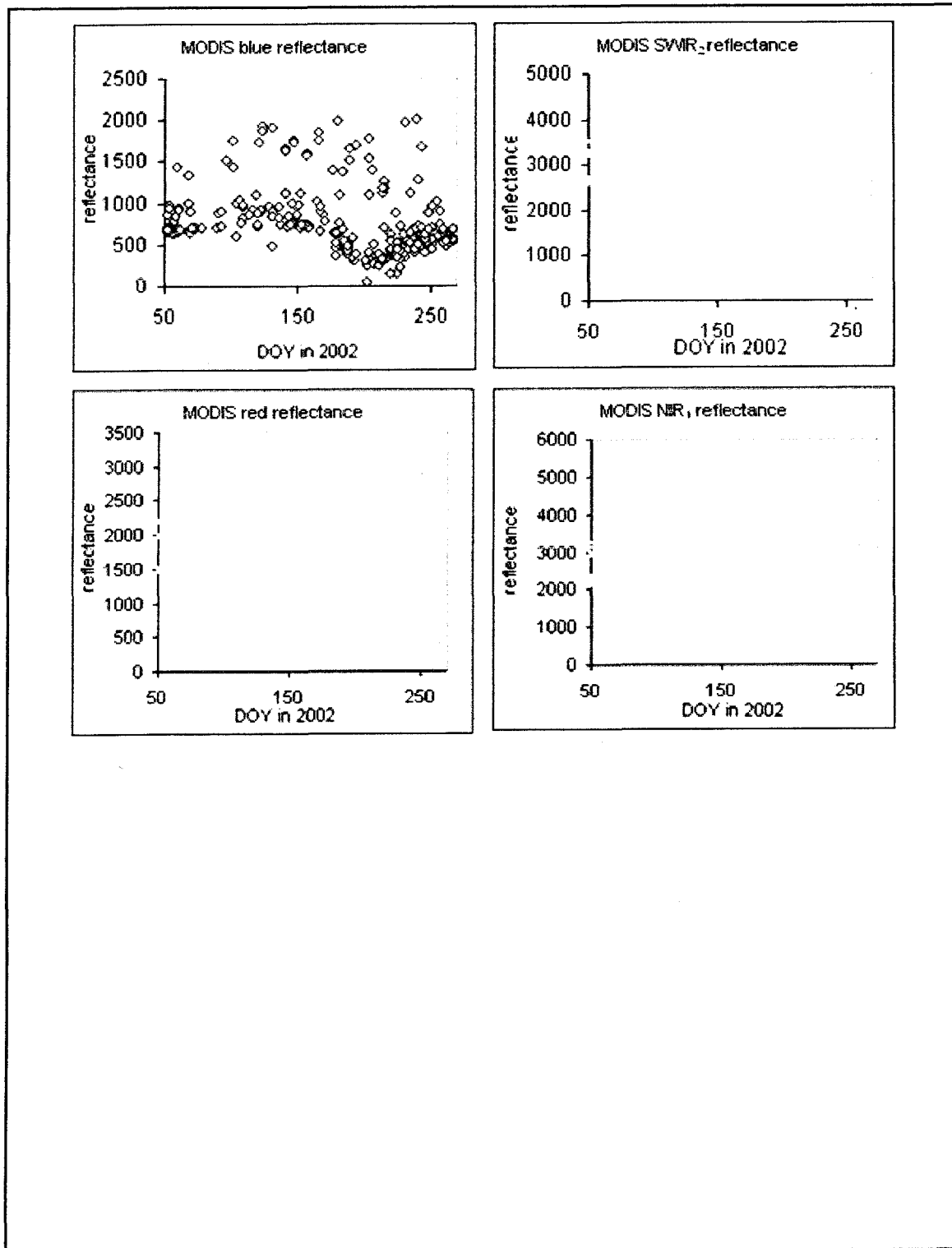


Figure 2.5 MODIS daily observations (blue reflectance $\leq$ 0.2) of the Xilingol grassland site in DOY 50 to 270, 2002 (reflectance scale=0.0001)

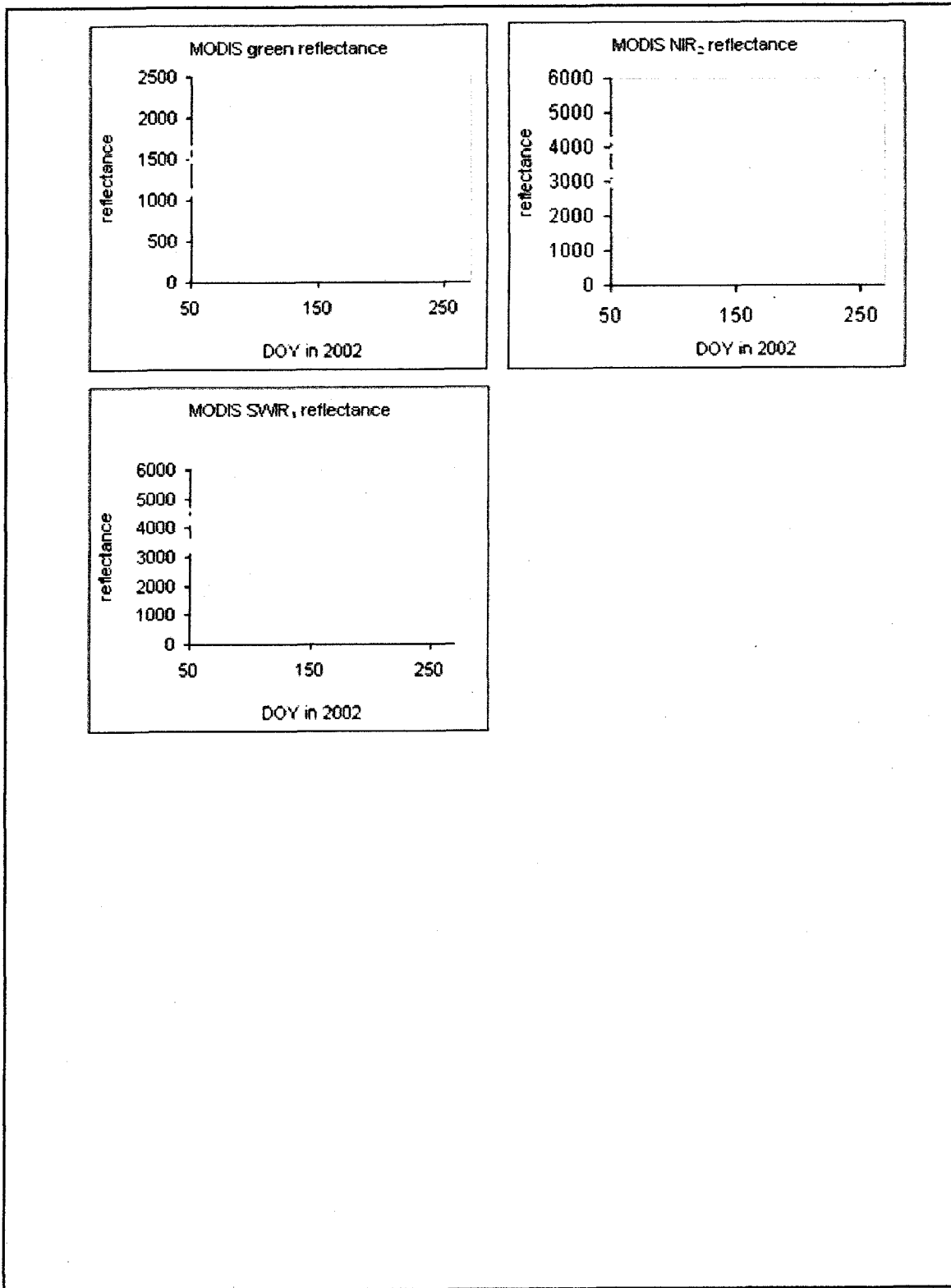


Figure 2.5 (continued) MODIS daily observations (blue reflectance $\leq$ 0.2) of Xilingol grassland site in DOY 50 to 270, 2002 (reflectance scale=0.0001)



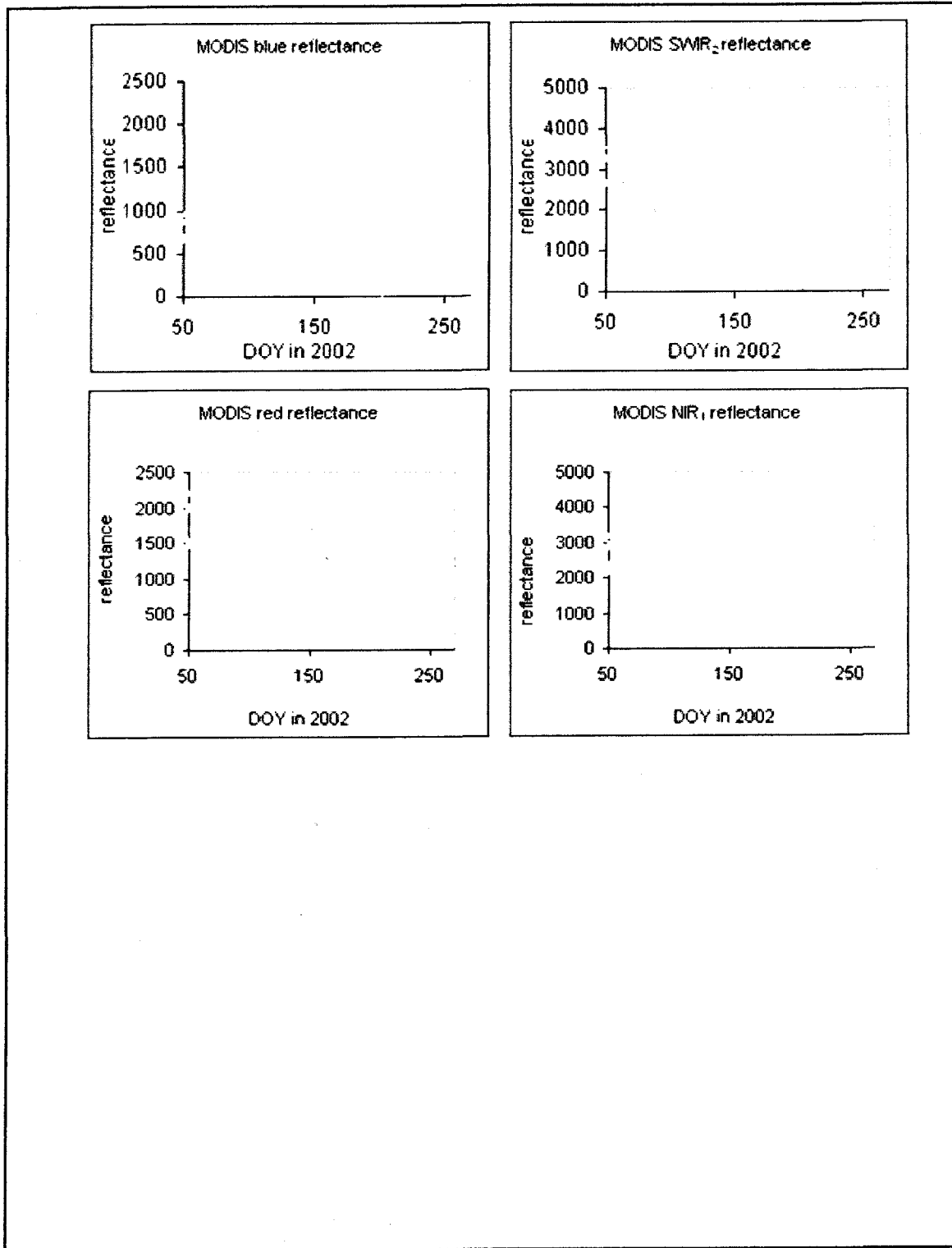


Figure 2.6 MODIS daily observations of the Xilingol grassland site in DOY 50 to 270, 2002 (reflectance scale=0.0001) after discarding the observations with scattering blue reflectance

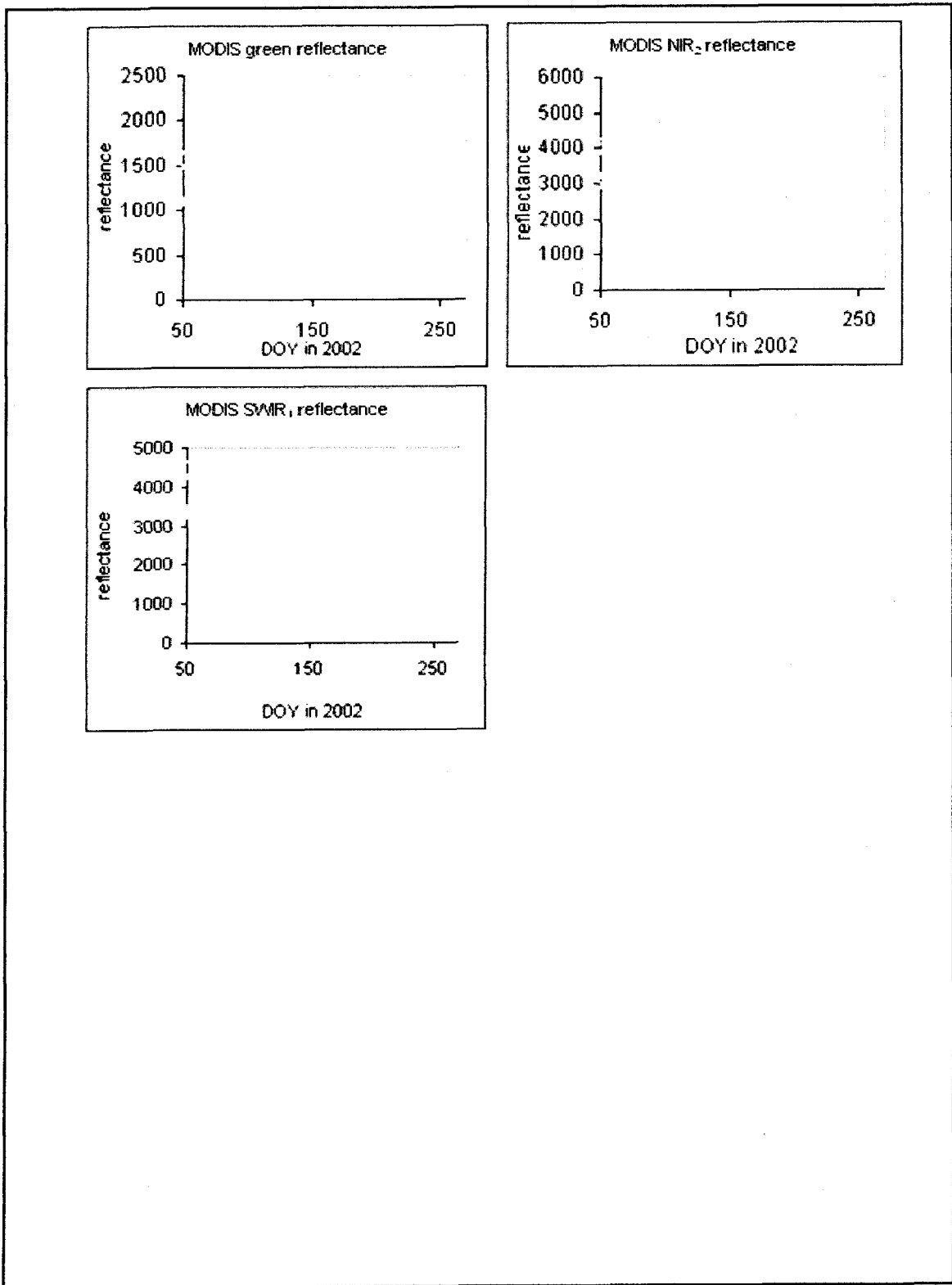


Figure 2.6 (continued) MODIS daily observations of the Xilingol grassland site in DOY 50 to 270, 2002 (reflectance scale=0.0001) after discarding the observations with scattering blue reflectance

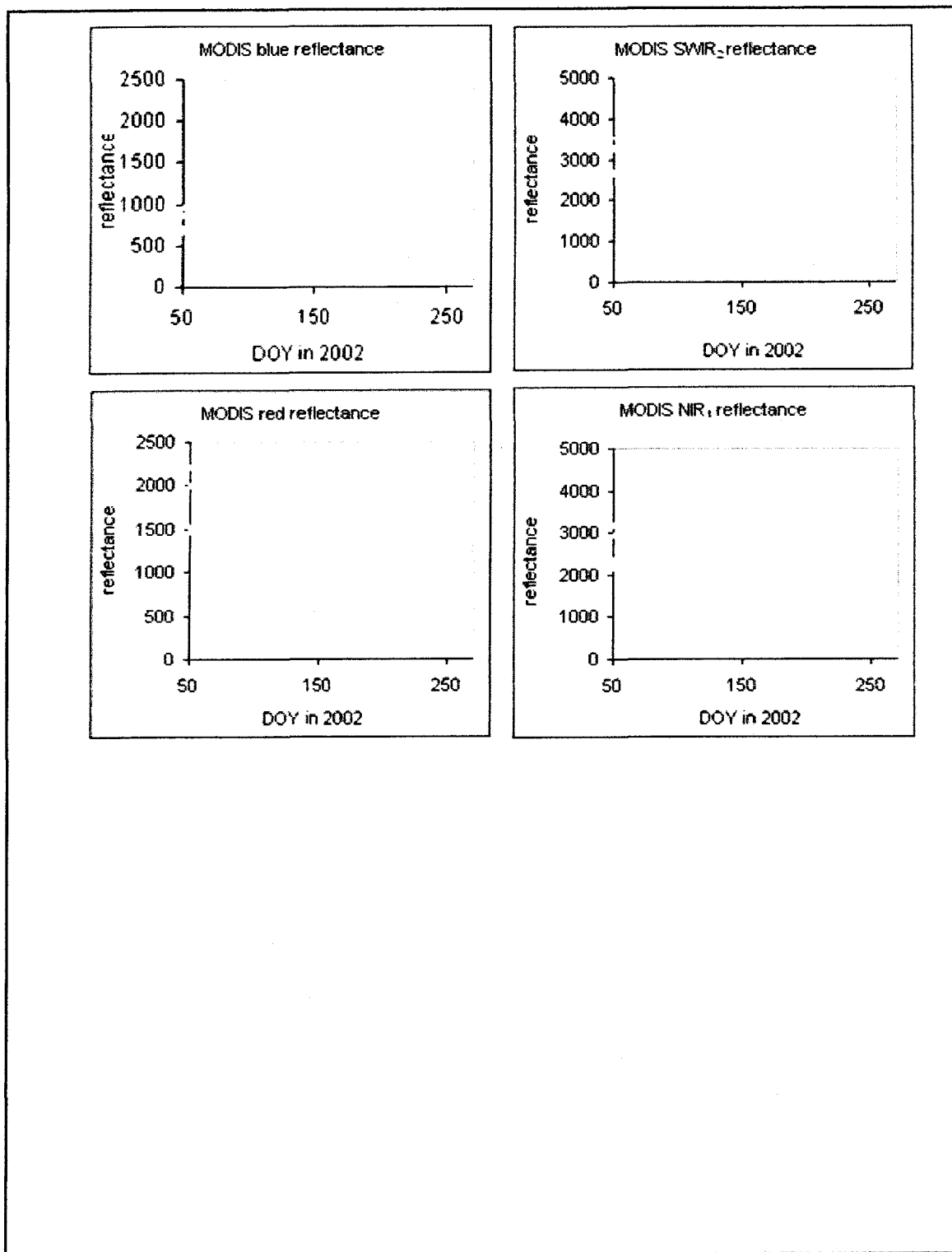


Figure 2.7 MODIS daily observations of the Xilingol grassland site in DOY 50 to 270, 2002 (reflectance scale=0.0001) after discarding the observations with scattering too low reflectance of all the seven bands

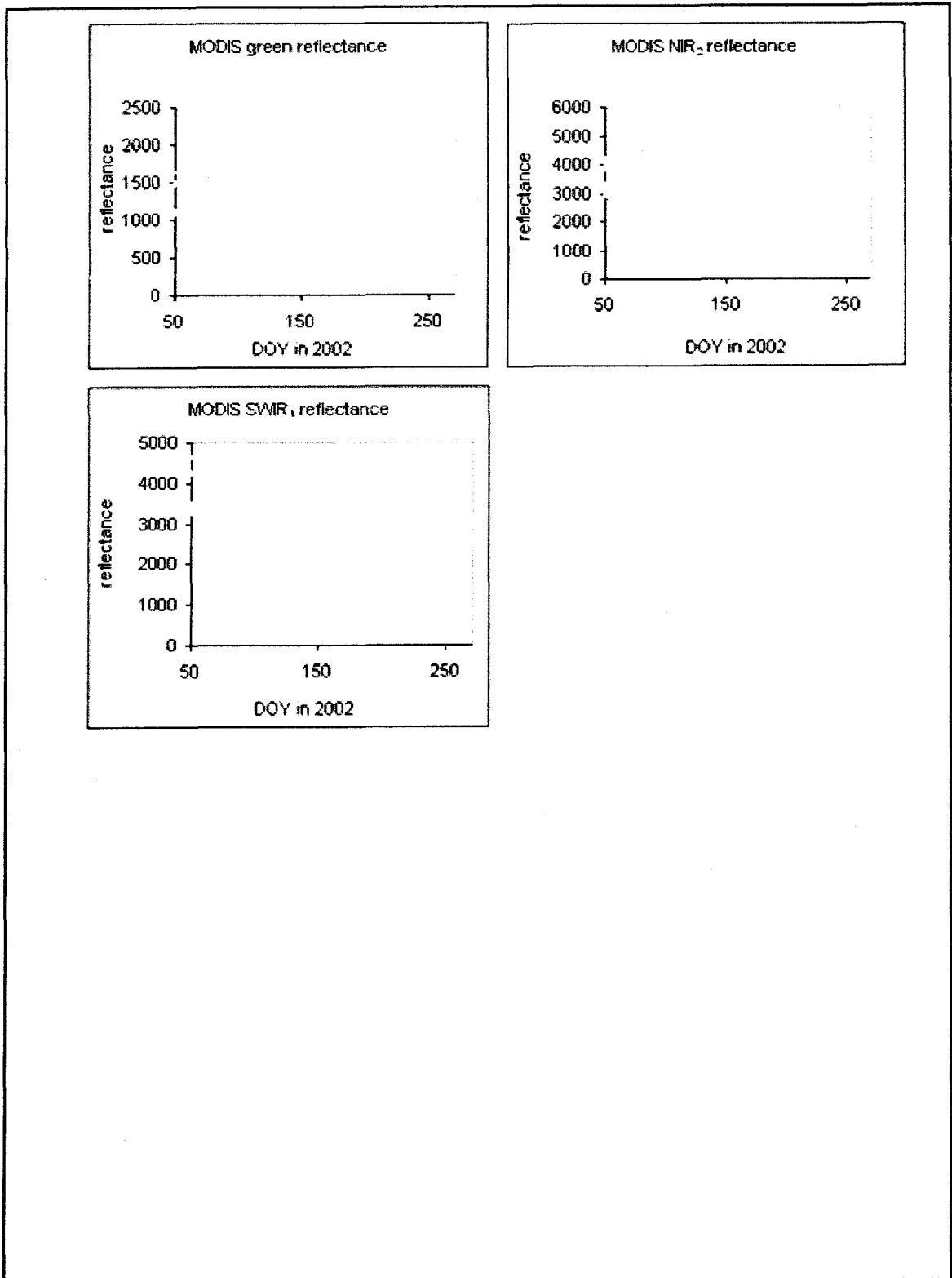


Figure 2.7 (continued) MODIS daily observations of the Xilingol grassland site in DOY 50 to 270, 2002 (reflectance scale=0.0001) after discarding the observations with scattering too low reflectance of all the seven bands

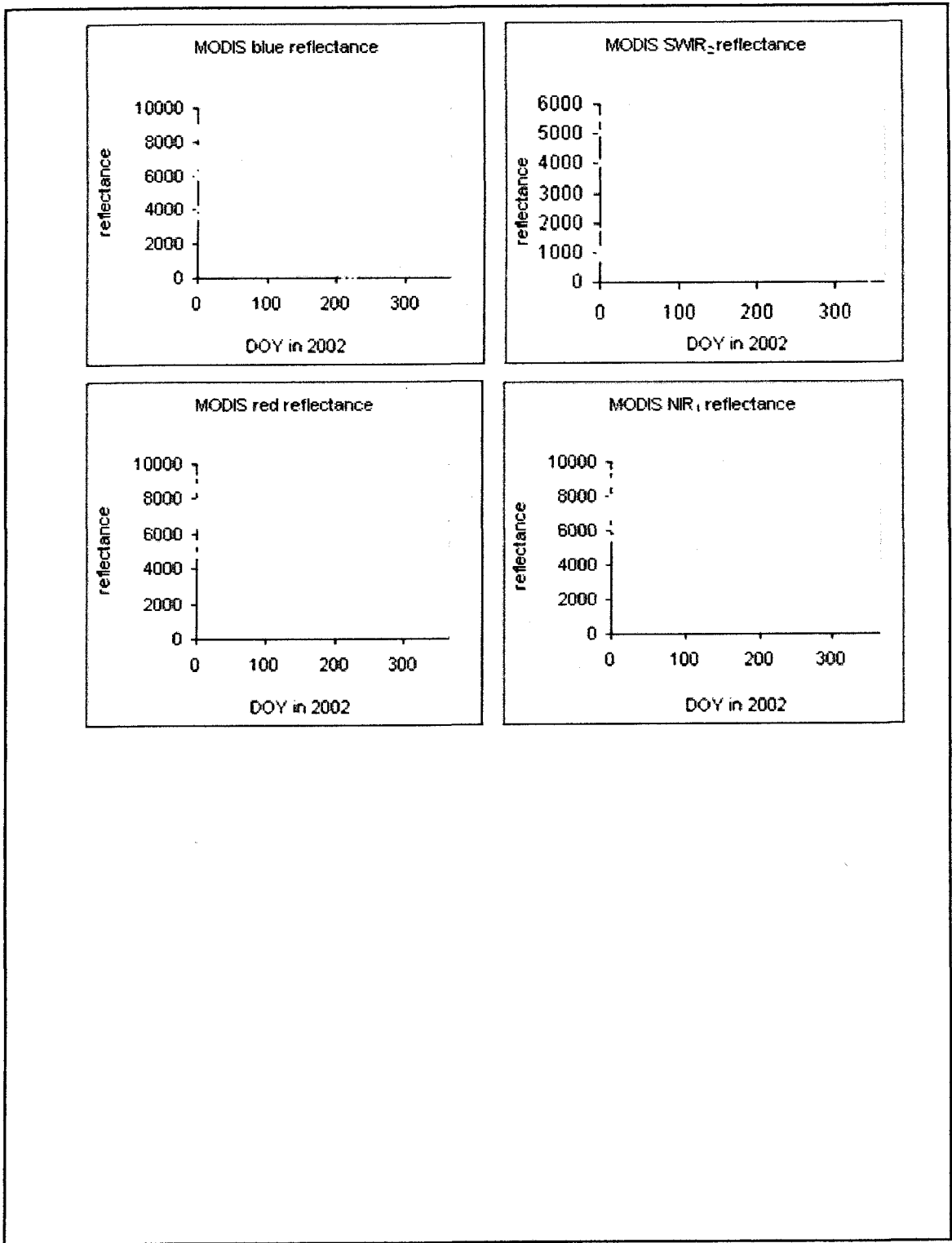


Figure 2.8 MODIS daily observations of the Xilingol grassland site in DOY 50 to 270 (reflectance scale=0.0001) in Figure 2.7, observations before DOY 50, observations after DOY 270 and relative annual NDVI, EVI and LSWI in 2002

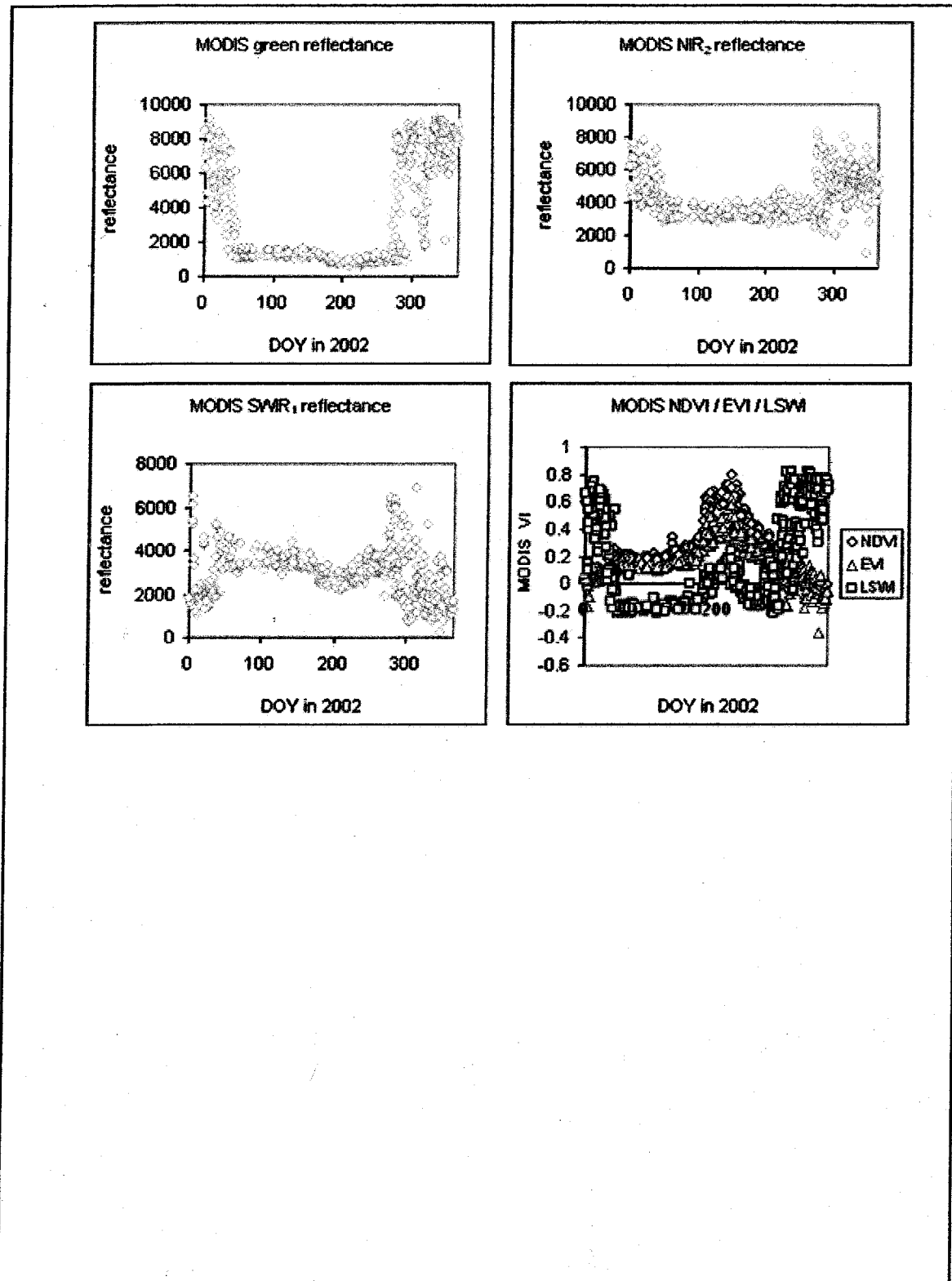


Figure 2.8 (continued) MODIS daily observations of the Xilingol grassland site in DOY 50 to 270 (reflectance scale=0.0001) in Figure 2.7, observations before DOY 50, observations after DOY 270 and relative annual NDVI, EVI and LSWI in 2002

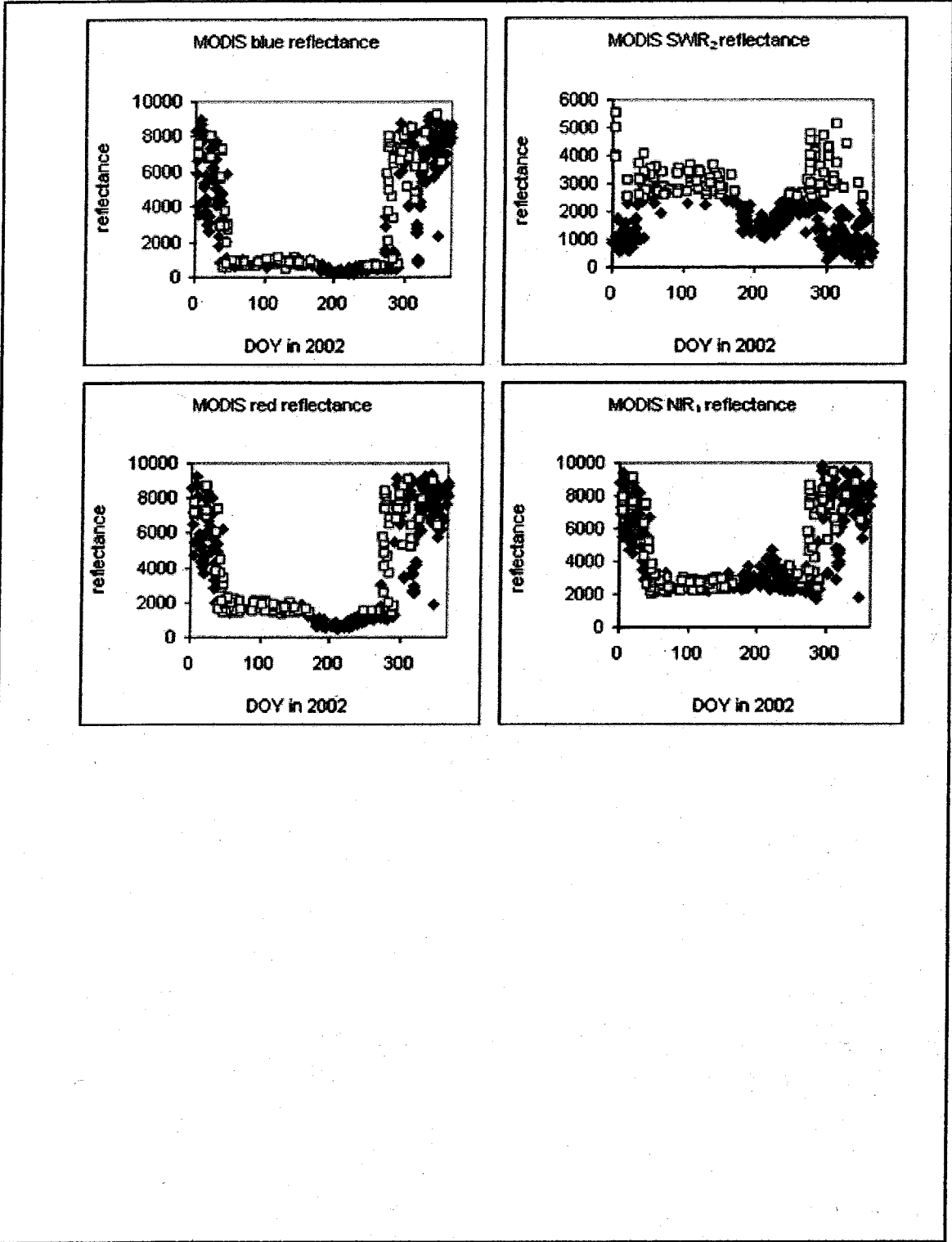


Figure 2.9 MODIS daily observations of the Xilingol grassland site in Figure 2.8 (reflectance scale=0.0001) were partitioned into two parts: the observations with SWIR<sub>2</sub> less than 0.25 (black blue points); the others with SWIR<sub>2</sub> greater than 0.25 (pink points)

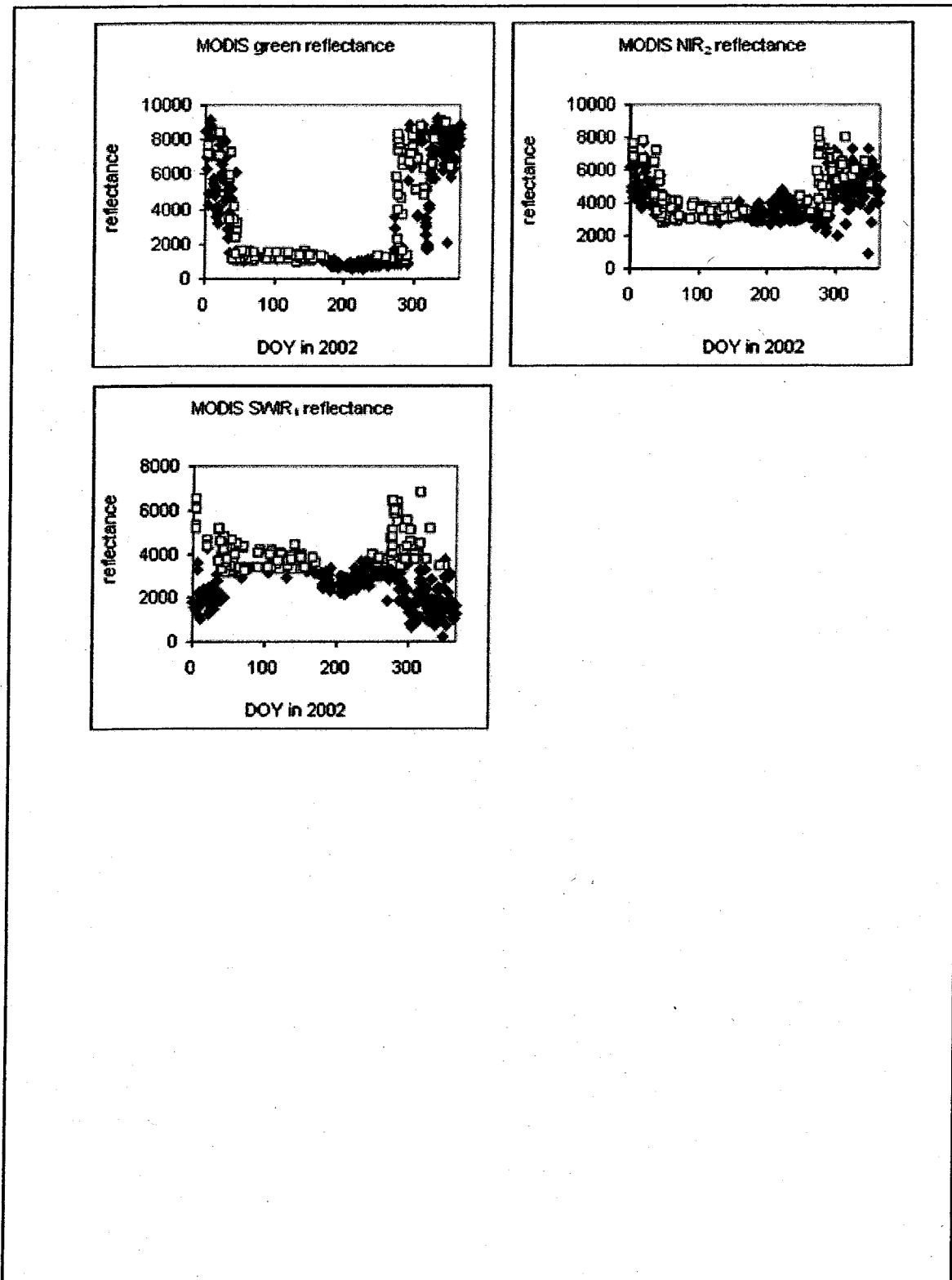


Figure 2.9 (continued) MODIS daily observations of the Xilingol grassland site in Figure 2.8 (reflectance scale=0.0001) were partitioned into two parts: the observations with SWIR<sub>2</sub> less than 0.25 (black blue points); the others with SWIR<sub>2</sub> greater than 0.25 (pink points)



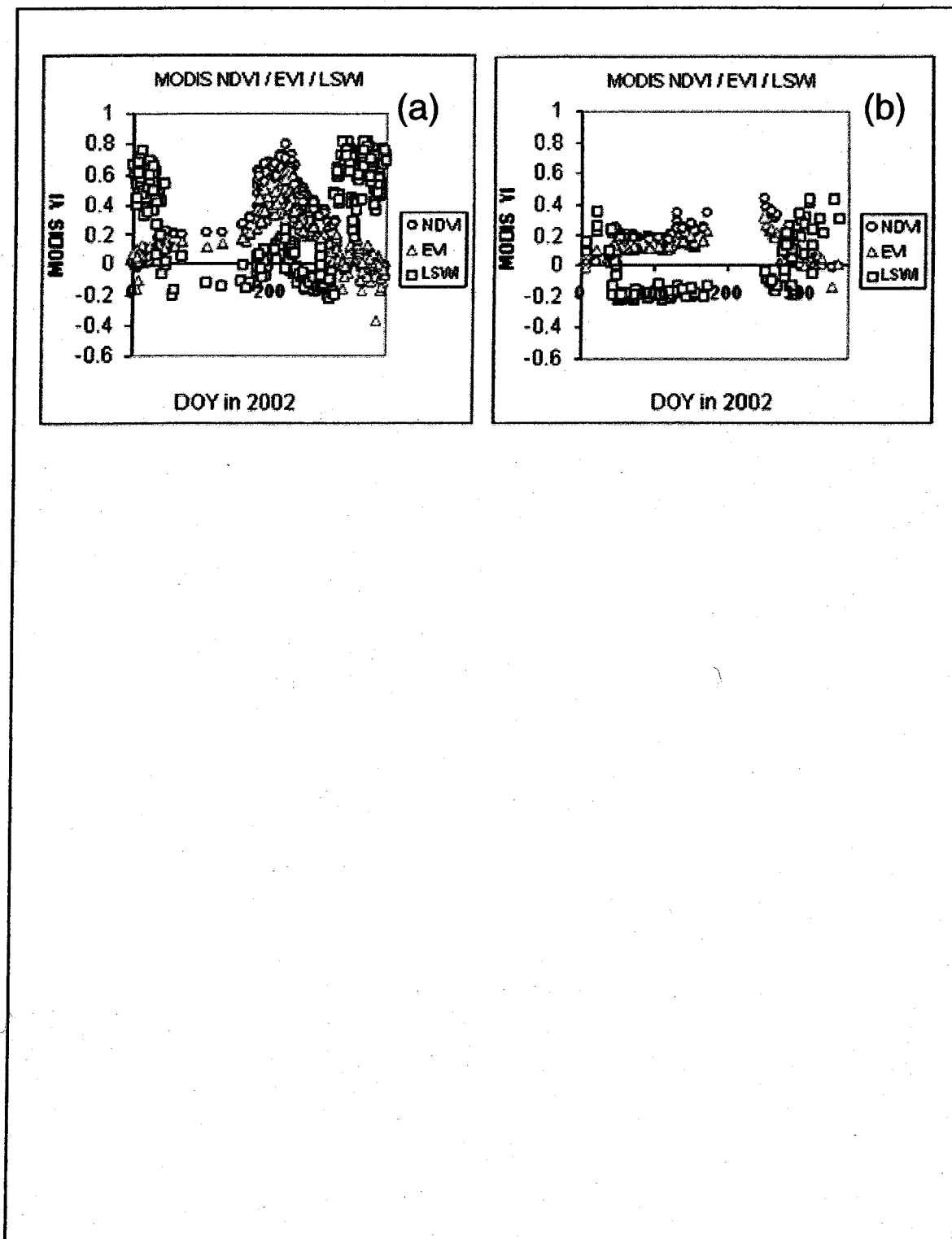


Figure 2.10 (a) NDVI, EVI and LSWI of the observations in Figure 2.9 with  $SWIR_2$  less than 0.25; (b) NDVI, EVI, and LSWI of the others in Figure 2.9 with  $SWIR_2$  greater than 0.25

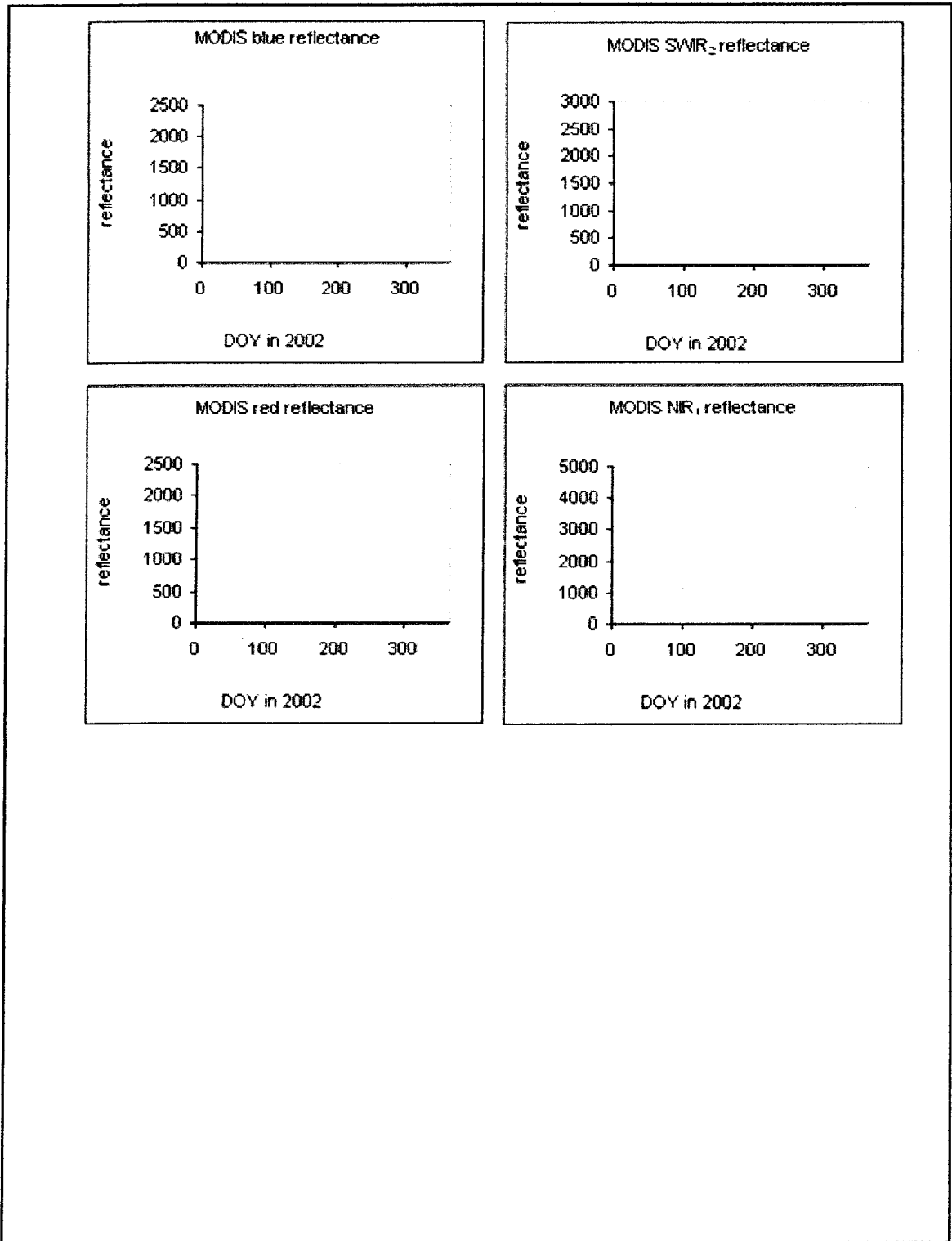


Figure 2.11 Subset ( $SWIR_2 < 0.25$ ) of MODIS daily clustering observations of the Xilingol grassland site in 2002 (reflectance scale=0.0001) without snow covered and relative NDVI, EVI, LSWI and snow cover fraction (cfsnow)

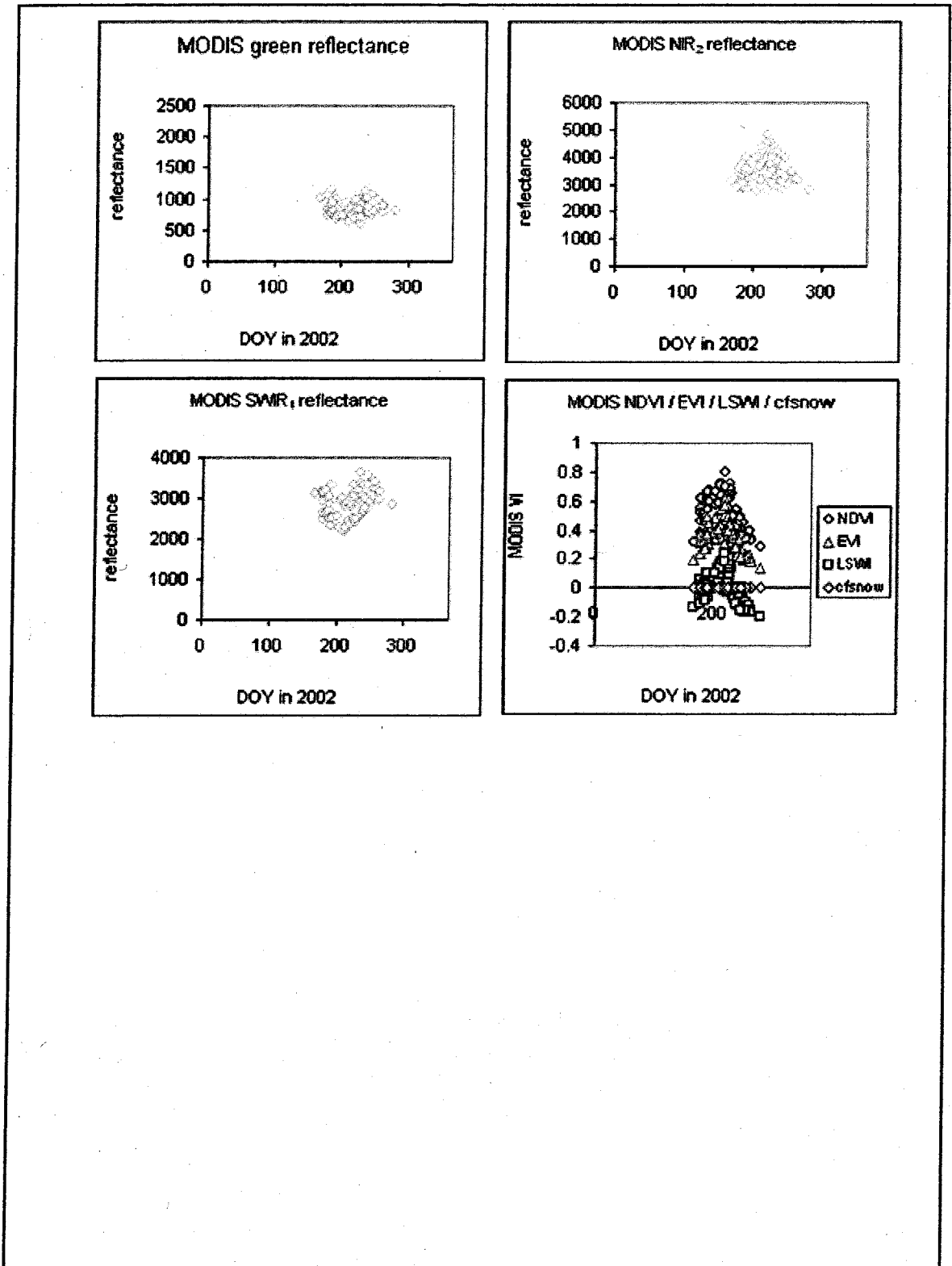


Figure 2.11 (continued) Subset ( $SWIR_2 < 0.25$ ) of MODIS daily clustering observations of the Xilingol grassland site in 2002 (reflectance scale = 0.0001) without snow covered and relative NDVI, EVI, LSWI and snow cover fraction (cfsnow)

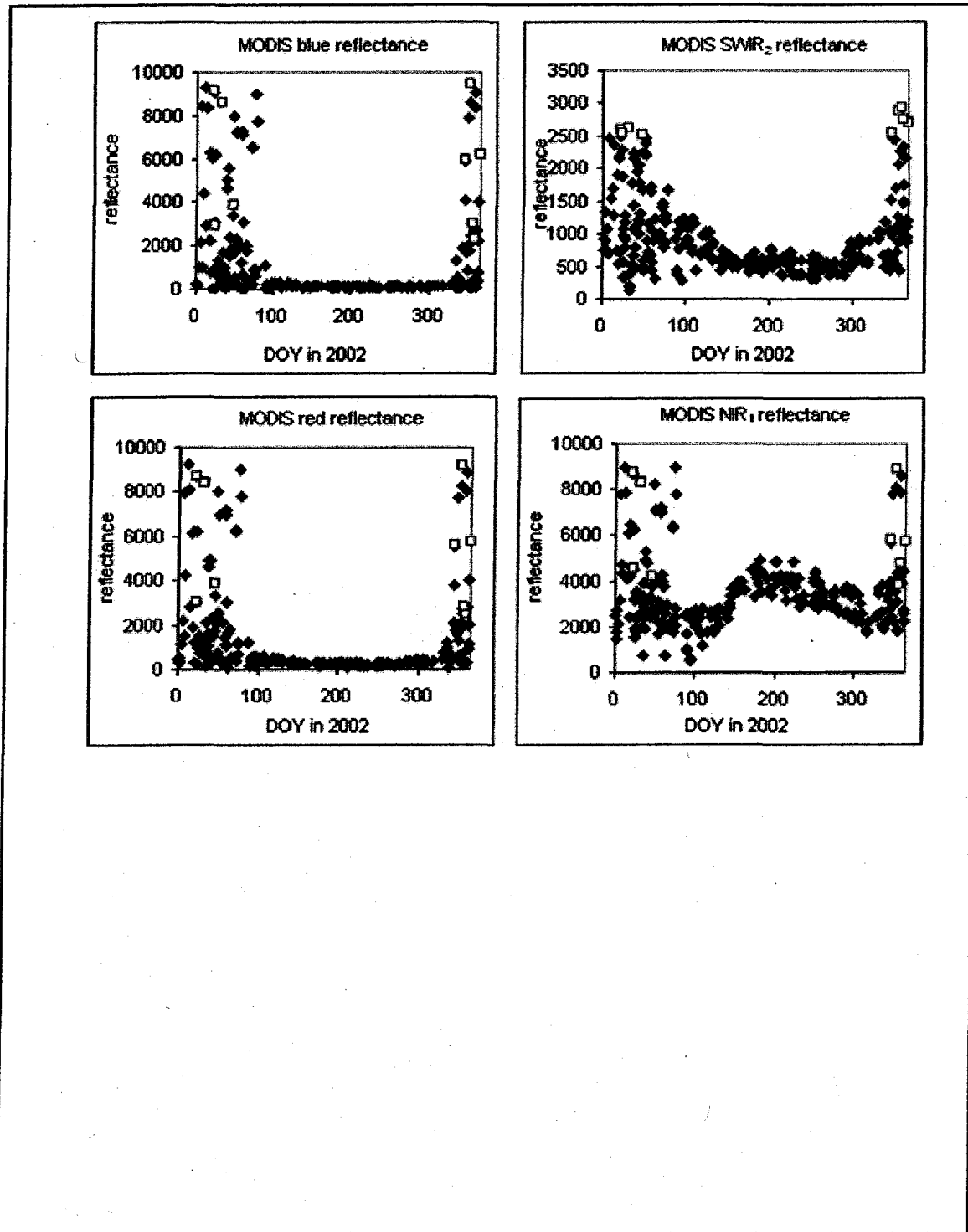


Figure 2.12 MODIS daily observations of the Harvard Forest site in 2002 (reflectance scale=0.0001) were collected as atmospheric contamination free observations from DOY 90 to 318 plus observations before and after the period, and were partitioned into two parts: the observations with SWIR<sub>2</sub> less than 0.25 (black blue points); the others with SWIR<sub>2</sub> greater than 0.25 (pink points)

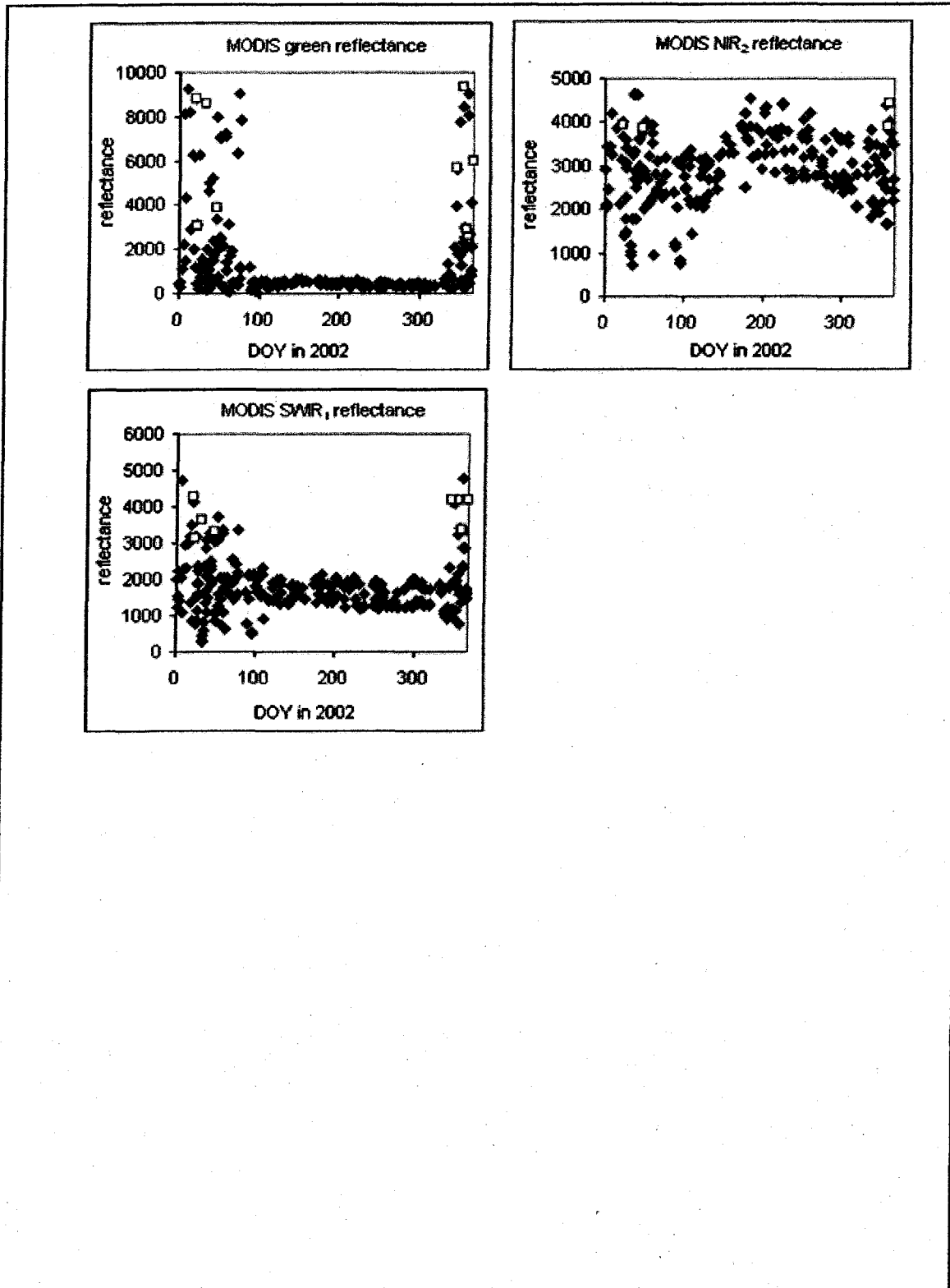


Figure 2.12 (continued) MODIS daily observations of the Harvard Forest site in 2002 (reflectance scale=0.0001) were collected as atmospheric contamination free observations from DOY 90 to 318 plus observations before and after the period, and were partitioned into two parts: the observations with SWIR<sub>2</sub> less than 0.25 (black blue points); the others with SWIR<sub>2</sub> greater than 0.25 (pink points)

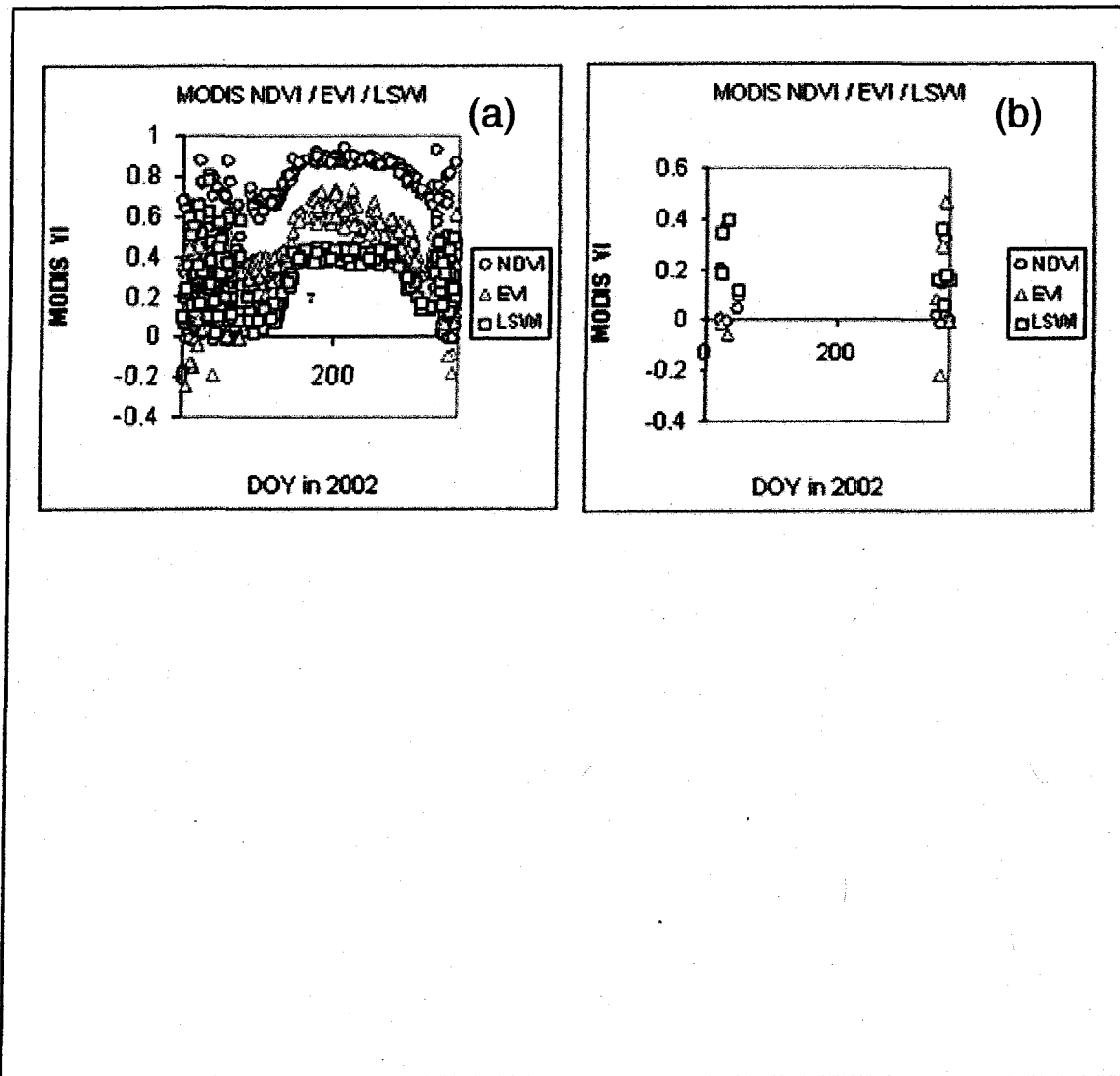


Figure 2.13 (a) NDVI, EVI and LSWI of the observations with  $SWIR_2$  less than 0.25 in Figure 2.12; (b) NDVI, EVI, and LSWI of the others with  $SWIR_2$  greater than 0.25 in Figure 2.12

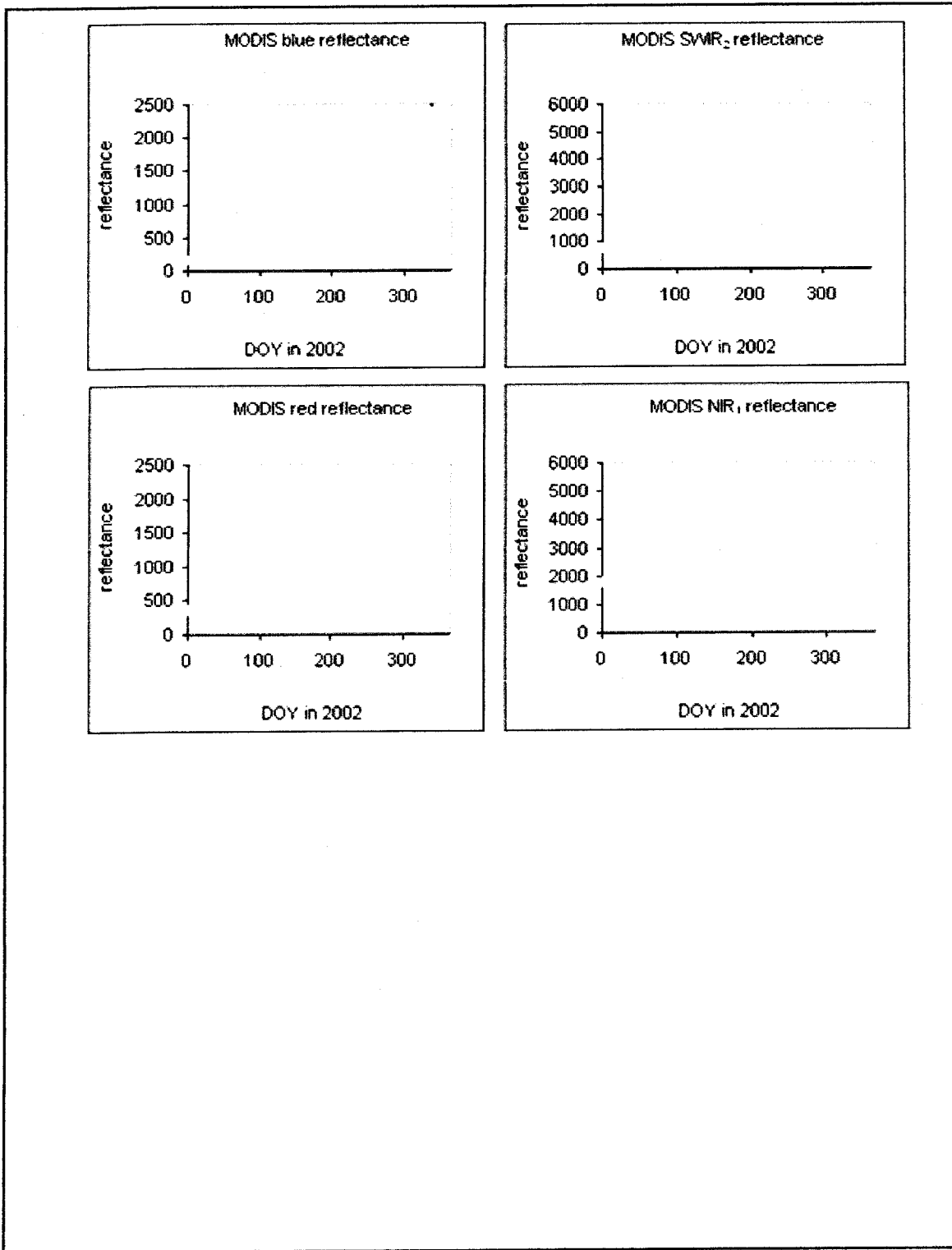


Figure 2.14 Subset ( $SWIR_2 < 0.25$ ) of MODIS daily observations (reflectance scale=0.0001) of the Harvard Forest site in 2002 in Figure 2.12 without snow covered and relative NDVI, EVI, and LSWI

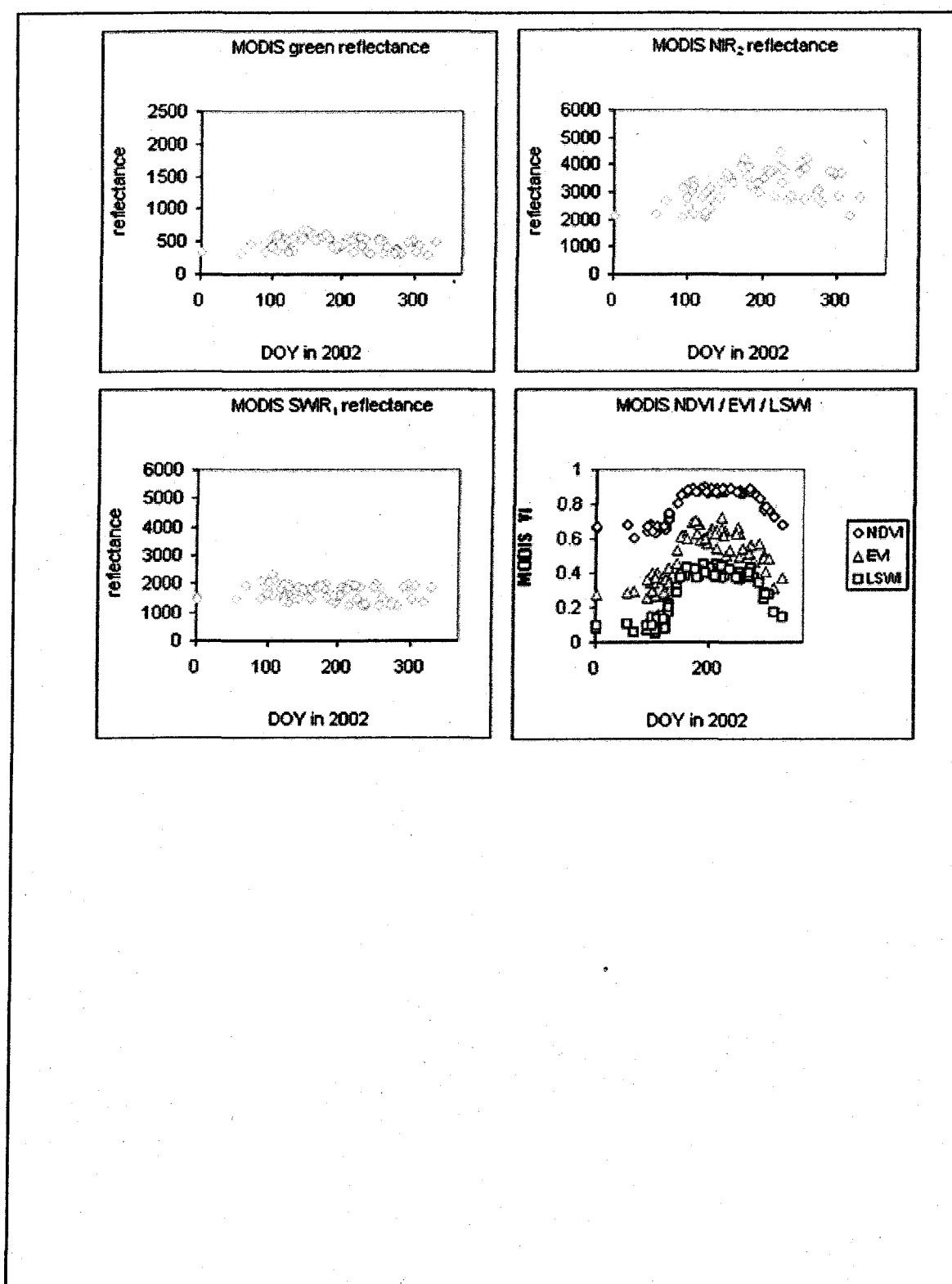


Figure 2.14 (continued) Subset ( $SWIR_2 < 0.25$ ) of MODIS daily observations (reflectance scale=0.0001) of the Harvard Forest site in 2002 in Figure 2.12 without snow covered and relative NDVI, EVI, and LSMI



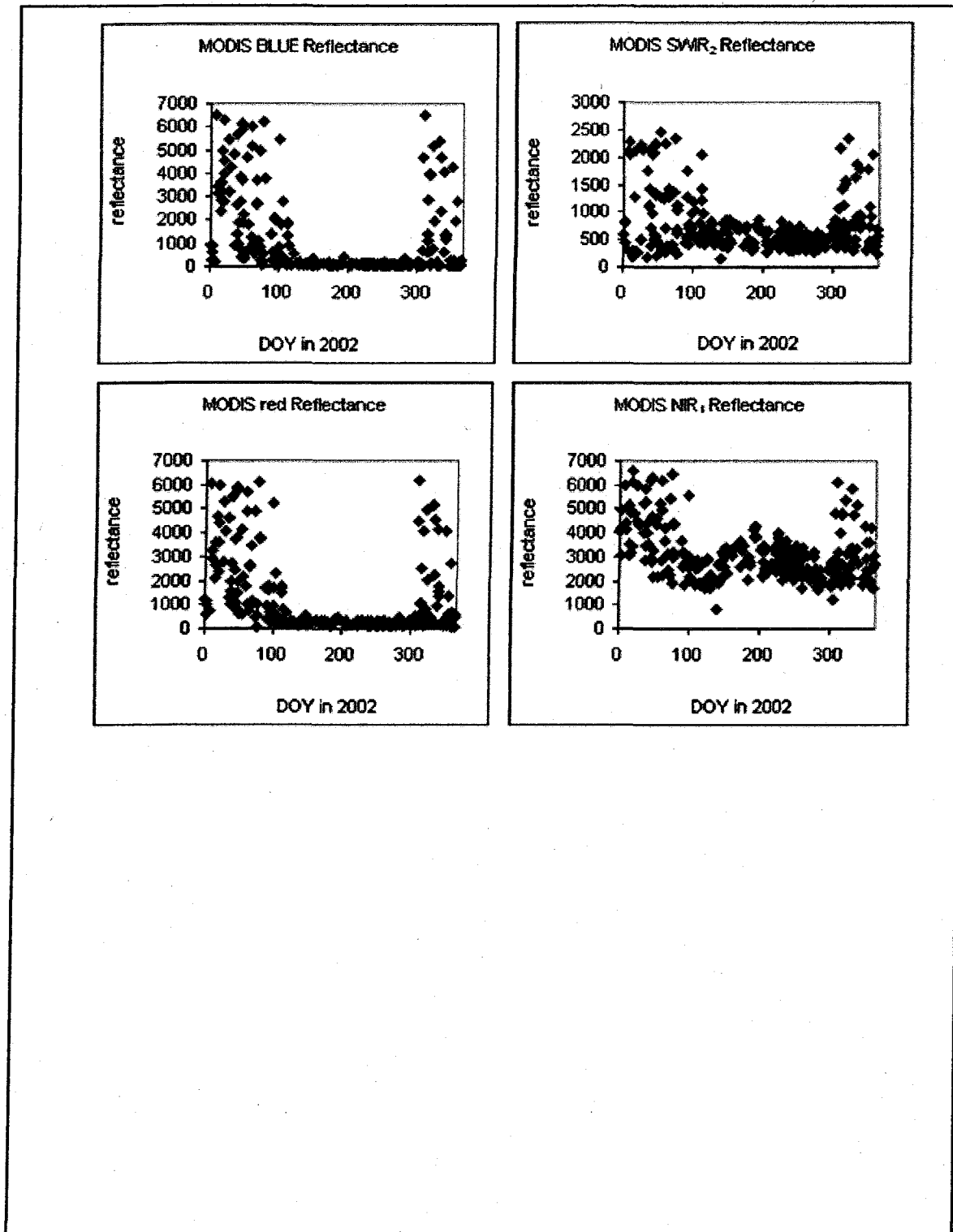


Figure 2.15 MODIS daily observations of the Howland Forest site in 2002 (reflectance scale=0.0001) were collected as atmospheric contamination free observations from DOY 115 to 318 plus observations before and after the period, and relative NDVI, EVI and LSWI were calculated

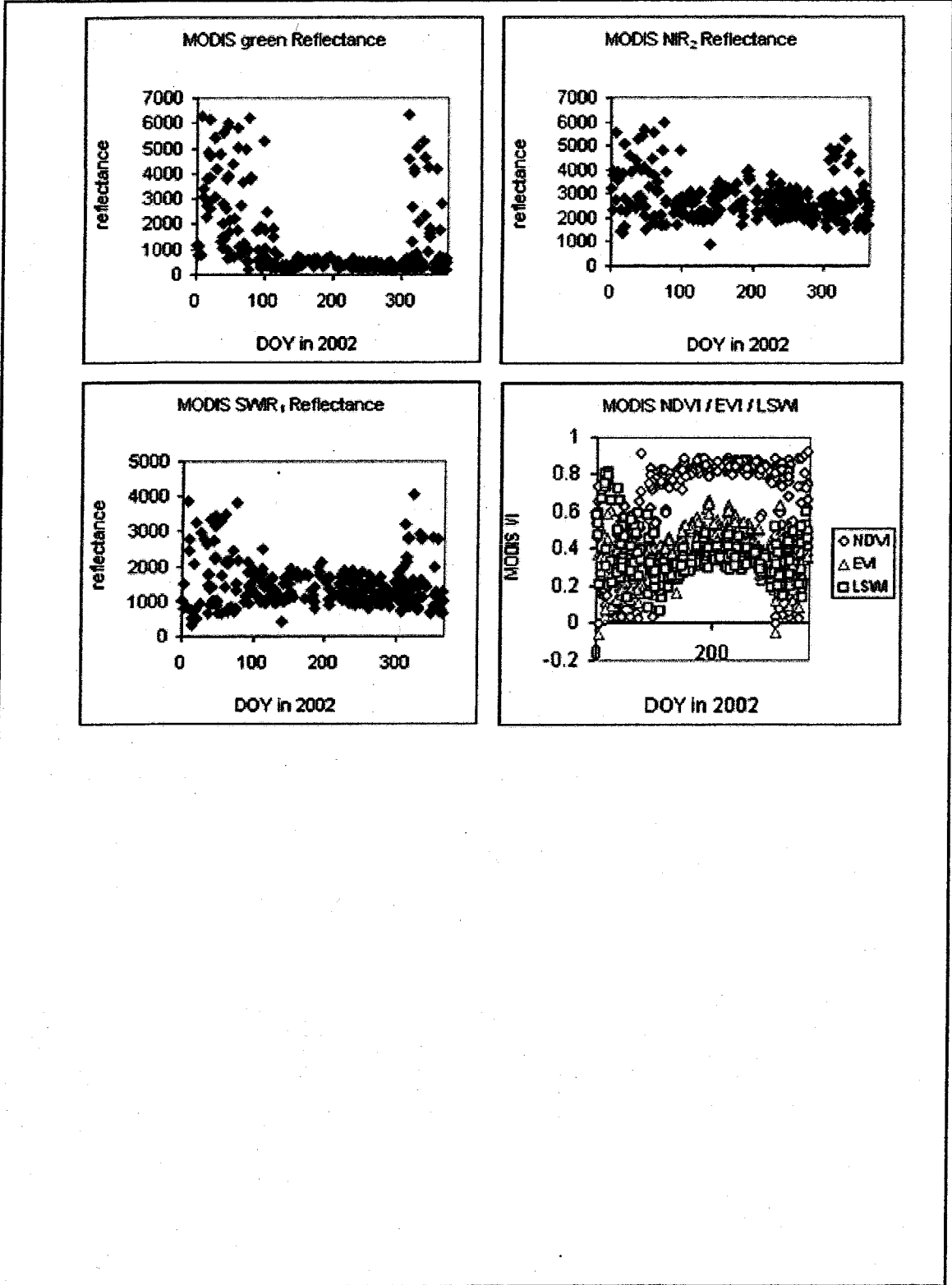


Figure 2.15 (continued) MODIS daily observations of the Howland Forest site in 2002 (reflectance scale=0.0001) were collected as atmospheric contamination free observations from DOY 115 to 318 plus observations before and after the period, and relative NDVI, EVI and LSWI were calculated

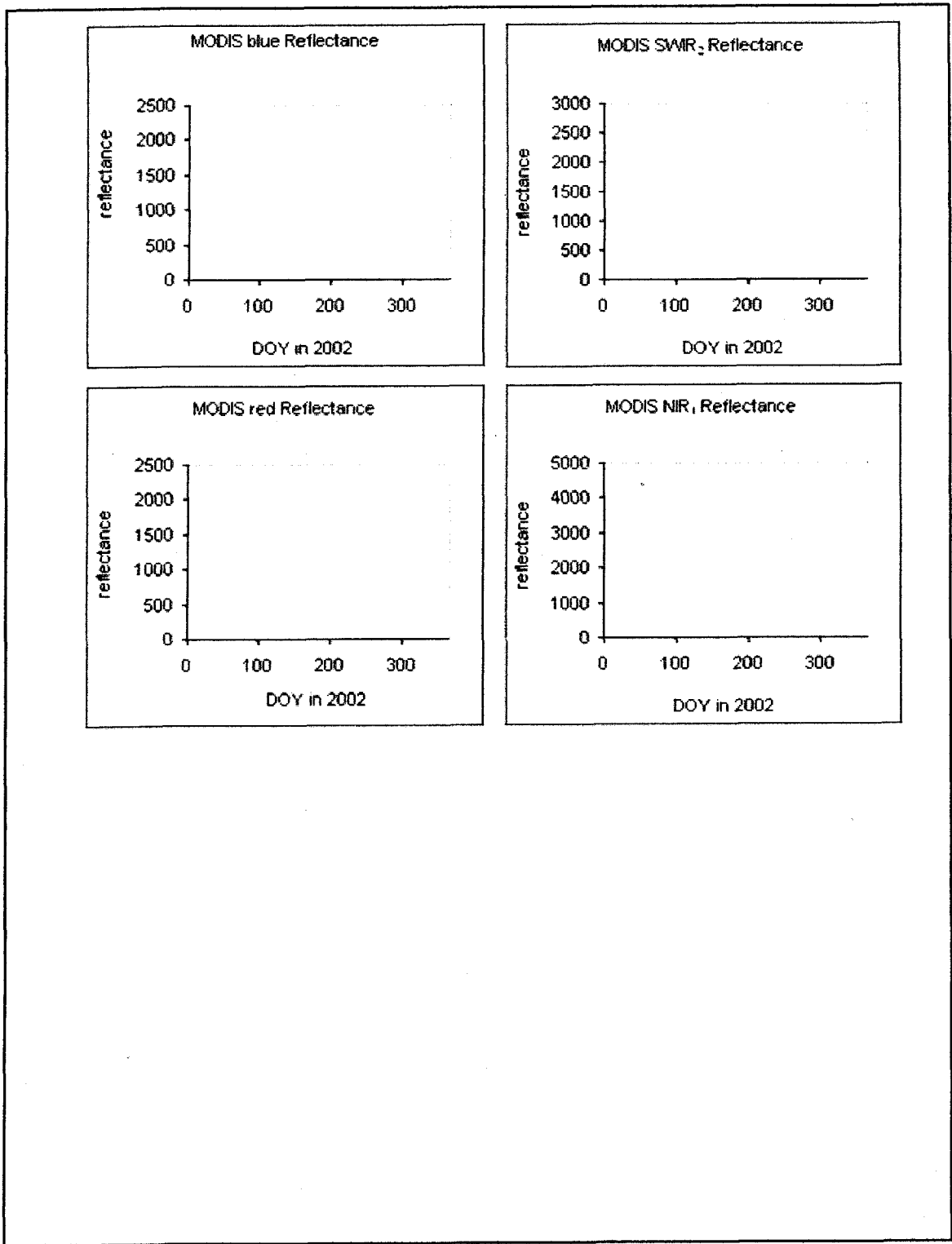


Figure 2.16 Subset ( $SWIR_2 < 0.25$ ) of MODIS daily observations (reflectance scale=0.0001) of the Howland Forest site in 2002 without snow covered and relative NDVI, EVI, and LSWI

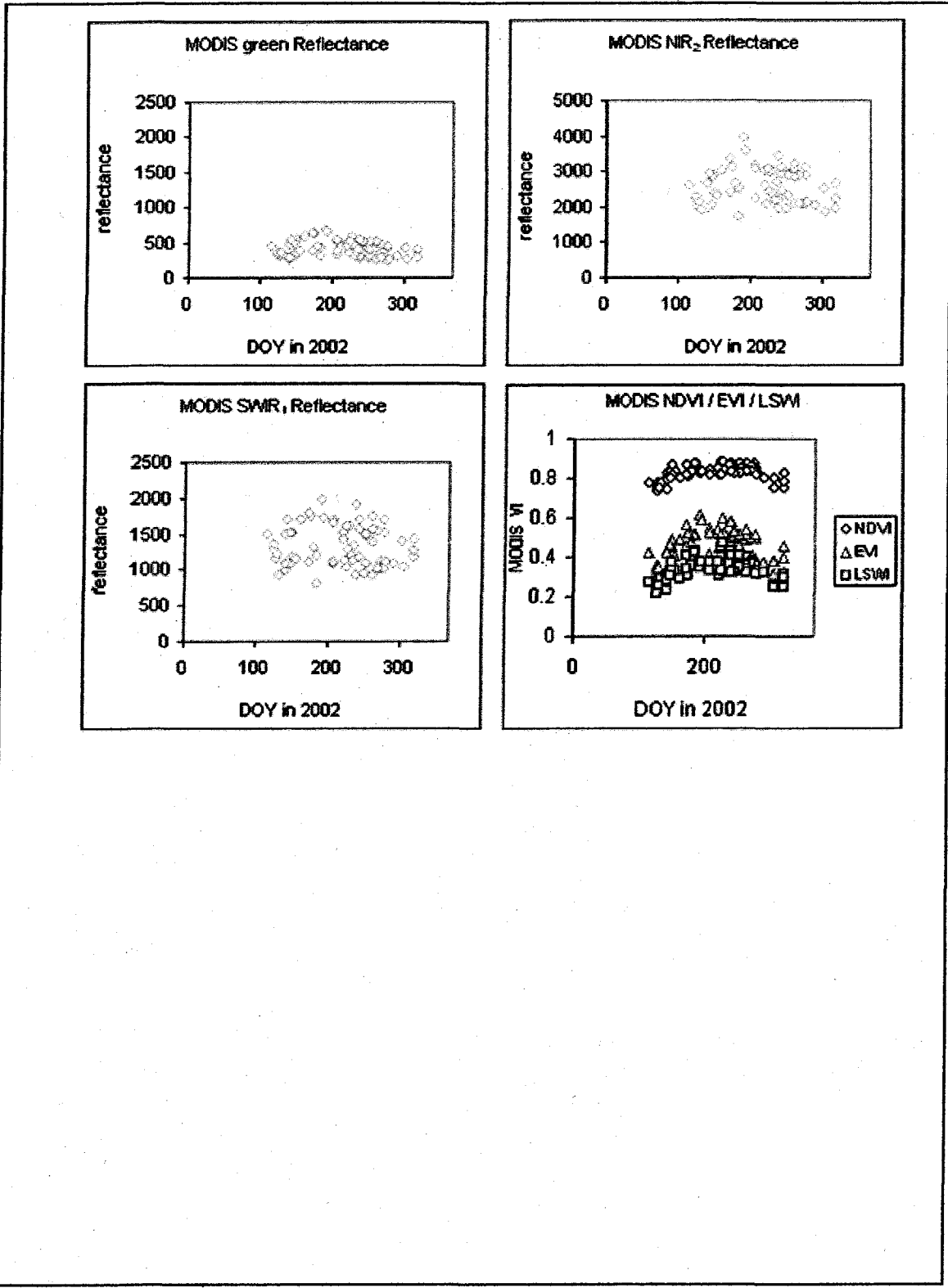


Figure 2.16 (continued) Subset ( $SWIR_2 < 0.25$ ) of MODIS daily observations (reflectance scale=0.0001) of the Howland Forest site in 2002 without snow covered and relative NDVI, EVI, and LSM

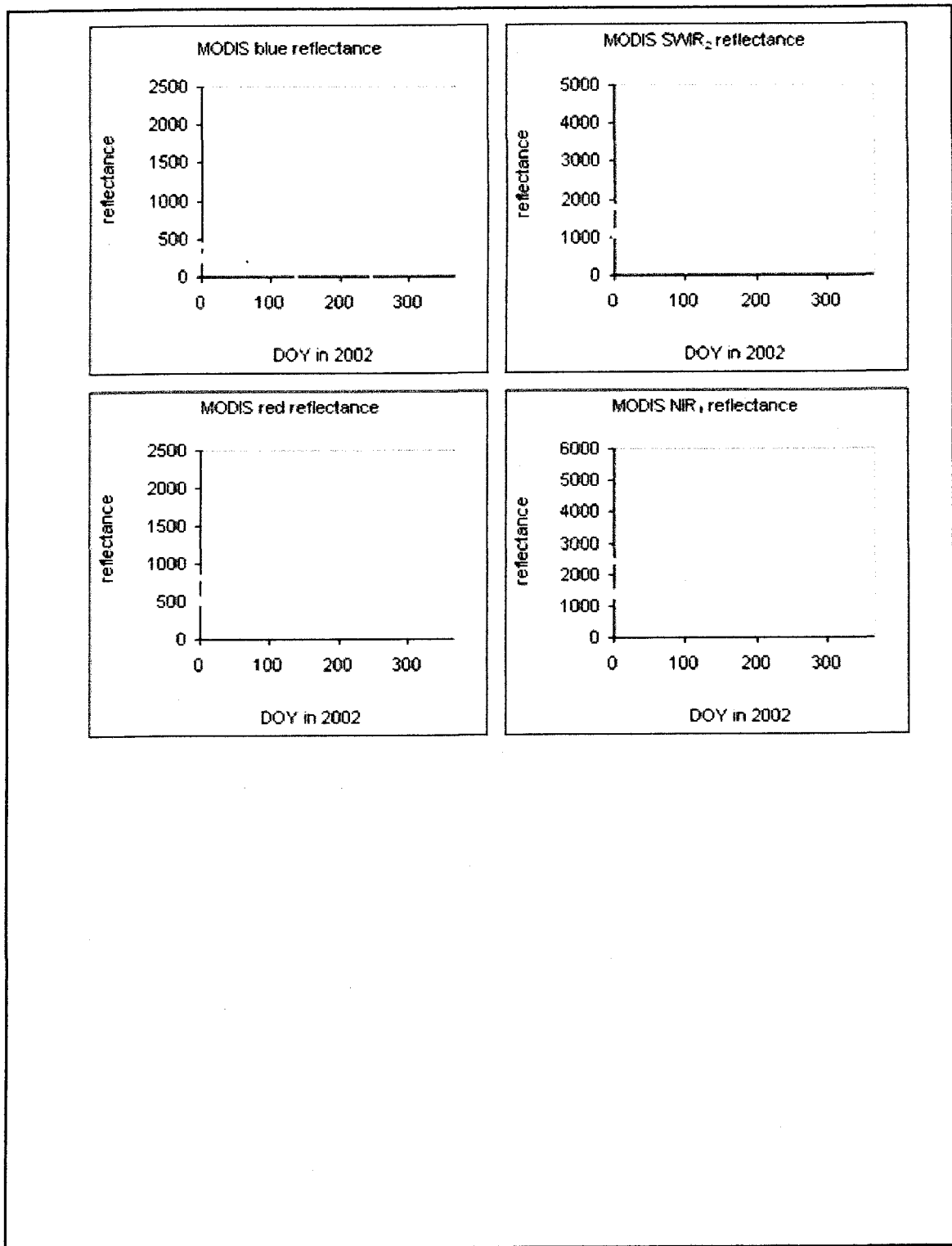


Figure 2.17 MODIS daily atmospheric contamination free observations of the Walker Branch Watershed Forest site in 2002 (reflectance scale=0.0001) and relative NDVI, EVI and LSWI. Note that all of the observations were snow free

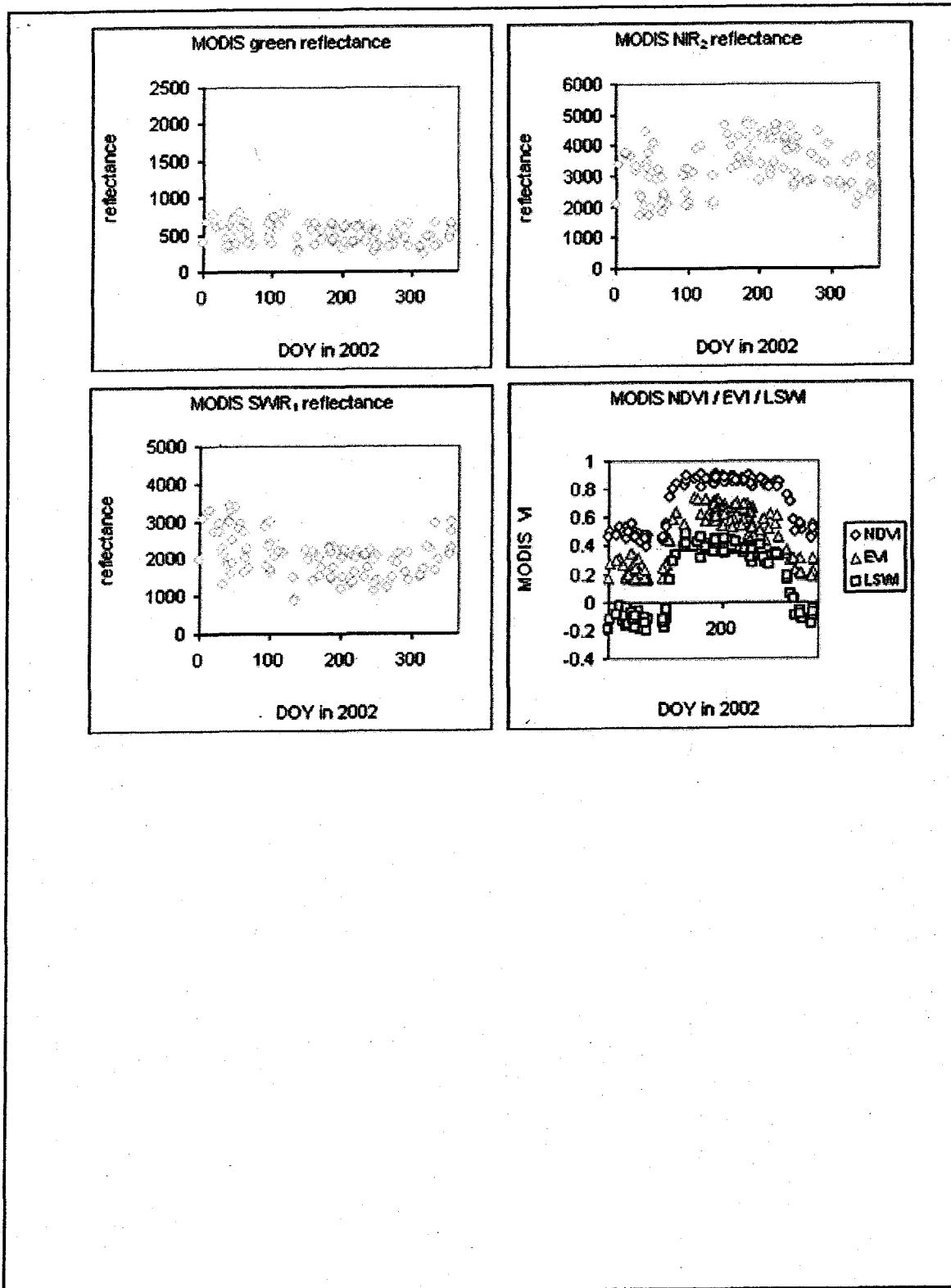


Figure 2.17 (continued) MODIS daily atmospheric contamination free observations of the Walker Branch Watershed Forest site in 2002 (reflectance scale=0.0001) and relative NDVI, EVI and LSWI. Note that all of the observations were snow free

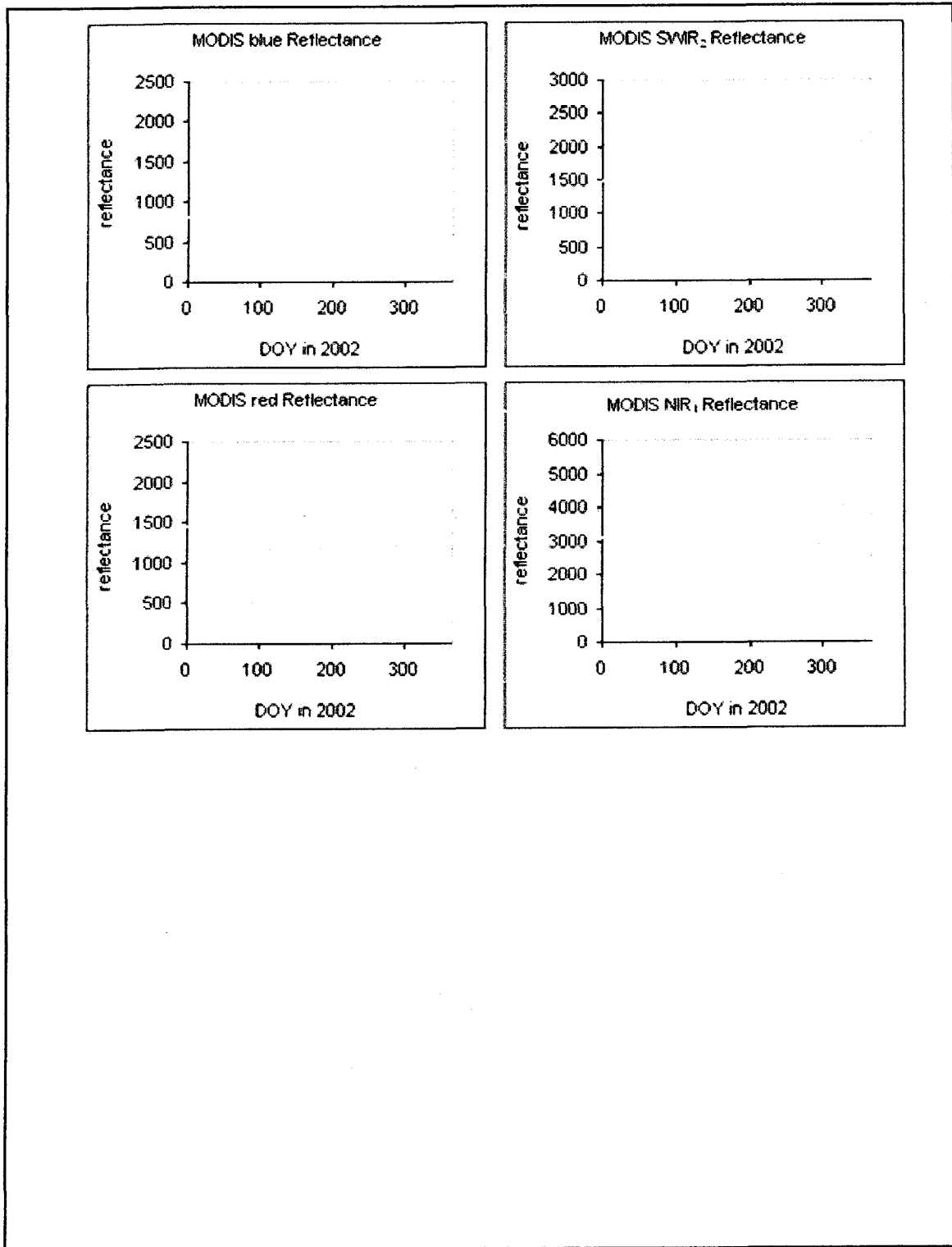


Figure 2.18 MODIS daily clustering observations of the Soybean site in 2002 (reflectance scale=0.0001) and relative NDVI, EVI and LSWI

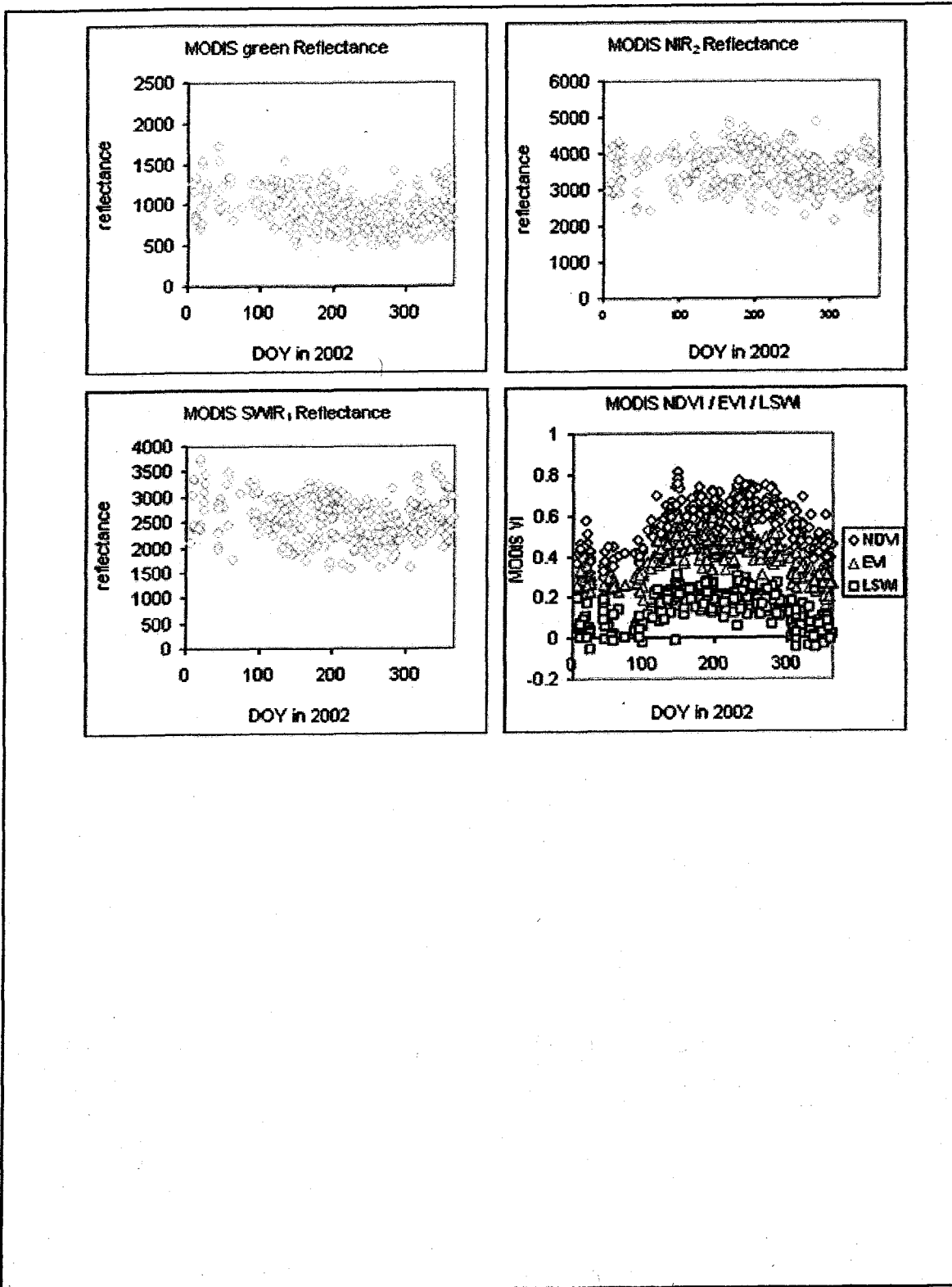


Figure 2.18 (continued) MODIS daily clustering observations of the Soybean site in 2002 (reflectance scale=0.0001) and relative NDVI, EVI and LSWI



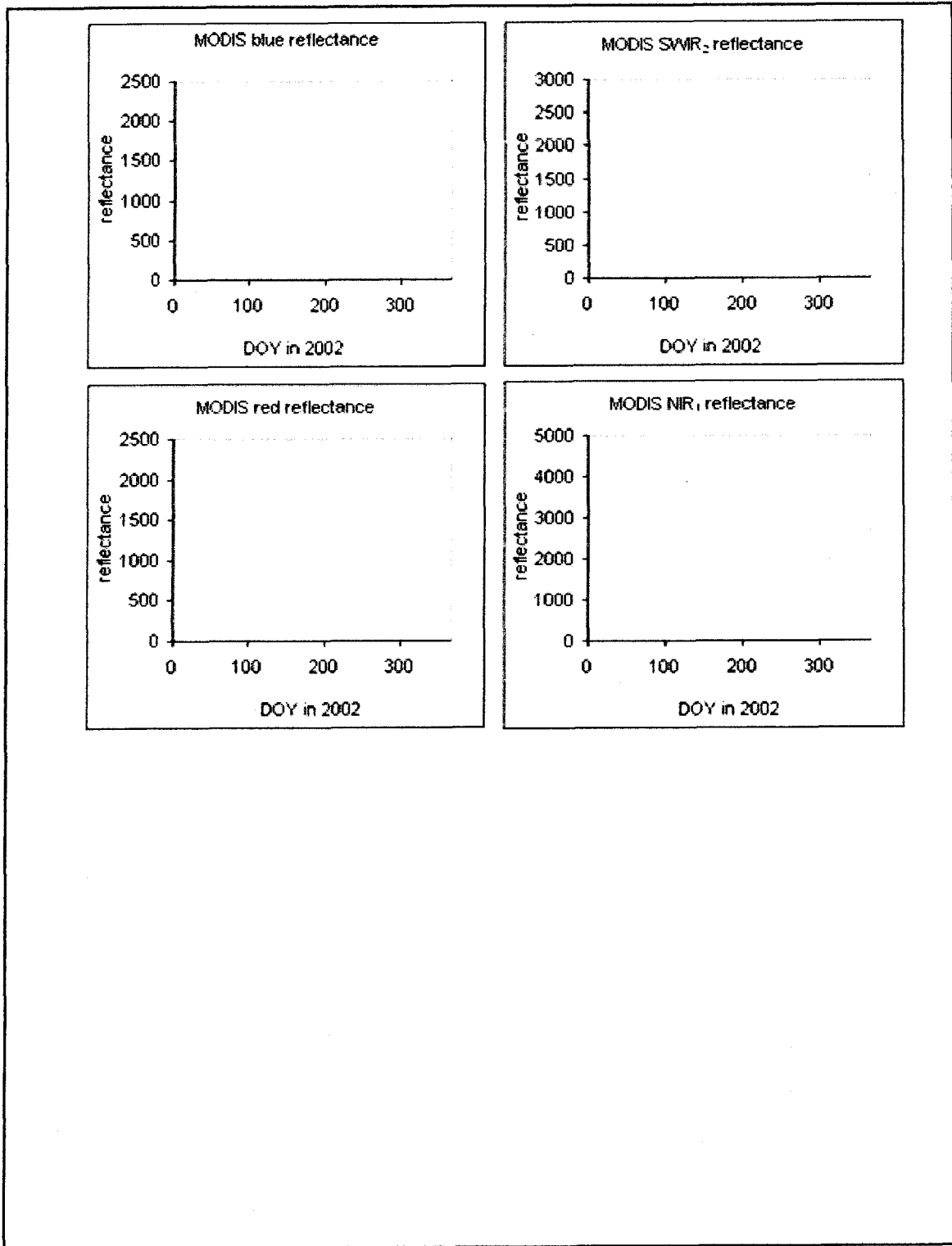


Figure 2.19 Subset ( $SWIR_2 < 0.25$ ) of MODIS daily clustering observations (reflectance scale=0.0001) of the Soybean site in 2002 in Figure 2.18 after discarding the observations that have atmospheric effect and relative NDVI, EVI and LSWI

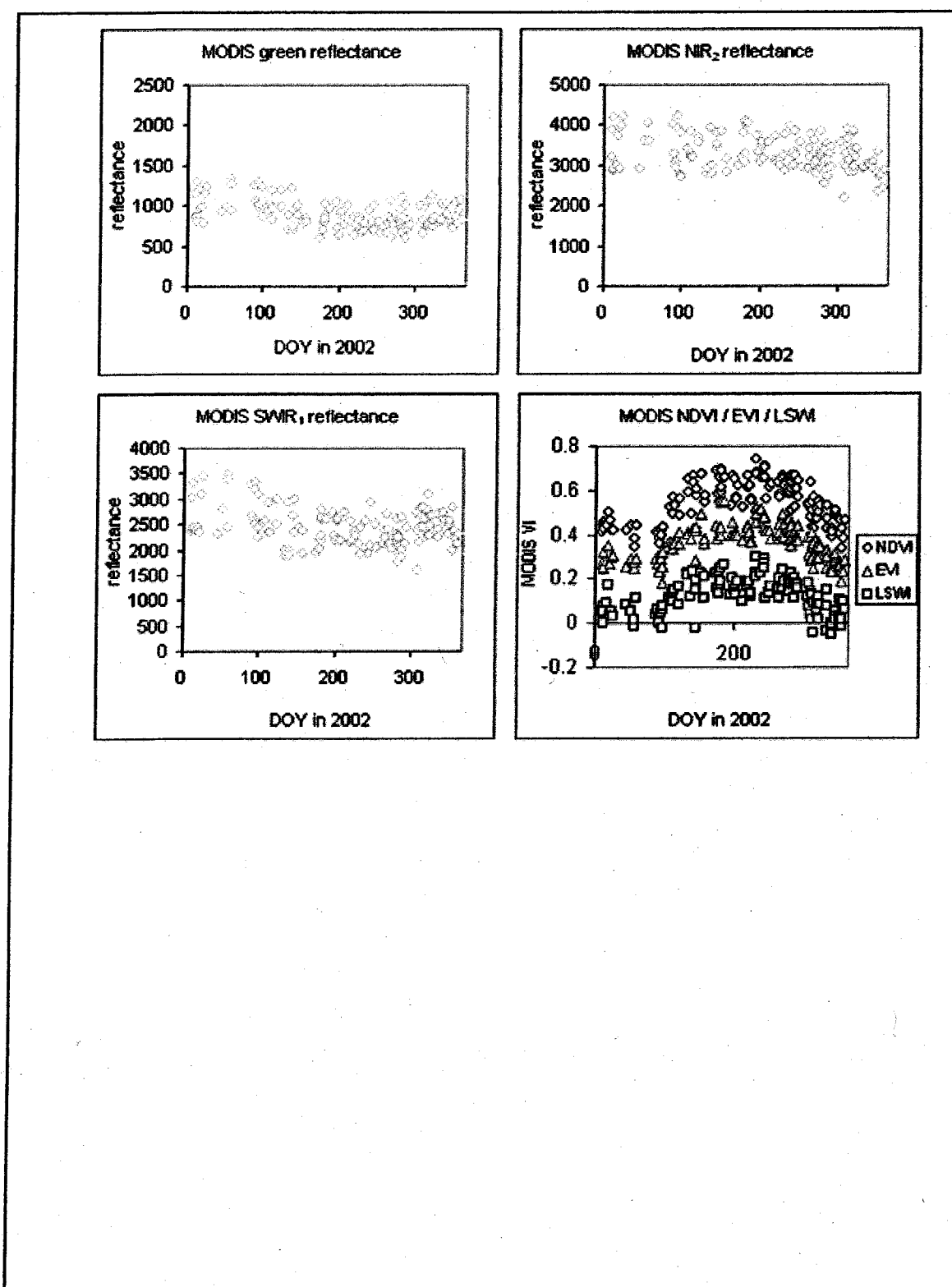


Figure 2.19 (continued) Subset ( $SWIR_2 < 0.25$ ) of MODIS daily clustering observations (reflectance scale=0.0001) of the Soybean site in 2002 in Figure 2.18 after discarding the observations that have atmospheric effect and relative NDVI, EVI and LSWI

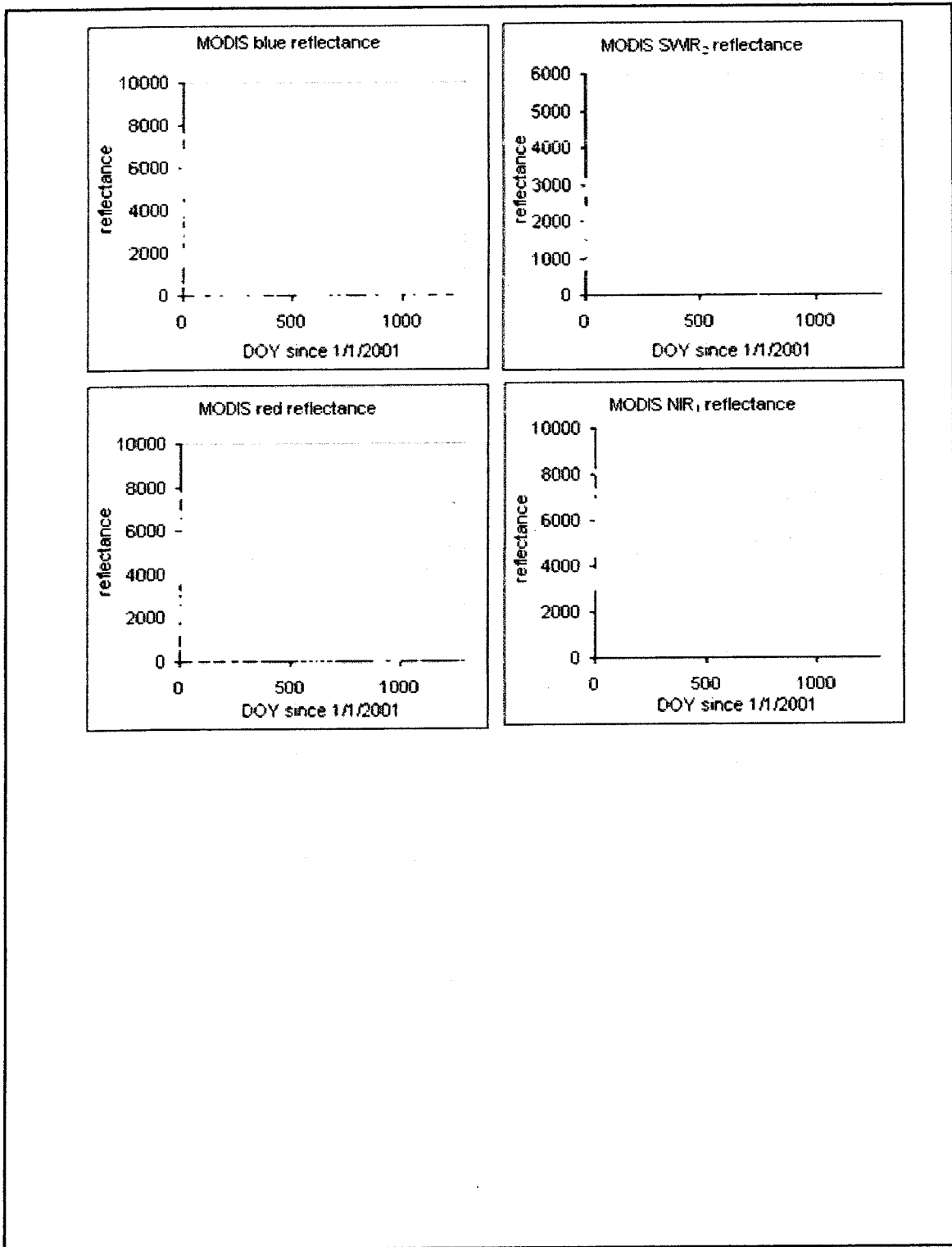


Figure 2.20 All MODIS daily observations (reflectance scale =0.0001) of the tropical km67 seasonal moist forest site since 1/1/2001 to 7/10/2004. DOY calculated beginning from 1/1/2001

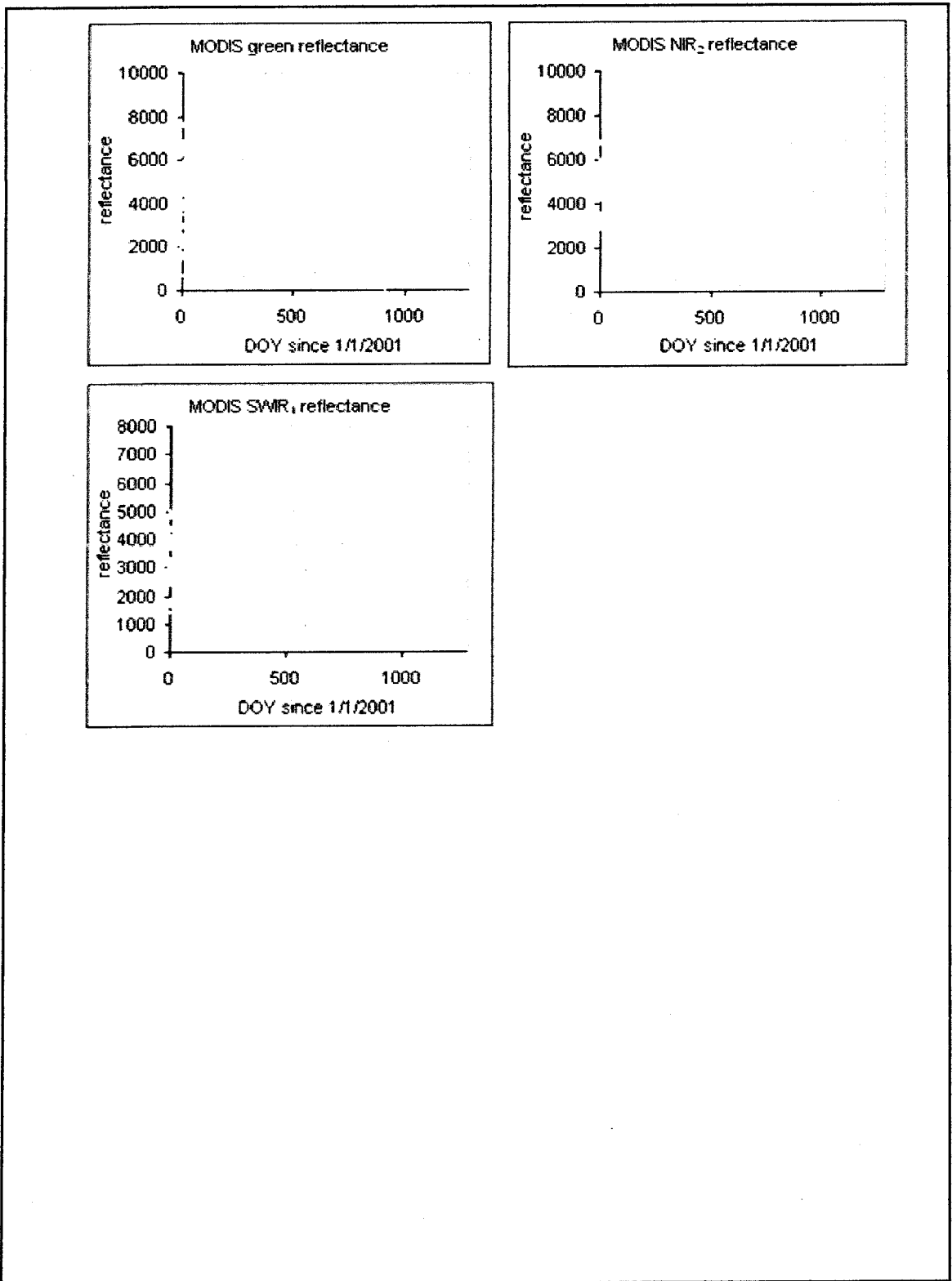


Figure 2.20 (continued) All MODIS daily observations (reflectance scale =0.0001) of the tropical km67 seasonal moist forest site since 1/1/2001 to 7/10/2004. DOY calculated beginning from 1/1/2001

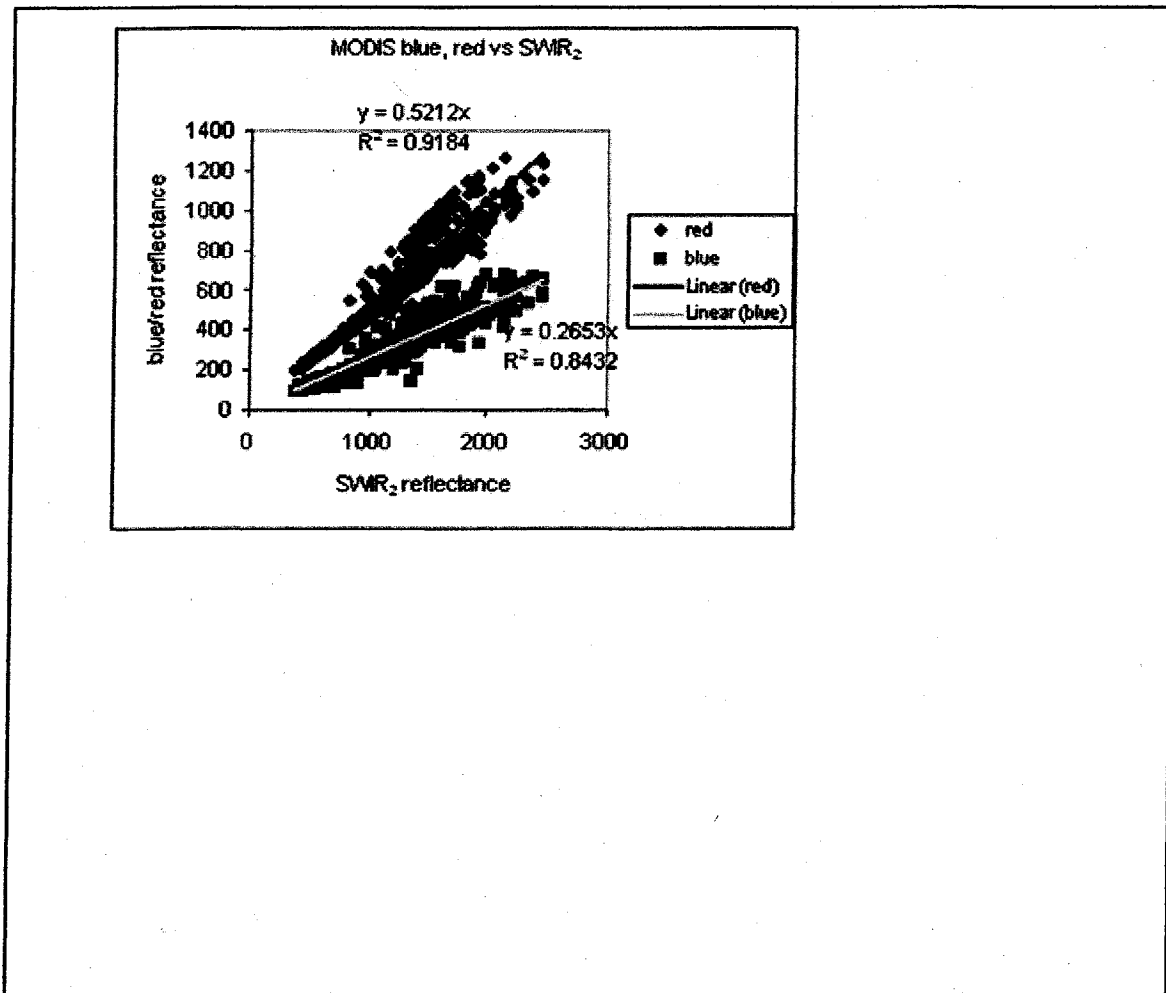


Figure 2.21 Comparison of MODIS blue, red and SWIR<sub>2</sub> reflectance of all contamination free observations of the Xilingol grassland site, Harvard Forest site, Howland Forest site, Walker Branch Watershed site and Soybean site in 2002 (reflectance scale=0.0001)

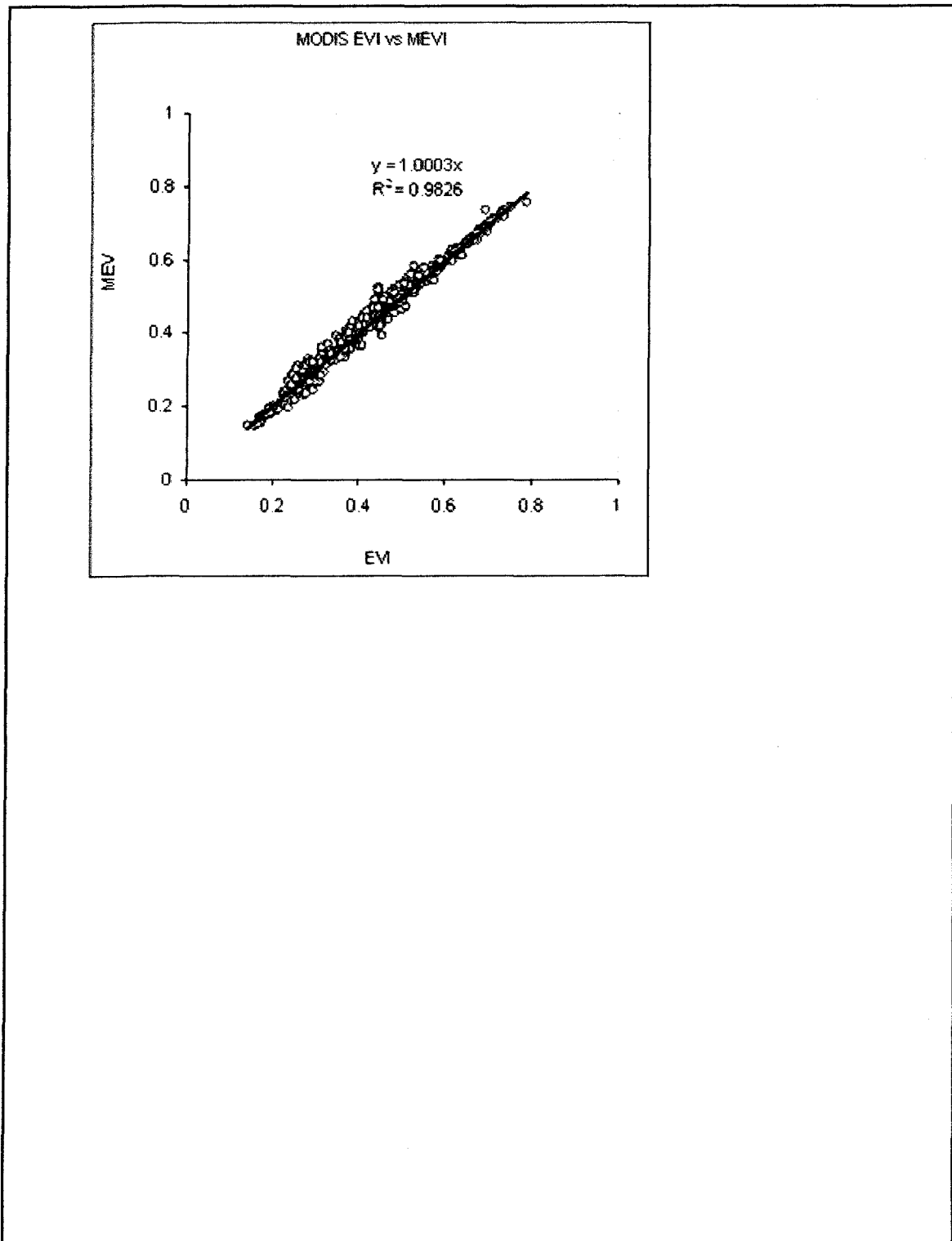


Figure 2.22 Comparison of MEVI and EVI of all contamination free observations of the Xilingol grassland site, Harvard Forest site, Howland Forest site, Walker Branch Watershed site and Soybean site in 2002 (reflectance scale=0.0001)

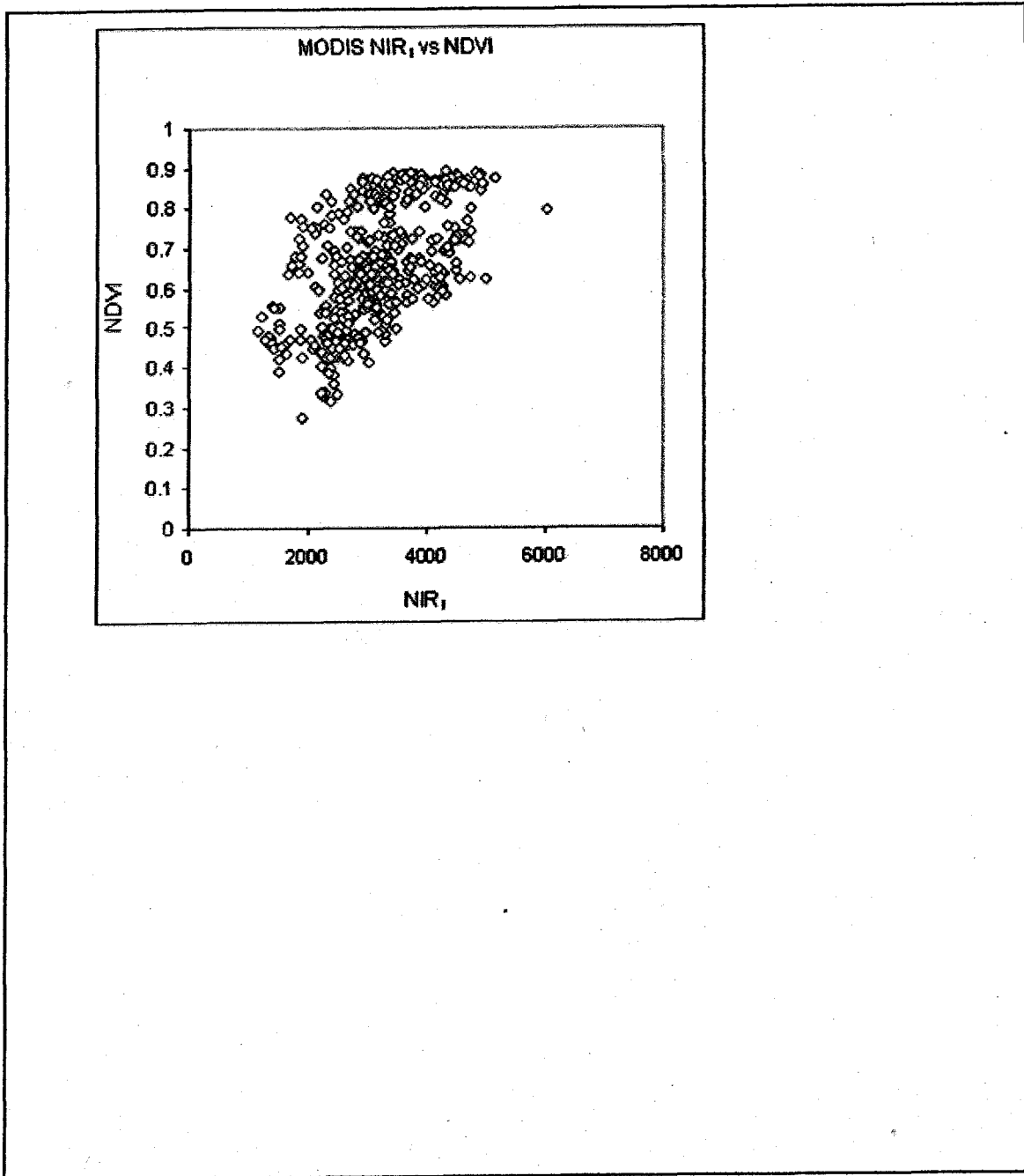


Figure 2.23 Comparison of NDVI and NIR<sub>1</sub> of all contamination free observations of the Xilingol grassland site, Harvard Forest site, Howland Forest site, Walker Branch Watershed site and Soybean site in 2002 (reflectance scale=0.0001)

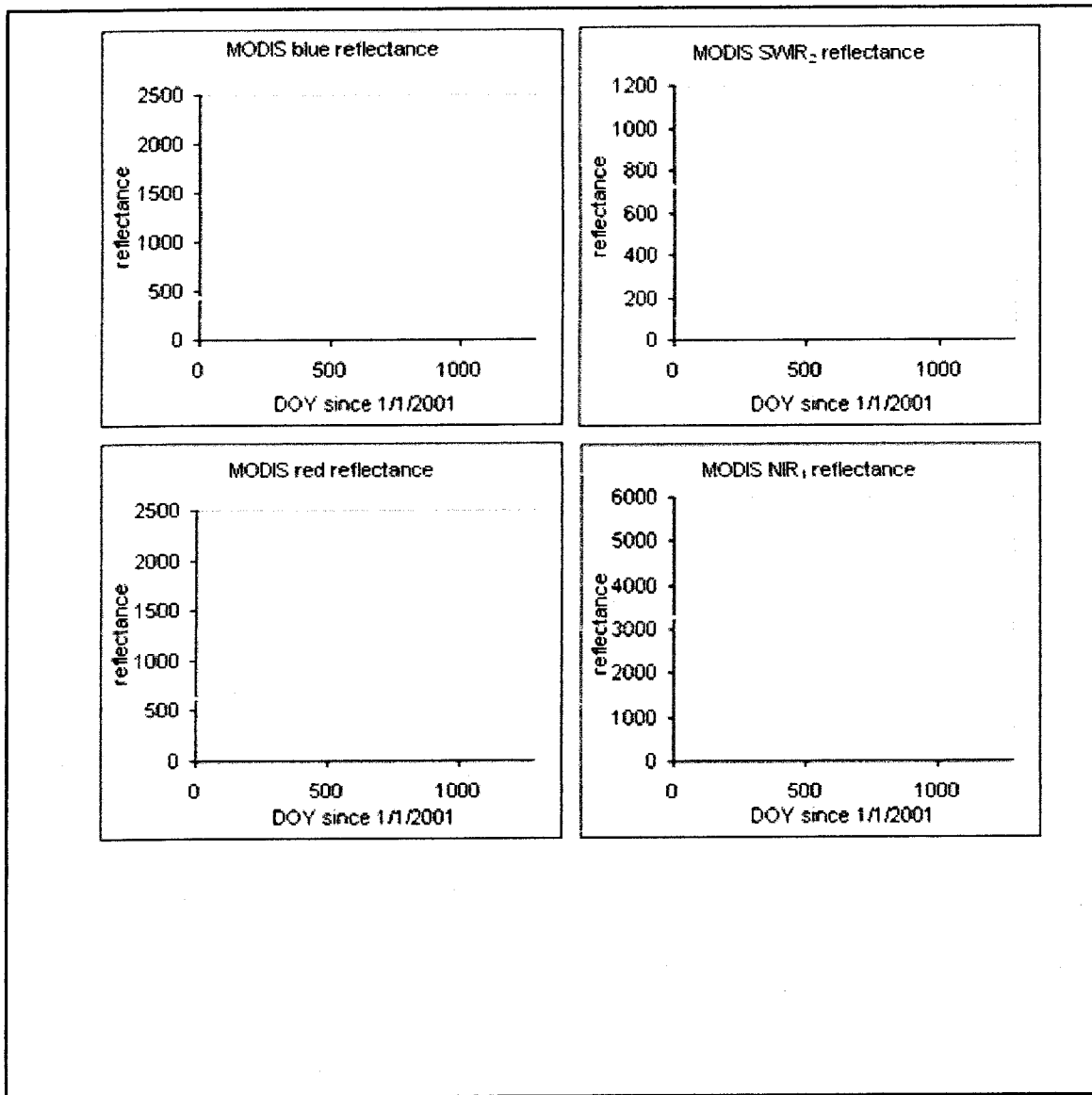


Figure 2.24 Selected MODIS daily observations (reflectance scale =0.0001) of the tropical km67 seasonal moist forest site since 1/1/2001 to 7/10/2004 (DOY calculated beginning from 1/1/2001) that satisfy the following criteria: (1)  $0.03 \leq \rho_{SWIR_2} \leq 0.1$ ; (2)  $\rho_{blue} \leq 0.3$ ; (3)  $NDVI \geq \frac{1}{6}$ ; (4) if  $\rho_{NIR_1} \geq 0.45$ ,  $NDVI \geq \frac{3}{5}$ ; (5)  $-0.004 \leq \rho_{blue} - 0.25\rho_{SWIR_2} \leq 0.04$  and (6)  $-0.004 \leq \rho_{red} - 0.5\rho_{SWIR_2} \leq 0.04$



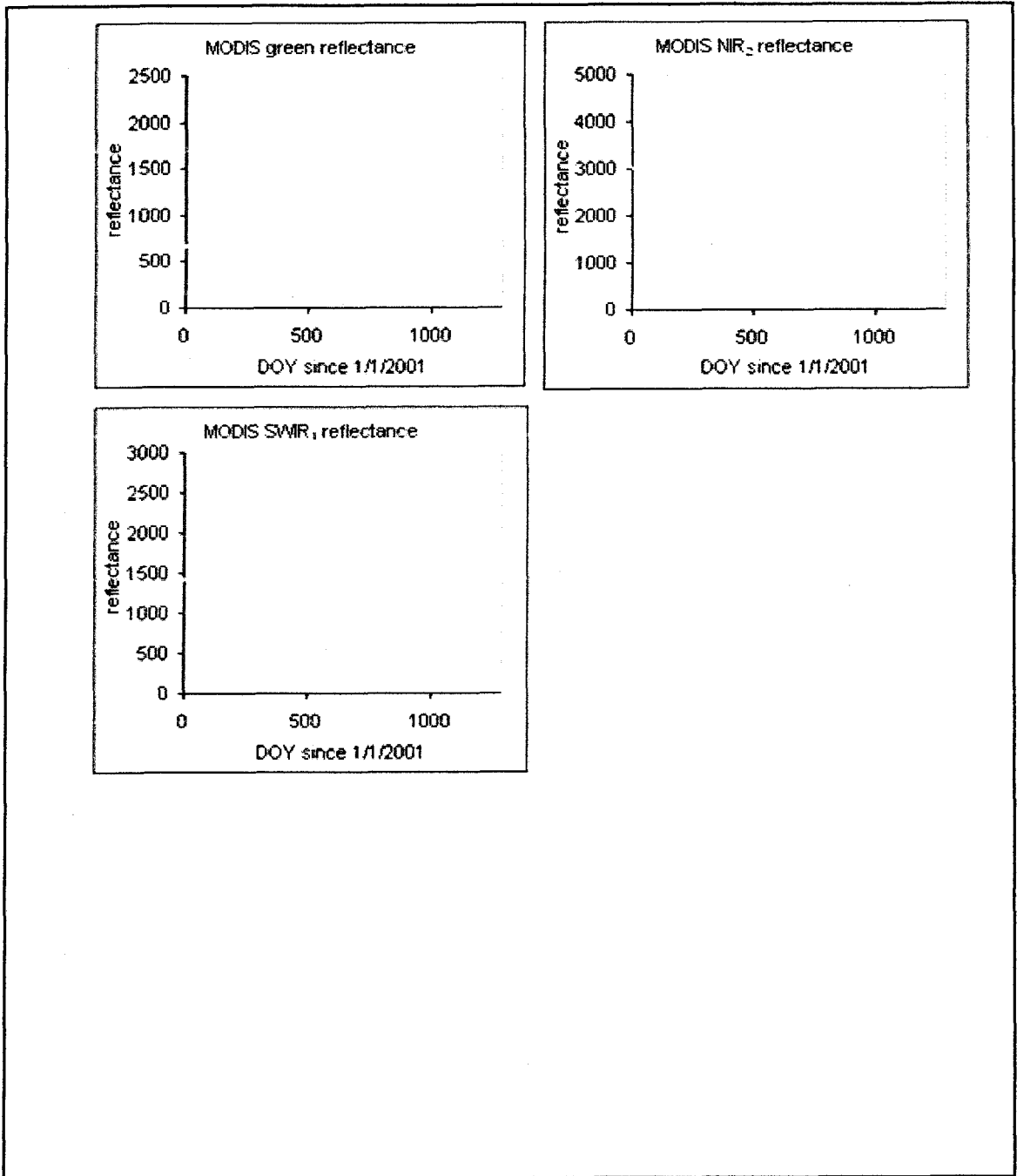


Figure 2.24 (continued) Selected MODIS daily observations (reflectance scale =0.0001) of the tropical km67 seasonal moist forest site since 1/1/2001 to 7/10/2004 (DOY calculated beginning from 1/1/2001) that satisfy the above criteria

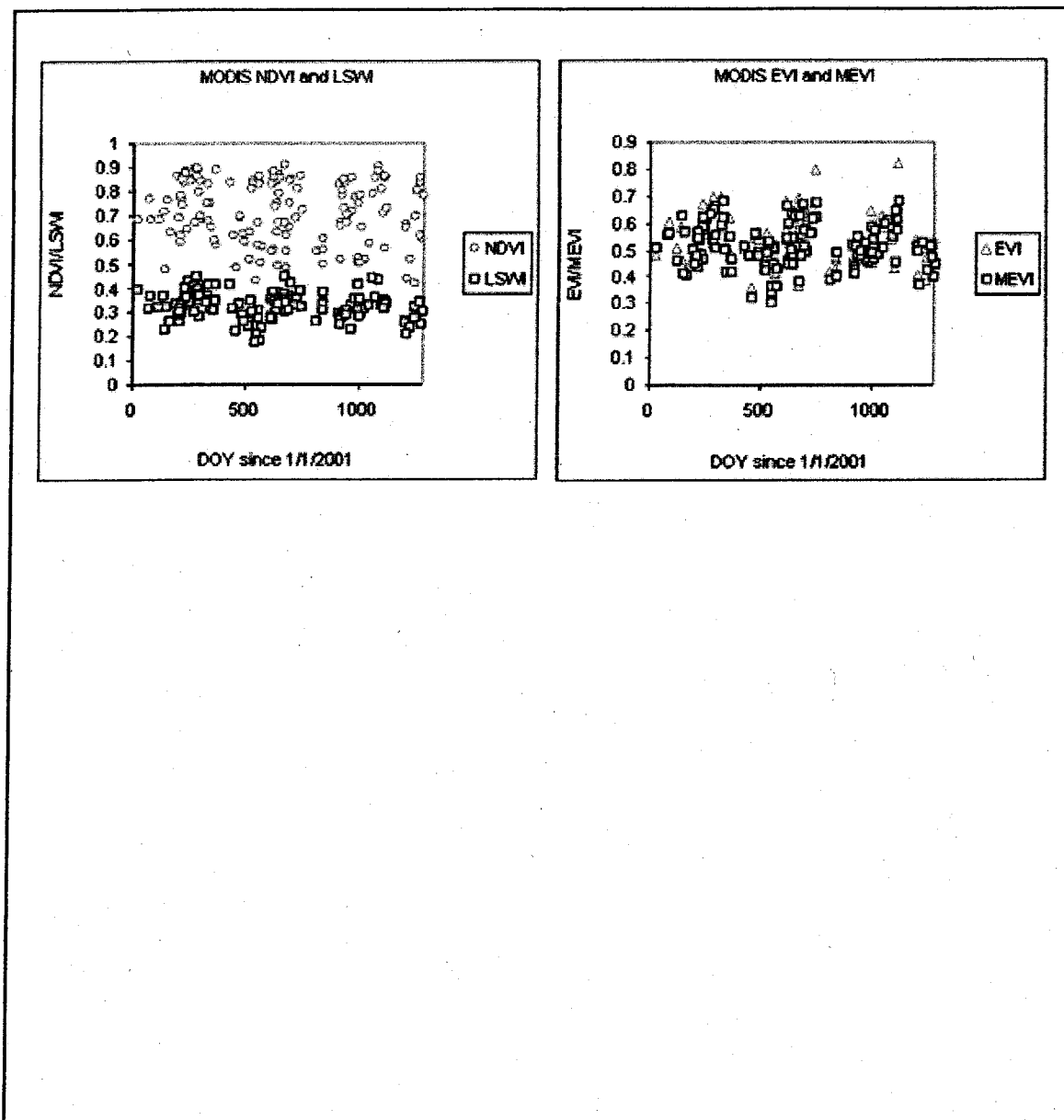


Figure 2.25 NDVI, LSWI, EVI and MEVI of the selected MODIS daily observations (reflectance scale =0.0001) of the tropical km67 seasonal moist forest site since 1/1/2001 to 7/10/2004 (DOY calculated beginning from 1/1/2001)

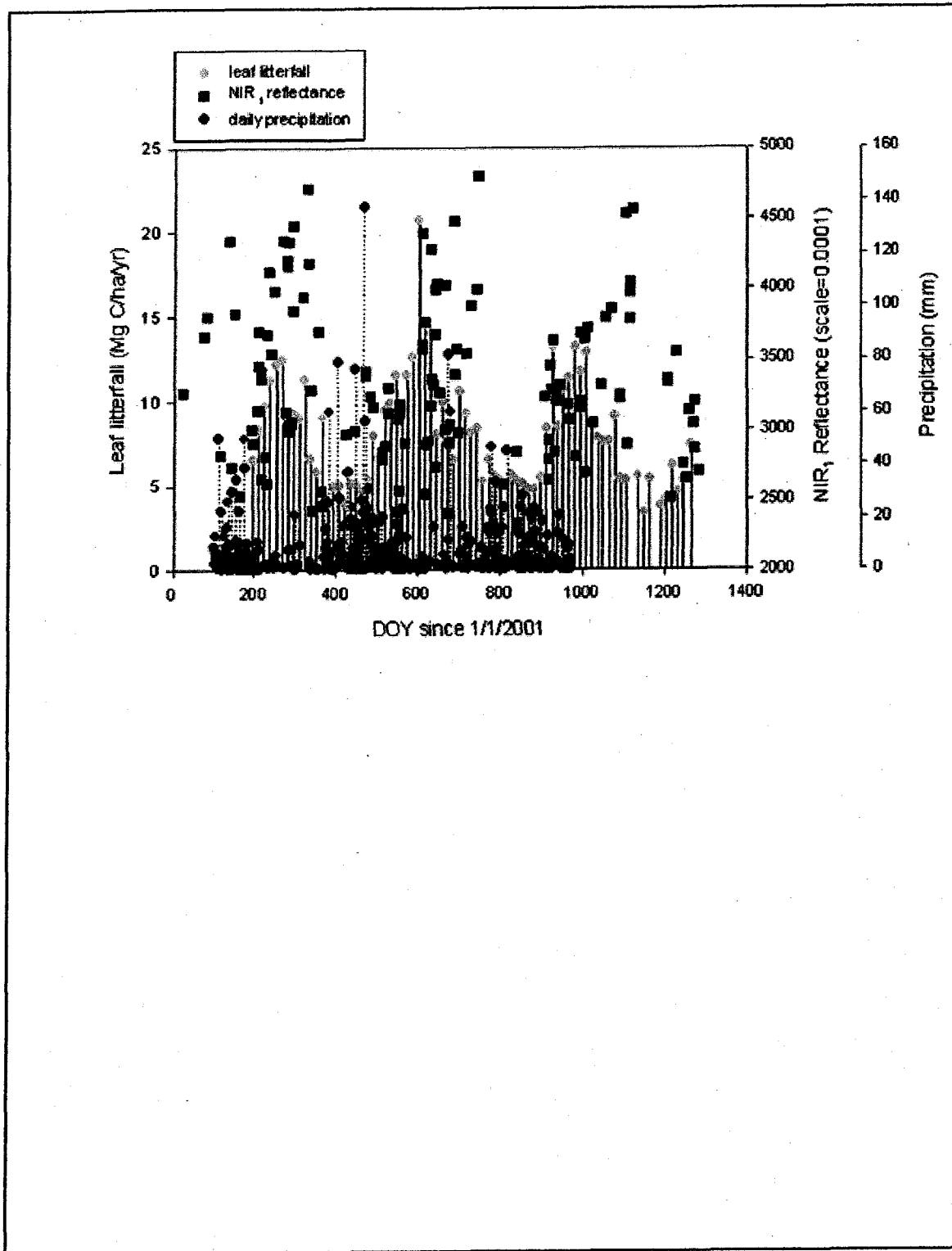


Figure 2.26 MODIS daily NIR<sub>1</sub> reflectance from Figure 2.24 and seasonal dynamics of precipitation and leaf litterfall at the km67 site (precipitation and leaf litterfall from Saleska et al., 2003)

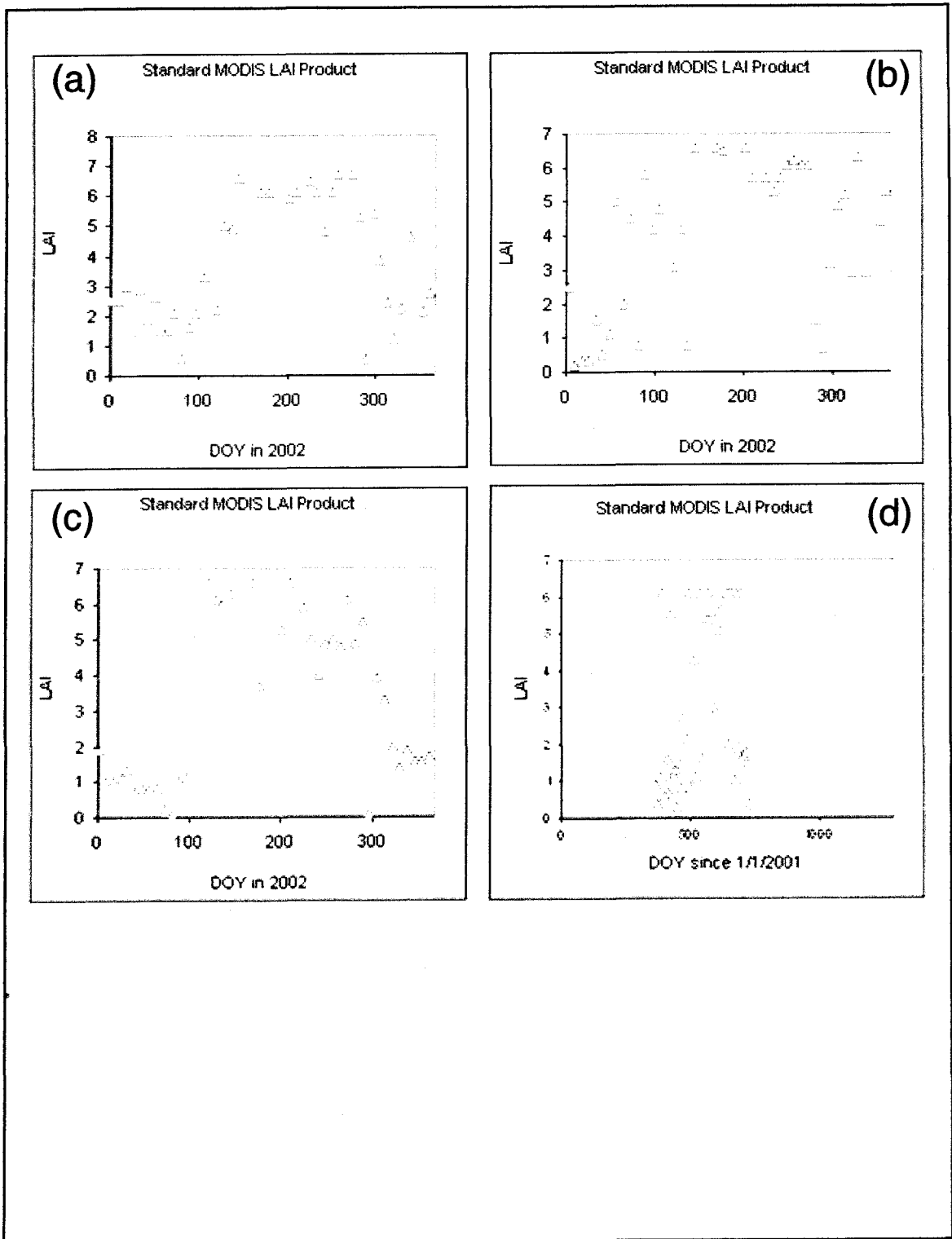


Figure 2.27 Standard LAI product in 2002 of: (a) the Harvard Forest site; (b) the Howland Forest site; (c) the Walker Branch Watershed Forest site and (d) the km67 site

## CHAPTER 3

### LESSONS LEARNED FROM INVERSION OF PROSAIL WITH MULTIPLE DAILY MODIS DATA

#### **3.1 Introduction**

The analysis of Chapter 2 showed that the assumption that the leaf spectral reflectance of a given biome type is constant anywhere and anytime should be modified, otherwise one will see the conflicting results: LAI from the MODIS FPAR/LAI products does not follow the seasonal patterns of MODIS NIR<sub>1</sub>. Therefore I soften the assumption; hence leaf optical properties and spectral characteristics are not constant during the plant growing season. Following seasonal variations of leaf structure and chemistry, fraction of absorption of photosynthetically active radiation by chlorophyll in leaves (FAPAR<sub>chl</sub>) will change during the plant growing season. To estimate LAI, FAPAR<sub>chl</sub> and other biophysical/biochemical variables, a canopy radiative transfer model and a leaf radiative transfer model need to be coupled. Bobby Braswell kindly offered me his SAIL version (SAIL-2) and PROSPECT version in Matlab. The SAIL-2 model is credited to the former studies (Goel et al., 1984c; Badhwar et al., 1985; Goel et al., 1985; Major et al., 1992; Braswell et al., 1996; Andrieu et al., 1997; Jacquemoud et al., 2000). The SAIL-2 model decomposes a canopy into stems and leaves. Stems and leaves have different spectral characteristics. Inclination angles and BRDF (bi-directional reflectance distribution

function) effect of both leaves and stems were considered. The PROSPECT offered by Bobby Braswell has four leaf-level variables: leaf internal structure variable ( $N$ ), leaf chlorophyll content ( $C_{ab}$ ), leaf dry matter content ( $C_m$ ), and leaf water thickness ( $C_w$ ) (Jacquemoud et al., 1990; Hosgood et al., 1995; Baret et al., 1997; Demarez et al., 1999). I coupled the leaf-canopy PROSPECT+SAIL-2 model by replacing the component of leaves in the SAIL-2 model with the four-variable PROSPECT model. I also got the information about the leaf brown pigment ( $C_{brown}$ ) from Fred Baret in France and added it to the code. The PROSPECT+SAIL-2 model has three groups of variables: (1) observation viewing geometry variables, (2) atmospheric condition variable (visibility) and (3) biophysical and biochemical variables (Table 1). Because the MODIS data used here were well but not perfectly atmospherically corrected, the atmospheric visibility variable ( $VIS$ , in Table 1) was assumed as a constant during inversion. The other sixteen variables are plant area index ( $PAI$ ), stem fraction ( $SFRAC$ ), leaf inclination angle ( $LFINC$ ), stem inclination angle ( $STINC$ ), leaf hot spot parameter ( $LFHOT$ ), stem hotspot parameter ( $STHOT$ ), cover fraction ( $CF$ ), five leaf parameters ( $N$ ,  $C_{ab}$ ,  $C_m$ ,  $C_w$ ,  $C_{brown}$ ), two parameters to simulate soil optical properties ( $SOIL_A$ ,  $SOIL_B$ ), and two parameters to simulate stem optical properties ( $STEM_A$ ,  $STEM_B$ ).

The objective of this chapter is to record the steps I have performed and the lessons I have learned from the experiments: how fast the Matlab version runs; which daily MODIS observations may be used as inputs to invert the radiative transfer model; can all the seven MODIS bands be used to do inversion; should the brown pigment consideration be added into the PROSPECT model?

### **3.2 Metropolis algorithm for inversion**

Inversion of a radiative transfer model is computation intensive and requires careful choice of optimization procedures. The iterative optimization procedures, the most common approaches to invert a radiative transfer model (e.g., Bacour et al., 2002a), were not used in this study. The iterative optimization procedures are local optimization techniques and they have limited potential to search ‘global’ optimal solutions. For instance, if there are a few minimum points within a search space, the iterative procedures could offer a local extreme-point solution and might fail to provide a global extreme-point solution given an initial guess. As an alternative, a new method based on a Metropolis algorithm (Metropolis et al., 1953; Hurtt et al., 1996; Braswell et al., 2005) was developed. This method simulates the distribution of variables and can provide estimates of uncertainty (i.e., standard deviation) of individual variables. The Metropolis algorithm is computation intensive.

The inversion algorithm we used in this study is a modified version of the Metropolis algorithm (Metropolis et al., 1953), one algorithm often used in Markov Chain Monte Carlo (MCMC) estimation. In each iteration, the algorithm uses the current variable estimate to randomly generate a new “proposal” estimate in variable space. This new variable estimate will be the input for a new model run. Model-retrieved and observed reflectance values are used to calculate the likelihood of an error probability model. The Metropolis algorithm then accepts the new variable point with a certain probability. The resulting Markov chain of accepted variable values converges after a certain burn-in period to the posterior distribution of the variables conditional on the observations. In the following, Pr denotes Probability in a general sense, or, more

specifically, the value of a probability density function.  $Pr(\text{new}|\text{data})$  and  $Pr(\text{old}|\text{data})$  mean conditional probabilities of “new” and “old” variable estimates (points) given the known “data”.

According to Bayes’ theorem,

$$Pr(\text{variable point} | \text{data}) \propto Pr(\text{variable point}) Pr(\text{data} | \text{variable point})$$

Let  $L(\text{variable point}) = Pr(\text{data} | \text{variable point})$ , then

$$Pr(\text{variable point} | \text{data}) \propto Pr(\text{variable point}) L(\text{variable point})$$

where  $L(\cdot)$  is the likelihood function.  $Pr(\text{variable point})$  denotes the prior distribution assumed for the set of variables. In this study we assume a set of independent uniform prior distributions for the variables. Let  $X_i = [x_{i1}, \dots, x_{ip}]$  ( $p > 1$ ),  $i$  is the subscript of data point, subscripts 1, ...,  $p$  mean spectral bands, and  $x$  is reflectance.

This study assumes that the observed spectral values  $X_i$  differ from the model predicted values  $U_i = [u_{i1}, \dots, u_{ip}]$  according to a mean zero  $p$ -variate Gaussian error model that results in the likelihood function

$$L = \prod_{i=1}^n \frac{1}{(\sqrt{2\pi})^p |\Sigma|^{1/2}} e^{-\frac{1}{2}(X_i - U_i)' \Sigma^{-1} (X_i - U_i)} \quad (1)$$

where  $n$  is the number of data points and  $\Sigma$  is the variance - covariance matrix of  $X$ .  $\Sigma$  is estimated by the usual sample variances – covariances in each step of the algorithm:

$$\Sigma_e = (s_{ij})_{p \times p} \quad (2)$$

$$s_{ij} = \frac{1}{n} \sum_{k=1}^n (x_{ki} - u_{ki})(x_{kj} - u_{kj}) \quad i, j = 1, \dots, p$$



The natural logarithm of the likelihood, the “log-likelihood” ( $\log(L)$ ), is used in the algorithm during operation (e.g., Bishop, 1995).

The algorithm defines the probability to accept the new point as following:

$$\Pr_{accept} = \min \left( 1, \frac{\Pr(new | data)}{\Pr(old | data)} \right), \quad (3)$$

If the algorithm accepts the new point, it will become “old” point in next iteration; otherwise, the old point will still be the “old” point in next iteration.

To accelerate the speed of convergence of the Metropolis algorithm, we modified the adaptive algorithm used in other studies (e.g., Hurtt et al., 1996; Braswell et al., 2005) as following:

In each iteration, one variable is selected to change as

$$variable_{new,s} = variable_{old,s} + r \times (variable_{max,s} - variable_{min,s}) \quad (4)$$

where  $s=1, \dots, 16$ , the number of variables in PROSAIL-2 model that are allowed to search for solutions,  $r$  is randomly selected at each step between  $\pm 0.5 \cdot temperature_s$ ,

$variable_{max,s}$ ,  $variable_{min,s}$  are the maximum and minimum values allowed to search. If

$variable_{new,s}$  is accepted, then  $temperature_s$  is increased by a factor of 1.006569

(personal communication with Dr. William Sacks). If it is rejected, then  $temperature_s$  is

decreased by a factor of 0.99. By changing the  $temperatures$  in this way, the

$temperatures$  of all variables are adjusted until varying any given variable leads to

acceptance of about 23% to 44% of the time, which is considered an ideal acceptance rate

for the Metropolis algorithm (Gelman et al., 2000).

### 3.3 Results

#### TASK 1: How fast does the Matlab version run?

I simulated ten MODIS observations as input for inversion of all the fifteen variables in Table 1 with the Metropolis algorithm. It spent 4 hours, 39 minutes and 27 seconds on workstation dragon of Complex Systems Research Center, UNH to run 42000 iterations. If I want to run 2,250,000 iterations, it will need 10days, 10 hours, 3 minutes and 50 seconds.

#### TASK 2: Which daily MODIS observations may be used as inputs to invert the radiative transfer model?

In Chapter 2, I described and analyzed the procedures in detail about how to determine if one daily MODIS observation is cloud-free and snow-free, or if it is a noise-contaminated observation. For example, the cloud-free and snow-free daily MODIS observations of the Harvard Forest site in 2002 had BLUE reflectance less than 0.05 (Figure 2.14). The SWIR<sub>2</sub> reflectance of cloud-free and snow-free observations over Harvard Forest site should be not greater than 0.25. Following the procedures in Chapter II, one can select the cloud-free and snow-free observations as input of radiative transfer models.

#### TASK 3: Which MODIS bands should be used and should brown pigments be considered?

In order to test which MODIS bands should be used and if brown pigments in leaf should be considered, I collected daily MODIS observations from day of year (DOY) 201

to 211 in 2001 over Harvard Forest site (see description of the site in Chapter 4), a deciduous broadleaf forest site. The data collection set was used for the task. Description about daily MODIS observations in detail is available in Chapters 2 and 4. The strength of the Metropolis inversion algorithm is to provide distributions for individual variables. The posterior distributions offer histograms of the variables and their standard deviations (uncertainties).

TASK 3.1.....inverted results using all seven MODIS bands without consideration of leaf brown pigment (i.e., assume that there is no brown pigment in leaf)

Here I reported the histograms of the sixteen variables (see Figure 3.1) from inversion of the MODIS data collection using all the seven MODIS bands with the assumption that leaf brown pigments be zero. The mode of cover fraction histogram (Figure 3.1 (c)) is close to its allowable right range, i.e. 100%. It is reasonable because the Harvard Forest was almost completely covered by forests (Turner et al., 2003). However, the LAI ( $LAI=PAI*(1-SFRAC)$ ) (see Figures 3.1 (a) and (b)) is much lower than the field measurements (Xiao et al., 2004c) and the estimates from intensive field measurements and Landsat ETM + (Cohen et al., 2003) during summer peak growing season. Leaf chlorophyll mean value (Figure 3.1 (e)) was greater than  $110 \mu\text{g}/\text{cm}^2$ . The value is much greater than the measurements in the Harvard Forest reported by other researchers in earlier studies (Waring et al., 1995; Cavender-Bares et al., 2000) and greater than the measurements of needles reported earlier (Zarco-Tejada et al., 2004). Aber and colleagues (Aber et al., 1996) used specific leaf weight  $0.028 \text{ g}/\text{cm}^2$  for pine

and  $0.01 \text{ g/cm}^2$  for deciduous leaf. The mean value of inverted leaf dry matter was around  $0.052 \text{ g/cm}^2$  (Figure 3.1 (g)), much greater than the former. Using mean values of the retrieved variable distributions, the reflectance was reproduced with PROSAIL-2. Blue,  $\text{NIR}_2$  and  $\text{SWIR}_1$  were not well reproduced (Figure 3.1 (p)).

TASK 3.2 ..... inverted results using all seven MODIS bands with consideration of leaf brown pigment

Compared with the results in Figure 3.1, the results with the consideration of brown pigments in leaf (Figure 3.2) improved in some aspects. LAI and leaf dry matter (Figures 3.2 (a), (b) and (h)) were more consistent with other research results in literature (Aber et al., 1996; Cohen et al., 2003). Leaf chlorophyll estimates (Figure 3.2 (e)), compared to the literature results, were reasonable. However, Reproduced blue and  $\text{SWIR}_2$  were much less than observed data (Figure 3.2 (q)). The results hint that it is a better choice to use only five-spectral information with the consideration of brown pigments. Actually, we may expect some yellow/dead leaves of forests at the scale of 500m, the MODIS scale used in this study.

TASK 3.3 ..... inverted results using five MODIS bands excluding blue and  $\text{SWIR}_2$  without consideration of leaf brown pigment

The reproduced red, green and  $\text{SWIR}_1$  reflectance matched well with observed data while the reproduced  $\text{NIR}_1$  and  $\text{NIR}_2$  were lower than observed data (Figure 3.3 (p)). However, the retrieved chlorophyll concentration (Figure 3.3 (e)) hit the right edge of the allowable search range. The estimate of chlorophyll could not match the reality. Without

including of brown pigment in inversion at the 500m scale of MODIS data, some of the inverted results will be unreasonable.

TASK 3.4 inverted results using five MODIS bands excluding blue and SWIR<sub>2</sub> with consideration of leaf brown pigment

Comparing the LAI, chlorophyll concentration, leaf dry matter and reproduced reflectance of Figures 3.1 -3.4, the results using only five MODIS bands and with the consideration of leaf brown pigments were the most reasonable. The retrieved mean LAI was 4.44 that is reasonable when compared to 4.9 reported by Cohen and colleagues (Cohen et al., 2003). The retrieved mean chlorophyll content was  $49.89\mu\text{g}/\text{cm}^2$  that fall between the measurements of broadleaf species and needles from the literatures (Waring et al., 1995; Cavender-Bares et al., 2000; Zarco-Tejada et al., 2004). Retrieved mean leaf dry matter also fall between specific leaf weight  $0.028\text{ g}/\text{cm}^2$  for pine and  $0.01\text{ g}/\text{cm}^2$  for deciduous leaf (Aber et al., 1996). The reproduced reflectance matched well with the observed MODIS five bands data.

### **3.4 Conclusions and summary**

The blue band is very sensitive to aerosols in the atmosphere. The SWIR<sub>2</sub> band is very sensitive to water and it can be saturated if there is sub-pixel water body under clear atmospheric condition (King et al., 1999). The MODIS daily reflectance data are not perfectly atmospherically corrected. Based on the above experiments the blue and SWIR<sub>2</sub> bands should be excluded from the inversion.

There are still some non-green pigments of the forests that can be detected by the MODIS optical sensors at 500m scale in spite of the common assumption that the forest leaves in summer are green. When brown pigments are not considered, green pigments will be treated as both green pigments and non-green pigments in the inversion procedures. It can be a source of error and uncertainties of the inversion.

Hereafter, I will use only five MODIS bands and consider brown pigments during inversion procedures.

Table 3.1 A list of variables in the PROSAIL-2 model and their search ranges

	Variable	Description	Unit	Search range
Biophysical /biochemical variables	PAI	plant area index, i.e., leaf +stem area index		1 – 7.5
	SFRAC	Stem fraction		0 – 1
	CF	Cover fraction: area of land covered by vegetation/ total area of land		0.5 – 1
	C <sub>ab</sub>	Leaf chlorophyll a+b content	µg/cm <sup>2</sup>	0 – 80
	N	Leaf structure variable: measure of the internal structure of the leaf		1.0 – 4.5
	C <sub>w</sub>	Leaf equivalent water thickness	cm	0.001 – 0.15
	C <sub>m</sub>	Leaf dry matter content	g/cm <sup>2</sup>	0.001 – 0.04
	C <sub>brown</sub>	Leaf brown pigment content		0.00001 – 8
	LFINC	Mean leaf inclination angle	degree	10 – 89
	STINC	Mean stem inclination angle	degree	10 – 89
	LFHOT	Leaf BRDF variable: length of leaf/ height of vegetation		0 – 0.9
	STHOT	Stem BRDF variable: length of stem / height of vegetation		0 – 0.9
	STEM <sub>A</sub>	Stem reflectance variable: maximum (for a fitted function)		0.2 – 20
	STEM <sub>B</sub>	Stem reflectance variable range (for same fitted function)		50 – 5000
	SOIL <sub>A</sub>	Soil reflectance variable: maximum (for a fitted function)		0.2 – 20
SOIL <sub>B</sub>	Soil reflectance variable: range (for same fitted function)		50 – 5000	
Atmospheric condition variable	VIS	Diffuse/ direct variable: scope of atmospheric clarity	km	50

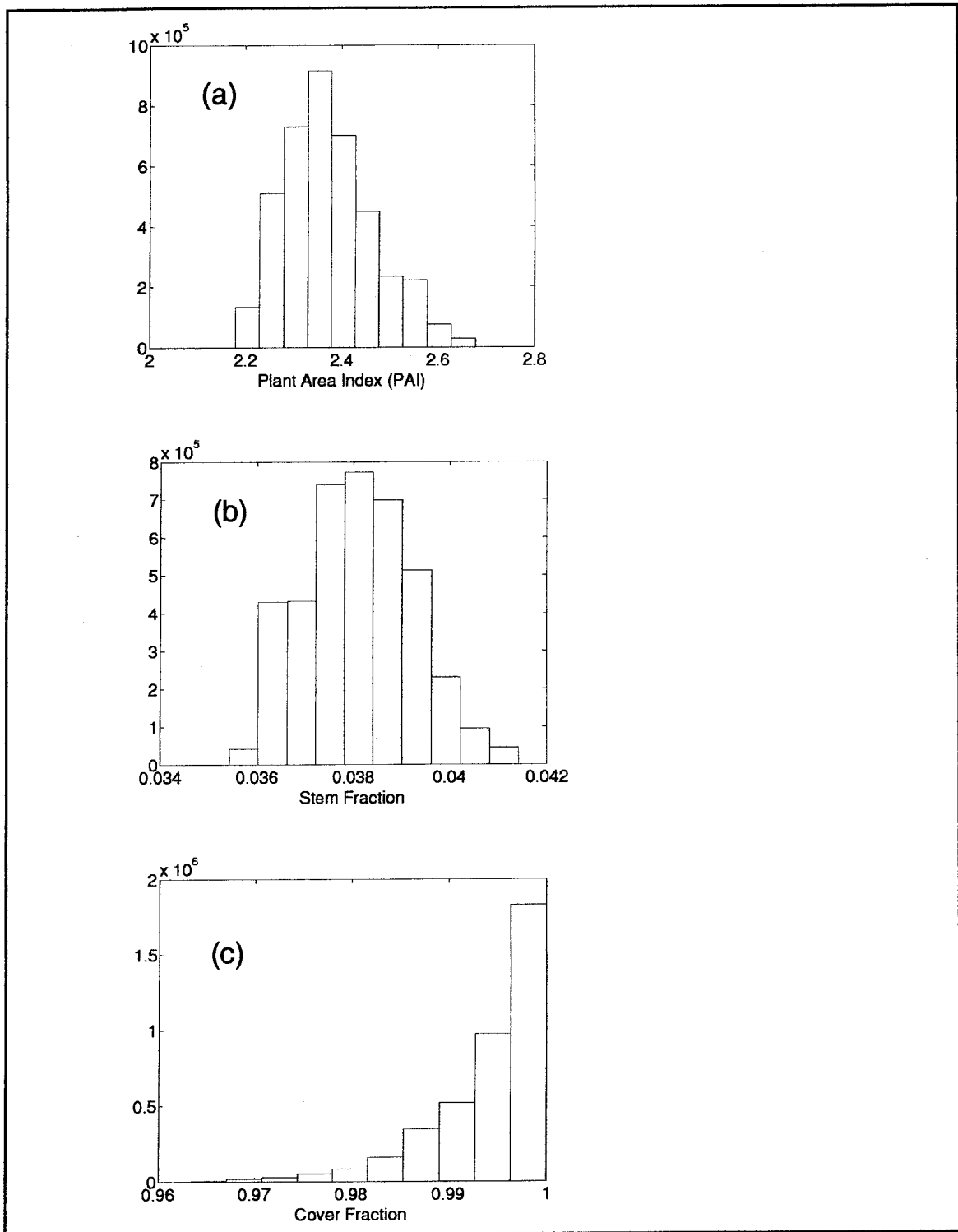


Figure 3.1 Retrieved results using seven MODIS bands without consideration of brown pigments for the Harvard Forest for MODIS data collection from day of year (DOY) 201 to 214 in 2001: retrieved histograms: (a) plant area index (PAI), (b) stem fraction, and (c) cover fraction



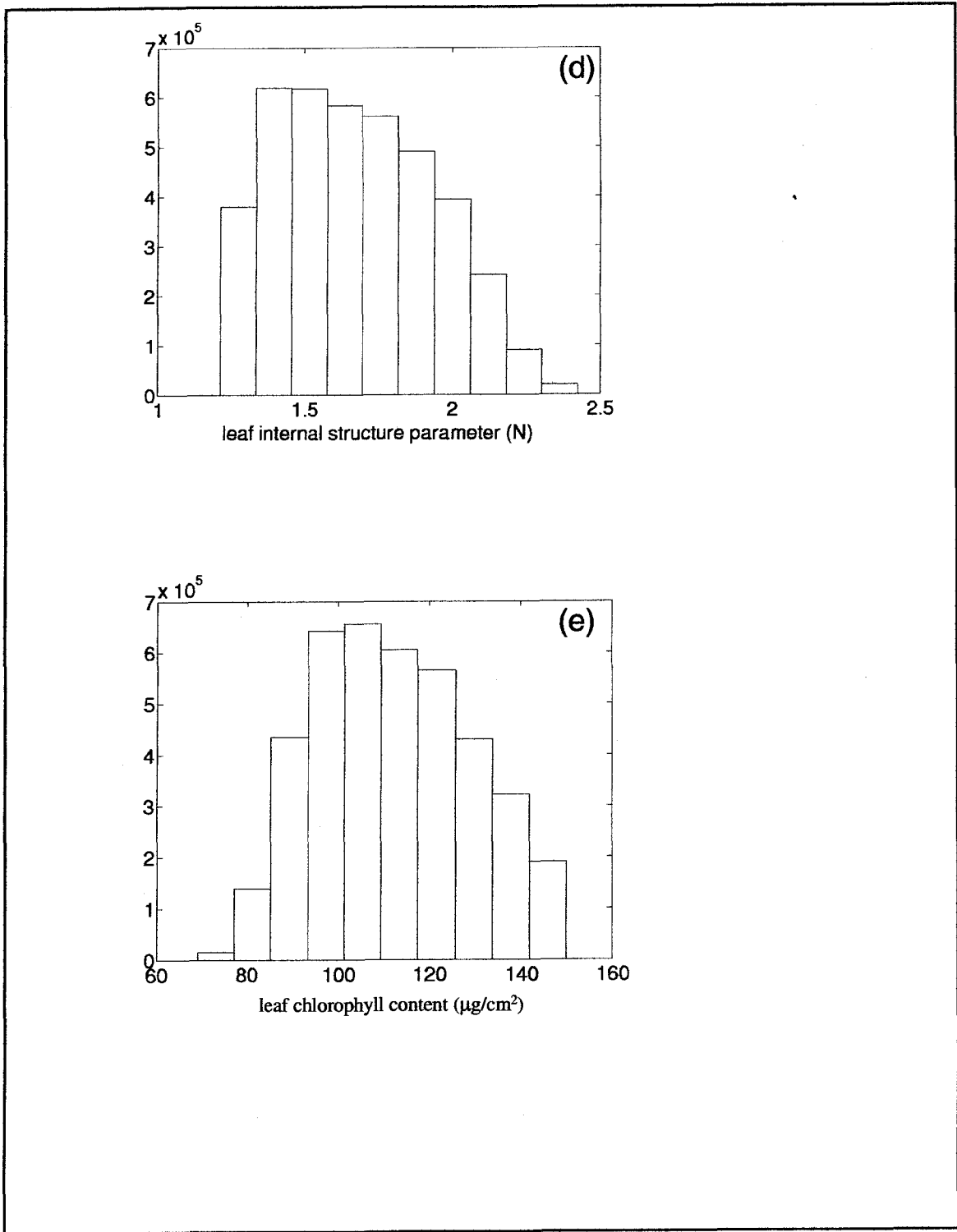


Figure 3.1 (continued) Retrieved histograms: (d) leaf internal structure parameter (N) , and (e) leaf chlorophyll content ( $C_{ab}$ :  $\mu\text{g}/\text{cm}^2$ )

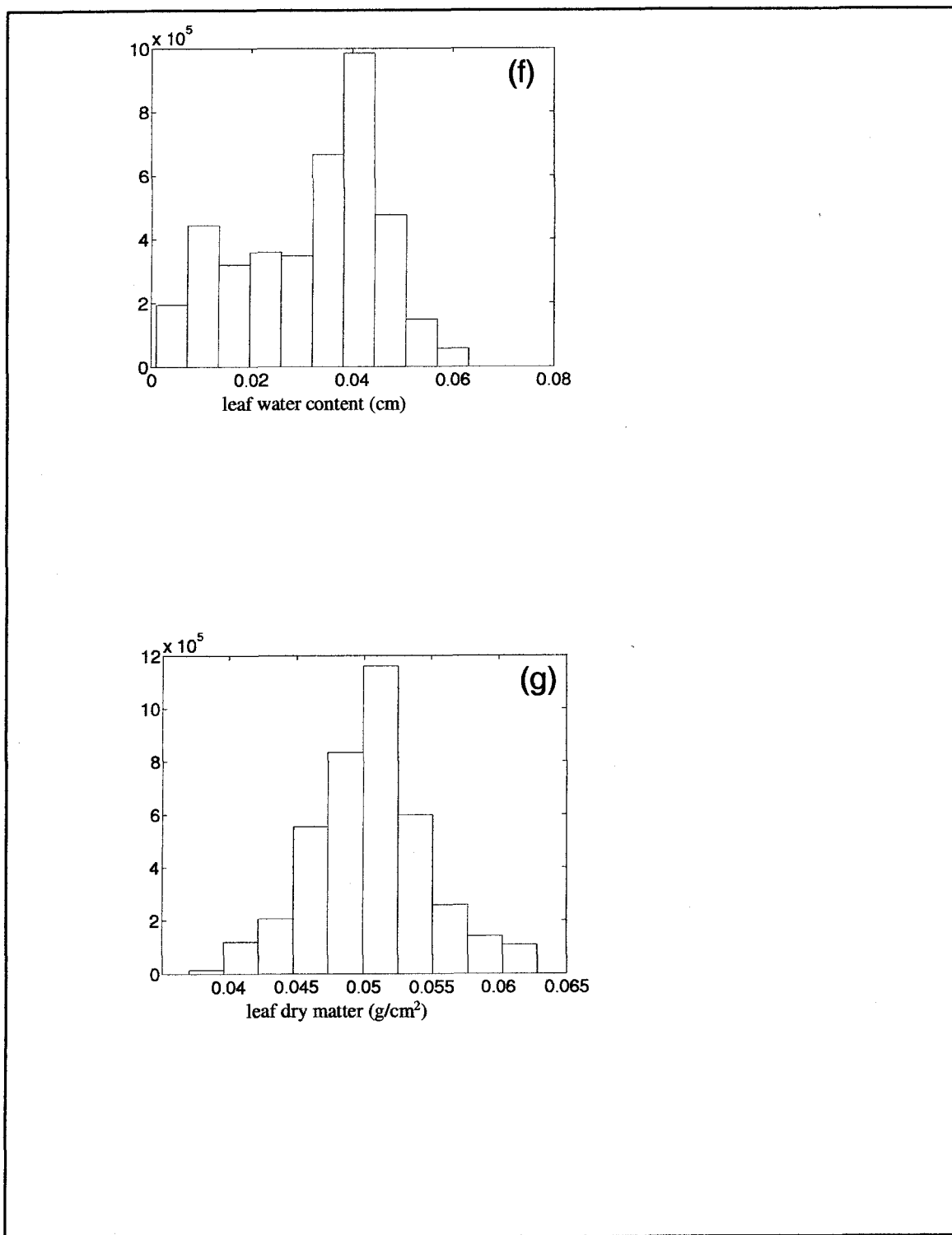


Figure 3.1(continued) Retrieved histograms: (f) leaf water content ( $C_w$  : cm), and (g) leaf dry matter ( $C_m$  :  $g/cm^2$ )

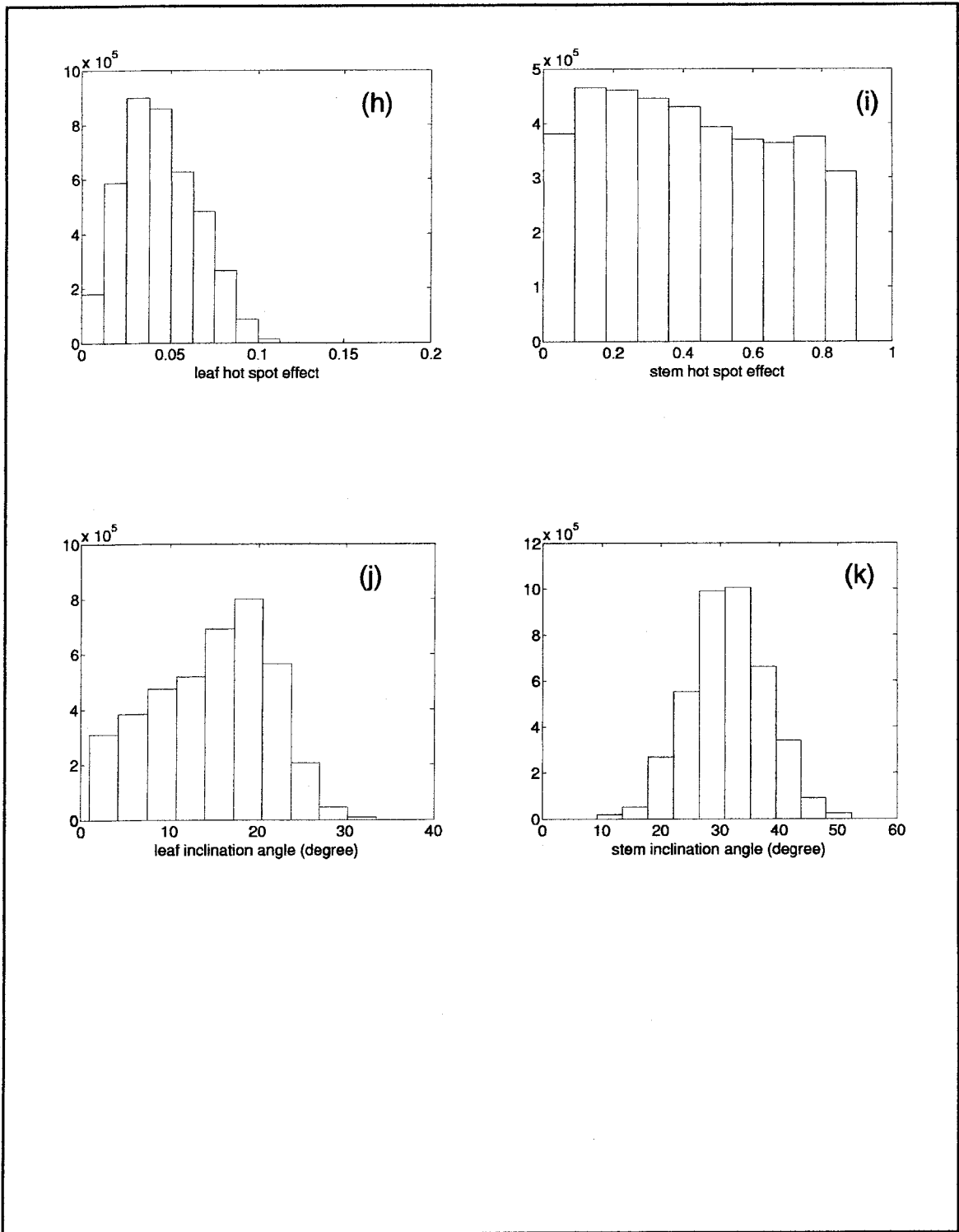


Figure 3.1 (continued) Retrieved histograms: (h) leaf hot spot parameter, (i) stem hot spot parameter, (j) leaf inclination angle (degree), and (k) stem inclination angle (degree)

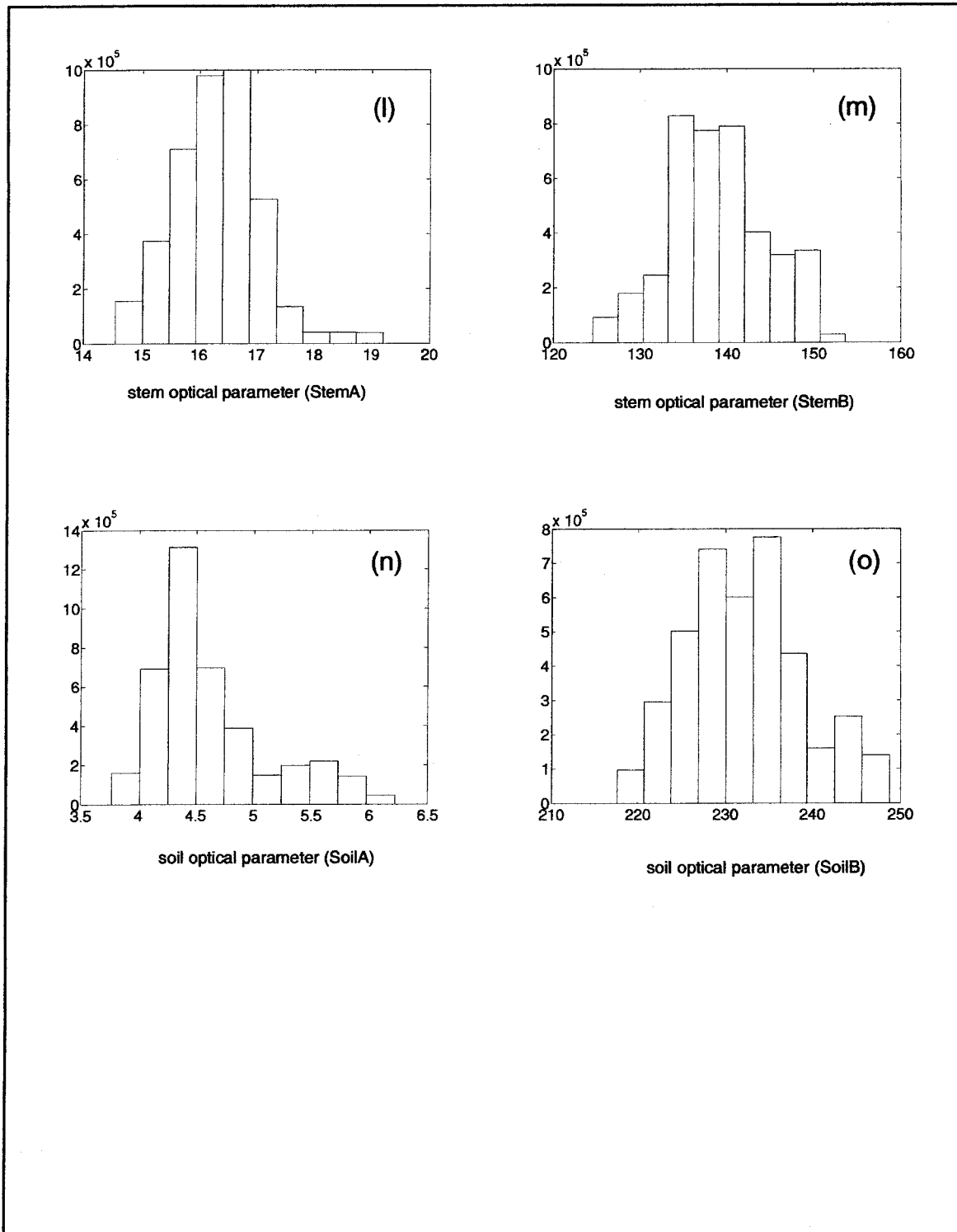


Figure 3.1 (continued) Retrieved histograms: (l) stem optical parameter (StemA), (m) stem optical parameter (StemB), (n) soil optical parameter (SoilA), and (o) soil optical parameter (SoilB)

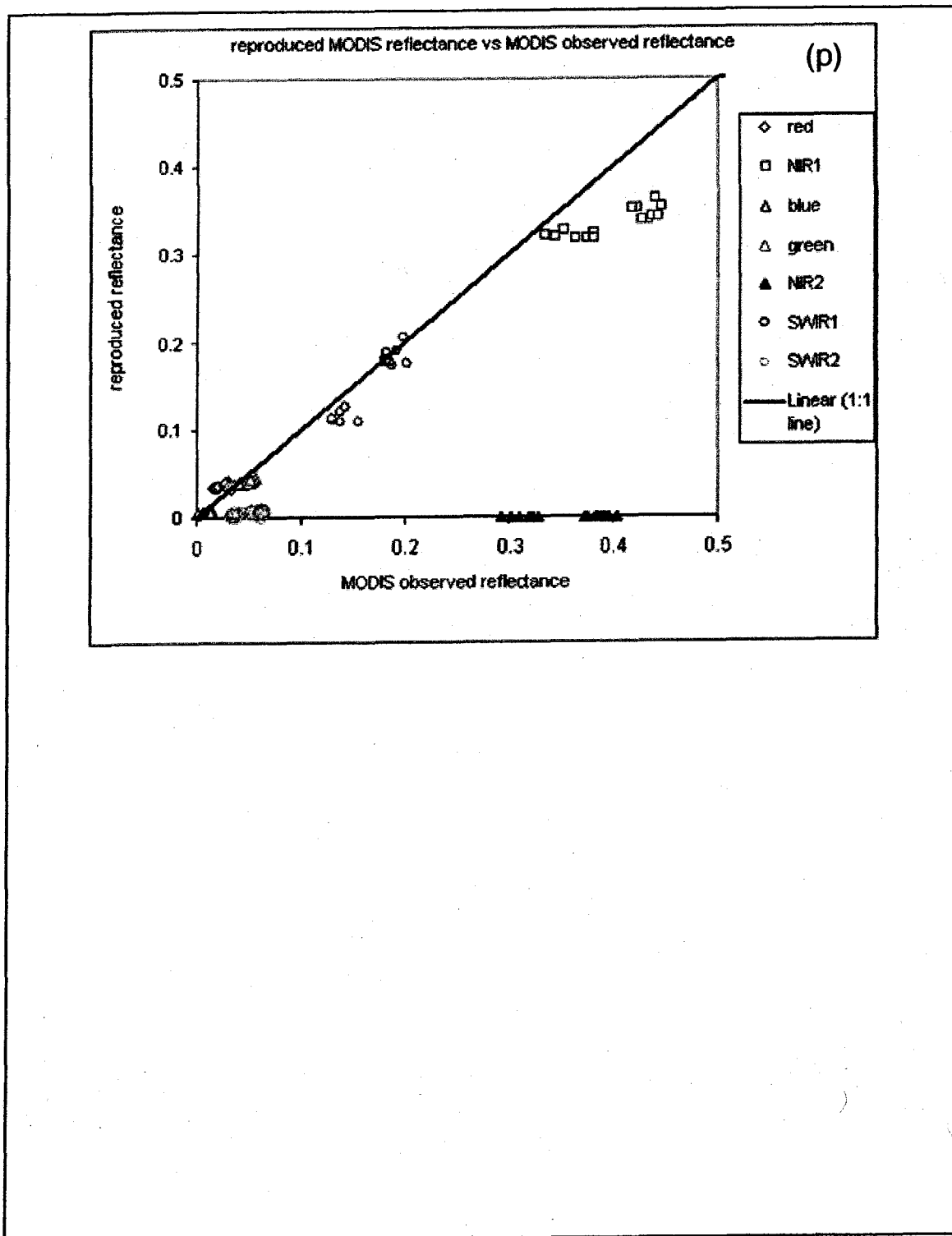


Figure 3.1(continued) (p) a comparison between the reproduced reflectance using retrieved mean values of (a) – (o) and MODIS observed reflectance

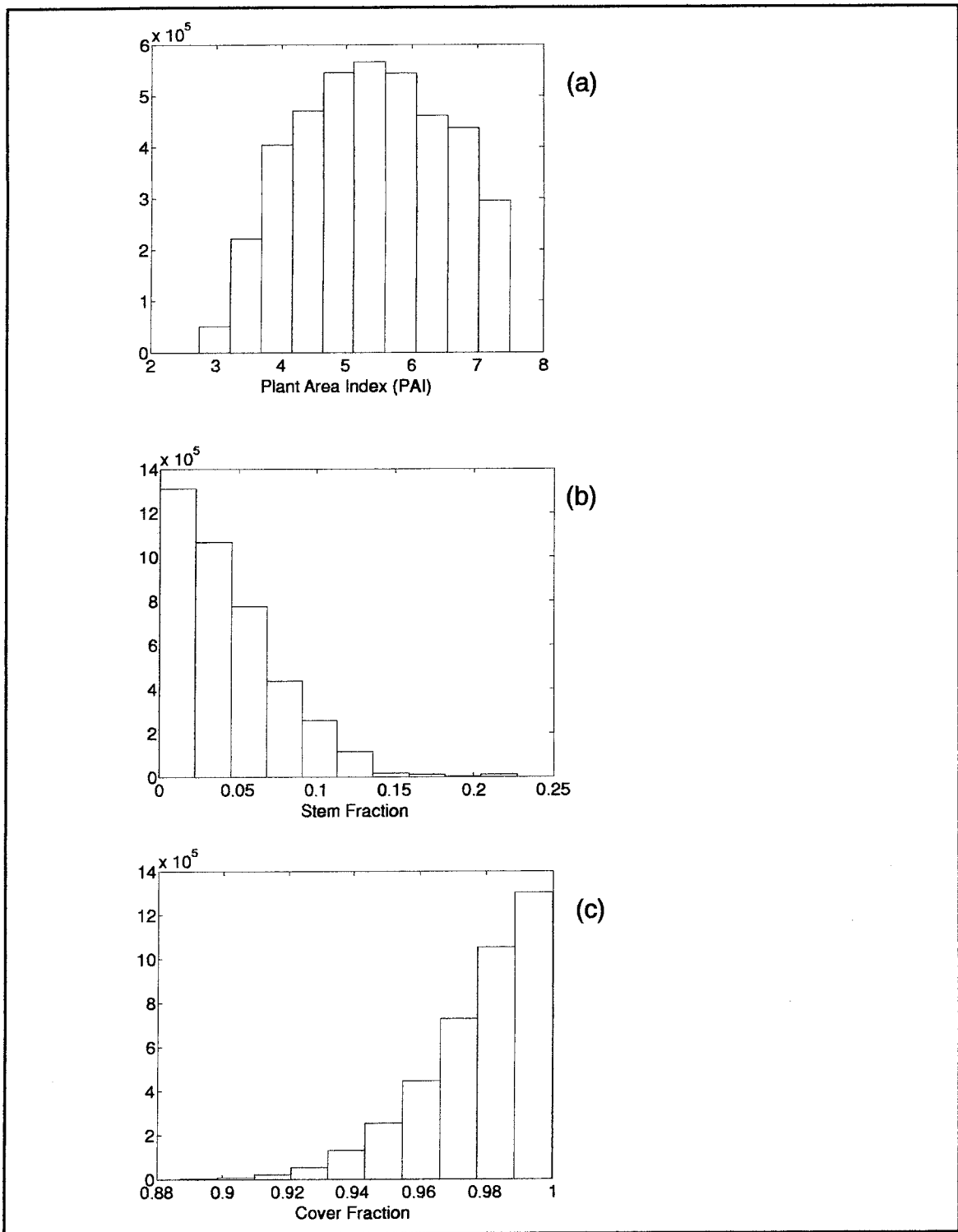


Figure 3.2 Retrieved results using seven MODIS bands with consideration of brown pigments for the Harvard Forest for MODIS data collection from day of year (DOY) 201 to 214 in 2001: retrieved histograms: (a) plant area index (PAI), (b) stem fraction, and (c) cover fraction

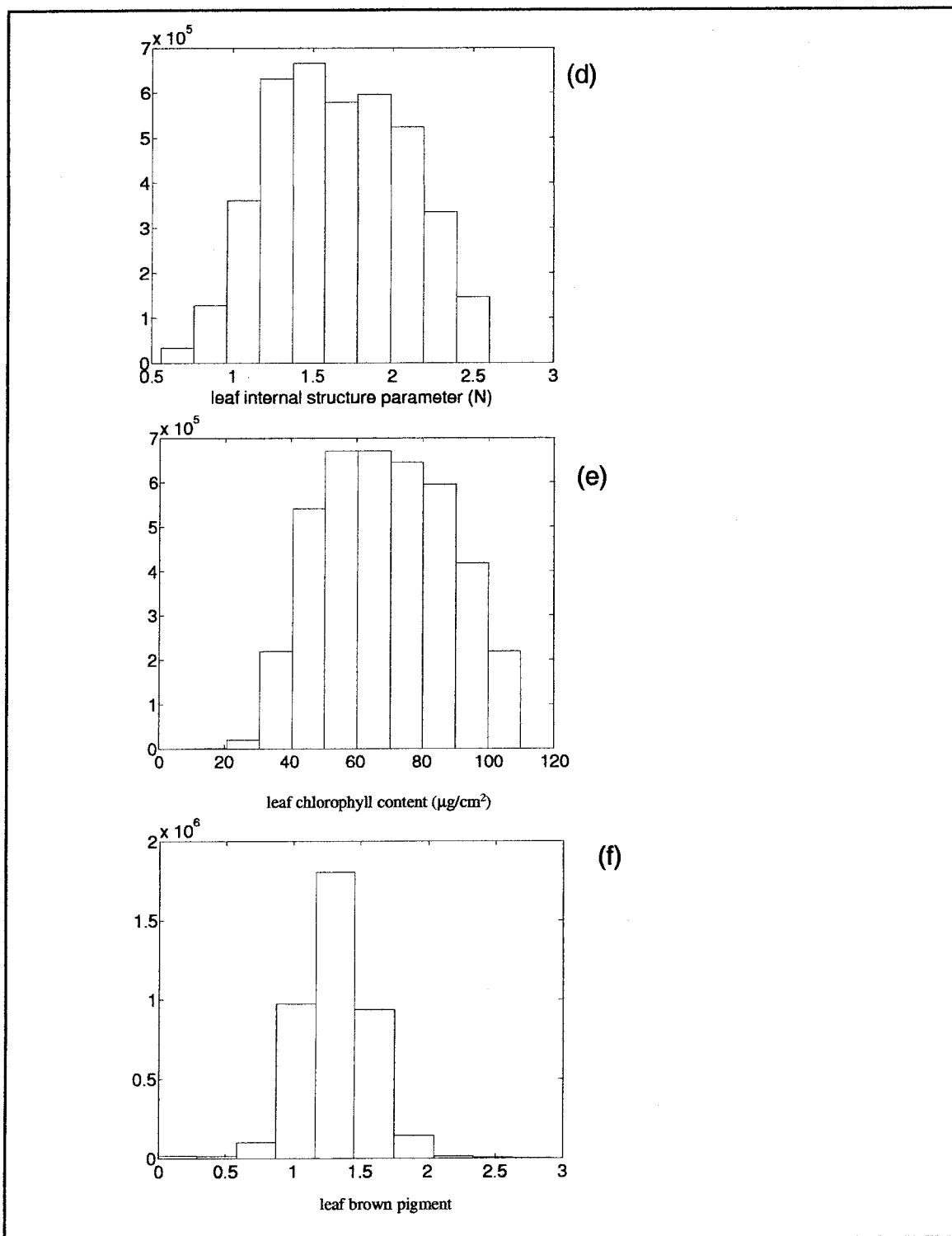


Figure 3.2 (continued) Retrieved histograms: (d) leaf internal structure parameter (N) , (e) leaf chlorophyll content ( $C_{ab}$ :  $\mu\text{g}/\text{cm}^2$ ), and (f) brown pigment

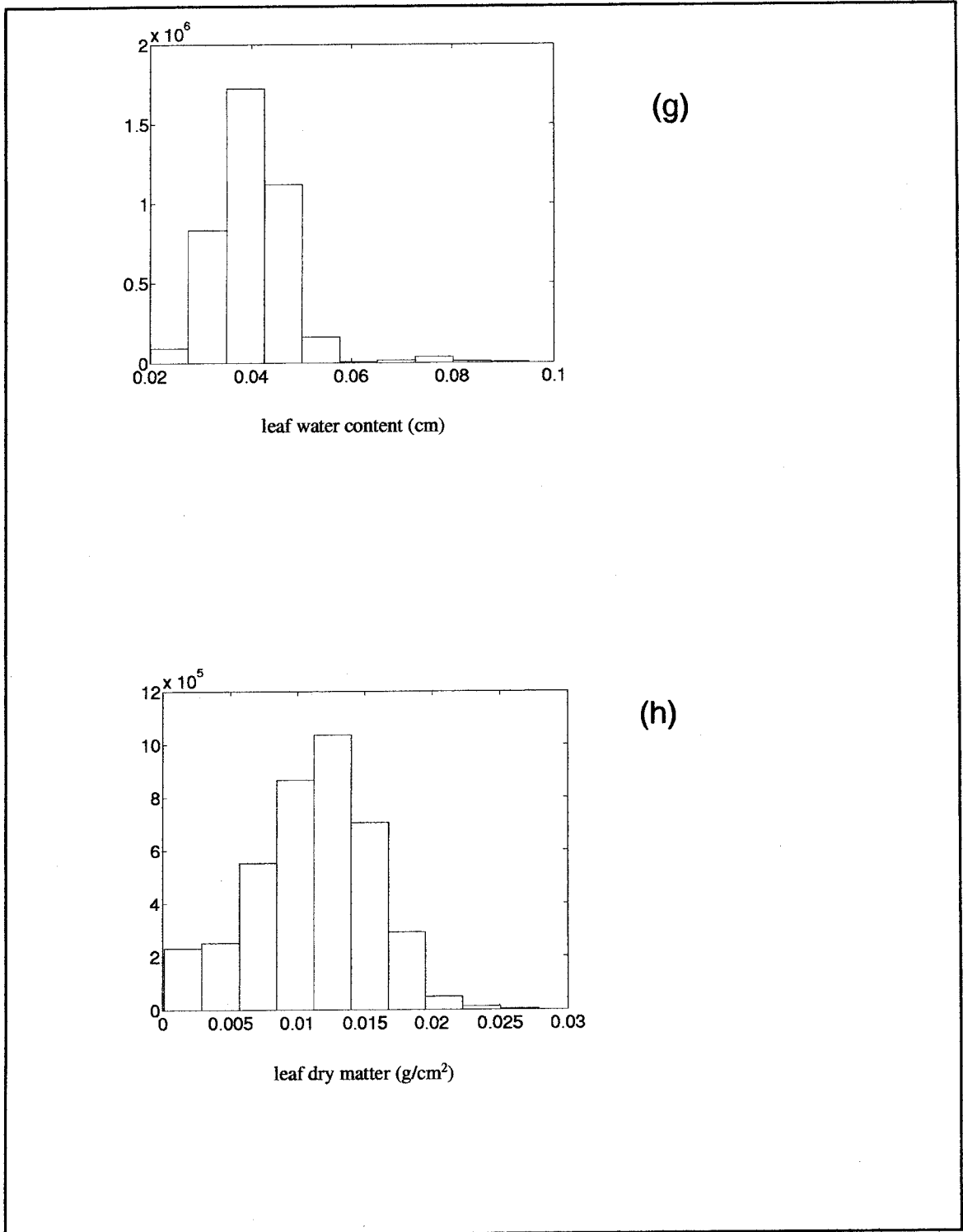


Figure 3.2 (continued) Retrieved histograms: (g) leaf water content ( $C_w$  : cm), and (h) leaf dry matter ( $C_m$  : g/cm<sup>2</sup>)



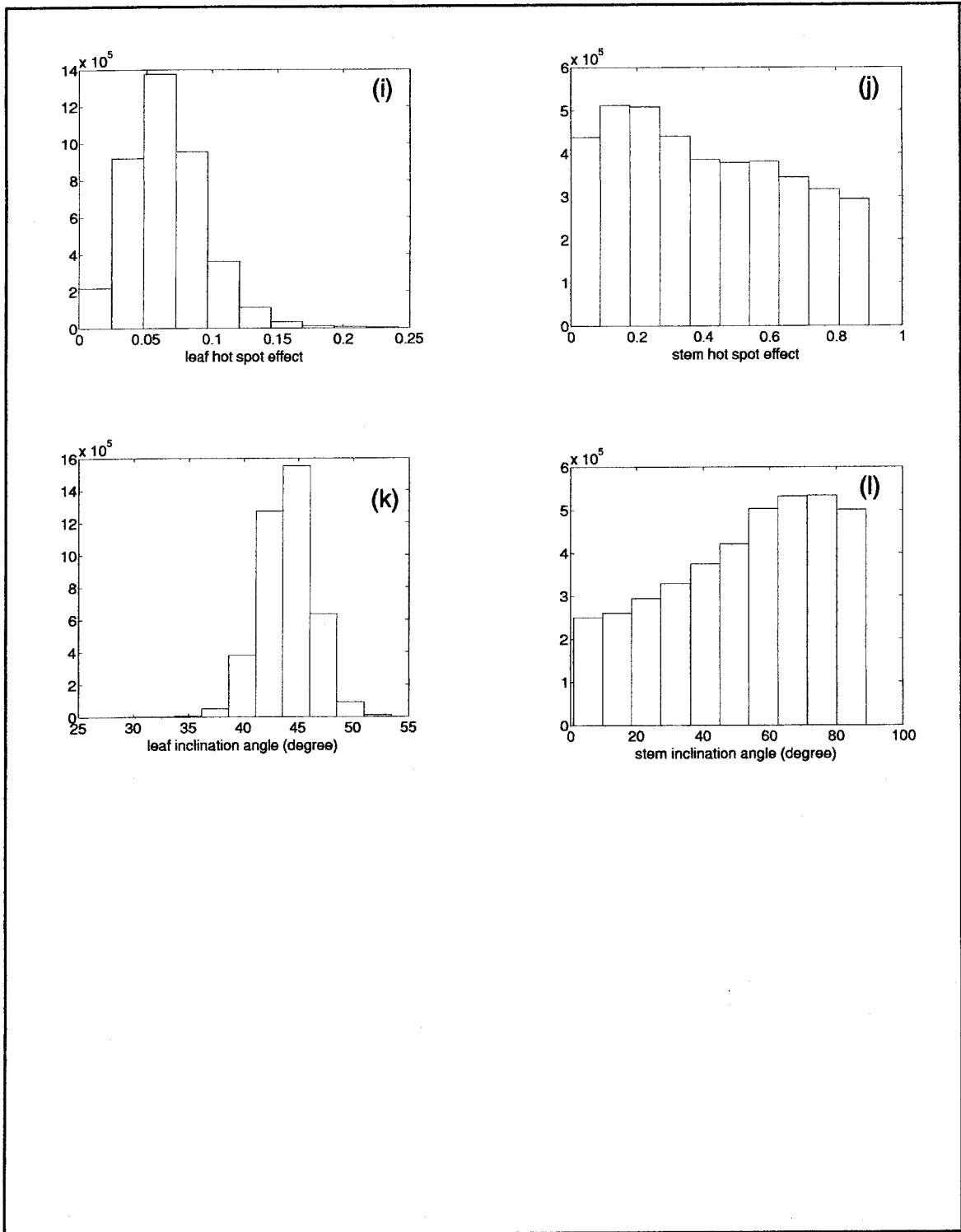


Figure 3.2 (continued) Retrieved histograms: (i) leaf hot spot parameter, (j) stem hot spot parameter, (k) leaf inclination angle (degree), and (l) stem inclination angle (degree)

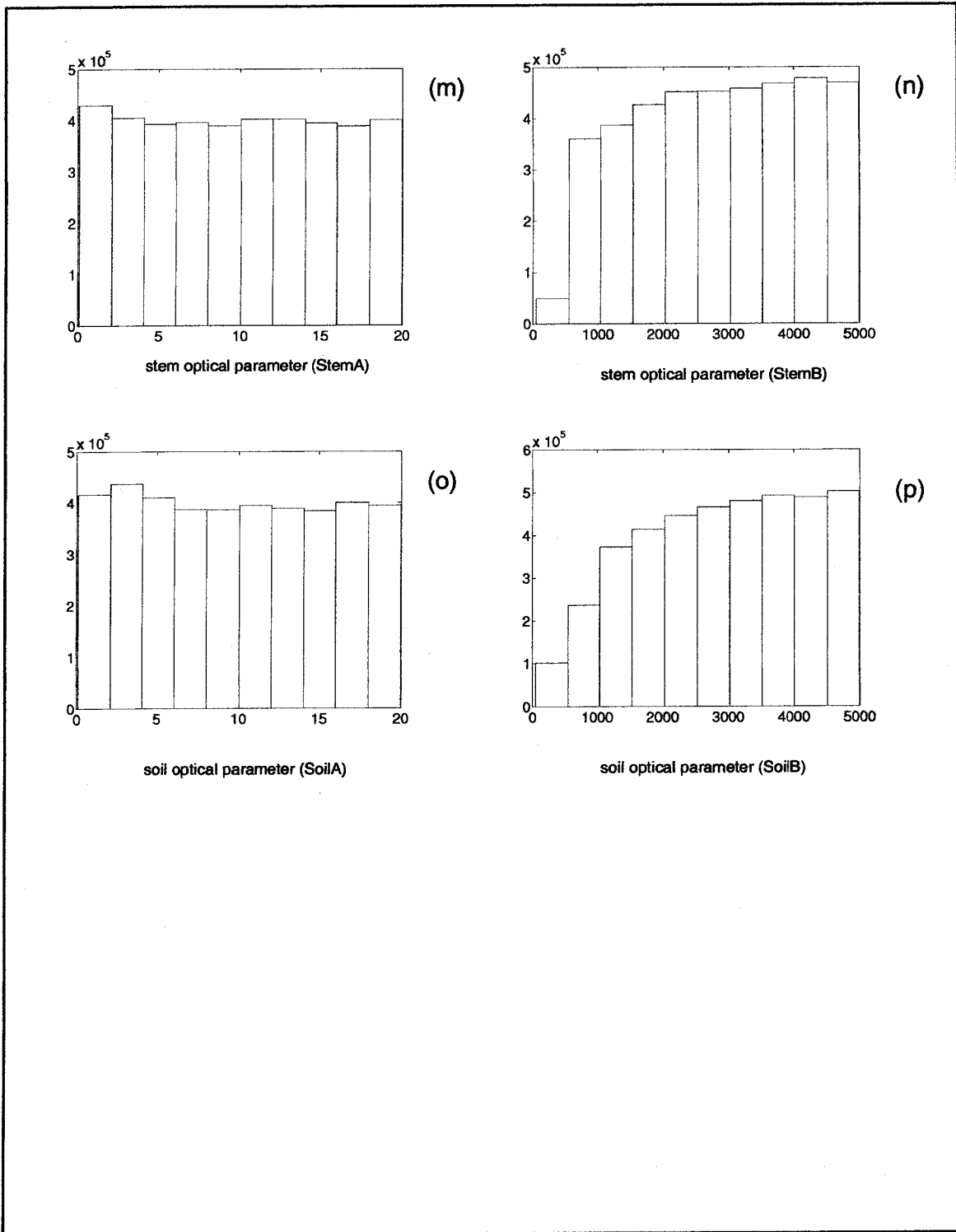


Figure 3.2 (continued) Retrieved histograms: (m) stem optical parameter (StemA), (n) stem optical parameter (StemB), (o) soil optical parameter (SoilA), and (p) soil optical parameter (SoilB)

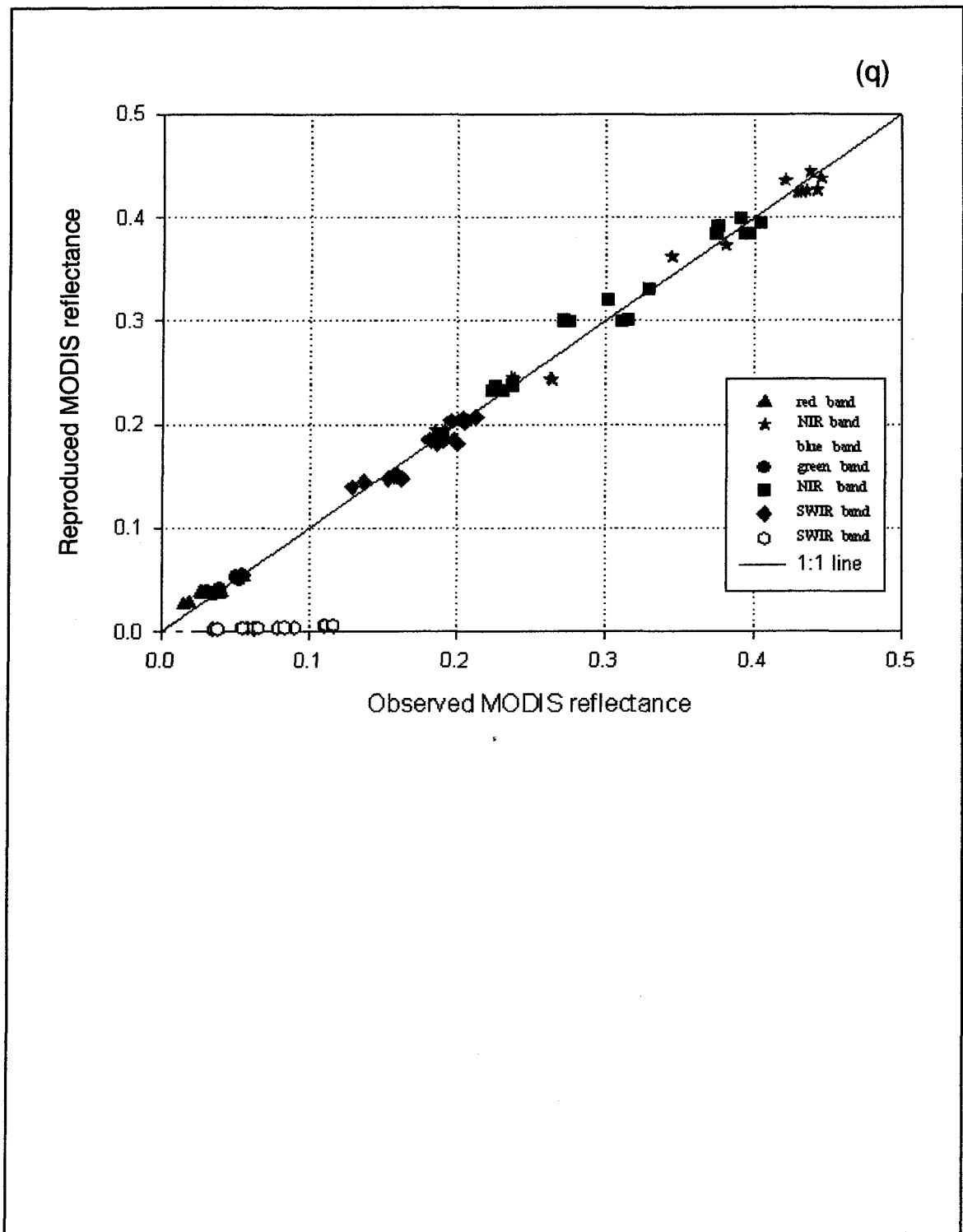


Figure 3.2 (continued) (q): a comparison between the reproduced reflectance using retrieved mean values of (a) – (p) and MODIS observed reflectance

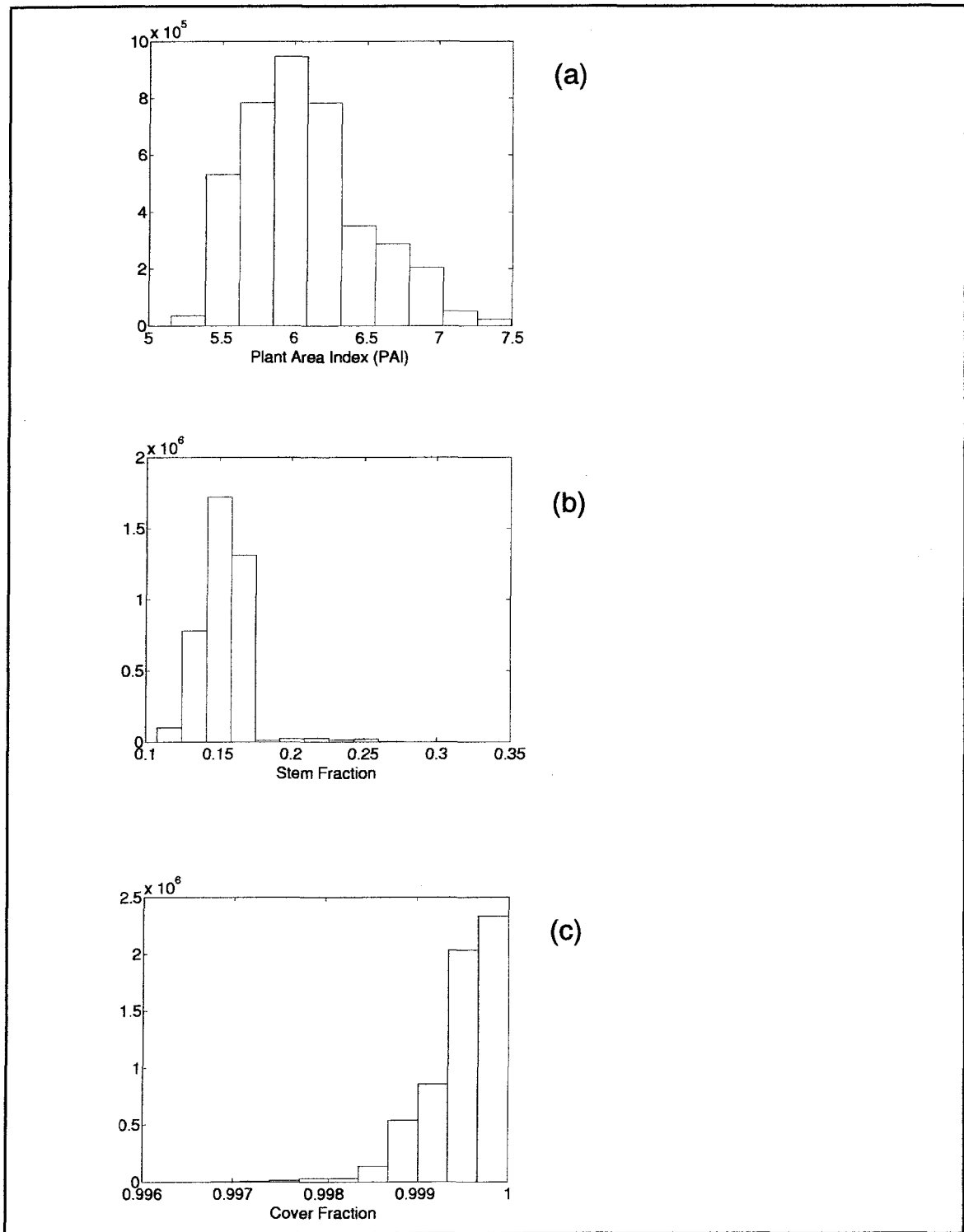


Figure 3.3 Retrieved results using MODIS bands except blue and SWIR<sub>2</sub> without consideration of brown pigment for the Harvard Forest for MODIS data collection from day of year (DOY) 201 to 214 in 2001: retrieved histograms: (a) plant area index (PAI), (b) stem fraction, and (c) cover fraction

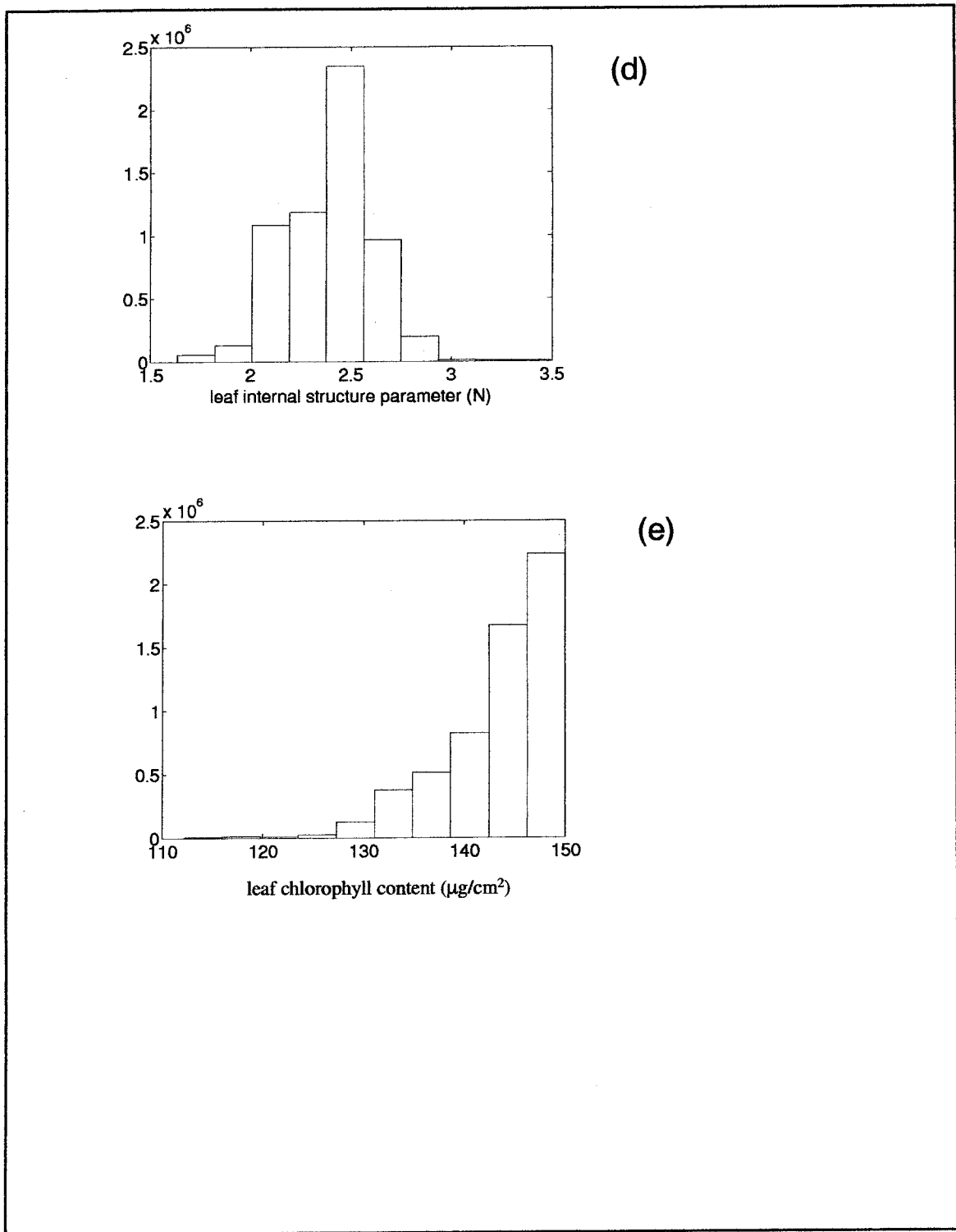


Figure 3.3 (continued) Retrieved histograms: (d) leaf internal structure parameter (N) , and (e) leaf chlorophyll content (C<sub>ab</sub>: μg/cm<sup>2</sup>)

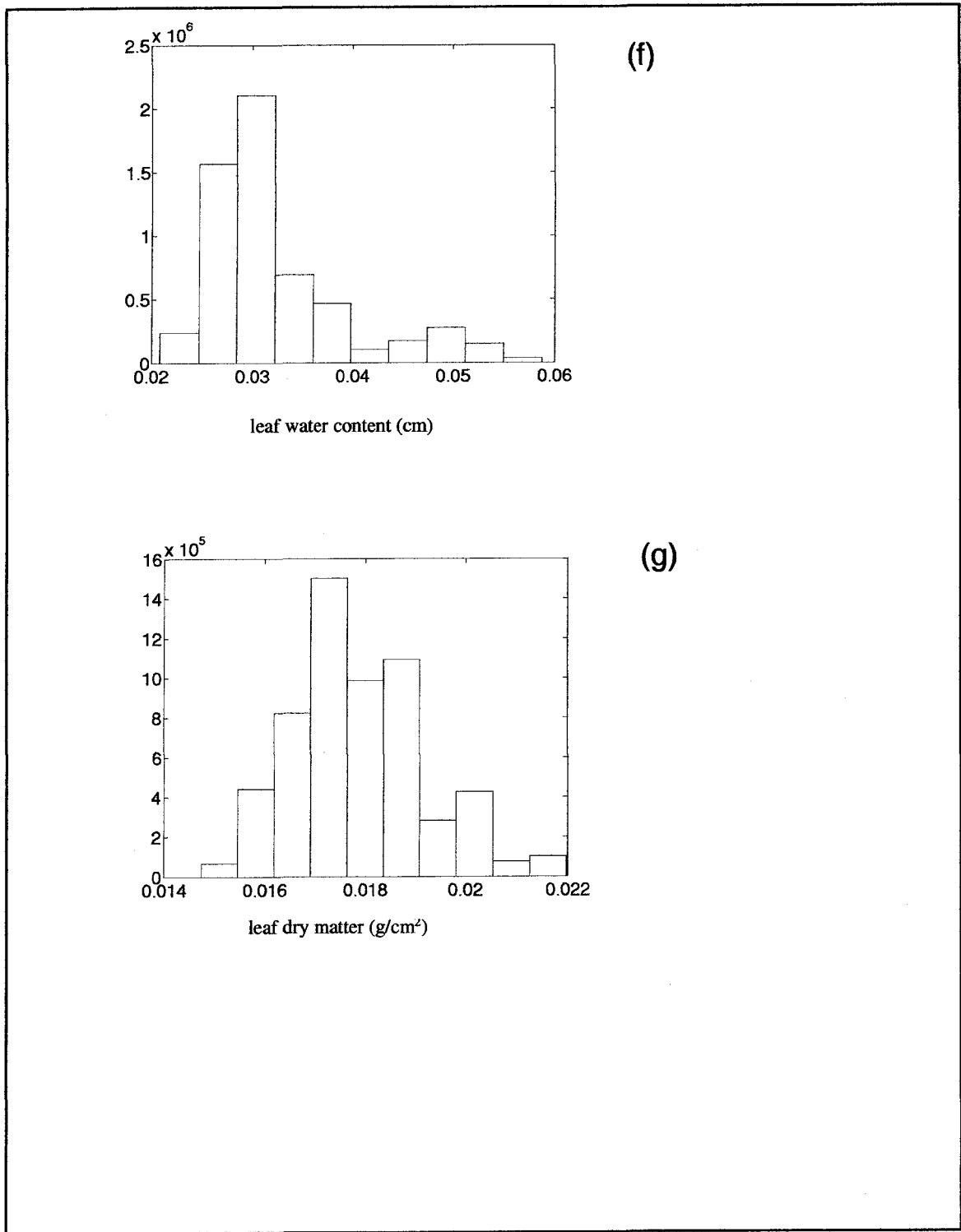


Figure 3.3 (continued) Retrieved histograms: (f) leaf water content ( $C_w$  : cm), and (g) leaf dry matter ( $C_m$  :  $g/cm^2$ )

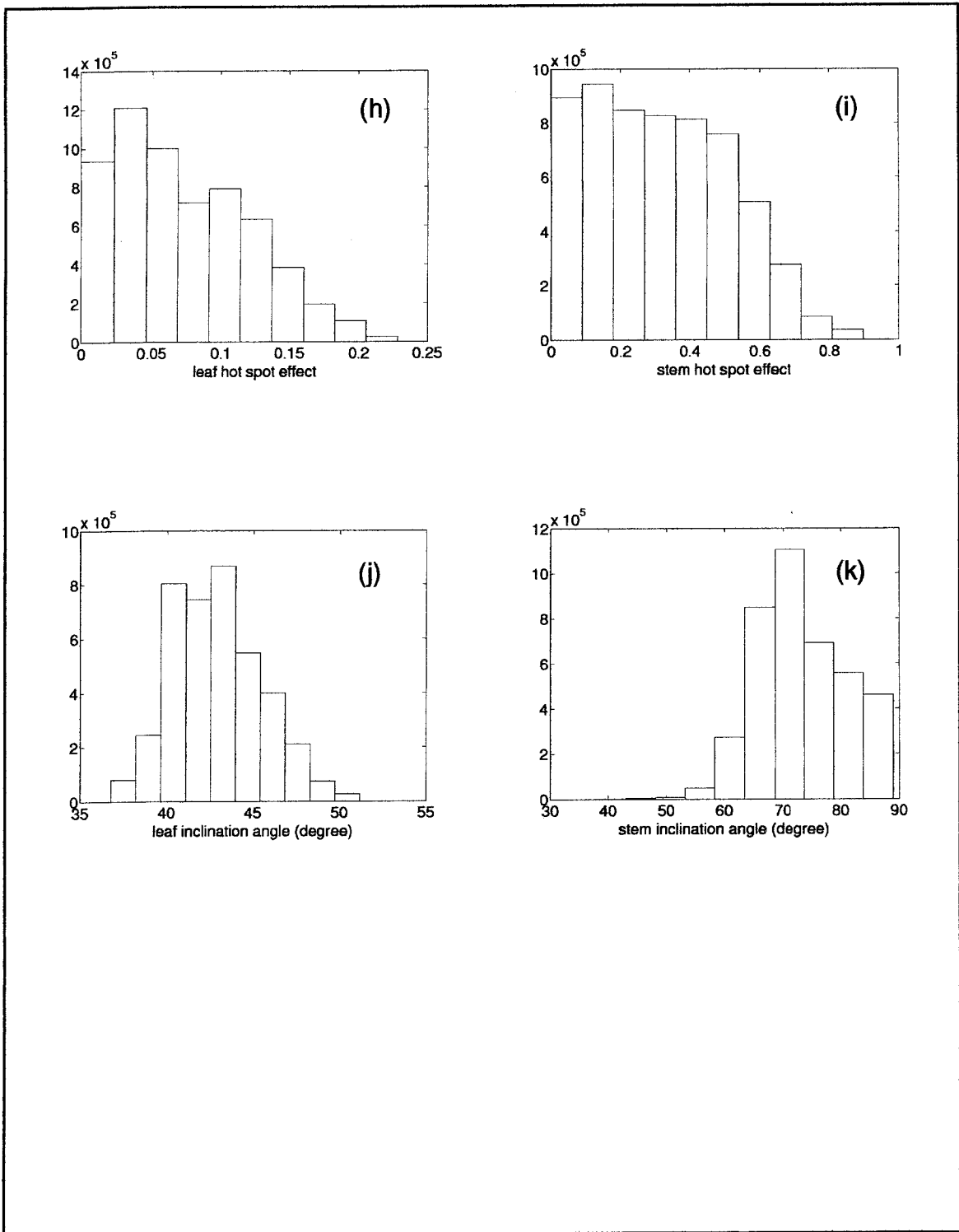


Figure 3.3 (continued) Retrieved histograms: (h) leaf hot spot parameter, (i) stem hot spot parameter, (j) leaf inclination angle (degree), and (k) stem inclination angle (degree)

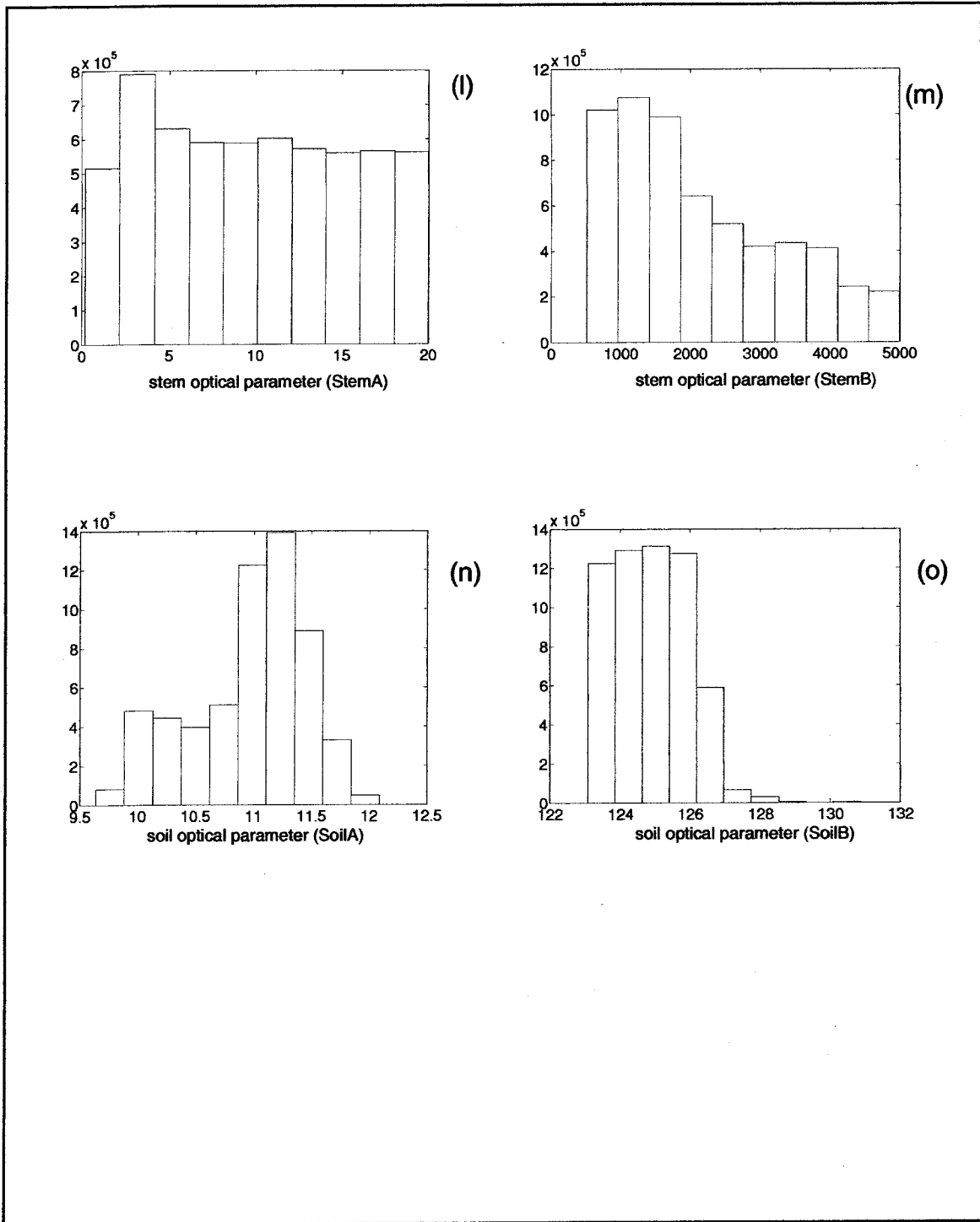


Figure 3.3 (continued) Retrieved histograms: (l) stem optical parameter (StemA), (m) stem optical parameter (StemB), (n) soil optical parameter (SoilA), and (o) soil optical parameter (SoilB)



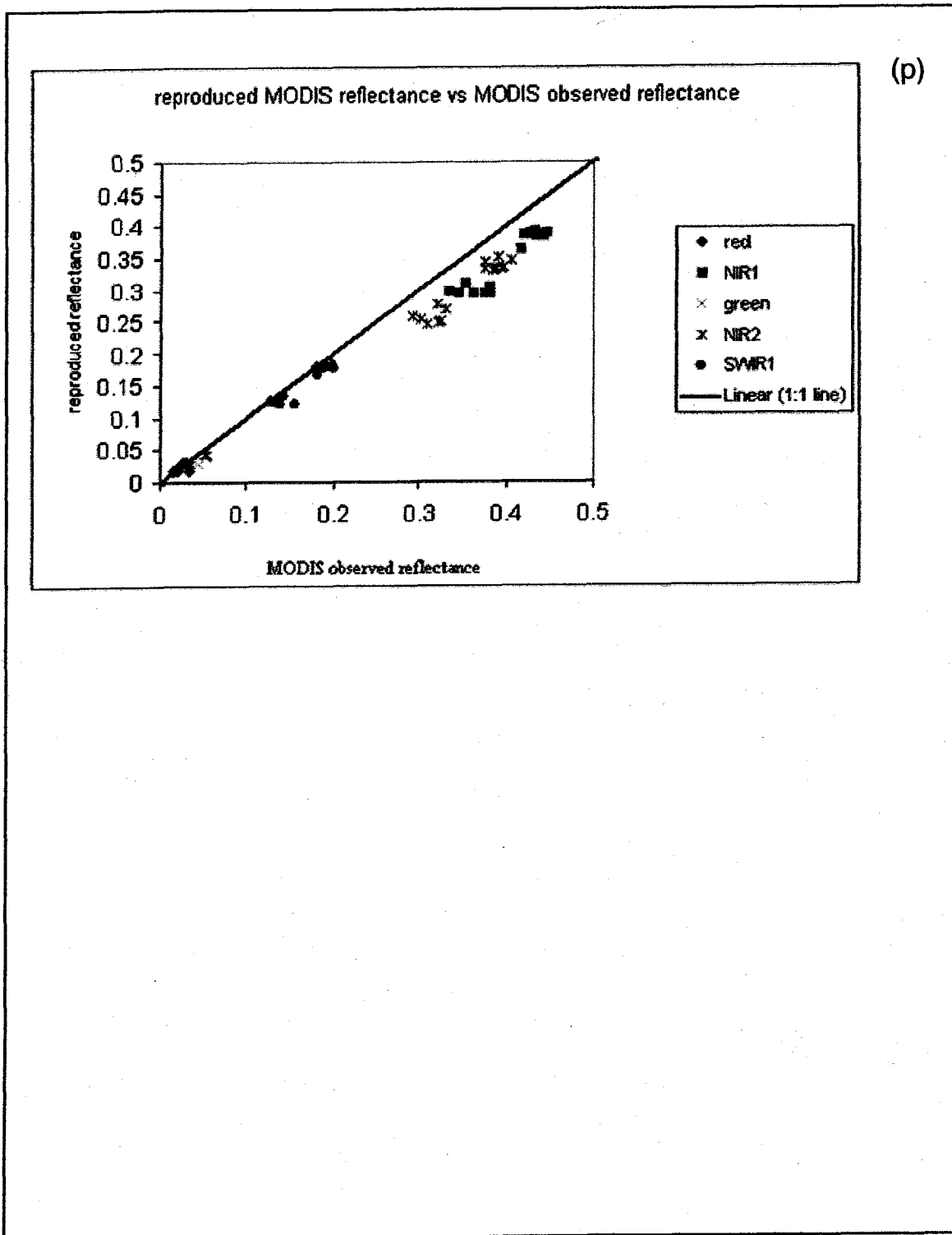


Figure 3.3 (continued) (p) a comparison between the reproduced reflectance using retrieved mean values of (a) – (o) and MODIS observed reflectance

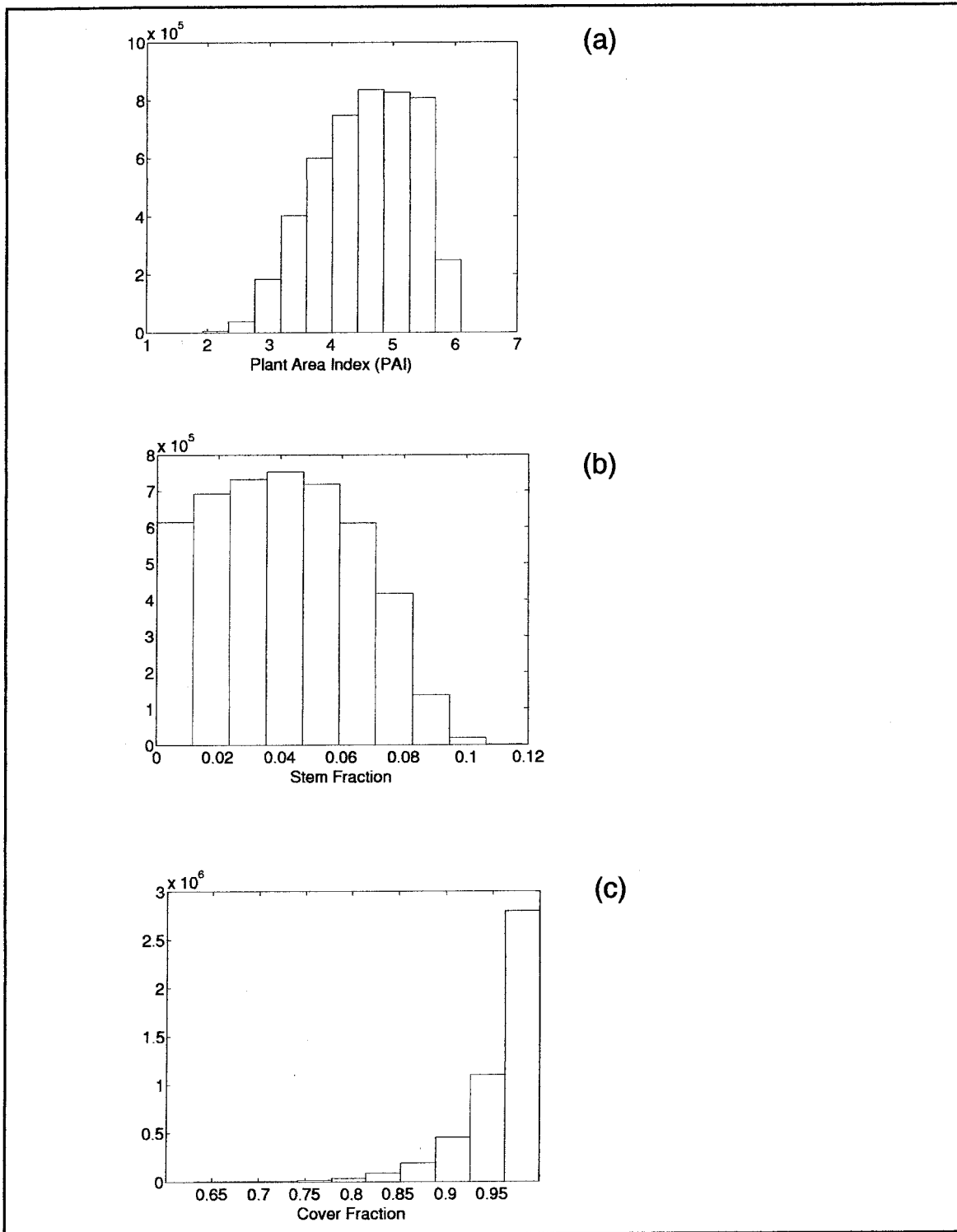


Figure 3.4 Retrieved results using MODIS bands except blue and SWIR<sub>2</sub> with consideration of brown pigments for the Harvard Forest for MODIS data collection from day of year (DOY) 201 to 214 in 2001: retrieved histograms: (a) plant area index (PAI), (b) stem fraction, and (c) cover fraction

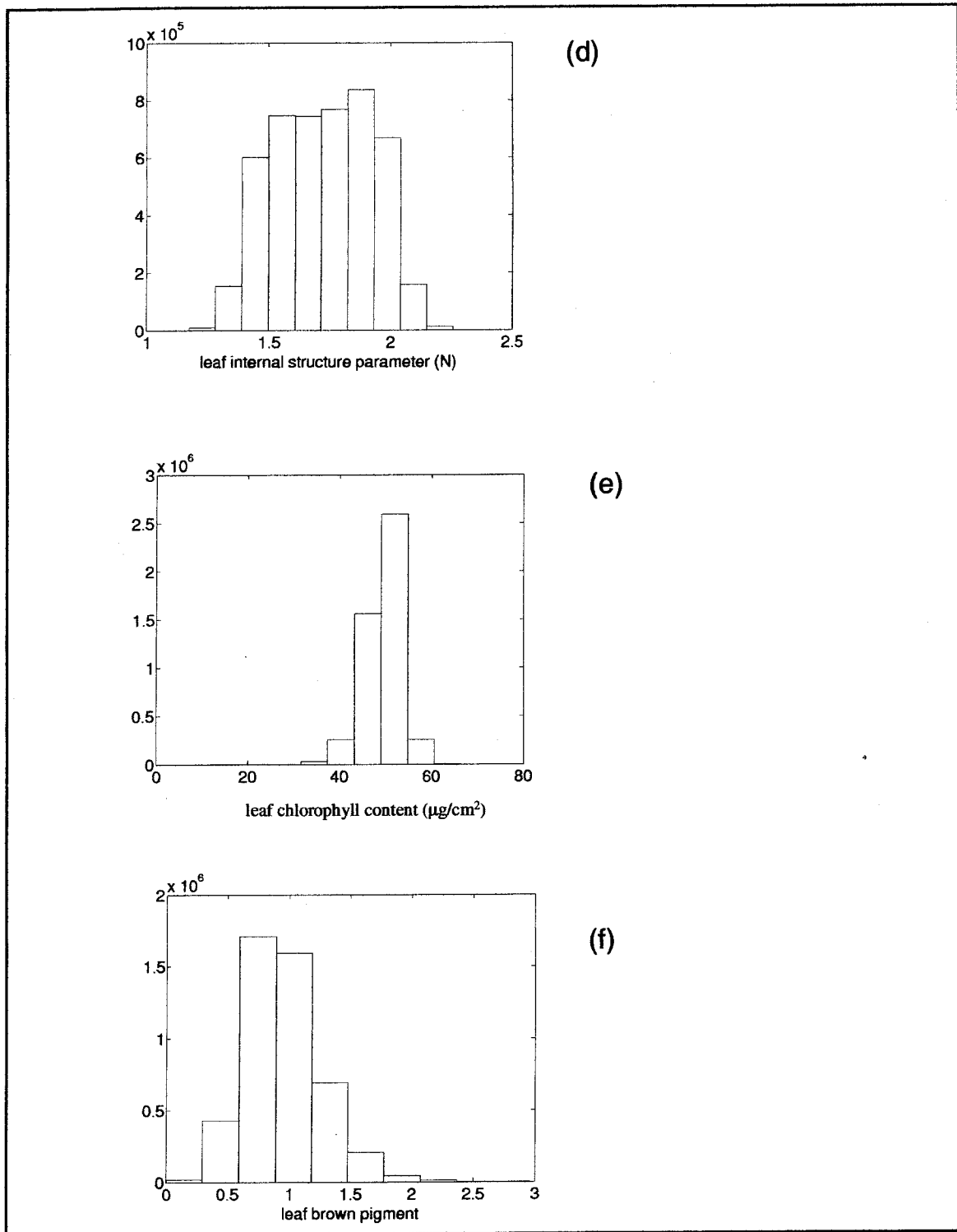


Figure 3.4 (continued) Retrieved histograms: (d) leaf internal structure parameter (N) , (e) leaf chlorophyll content ( $C_{ab}$ :  $\mu\text{g}/\text{cm}^2$ ), and (f) brown pigment

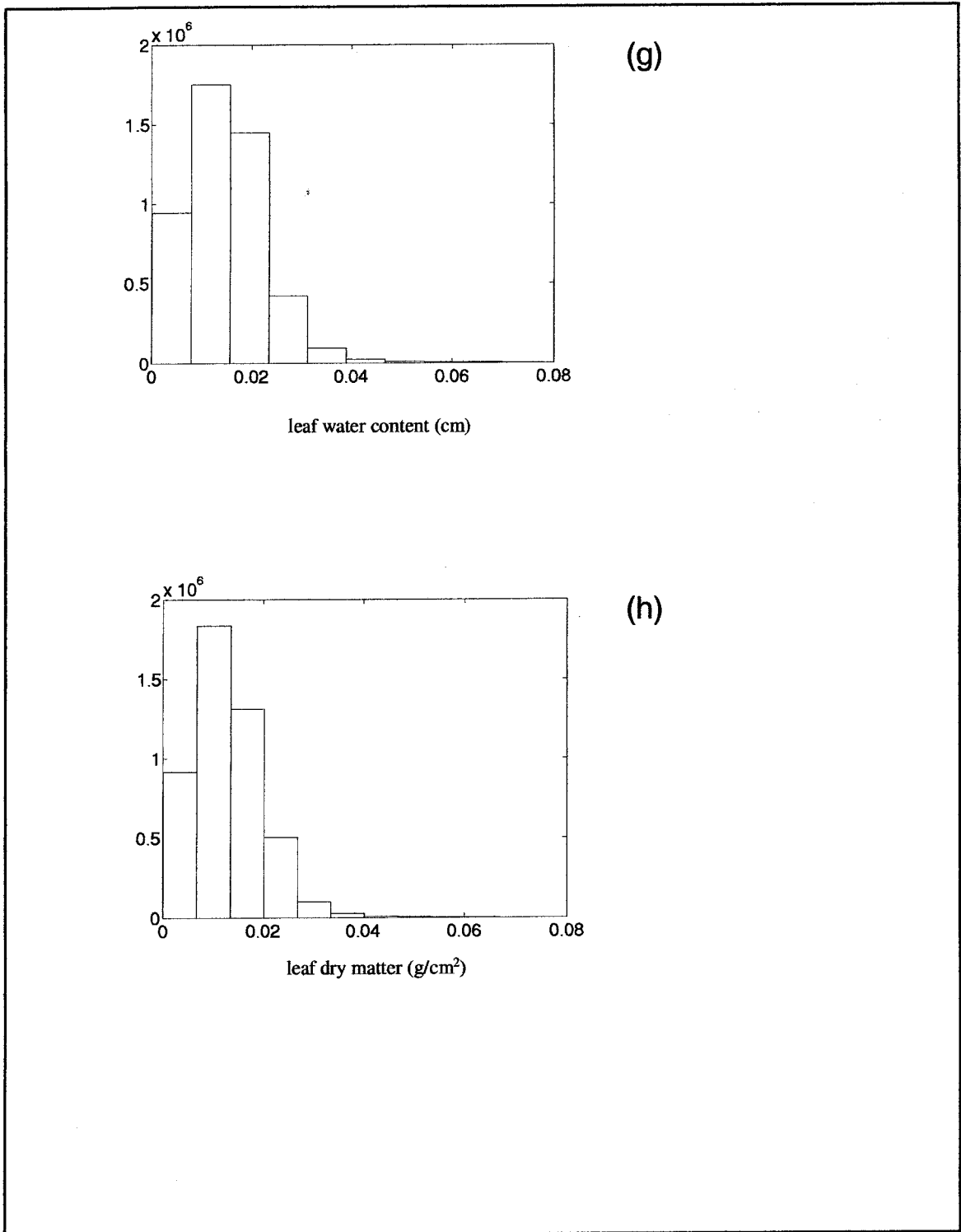


Figure 3.4 (continued) Retrieved histograms: (g) leaf water content ( $C_w$  : cm), and (h) leaf dry matter ( $C_m$  :  $g/cm^2$ )

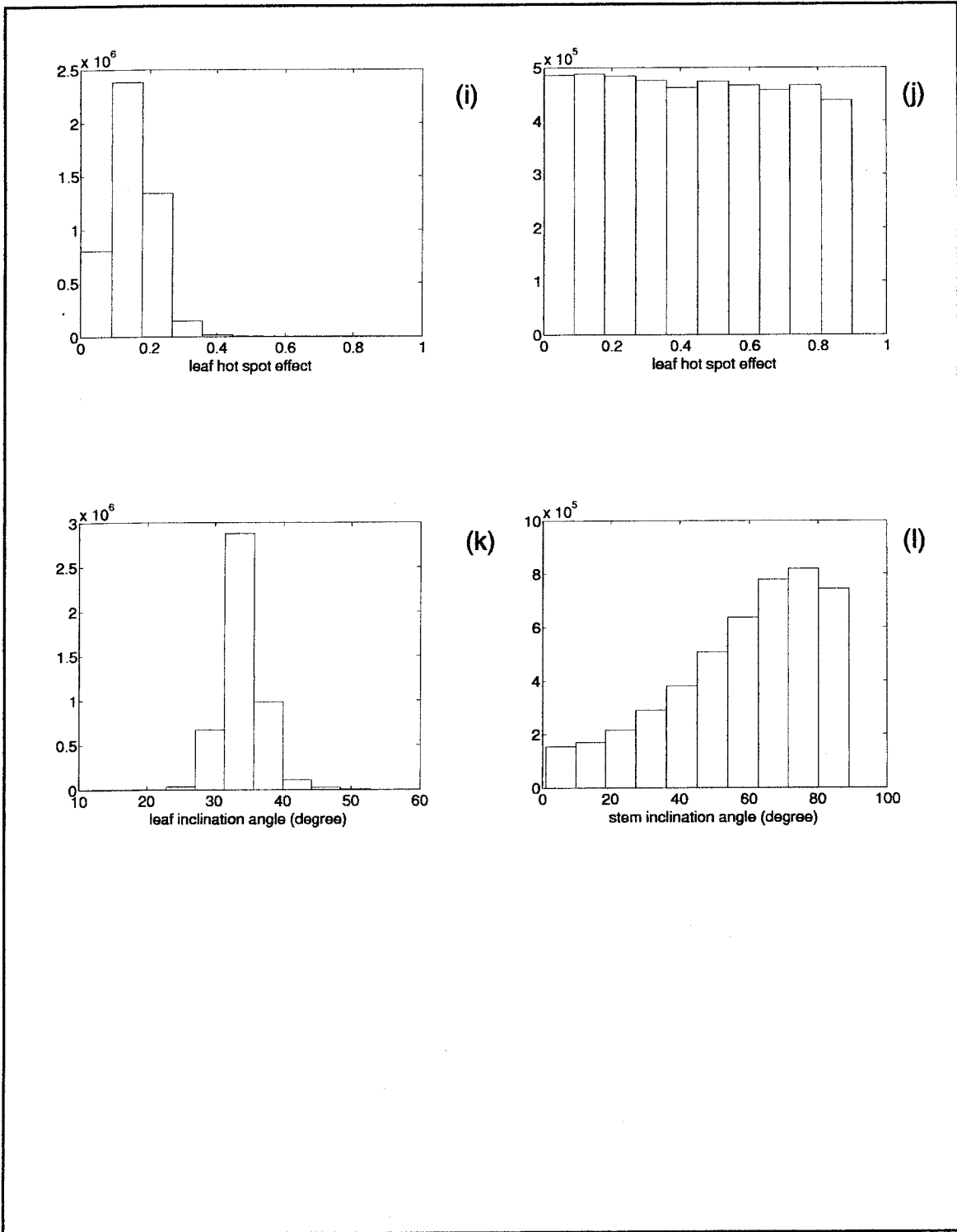


Figure 3.4 (continued) Retrieved histograms: (i) leaf hot spot parameter, (j) stem hot spot parameter, (k) leaf inclination angle (degree), and (l) stem inclination angle (degree)

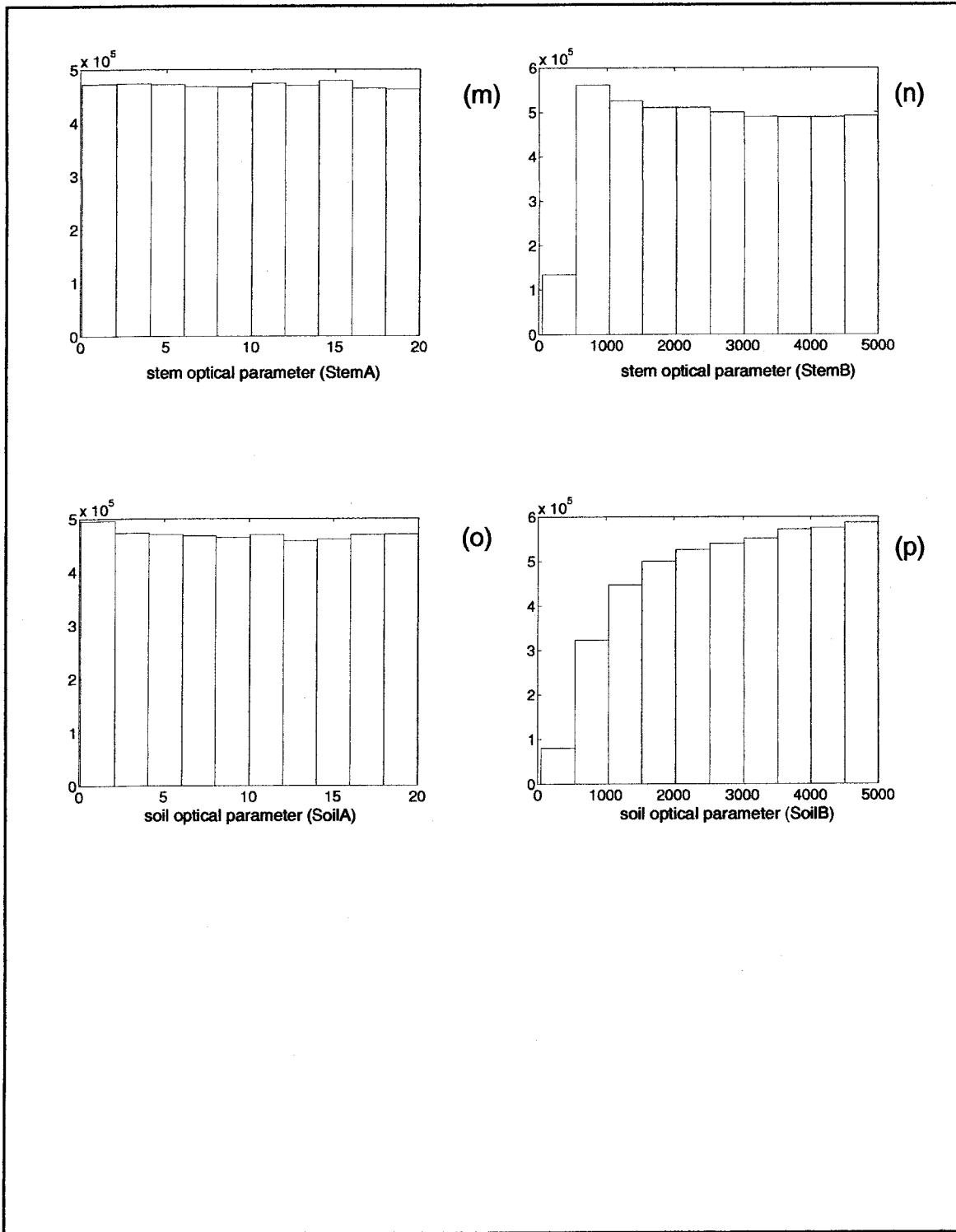


Figure 3.4 (continued) Retrieved histograms: (m) stem optical parameter (StemA), (n) stem optical parameter (StemB), (o) soil optical parameter (SoilA), and (p) soil optical parameter (SoilB)

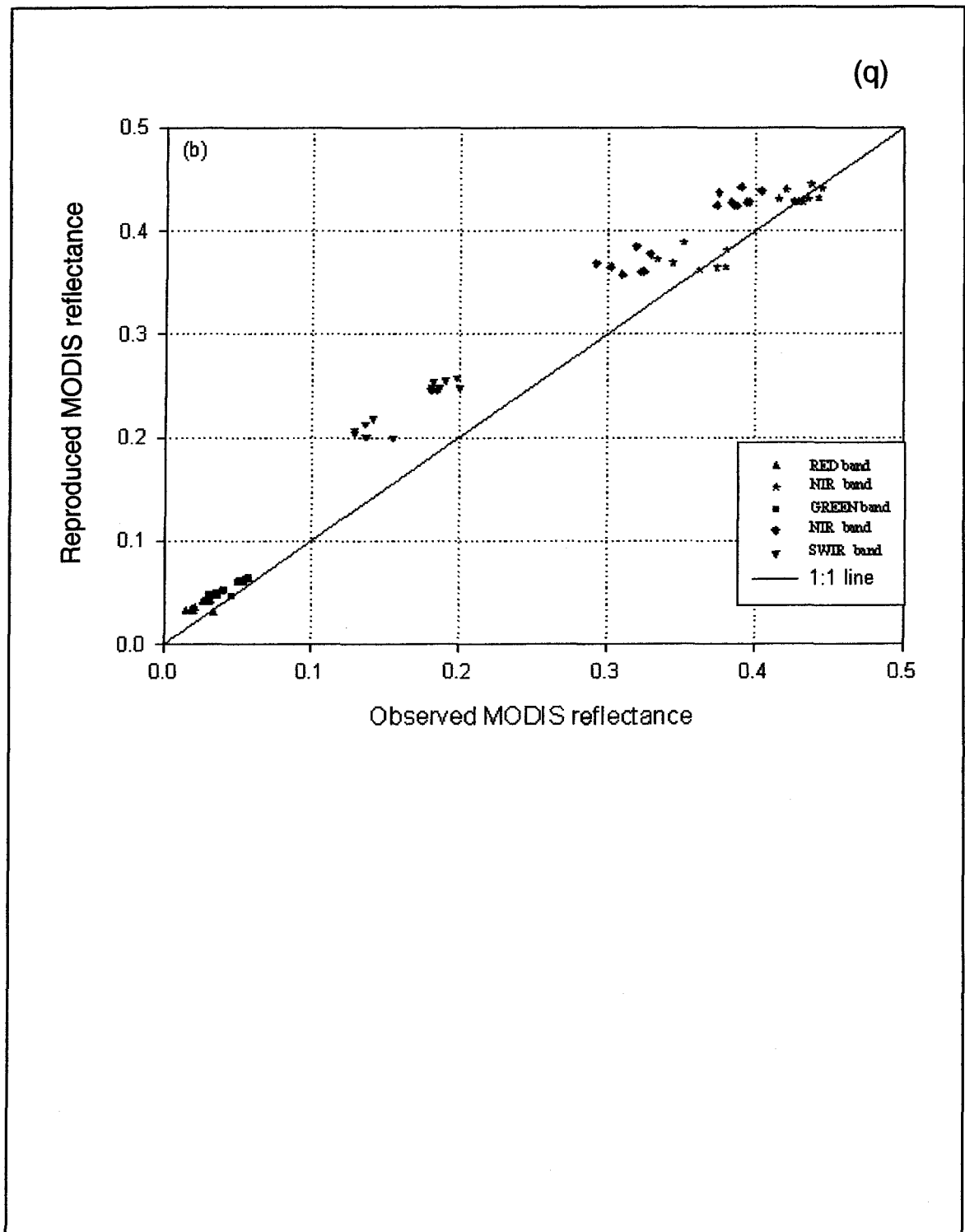


Figure 3.4 (continued) (q) comparison between the reproduced reflectance using retrieved mean values of (a) – (p) and MODIS observed reflectance

## CHAPTER 4

# ESTIMATING LIGHT ABSORPTION BY CHLOROPHYLL, LEAF AND CANOPY IN A DECIDUOUS BROADLEAF FOREST USING MODIS DATA AND A RADIATIVE TRANSFER MODEL<sup>1</sup>

### 4.1 Introduction

Gross primary production (GPP) is a key terrestrial ecophysiological process that links atmospheric composition and vegetation processes. One of the most important of these processes, plant photosynthesis, requires solar radiation in the 0.4-0.7  $\mu\text{m}$  range (also known as photosynthetically active radiation or PAR), water, carbon dioxide ( $\text{CO}_2$ ), and nutrients. The fraction of PAR absorbed by the vegetation canopy ( $\text{FAPAR}_{\text{canopy}}$ ) is therefore an important biophysical variable and is widely used in satellite-based Production Efficiency Models (Potter et al., 1993; Prince et al., 1995; Ruimy et al., 1996; Running et al., 2004) to estimate GPP or net primary production (NPP). In remote sensing studies,  $\text{FAPAR}_{\text{canopy}}$  is usually estimated as a linear or non-linear function of Normalized Difference Vegetation Index (NDVI) (Prince et al., 1995; Tucker, 1979).  $\text{FAPAR}_{\text{canopy}}$  is also related to leaf area index (LAI), and is estimated as a function of LAI and a light extinction coefficient in a number of process-based biogeochemical models (Ruimy et al., 1999). The LAI- $\text{FAPAR}_{\text{canopy}}$  and NDVI- $\text{FAPAR}_{\text{canopy}}$  relationships have been the

---

<sup>1</sup> This chapter is already published in *Remote Sensing of Environment* (2005), vol. 99, 357-371



dominant paradigm in the literature for estimating GPP and NPP of terrestrial vegetation at various spatial scales (Field et al., 1995; Running et al., 2004).

A vegetation canopy is composed primarily of photosynthetically active vegetation (PAV) and non-photosynthetic vegetation (NPV; e.g., senescent foliage, branches and stems). The presence of NPV has a significant effect on  $FAPAR_{canopy}$ . For example, in forests with an LAI less than 3.0, an earlier study (Asner et al., 1998b) found that stems increased canopy FAPAR by 10-40%. There is then, in principal, a need to partition  $FAPAR_{canopy}$  into the fractions of PAR absorbed by green leaves and by NPV.

Furthermore, it is important to note that a green leaf is composed of chlorophyll and various proportions of non-photosynthetic components (e.g., other pigments in the leaf, primary/secondary/tertiary veins, and cell walls). Non-photosynthetic absorption in PAR wavelengths can vary in magnitude (e.g., 20-50%) among different species, leaf morphology, leaf age and growth history (Hanan et al., 1998; Lambers et al., 1998; Hanan et al., 2002). We argue that  $FAPAR_{canopy}$  should be partitioned into the fractions of PAR absorbed by chlorophyll ( $FAPAR_{chl}$ ) and by NPV ( $FAPAR_{NPV}$ , including all the non-chlorophyll pigments in leaf, cell walls, veins, branches and stems).

Only the PAR absorbed by chlorophyll (a product of  $FAPAR_{chl} \times PAR$ ) is used for photosynthesis. Therefore, remote sensing-driven biogeochemical models that use  $FAPAR_{chl}$  in estimating GPP are more likely to be consistent with plant photosynthesis processes (Xiao et al., 2004b, b). It is important to understand to what extent  $FAPAR_{canopy}$  can be partitioned into  $FAPAR_{chl}$  and  $FAPAR_{NPV}$  given imperfect models and data. In an earlier study (Depury et al., 1997), a process-based leaf photosynthesis model estimated PAR effectively absorbed by PSII system per unit leaf area. However, the partitioning

issue has not been studied extensively in both remote sensing and ecological communities that focus on large scales.

Quantifying the temporal evolution of  $FAPAR_{chl}$  for a forest ecosystem represents an important challenge for remote sensing and ecology researchers, as it is extremely difficult to directly measure  $FAPAR_{chl}$  and  $FAPAR_{NPV}$  at the leaf and canopy levels on large scales over plant growing seasons. To our knowledge, no field and laboratory experiments to measure  $FAPAR_{chl}$  at the leaf and canopy levels over plant growing seasons have been reported, and similarly we found no published efforts to calculate  $FAPAR_{chl}$  with physics-based radiative transfer models.

In this study, we aim to develop a theoretical and technical framework for quantifying and evaluating the fractions of PAR absorbed by chlorophyll, leaf and canopy. The specific objectives of this study are twofold: (1) to clarify the concepts of  $FAPAR_{chl}$ ,  $FAPAR_{leaf}$  and  $FAPAR_{canopy}$ ; (2) to explore the potential of estimating  $FAPAR_{canopy}$ ,  $FAPAR_{leaf}$  and  $FAPAR_{chl}$ , using a coupled leaf-canopy radiative transfer model with multiple daily images from the MODerate resolution Imaging Spectroradiometer (MODIS) onboard NASA Terra satellite. We used a coupled leaf-canopy radiative transfer model (PROSPECT model +SAIL-2 model) to calculate  $FAPAR_{chl}$ ,  $FAPAR_{canopy}$  and  $FAPAR_{leaf}$ . These models have been discussed extensively in the published literature, both separately and in combination (Verhoef, 1984; Kuusk, 1985; Verhoef, 1985; Jacquemoud et al., 1990; Braswell et al., 1996; Jacquemoud et al., 1996; Baret et al., 1997; Gond et al., 1999; Jacquemoud et al., 2000; Weiss et al., 2000; Bacour et al., 2002a; Combal et al., 2002; Verhoef et al., 2003; Zarco-Tejada et al., 2003; Di Bella et al., 2004). As a case study, we selected a deciduous broadleaf forest at the

Harvard Forest in Massachusetts, USA, where earlier studies reported field-based observations of leaf chlorophyll content (Waring et al., 1995) and LAI (Cohen et al., 2003; Xiao et al., 2004c). This radiative transfer based modeling exercise will help us to address an important scaling issue – light absorption from chlorophyll to leaf and to canopy. Our analysis also provides guidance for designing and conducting field measurement and observations of forest canopies in the near future.

## **4.2 Description of the radiative transfer model and the inversion algorithm**

### **4.2.1 Brief description of the PROSPECT+SAIL-2 model**

The PROSPECT model is a leaf radiative transfer model. Previous studies used the PROSPECT model with four variables - leaf internal structure variable ( $N$ ), leaf chlorophyll content ( $C_{ab}$ ), leaf dry matter content ( $C_m$ ), and leaf water thickness ( $C_w$ ) (Jacquemoud et al., 1990; Hosgood et al., 1995; Demarez et al., 1999; Newnham et al., 2001). A number of other studies used the PROSPECT model with five variables - leaf internal structure variable ( $N$ ), leaf chlorophyll content ( $C_{ab}$ ), leaf dry matter content ( $C_m$ ), leaf water thickness ( $C_w$ ) and leaf brown pigment ( $C_{brown}$ ) (Baret et al., 1997; Verhoef et al., 2003; Di Bella et al., 2004). We used the five-variable PROSPECT model in this study because the addition of brown pigment is useful for discriminating between photosynthetic and non-photosynthetic light absorption.

The SAIL (Scattering from Arbitrarily Inclined Leaves) model is a canopy radiative transfer model. The SAIL model has been developed by several earlier researchers, evolving gradually over time with minor changes reflecting individual study objectives (e.g., Goel et al., 1984c; Verhoef, 1984; Badhwar et al., 1985; Goel et al., 1985;

Kuusk, 1985; Verhoef, 1985; Major et al., 1992; Braswell et al., 1996; Andrieu et al., 1997; Jacquemoud et al., 2000). In this study we used the version of SAIL presented by Braswell et al. (SAIL-2; Braswell et al., 1996). The SAIL-2 model decomposes a vegetation canopy into stems and leaves. In a typical parameterization, stems have spectral properties that are more similar to soil and litter than leaves. Leaf and stem mean inclination angles, and the self-shading effect of both leaves and stems are also considered.

In this study, we coupled the modified PROSPECT model with the SAIL-2 model (hereafter called PROSAIL-2) by replacing the leaf reflectance component in the SAIL-2 model with the five-variable PROSPECT model. The coupled PROSAIL-2 model was used to describe optical characteristics (reflectance, absorption and transmittance) of the canopy and its components. The PROSAIL-2 model has three groups of parameters: (1) observation viewing geometry variables; (2) an atmospheric condition (visibility) variable; and (3) biophysical and biochemical variables (Table 1). Table 1 lists the search range of the sixteen biophysical/ biochemical variables, based on an extensive literature review. The sixteen biophysical and biochemical variables are plant area index (PAI), stem fraction (SFRAC), cover fraction (CF), stem inclination angle (STINC), stem BRDF effect variable (STHOT), leaf inclination angle (LFINC), leaf BRDF effect variable (LFHOT), five leaf variables that simulate leaf optical properties ( $N$ ,  $C_{ab}$ ,  $C_m$ ,  $C_w$ ,  $C_{brown}$ ), two soil/litter variables that simulate soil/litter optical properties ( $SOIL_A$ ,  $SOIL_B$ ), and two stem variables that simulate stem optical properties ( $STEM_A$ ,  $STEM_B$ ). Because the MODIS data used in the study were atmospherically corrected, we set the

atmospheric visibility variable (VIS, in Table 4.1) to be large and constant throughout this analysis.

#### 4.2.2 Description of inversion algorithm -- the Metropolis algorithm

Inversion of a radiative transfer model is computationally intensive and requires careful choices of optimization procedures. Iterative steepest-descent optimization procedures, the most commonly used approaches to invert radiative transfer models (e.g., Bacour et al., 2002a), were not used in this study. These procedures are local optimization techniques with limited potential to locate globally optimal solutions. For example, if there are a few minimum points within a search space, the iterative procedures could offer a local extreme-point solution and might fail to provide a global extreme-point solution given an initial guess. As an alternative, a method based on the Metropolis algorithm (Metropolis et al., 1953; Hurtt et al., 1996; Braswell et al., 2005) was employed. This method estimates posterior probability distributions of the variables and thus can provide estimates of uncertainty (such as standard deviations and confidence intervals) of individual variables, by inspection of the retrieved distributions. The Metropolis algorithm is relatively computationally intensive, owing to the need for simulation of a large number of samples required to obtain a reliable estimate of the variables' distributions.

The Metropolis algorithm (Metropolis et al., 1953), is a type of Markov Chain Monte Carlo (MCMC) estimation procedure. At each step out of a predetermined number of iterations, the algorithm uses the current variable estimate to randomly generate a new "proposal" estimate in variable space. This new variable estimate will be the input for a

new model run. Model-retrieved and observed reflectance values are used to calculate the likelihood of an error probability model. The Metropolis algorithm then accepts the new variable estimate with a certain probability. The resulting Markov Chain of accepted variable values converges to the posterior distribution of the variables conditional on the observations after a transient “burn-in” period. MCMC theory assures that such a sampling scheme provides Markov chains whose values represent draws from the posterior distributions. In the following formalism,  $\Pr(\cdot)$  denotes probability in a general sense, or more specifically, the value of a probability density function.  $\Pr(v)$  denotes the prior distribution assumed for the set of variables.  $\Pr(v_{\text{new}}|\text{data})$  and  $\Pr(v_{\text{old}}|\text{data})$  refer to the conditional probabilities of “new” and “old” variable estimates (variable points) given the known “data”.

According to Bayes’ theorem,

$$\Pr(v | \text{data}) \propto \Pr(v)\Pr(\text{data} | v)$$

$$\text{Let } L(v) = \Pr(\text{data} | v)$$

$$\Pr(v | \text{data}) \propto \Pr(v)L(v)$$

where  $L(\cdot)$  is the likelihood function. In this study we assume a set of independent uniform prior distributions for the variables. Let  $X_i = [x_{i1}, \dots, x_{ip}]$  ( $p > 1$ ),  $i$  is the subscript of data point, subscripts 1, ...,  $p$  mean spectral bands, and  $x$  is reflectance.

This study assumes that the observed spectral values  $X_i$  differ from the model predicted values  $U_i = [u_{i1}, \dots, u_{ip}]$  according to a mean zero  $p$ -variate Gaussian error model that results in the likelihood function

$$L = \prod_{i=1}^n \frac{1}{(\sqrt{2\pi})^p |\Sigma|^{1/2}} e^{-(X_i - U_i)' \Sigma^{-1} (X_i - U_i) / 2} \quad (1)$$

where  $n$  is the number of data points and  $\Sigma$  is the variance-covariance matrix of  $X$ .  $\Sigma$  is estimated by the usual sample variances and covariances in each step of the algorithm:

$$\begin{aligned} \Sigma_e &= (s_{ij})_{p \times p} \\ s_{ij} &= \frac{1}{n} \sum_{k=1}^n (x_{ki} - u_{ki})(x_{kj} - u_{kj}) \quad i, j = 1, \dots, p \end{aligned} \quad (2)$$

The natural logarithm of the likelihood, the “log-likelihood” ( $\log(L)$ ), is used in the algorithm during its operation (e.g., Bishop, 1995).

The algorithm defines the probability to accept the new point as following:

$$\Pr_{accept} = \min \left( 1, \frac{\Pr(v_{new} | data)}{\Pr(v_{old} | data)} \right) \quad (3)$$

If the algorithm accepts the new point, it will become the “old” point in next iteration; otherwise, the old point will still be the “old” point in next iteration.

To accelerate the speed of convergence of the Metropolis algorithm, we modified the adaptive algorithm used in other studies (e.g., Hurtt et al., 1996; Braswell et al., 2005) as following:

In each iteration, one variable is selected to change as

$$v_{new,s} = v_{old,s} + r \times (v_{max,s} - v_{min,s}) \quad (4)$$

where  $s=1, \dots, 16$ , is the number of variables in PROSAIL-2 model that are allowed to search for solutions,  $r$  is randomly selected at each step between  $\pm 0.5 \cdot T_s$ ,  $v_{max,s}$ ,  $v_{min,s}$  are the maximum and minimum values allowed to search, and  $T_s$  is temperature. If  $v_{new,s}$  is

accepted, then  $T_s$  is increased by a factor of 1.006569. If it is rejected, then  $T_s$  is decreased by a factor of 0.99. By changing the *temperatures* in this way, the  $T_s$  ( $s=1, \dots, 16$ ) of all variables are adjusted until varying any given variable leads to acceptance of about 23% to 44% of the time, which is considered an ideal acceptance rate for the Metropolis algorithm (Gelman et al., 2000).

#### 4.2.3 Calculation of $FAPAR_{canopy}$ , $FAPAR_{leaf}$ , and $FAPAR_{chl}$

To calculate  $FAPAR_{chl}$ ,  $FAPAR_{leaf}$  and  $FAPAR_{canopy}$  using the PROSAIL-2 model, we need to know the values of the input variables used in the model. Our strategy is to first invert the biophysical and biochemical variables using the coupled PROSAIL-2 model with observed spectral reflectance data (reflectance plus relative observation geometry), and then to calculate  $FAPAR_{chl}$ ,  $FAPAR_{leaf}$  and  $FAPAR_{canopy}$  using forward simulations.

We calculated  $FAPAR_{canopy}$  (Goward et al., 1992),  $FAPAR_{leaf}$  (Braswell et al., 1996), and  $FAPAR_{chl}$  (see equations 5 - 9) using the PROSAIL-2 model with the variable values from the inversion.

$$FAPAR_{canopy} = \frac{APAR_{canopy}}{PAR_0} \quad (5)$$

$$FAPAR_{leaf} = \frac{APAR_{leaf}}{PAR_0} \quad (6)$$

$$FAPAR_{chl} = \frac{APAR_{chl}}{PAR_0} \quad (7)$$

$$APAR_{canopy} = APAR_{leaf} + APAR_{stem} \quad (8)$$



$$APAR_{leaf} = APAR_{chl} + APAR_{dry\ matter} + APAR_{brown\ pigment} \quad (9)$$

where  $PAR_0$  is the incoming PAR at the top of the canopy, and APAR is the absorbed PAR.  $APAR_{canopy}$ ,  $APAR_{leaf}$ ,  $APAR_{stem}$ ,  $APAR_{chl}$ ,  $APAR_{dry\ matter}$ , and  $APAR_{brown\ pigment}$  are absorbed PAR by canopy, leaf, stem, chlorophyll in leaf, dry matter in leaf, and brown pigment in leaf, respectively.

#### 4.2.4 Inversion of the PROSAIL-2 model with simulated data

After integration of the coupled PROSAIL-2 model with the Metropolis inversion algorithm, we conducted a number of model inversion runs with simulated data to examine the performance of the modeling framework. Here we report results from one typical group of these model-simulated data (Table 4.2). We used the values of individual variables in Table 4.2 to simulate reflectance as the first simulated data set. For the second simulated data set, we added random noise (mean=0, standard deviation=5% of reflectance) to represent error in the reflectance prior to inversion. In the third simulated data set, we added a different amount of random noise (mean=0, standard deviation=10% of reflectance) to the reflectance. Inversion of the PROSAIL-2 model was conducted for the three simulated data sets, using the MCMC algorithm (see Section 2.2). All the sixteen variables (Table 4.1) were estimated simultaneously for the three simulated data sets.

The strength of the Metropolis algorithm is that it provides posterior distributions of retrieved variables, which present a detailed picture of the behavior and uncertainty of individual variables, conditioned on both the model and the observed data. Therefore the retrieved distributions provide information about the parameter sensitivity of the

PROSAIL-2 model. For simplicity, we have grouped variable behavior into three major categories: well-constrained, edge-hitting and poorly-constrained (Braswell, et al., 2005). The “well-constrained” variables usually have a well-defined distribution, with small standard deviations relative to their allowable ranges. The “poorly-constrained” variables have relatively flat distributions with large standard deviations relative to their allowable ranges. Edge-hitting variables are those for which the modes of their retrieved values occurred near one of the edges of their allowable ranges and most of the retrieved values were clustered near this edge. As shown in Table 4.2, among the 16 biophysical/biochemical variables in the PROSAIL-2 model, nine variables had “well-constrained” distributions, six variables had “poorly-constrained” distributions, and one variable had “edge-hitting” distribution. By forward calculation with the retrieved distributions, we found that  $FAPAR_{canopy}$ ,  $FAPAR_{leaf}$  and  $FAPAR_{chl}$  were also “well-constrained”. Because of page limits we did not present the graphs to show the histograms of individual variables from the simulated data. Graphs showing the histograms of individual variables retrieved from the MODIS data (see Section 3.2) illustrate the parameter behaviors we discussed in this section.

### **4.3 Description of the Harvard Forest site and multiple daily MODIS data collections**

#### **4.3.1 Brief description of the Harvard Forest site**

The Harvard Forest eddy flux tower site (42.54°N and 72.18°W, 180 - 490 m elevation) is located in western Massachusetts, USA. The vegetation is primarily deciduous broadleaf forest, dominated by red oak (*Quercus rubra*), red maple (*Acer*

*rubrum*), black birch (*Betula lenta*) and white pine (*Pinus strobus*). There are also some evergreen needleleaf species within the forest, for example, eastern hemlock (*Tsuga canadensis*) (Waring et al., 1995). Altogether, deciduous broadleaf forest occupies 56% of the land, conifer forest occupies 12%, and mixed forest occupies 20% (Turner et al., 2003). The canopy height is approximately 20 –24m. Soils are mainly sandy loam glacial till with some alluvial and colluvial deposits. The climate is cool, moist temperate with July mean temperature 20°C. Annual mean precipitation is about 110 cm, and the precipitation is distributed approximately evenly throughout the year. Most areas are at least moderately well-drained (Wofsy et al., 1993; Goulden et al., 1996; Barford et al., 2001). The major deciduous species of Harvard Forest commenced senescence on about September 17<sup>th</sup> in 1991 and 1992 (Bassow et al., 1998). Intensive field work has been conducted at the site for measuring leaf chlorophyll content by species (Waring et al., 1995) and LAI (Cohen et al., 2003; Xiao et al., 2004c). These field data are useful and available for evaluating estimated values of chlorophyll content and LAI from inversion of the PROSAIL-2 model.

#### 4.3.2 Collection of multiple daily MODIS data over the Harvard Forest site

Three MODIS standard products are used in this study: MODIS daily surface reflectance (MOD09GHK, v004), MODIS daily observation viewing geometry (MODMGGAD, v004), and MODIS daily observation pointers (MODPTHKM, v004). The MODIS daily surface reflectance product has surface reflectance values of seven spectral bands (500m spatial resolution) that are primarily designed for study of vegetation and land surface: red (620-670 nm), blue (459 – 479 nm), green (545-565 nm),

near infrared (NIR<sub>1</sub>, 841-875 nm, and NIR<sub>2</sub>, 1230 – 1250 nm), short-wave infrared (SWIR<sub>1</sub>, 1628 – 1652 nm, and SWIR<sub>2</sub>, 2105-2155 nm). The MODIS daily observation viewing geometry product contains observation viewing geometry information (view zenith angle, view azimuth angle, sun zenith angle and sun azimuth angle) at a nominal 1-km scale. The MODIS daily observation pointers product provides a reference, at the 500 m scale, to observations that intersect each pixel of MODIS daily surface reflectance product in MODIS daily observation viewing geometry product (personal communication with Dr. Robert Wolfe). All these three MODIS data products are freely available at USGS EROS Data Center (<http://www.edc.usgs.gov/>).

The quality control (QC) data layer from the MODIS daily surface reflectance product includes information about errors and missing data in the daily surface reflectance product, for each of the seven MODIS bands, as well as information about whether an atmospheric correction was performed, and information about whether an adjacency correction was performed. If the QC value indicates any quality problem, the observation was not used in our analysis. In addition, we tried to avoid residual cloud-contaminated observations by carefully screening reflectance values of the MODIS blue band (459 – 479 nm). The reflectance of forested and other vegetated areas is generally less than 0.05 (Kaufman et al., 1997) under cloud-free conditions. If the MODIS blue band reflectance is greater than 0.05, and the QC flag indicates no quality problem, the observation is still excluded from the analysis. In addition, the blue band is very sensitive to residual aerosol, and the SWIR<sub>2</sub> band is very sensitive to subpixel water bodies (King et al., 1999). Therefore, both the blue and SWIR<sub>2</sub> bands were not used for inversion of PROSAIL-2 model. In this study, we used information from the other five MODIS bands

to invert PROSAIL-2 model. Thus, in Equations (1) and (2),  $p$  is equal to five,

$X_i = [x_{i1}, x_{i2}, x_{i3}, x_{i4}, x_{i5}]$ , and  $U_i = [u_{i1}, u_{i2}, u_{i3}, u_{i4}, u_{i5}]$ , where subscripts 1, 2, 3, 4, 5 refer to red, NIR<sub>1</sub>, green, NIR<sub>2</sub>, and SWIR<sub>1</sub> bands of MODIS, respectively.

We acquired daily MODIS data (year 2001 through year 2003) from the NASA data archive, for an area containing the Harvard Forest site. To invert all the sixteen variables of the PROSAIL-2 model simultaneously with daily MODIS data, one needs to have sufficient satellite observations of adequate quality. For the MODIS sensor onboard the Terra satellite, there are not enough satellite observations over Harvard Forest site within one day to allow a stable inversion of the PROSAIL-2 model (the problem is underdetermined). One solution is to collect satellite observations over a longer period of time, for example, over a 16 days period as is done in the production of the standard MODIS nadir-adjusted product (MOD43; Strahler, 1999). To balance the need for many satellite observations and the need for collecting observations over a short period of time, we used a flexible scheme for organizing observations for inversion of the PROSAIL-2 model (Table 4.3). We assumed that there is negligible variation of the canopy and the leaf within the period of each data collection in Table 4.3. This assumption is commonly used when researchers need many observations during a short period (e.g., Strahler, 1999). Each of the six data collections in Table 4.3 has 10 to 17 good-quality observations and covers no more than sixteen consecutive days. The MODIS observations associated with the individual data collections have large variations in observation geometry. For example, Figure 4.1 shows the variation of observation geometry for the data collection from DOY 201 to 214 in 2001.

### 4.3.3 Inversion of the PROSAIL-2 model with MODIS data

For this paper, we designed an inversion scheme to estimate the sixteen biophysical and biochemical variables using observed spectral reflectance data. We performed inversions of the PROSAIL-2 model for each of the six data collections using the Metropolis algorithm, resulting in the distributions of individual variables for each data collection. We evaluated the inversions of the PROSAIL-2 model in three ways. First, we compared observed surface reflectance from the MODIS image with surface reflectance retrieved using PROSAIL-2. For the forward calculations of reflectance we used the mean values of variables taken from the posterior distributions. Secondly, we examined the temporal variations of a few key variables from inversion of the PROSAIL-2 model, with available data about LAI and chlorophyll content from the literature. Thirdly, we examined the temporal variation of  $FAPAR_{canopy}$ ,  $FAPAR_{leaf}$  and  $FAPAR_{chl}$ , and compared them with two commonly used vegetation indices, NDVI and the Enhanced Vegetation Index (EVI, Huete et al., 1997), showing their temporal patterns and magnitudes with respect to FAPAR values.

$$NDVI = \frac{\rho_{NIR_1} - \rho_{red}}{\rho_{NIR_1} + \rho_{red}} \quad (10)$$

$$EVI = 2.5 \times \frac{\rho_{NIR_1} - \rho_{red}}{\rho_{NIR_1} + 6 \times \rho_{red} - 7.5 \times \rho_{blue} + 1} \quad (11)$$

where  $\rho_{blue}$ ,  $\rho_{red}$  and  $\rho_{NIR_1}$  are reflectance values of the blue, red and  $NIR_1$  bands.

## **4.4 Results**

### **4.4.1 Comparison between retrieved and observed reflectance values**

After the inversions of the PROSAIL-2 model, we utilized the mean values of the retrieved variable distributions for each data collection as inputs to calculate the reflectance with forward simulations of the PROSAIL-2 model. Figure 4.2 shows a comparison of PROSAIL-2 retrieved reflectance with observed reflectance of MODIS green, red, NIR<sub>1</sub>, NIR<sub>2</sub>, and SWIR<sub>1</sub> bands. The correlation coefficient between retrieved and observed MODIS visible reflectance is 0.75 for green band and 0.54 for red band. The root mean squared error (RMSE) between observed and retrieved MODIS visible reflectance is 0.9% for green band and 0.9% for red band. The correlation coefficient between retrieved and observed NIR/SWIR reflectance is 0.83, 0.67, and 0.50 for NIR<sub>1</sub>, NIR<sub>2</sub> and SWIR<sub>1</sub>, respectively. The RMSE between observed and retrieved NIR/SWIR reflectance is 2.8%, 4.0%, and 3.7% for NIR<sub>1</sub>, NIR<sub>2</sub> and SWIR<sub>1</sub>, respectively. Note that each data collection spanned approximately two weeks, and any variation of leaf and canopy during the period may have contributed to the discrepancies between our retrieved reflectance and MODIS observed reflectance. Possible errors introduced during MODIS pre-processing may also contribute to the discrepancies (e.g. imperfect atmospheric correction). The comparison suggests that PROSAIL-2 model with the retrieved mean values of individual variables reasonably reproduces the surface reflectance of the deciduous broadleaf forest site in 2001-2003.

#### 4.4.2 Temporal variation of eight variables (PAI, SFRAC, CF, $C_{ab}$ , $N$ , $C_w$ , $C_m$ , $C_{brown}$ ) in the PROSAIL-2 model

The strength of the Metropolis inversion algorithm is that it estimates probability distributions for individual model variables. Inspection of these posterior distributions offers a measure of uncertainty in the form of their standard deviations or other quantile intervals. As discussed previously, the shape of the distributions provide a measure of compatibility between model and data. We examined the histograms of the sixteen variables from inversion of each MODIS data collection, and ranked them into the categories of “well-constrained”, “poorly-constrained” and “edge-hitting”. For the MODIS data collection in DOY 147-162, nine variables belong to “well-constrained”, six variables to “poor-constrained” and one variable to “edge-hitting” (Table 4.4). For example, leaf chlorophyll content ( $C_{ab}$ ) has a bell-shaped “well-constrained” distribution (Figure 4.3), with a mean value of  $35.9 \mu\text{g}/\text{cm}^2$  and a standard deviation of  $5.6 \mu\text{g}/\text{cm}^2$ . Stem fraction (SFRAC) has a relatively “well-constrained” distribution (Figure 4.4) with a mean value of 8.8% and a standard deviation of 5.6%. In comparison, cover fraction (CF) has a distribution that clearly belongs to the “edge-hitting” category (Figure 4.5), with a mean value of 92% and a standard deviation of 7%. The soil variable ( $\text{SOIL}_A$ ) is “poorly-constrained” (Figure 4.6) and has a mean value of 9.94 and a standard deviation of 5.79. We calculated LAI, based on estimated values of PAI and SFRAC, and we see that its resultant distribution is “well constrained” (Figure 4.7) with a mean value of 4.2 and a standard deviation of 1.3. For the other five MODIS data collections, the results were similar. Both stem and soil variables contributed relatively little to surface reflectance, largely due to a very high percentage of forest cover and large values (4.9 in



peak growing season of 2001) of leaf area index in the Harvard Forest site (Cohen et al., 2003).

Figure 4.8 shows the temporal variation of the mean and standard deviation of three canopy-level variables in the PROSAIL-2 model. The mean value of plant area index (PAI) from DOY 147 to 260 in 2001 to 2003 varies between 4 and 5 (Figure 4.8a), with a slightly increasing tendency of PAI from DOY 147 to 210, and a slightly decreasing tendency of PAI from DOY 230 to DOY 260. The mean value of stem fraction from DOY 147 to 260 in 2001 to 2003 was within the range of about 2%-10%, and the data collection from DOY 147 to 162 in 2002 had the largest value of stem fraction among the six data collections (Figure 4.8b). Stem fraction explained why the difference between the mean value of  $FAPAR_{canopy}$  and the mean value of  $FAPAR_{leaf}$  of the data collection from DOY 147 to 162 in 2002 was the greatest among all the six data collections (Figure 4.10a). The mean value of cover fraction from DOY 147 to 260 in 2001 to 2003 was within the range of 92% - 99%, and the data collection from DOY 147 to 162 in 2002 had the smallest value of cover fraction among the six data collections (Figure 4.8c). The cover fraction histogram of the data collection from DOY 147 to 162 in 2002 is shown in Figure 4.5. Its mode appears near the right edge of its allowable range (Table 4.1). All other modes of cover fraction for the six data collections also appear near the right edge. This is why some of the “mean plus standard deviation” values are greater than 1.0 in Figure 4.8c. We calculated LAI using the equation  $LAI = (1 - SFRAC) \times PAI$ . The resultant LAI mean values vary between 3.9 in DOY 147-162 in 2002 and 4.4 in DOY 201-214 in 2001 (Figure 4.8d).

Figure 4.9 shows the temporal variation of the mean and standard deviation of the five leaf-level variables in the PROSAIL-2 model. At leaf level, the estimated mean leaf chlorophyll content ( $C_{ab}$ ) among the six data collections ranges from 35.9 - 51.7  $\mu\text{g}/\text{cm}^2$ . The  $C_{ab}$  content of the ata collection from DOY 147 to 162 in 2002 is the lowest retrieved value, and is statistically different from the other five data collections. The mean values of  $C_{ab}$  content for the five data collections from DOY 172 to 260 have only a slight variation, well within the range of 10% (Figure 4.9a). Leaf brown pigment ( $C_{\text{brown}}$ ) shows a distinct seasonality with an increasing tendency from DOY 150 to DOY 260 (Figure 4.9b). The data collection from DOY 172 to 187 in 2003 had the lowest mean value of leaf dry matter ( $C_m$ ), which is significantly different from the other five collections. The mean values of  $C_m$  vary between 0.009 and 0.015  $\text{g}/\text{m}^2$  among the other five data collections (Figure 4.9c). The structural variable of leaf ( $N$ ) had a distinct seasonality with an increasing tendency from DOY 147 to 260 (Figure 4.9d). Leaf equivalent water thickness ( $C_w$ ) ranged between 0.015 cm and 0.032 cm, with a distinct temporal variation (Figure 4.9e).

#### 4.4.3. Temporal variation of $FAPAR_{\text{canopy}}$ , $FAPAR_{\text{leaf}}$ , and $FAPAR_{\text{chl}}$

We estimated the distributions of  $FAPAR_{\text{canopy}}$ ,  $FAPAR_{\text{leaf}}$ , and  $FAPAR_{\text{chl}}$  for each data collection, and extracted their mean and standard deviation (Figure 4.10). The maximum mean values of  $FAPAR_{\text{canopy}}$ ,  $FAPAR_{\text{leaf}}$ , and  $FAPAR_{\text{chl}}$  were 0.92, 0.90, and 0.74, respectively. The minimum mean values were 0.83, 0.74, and 0.57, respectively. The ratios of minimum value to maximum value, a quantitative indicator of data dispersion, were 0.91, 0.83, and 0.77, respectively.  $FAPAR_{\text{canopy}}$ ,  $FAPAR_{\text{leaf}}$ , and

$FAPAR_{chl}$  exhibited different magnitudes of temporal variations, with  $FAPAR_{canopy}$  and  $FAPAR_{leaf}$  showing only slight changes throughout the peak growing season from DOY 172 to DOY 260, and  $FAPAR_{chl}$  showing a strong seasonal variation.

The difference between  $FAPAR_{canopy}$  and  $FAPAR_{leaf}$  is attributed to light absorption by stem ( $APAR_{stem}$ ), i.e., the non-leaf part of the canopy. During the peak growing season (mid-June to mid-September), the vegetation canopy is dominated by leaves, and only a very small proportion of stems are observed by the MODIS sensor. This may explain why  $FAPAR_{canopy}$  values are only slightly higher than  $FAPAR_{leaf}$  for the five data collections from DOY 172 to 260 (Figure 4.10a). In comparison,  $FAPAR_{canopy}$  in DOY147-162 in 2002 is much larger than  $FAPAR_{leaf}$ , which is likely to be due to a slightly higher proportion of stems observed by the MODIS sensor.

The difference between  $FAPAR_{leaf}$  and  $FAPAR_{chl}$  is attributed to light absorption by the non-chlorophyll component of the leaf.  $FAPAR_{chl}$  values are substantially lower than  $FAPAR_{leaf}$  (Figure 4.10a). Furthermore, the difference between  $FAPAR_{leaf}$  and  $FAPAR_{chl}$  increased over time from DOY172 to DOY260 (Figure 4.10a), which is attributed to increases of light absorption by NPV components within the leaves. This suggests that leaf age and associated changes in dry matter and brown pigment components may affect the proportions of light absorption by NPV in the leaf and by chlorophyll.

NDVI has been widely used for estimation of  $FAPAR_{canopy}$  and GPP. In recent years, EVI has been used frequently as well (Justice et al., 1998). We calculated the mean and standard deviation of NDVI and EVI using the same MODIS images for each data collection.

For the five data collections from DOY 172 to DOY 260, mean NDVI values are very similar to  $FAPAR_{leaf}$  (Figure 4.10b), which supports the earlier studies that used NDVI to approximate  $FAPAR_{canopy}$  (e.g., Goward et al., 1992), as  $FAPAR_{leaf}$  and  $FAPAR_{canopy}$  values are close to each other in those five data collections. However, the NDVI associated with the data collection from DOY 147 to 162 in 2002 is much greater than  $FAPAR_{leaf}$ , but close to  $FAPAR_{canopy}$  (Figure 4.10b). In general, mean EVI values vary substantially over time and are much closer to  $FAPAR_{chl}$  values than mean NDVI values (Figure 4.10c). Note that reflectance values in daily MODIS images are not BRDF corrected reflectance; therefore, the observation viewing geometry has an effect on the dynamics of NDVI and EVI. The standard deviation of EVI varies among the six data collections. For example, the EVI from DOY 248 to 255 in 2003 has a standard deviation of 0.057 (about 10% of mean EVI value). Therefore, caution should be taken when selecting daily MODIS images to calculate vegetation indices for use in estimation of  $FAPAR_{canopy}$  and  $FAPAR_{chl}$ .

#### **4.5 Discussion**

Satellite-based optical sensors provide daily observations of the land surface at moderate spatial resolution. Numerous studies have used various radiative transfer models (RTM) to retrieve LAI and estimate  $FAPAR_{canopy}$  (e.g., Myneni et al., 1997; Asner et al., 1998b; Bicheron et al., 1999). The MODIS Land Science Team has used a 3-dimensional radiative transfer model to provide standard products of  $FAPAR_{canopy}$  and LAI at 1-km spatial resolution (Justice et al., 1998; Knyazikhin et al., 1998b). In this study we used a relatively simple RTM (PROSAIL-2 model) to study light absorption by

chlorophyll, leaf and canopy over time. Our modified version of the PROSAIL-2 based inversion includes brown pigments for better characterization of leaf absorption, and the Metropolis inversion algorithm for estimation of variable uncertainties and model-data compatibility.

There is currently a paucity of *in situ* independent data for evaluation of retrieved LAI and  $FAPAR_{canopy}$  at moderate (500-m to 1-km) spatial resolution (e.g., Cohen et al., 2003; Turner et al., 2003). Though field-based analyses are currently underway, we have no field-based data of chlorophyll, leaf water content and leaf dry matter in 2001-2003. In addition, the scaling problems associated with translating leaf chlorophyll to an image pixel at 500-m spatial resolution have yet to be addressed. Here we discuss two variables (LAI and chlorophyll content) that are important for interpreting the results of inversion of the PROSAIL-2 model in this study.

LAI is an important canopy-level biophysical variable. In an effort to evaluate the standard product of LAI and  $FAPAR_{canopy}$  from the MODIS Land Science Team, the BigFoot project was funded to study the spatial variation of LAI through a combination of extensive field sampling and Landsat images across a number of sites in North America. As part of the BigFoot project, the field study (Cohen et al., 2003) estimated spatial distributions of LAI at Harvard Forest and reported an LAI value of 4.9 during its mid growing season in 2001. Field researchers at Harvard Forest also conducted multi-temporal measurements of LAI in 1998 and 1999, which ranged from 3.4 to 4.2 in June - September of 1998, and from 3.8 to 4.7 in June - September of 1999 (Xiao et al., 2004c). Our estimated LAI mean values are within the range of LAI measured in 1998-1999 (Figures 4.7 and 4.8d). The MODIS standard LAI/FPAR product (MOD15A2, v004)

estimates LAI values of  $> 6.0$  at the Harvard Forest during June – September of 2001 – 2003. In this study, estimated mean LAI value from inversion of the PROSAIL-2 model for the data collection from DOY 201 to 214 in 2001 is about 4.4 (Figure 4.8d), which is more consistent with the field-based estimate from Cohen et al. (2003). The differences in LAI values between the MOD15A2 standard product and PROSAIL-2 based estimates in this study are often larger than 1 at the Harvard Forest. It is beyond the scope of this paper to diagnose the errors of either LAI algorithm in detail, but we note that the MOD15A2 estimate assumes constant standard leaf optical properties for deciduous broadleaf forests throughout the entire plant growing season (Myneni et al., 2002). For inversions of the PROSAIL-2 model in this study, we assume that leaf-level variables (e.g., brown pigments, leaf dry matter) change over time. The good agreement between PROSAIL-2-retrieved LAI and observed field LAI values suggests that inversions of the PROSAIL-2 model in this study works reasonably well.

Leaf chlorophyll content ( $C_{ab}$ ) is an important biochemical variable and one of the major control factors of photosynthesis. Given light intensity and atmospheric  $CO_2$  concentration, it has been reported that the chlorophyll content of red oak, one of the major species of Harvard Forest, would not change during the peak plant growing season prior to senescence (Cavender-Bares et al., 2000). Furthermore, there was no observed significant inter-annual change of chlorophyll content of the major species of Harvard Forest between 1995 and 1996 during plant growing periods before senescence (personal communication with Dr. Jeannine Cavender-Bares). The chlorophyll content of red oak at Harvard Forest in August of 1991 was measured to be  $36.8 \mu g/cm^2$ , red maple  $35.5 \mu g/cm^2$ , white birch  $38.1 \mu g/cm^2$ , and yellow birch  $41.2 \mu g/cm^2$  (Waring et al., 1995). A

research group recently reported that their measurement of chlorophyll content of needles in late July of 1998 and 1999 was  $60.2 \mu\text{g}/\text{cm}^2$  (Zarco-Tejada et al., 2004), which was higher than the reported values of chlorophyll content of hardwood species of Harvard Forest by other studies (Cavender-Bares et al., 2000 and Waring et al., 1995). Needleleaf trees are distributed in parts of the Harvard Forest site. The chlorophyll content of Harvard Forest leaves at the MODIS scale (500-m) is therefore likely to fall between the hardwood and needleleaf values, dependent upon the mixing ratio of hardwood trees and needleleaf trees. In this study, the estimated mean  $C_{ab}$  value for the data collection from DOY 147 to 162 in 2002 was  $35.9 \mu\text{g}/\text{cm}^2$ , and the estimated mean  $C_{ab}$  values for the other five data collections were  $44.9 - 51.7 \mu\text{g}/\text{cm}^2$ . These  $C_{ab}$  estimates fall within the range between the  $C_{ab}$  of hardwood trees and  $C_{ab}$  of needles reported by other researchers. While measurement of leaf chlorophyll content at individual leaves is tractable, scaling measurements of individual leaves to a MODIS image pixel (500-m) represents a major leap requiring a rigorous field sampling design. The results of this study suggest that future field work in deciduous broadleaf forests should include multi-temporal measurements of leaf-level variables (chlorophyll and other pigments, leaf dry matter and leaf water content).

The number of variables in the PROSAIL-2 model that can be reasonably inverted simultaneously is still an unresolved issue. An earlier model simulation study (Jacquemoud et al., 2000) argued that the leaf structure variable (N) should be held at a fixed value during inversion of the other variables. Their inversion was conducted for the spectral range from 430 nm to 880 nm. Another study (Zarco-Tejada et al., 2003) inverted N,  $C_m$ , and  $C_w$  with the other variables held constant, using a MODIS 8-day

composite reflectance data (MOD09A1) and MODIS LAI data (MOD15A2). Inversion of the PROSAIL-2 in our study has a broader spectral range from 555 nm to 1640 nm. In this study, inversion of the PROSAIL-2 model estimates simultaneously both canopy-level variables (e.g., PAI) and leaf-level variables, using multiple daily MODIS data. To our knowledge, this is the first study that simultaneously retrieves both canopy- and leaf-level variables through inversion of the PROSAIL-2 model and multiple daily MODIS data. The results of this study have demonstrated the potential of the PROSAIL-2 model as a tool for quantifying biophysical and biochemical variables of vegetation at leaf- and canopy-levels over time.

The results of this study highlight the differences among  $FAPAR_{canopy}$ ,  $FAPAR_{leaf}$  and  $FAPAR_{chl}$  over time for a deciduous broadleaf forest. The substantial difference between  $FAPAR_{canopy}$  and  $FAPAR_{chl}$  may have significant implication for those biogeochemical models that estimate light absorption, GPP, and NPP using satellite data. A number of satellite-based Production Efficiency Models (Potter et al., 1993; Prince et al., 1995; Ruimy et al., 1996; Running et al., 2004) use  $FAPAR_{canopy}$  to estimate the amount of PAR absorbed by canopies.

#### **4.6 Summary**

This study has demonstrated the potential for combining radiative transfer modeling with a Bayesian parameter estimation scheme, utilizing real satellite data for estimating leaf- and canopy-level biophysical and biochemical properties of a deciduous broadleaf forest. We estimated the PROSAIL-2 model variables based on the surface reflectance of the five MODIS spectral bands (green, red,  $NIR_1$ ,  $NIR_2$  and  $SWIR_1$ ). We



also estimated the seasonal dynamics of FAPAR at canopy-, leaf- and chlorophyll- levels, respectively. Our results show that  $FAPAR_{chl}$  and  $FAPAR_{canopy}$  exhibit different behaviors for a deciduous broadleaf forest. This study represents our effort in using a radiative transfer model to partition canopy-level FAPAR into  $FAPAR_{chl}$  and  $FAPAR_{NPV}$ , following previous studies that proposed the conceptual partitioning ( $FAPAR_{canopy} = FAPAR_{chl} + FAPAR_{NPV}$ ) and showed the potential of  $FAPAR_{chl}$  in improving the quantification of GPP for forests. This study is another step that enables us to go beyond the LAI- $FAPAR_{canopy}$ -NDVI paradigm and explore the alternative chlorophyll- $FAPAR_{chl}$  approach that takes advantage of moderate resolution optical sensors (e.g. MODIS) in the era of the Earth Observing System. This study also suggests that both remote sensing and ecological research would benefit from season-long measurements of leaf-level variables (e.g., chlorophyll, other pigments, leaf dry matter, and leaf water content), in addition to measurements of canopy-level variables (e.g., LAI).

Table 4.1

A list of variables in the PROSAIL-2 model and their search ranges

	Variable	Description	Unit	Search range
Biophysical /biochemical variables	PAI	plant area index, i.e., leaf +stem area index		1 – 7.5
	SFRAC	Stem fraction		0 –1
	CF	Cover fraction: area of land covered by vegetation/ total area of land		0.5 –1
	C <sub>ab</sub>	Leaf chlorophyll a+b content	µg/cm <sup>2</sup>	0 – 80
	N	Leaf structure variable: measure of the internal structure of the leaf		1.0 – 4.5
	C <sub>w</sub>	Leaf equivalent water thickness	cm	0.001 – 0.15
	C <sub>m</sub>	Leaf dry matter content	g/cm <sup>2</sup>	0.001 – 0.04
	C <sub>brown</sub>	Leaf brown pigment content		0.00001 – 8
	LFINC	Mean leaf inclination angle	degree	10 – 89
	STINC	Mean stem inclination angle	degree	10 – 89
	LFHOT	Leaf BRDF variable: length of leaf/ height of vegetation		0 – 0.9
	STHOT	Stem BRDF variable: length of stem / height of vegetation		0 – 0.9
	STEM <sub>A</sub>	Stem reflectance variable: maximum (for a fitted function)		0.2 – 20
	STEM <sub>B</sub>	Stem reflectance variable range (for same fitted function)		50 – 5000
	SOIL <sub>A</sub>	Soil reflectance variable: maximum (for a fitted function)		0.2 – 20
SOIL <sub>B</sub>	Soil reflectance variable: range (for same fitted function)		50 – 5000	
Atmospheric condition variable	VIS	Diffuse/ direct variable: scope of atmospheric clarity	km	50

Table 4.2 Posterior means, standard deviations, variable behavior from inversion of the PROSAIL-2 model with the three simulated data sets: no data error, noise standard deviation  $\sigma=5\%$ \* data, noise standard deviation  $\sigma = 10\%$ \*data

Variable	actual	no error	
		mean $\pm$ standard deviation	Variable class
PAI	4.5	4.43 $\pm$ 1.25	well-constrained
SFRAC	0.1	0.102 $\pm$ 0.070	well-constrained
CF	0.9	0.88 $\pm$ 0.09	well-constrained
C <sub>ab</sub>	35.0	36.36 $\pm$ 8.89	well-constrained
N	1.5	1.43 $\pm$ 0.19	well-constrained
C <sub>w</sub>	0.03	0.0327 $\pm$ 0.0087	well-constrained
C <sub>m</sub>	0.01	0.0109 $\pm$ 0.007	well-constrained
C <sub>brown</sub>	0.7	0.7000 $\pm$ 0.240	well-constrained
LFINC	45.0	41.69 $\pm$ 8.36	well-constrained
STINC	50.0	43.51 $\pm$ 21.84	poorly-constrained
LFHOT	0.05	0.1896 $\pm$ 0.1998	edge-hitting
STHOT	0.05	0.3982 $\pm$ 0.2575	poorly-constrained
STEM <sub>A</sub>	10.0	9.7928 $\pm$ 5.7782	poorly-constrained
STEM <sub>B</sub>	2820	3025 $\pm$ 1210	poorly-constrained
SOIL <sub>A</sub>	10.0	9.9686 $\pm$ 5.8055	poorly-constrained
SOIL <sub>B</sub>	3525	3204 $\pm$ 1139	poorly-constrained
FAPAR <sub>canopy</sub>	0.84	0.84 $\pm$ 0.10	well-constrained
FAPAR <sub>leaf</sub>	0.76	0.76 $\pm$ 0.11	well-constrained
FAPAR <sub>chl</sub>	0.59	0.58 $\pm$ 0.11	well-constrained

Table 4.2 (continued)

$\sigma=5\% * data$		$\sigma = 10% * data$	
mean $\pm$ standard deviation	Variable class	mean $\pm$ standard deviation	Variable class
4.42 $\pm$ 1.29	well-constrained	4.57 $\pm$ 1.33	well-constrained
0.090 $\pm$ 0.070	well-constrained	0.088 $\pm$ 0.070	well-constrained
0.87 $\pm$ 0.11	well-constrained	0.87 $\pm$ 0.14	well-constrained
37.0 $\pm$ 8.91	well-constrained	36.61 $\pm$ 9.16	well-constrained
1.43 $\pm$ 0.19	well-constrained	1.42 $\pm$ 0.19	well-constrained
0.0328 $\pm$ 0.0084	well-constrained	0.033 $\pm$ 0.0086	well-constrained
0.0115 $\pm$ 0.007	well-constrained	0.0115 $\pm$ 0.0068	well-constrained
0.7264 $\pm$ 0.246	well-constrained	0.7346 $\pm$ 0.243	well-constrained
42.20 $\pm$ 8.37	well-constrained	41.40 $\pm$ 8.50	well-constrained
43.54 $\pm$ 22.15	poorly-constrained	43.28 $\pm$ 22.04	poorly-constrained
0.1784 $\pm$ 0.1844	edge-hitting	0.2021 $\pm$ 0.2108	edge-hitting
0.4074 $\pm$ 0.2552	poorly-constrained	0.4156 $\pm$ 0.2598	poorly-constrained
9.7494 $\pm$ 5.7937	poorly-constrained	9.7993 $\pm$ 5.7817	poorly-constrained
3061 $\pm$ 1207	poorly-constrained	3014 $\pm$ 1222	poorly-constrained
9.8590 $\pm$ 5.6977	poorly-constrained	9.9686 $\pm$ 5.8054	poorly-constrained
3205 $\pm$ 1123	poorly-constrained	3149 $\pm$ 1148	poorly-constrained
0.83 $\pm$ 0.11	well-constrained	0.83 $\pm$ 0.11	well-constrained
0.74 $\pm$ 0.12	well-constrained	0.73 $\pm$ 0.11	well-constrained
0.56 $\pm$ 0.13	well-constrained	0.56 $\pm$ 0.14	well-constrained

Table 4.3 A list of MODIS multiple daily data collections in 2001 through 2003 for inversion of the PROSAIL-2 model. DOY – day of year

YEAR	DOY period	# of valid observations
2001	201-214	17
	250-260	13
2002	147-162	10
	219-230	10
2003	172-187	13
	248-255	13

Table 4.4 Variable behavior from inversion of the PROSAIL-2 model with the MODIS data collection from DOY 147 to162 in 2002

Variable	variable behavior
PAI	well-constrained
SFRAC	well-constrained
CF	edge-hitting
$C_{ab}$	well-constrained
N	well-constrained
$C_w$	well-constrained
$C_m$	well-constrained
$C_{brown}$	well-constrained
LFINC	well-constrained
STINC	Poorly-constrained
LFHOT	well-constrained
STHOT	Poorly-constrained
STEM <sub>A</sub>	Poorly-constrained
STEM <sub>B</sub>	Poorly-constrained
SOIL <sub>A</sub>	Poorly-constrained
SOIL <sub>B</sub>	Poorly-constrained
FAPAR <sub>canopy</sub>	well-constrained
FAPAR <sub>leaf</sub>	well-constrained
FAPAR <sub>chl</sub>	well-constrained

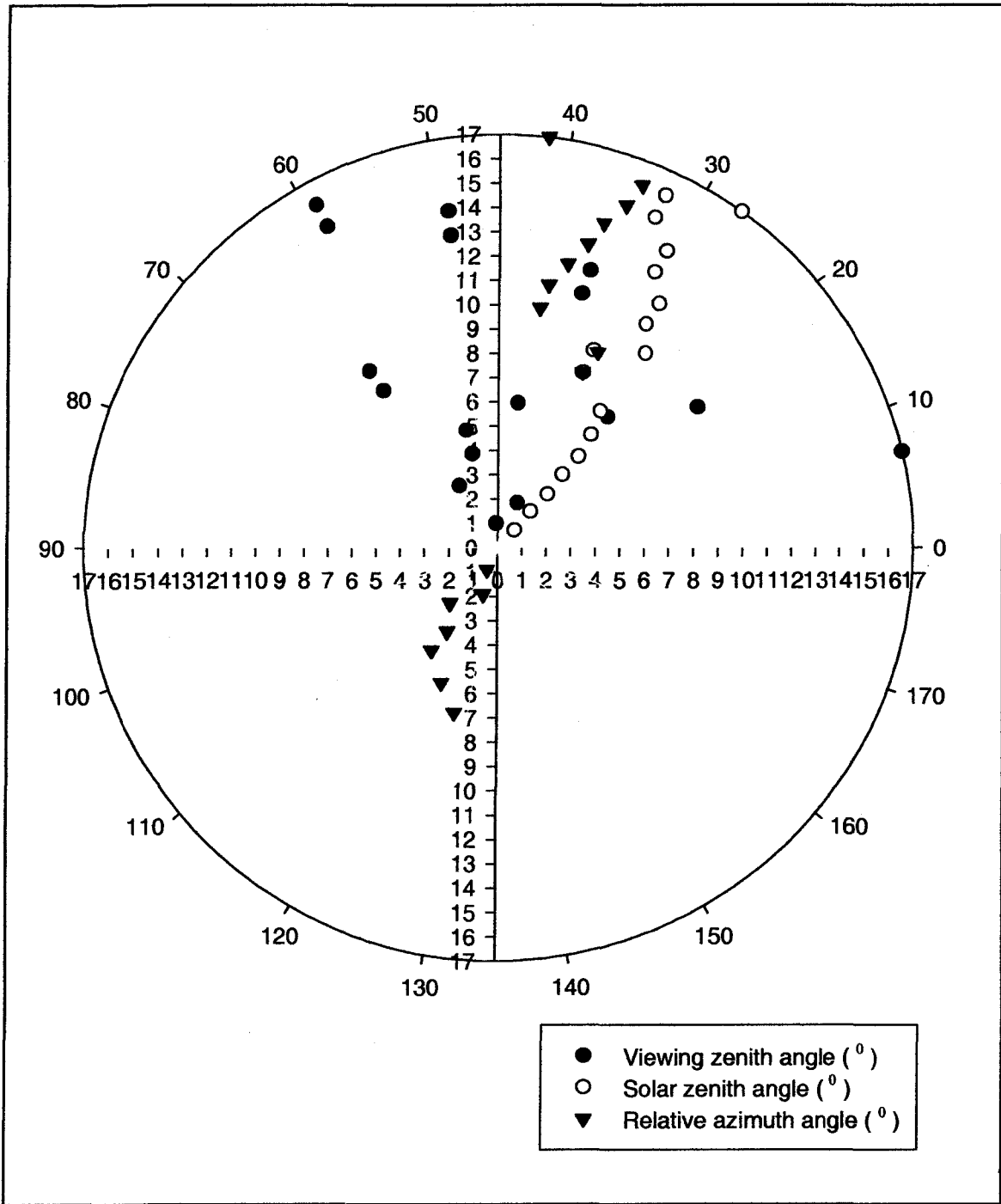


Figure 4.1 Viewing geometries of data collection from DOY 201 to 214 in 2001(17 observations)

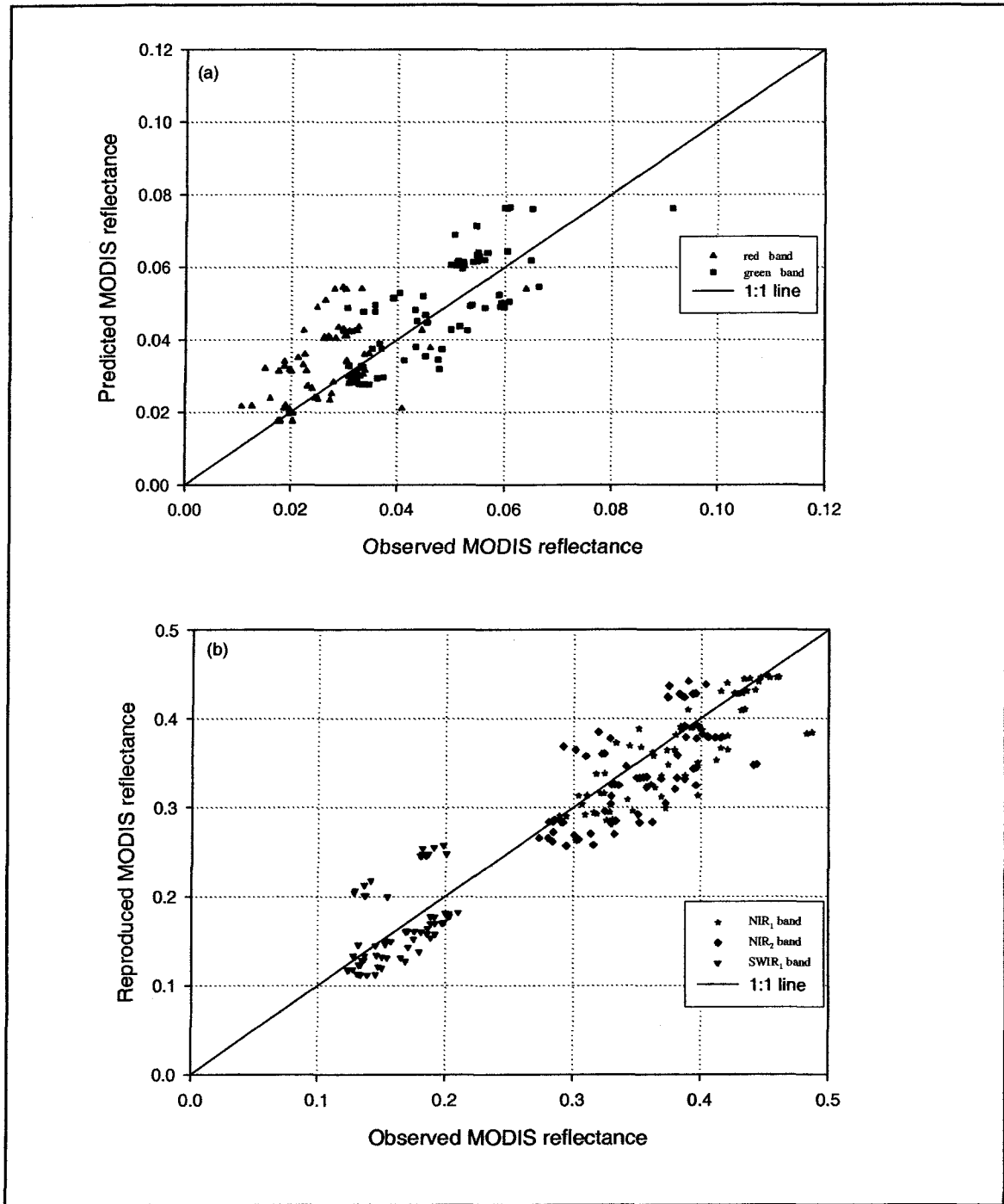


Figure 4.2 A comparison between the observed reflectance and PROSAIL-2-reproduced reflectance for five MODIS spectral bands (red, green, NIR<sub>1</sub>, NIR<sub>2</sub> and SWIR<sub>1</sub>). Surface reflectance were reproduced with the mean values of inverted variables from the PROSAIL-2 model in 2001, 2002 and 2003.(a) MODIS red and green bands and (b) MODIS NIR<sub>1</sub>, NIR<sub>2</sub>, and SWIR<sub>1</sub> spectral bands



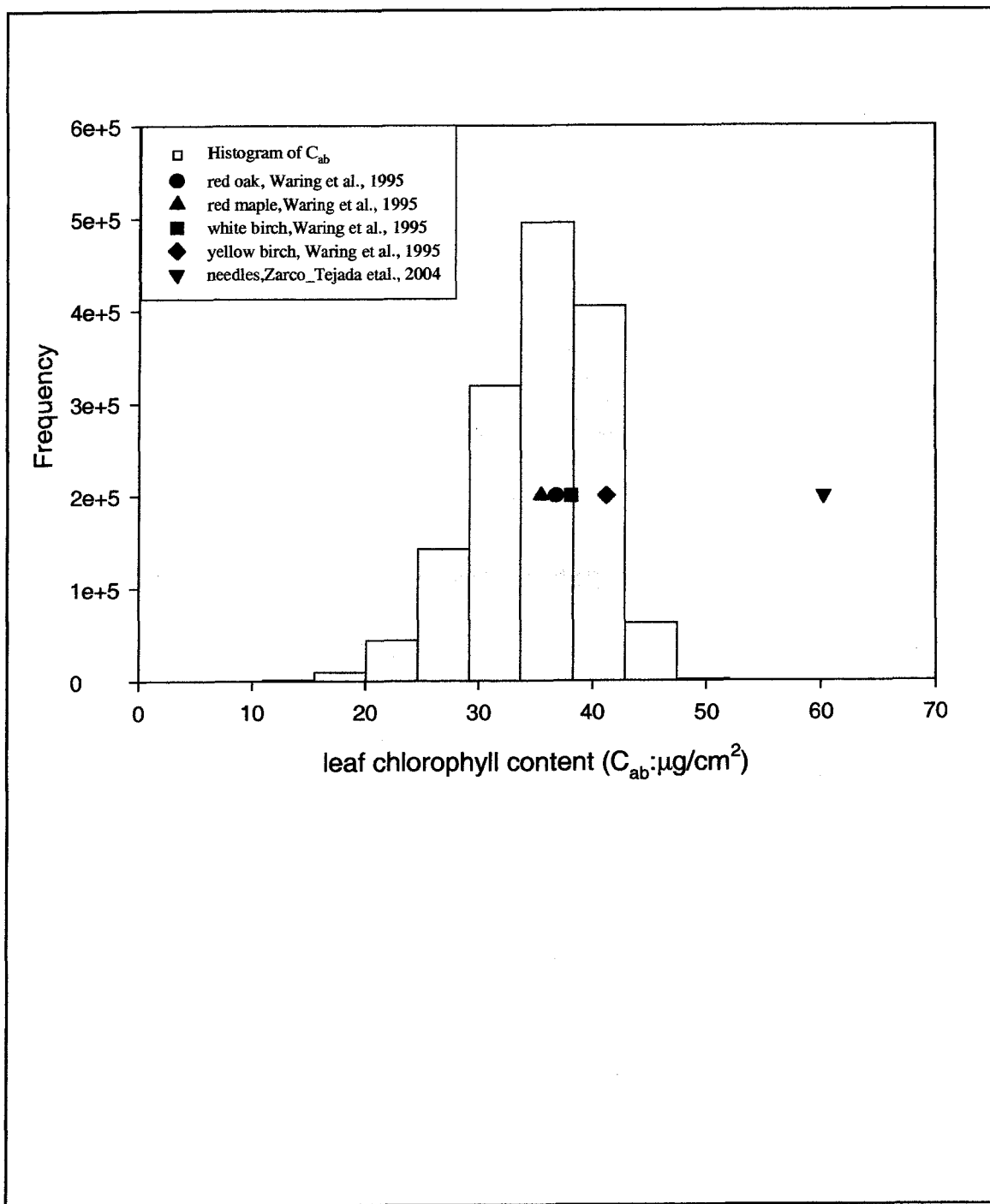


Figure 4.3 Histogram of leaf chlorophyll content ( $C_{ab}$ ,  $\mu\text{g}/\text{cm}^2$ ) for MODIS data collection from DOY 147 to 162 in 2002

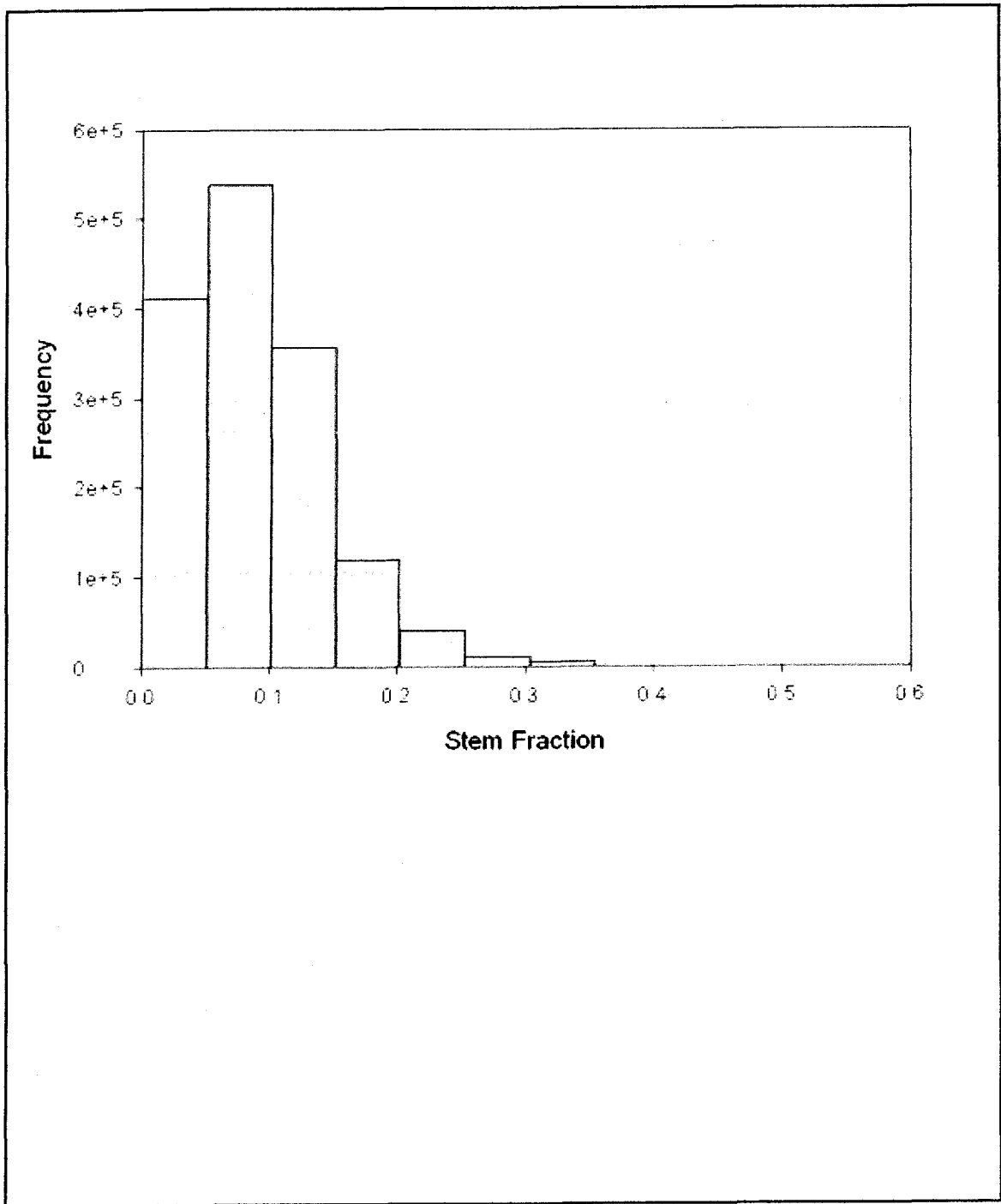


Figure 4.4 Histogram of stem fraction for MODIS data collection from DOY 147 to 162 in 2002

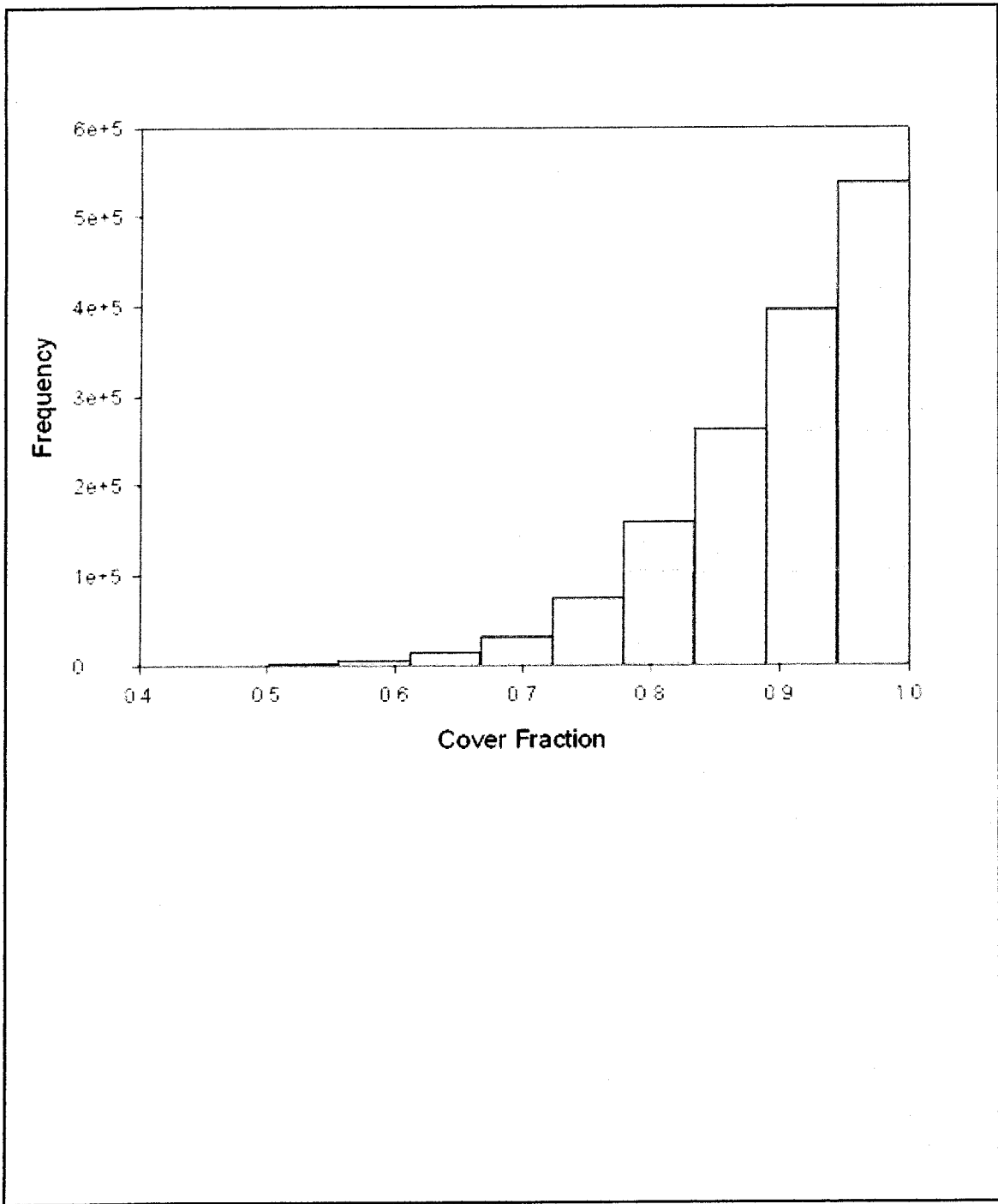


Figure 4.5 Histogram of cover fraction for MODIS data collection from DOY 147 to 162 in 2002

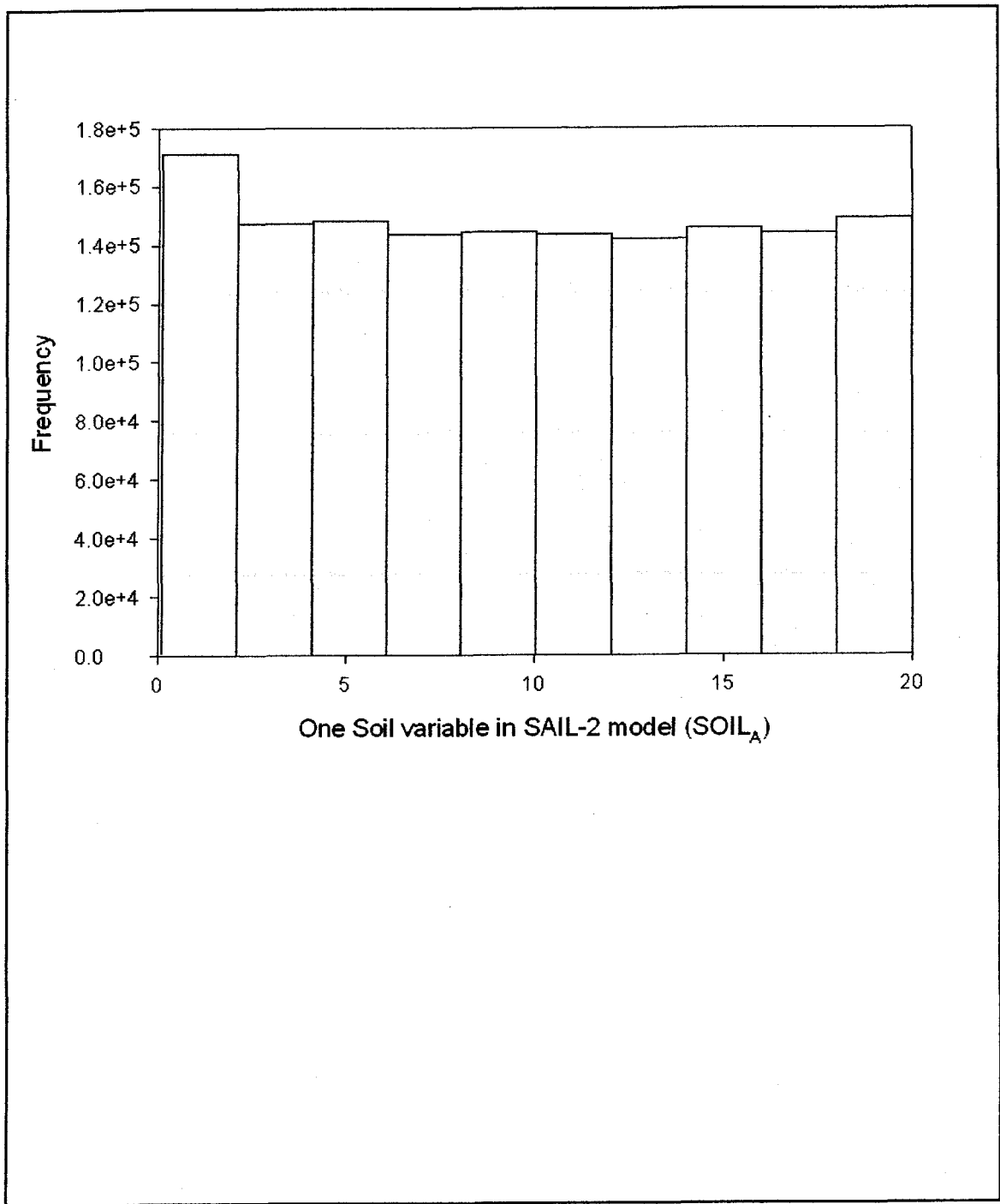


Figure 4.6 Histogram of one soil parameter in SAIL-2 (SOIL<sub>A</sub>) for MODIS data collection from DOY 147 to 162 in 2002

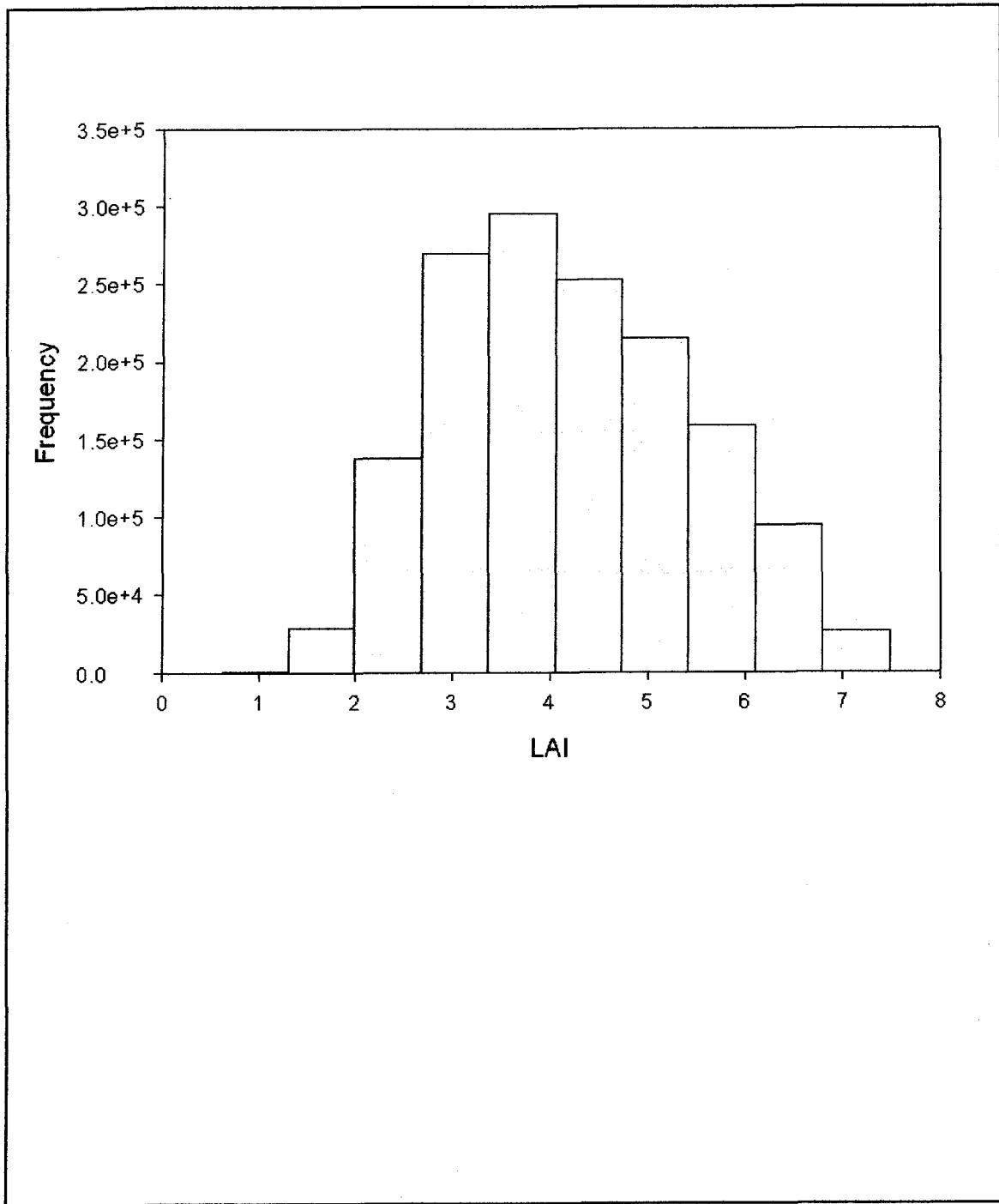


Figure 4.7 Histogram of leaf area index (LAI) for MODIS data collection from DOY 147 to 162 in 2002

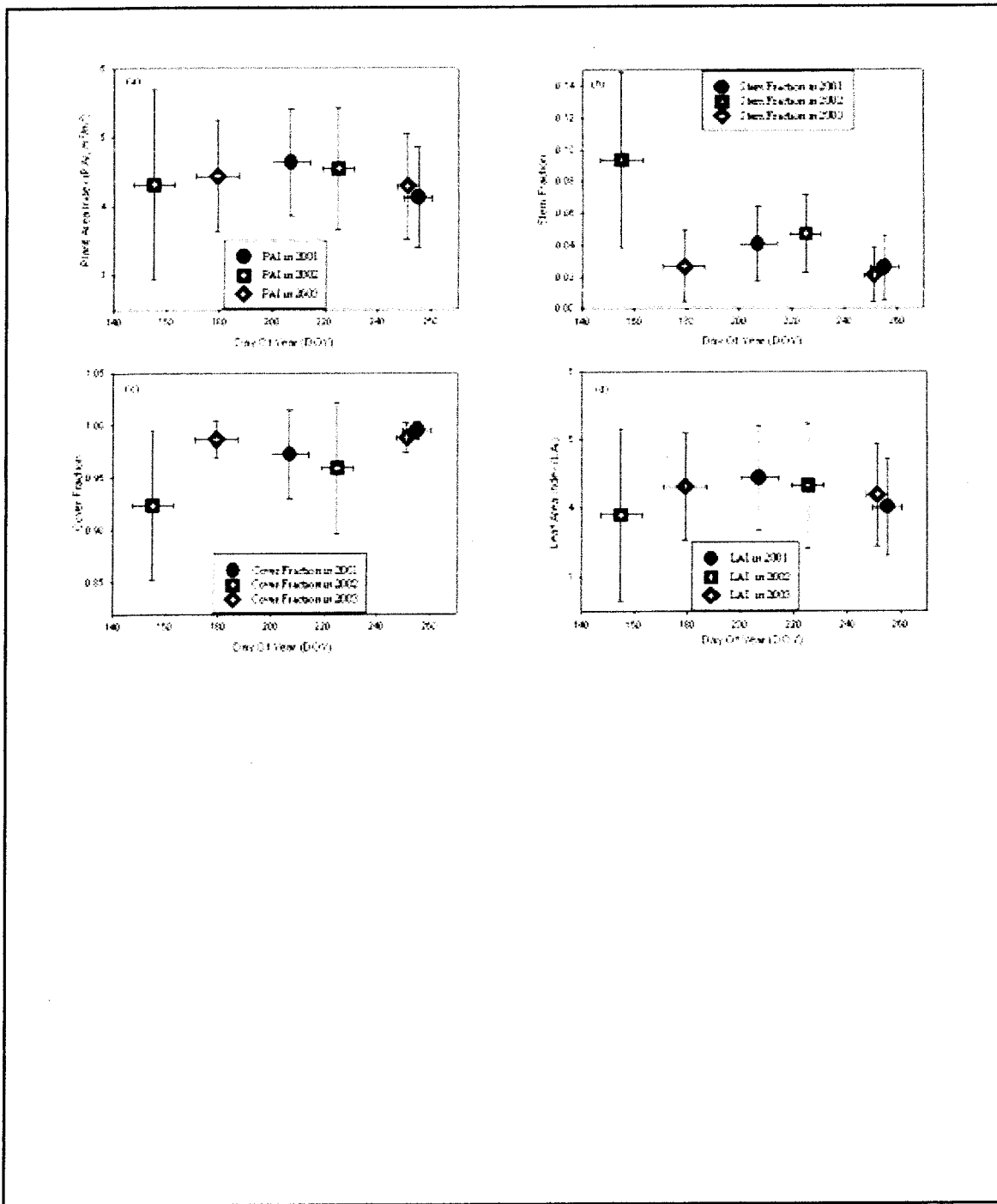


Figure 4.8 Temporal variation of canopy-level variables from inversion of PROSAIL-2 model and LAI at Harvard Forest in 2001, 2002 and 2003. (a) Plant Area Index (PAI); (b) Stem Fraction; (c) Cover Fraction; and (d) leaf area index (LAI)

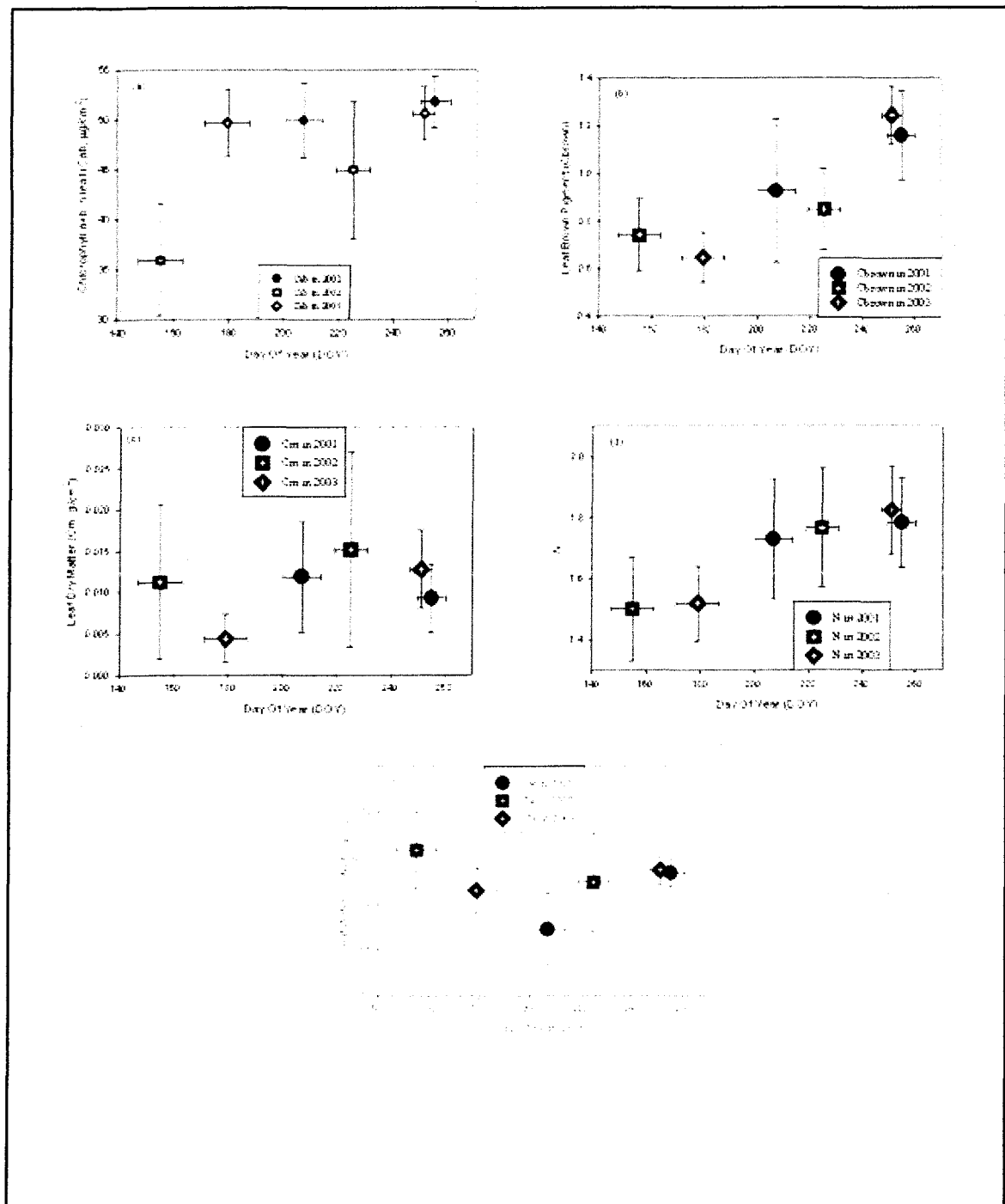


Figure 4.9 Temporal variation of leaf-level variables from inversion of PROSAIL-2 model at Harvard Forest in 2001, 2002 and 2003: (a) leaf chlorophyll content ( $C_{ab}$ ,  $\mu\text{g}/\text{cm}^2$ ) (b) leaf brown pigment ( $C_{\text{brown}}$ ); (c) leaf dry matter ( $C_m$ ,  $\text{g}/\text{cm}^2$ ); (d) N (structural parameter of leaf); and (e) leaf equivalent water thickness ( $C_w$ , cm)

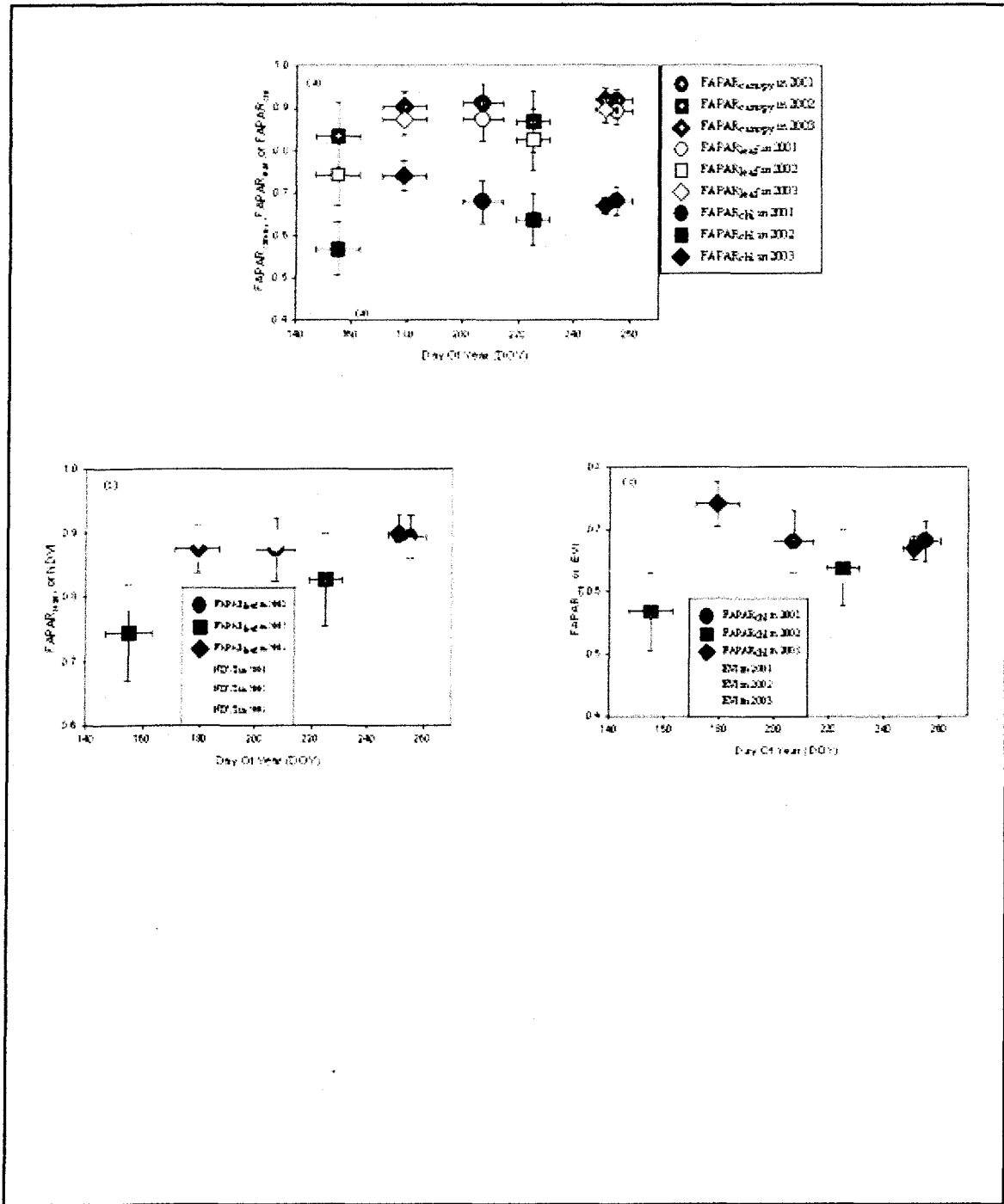


Figure 4.10 Temporal variations of the fraction of photosynthetically active radiation absorbed by chlorophyll, leaf and canopy, and vegetation indices at Harvard Forest in 2001, 2002, 2003. (a) A comparison of estimated  $FAPAR_{canopy}$ ,  $FAPAR_{leaf}$  and  $FAPAR_{chl}$ ; (b) a comparison between estimated  $FAPAR_{leaf}$  and NDVI; and (c) a comparison between estimated  $FAPAR_{chl}$  and EVI



## CHAPTER 5

# CHARACTERIZATION OF SEASONAL SPECTRAL VARIATION OF FOREST CANOPY IN A TEMPERATE DECIDUOUS BROADLEAF FOREST USING DAILY MODIS DATA<sup>2</sup>

### **5.1 Introduction**

Seasonal variations of vegetation dynamics (e.g., leaf area index [LAI], fraction of photosynthetically active radiation [PAR] absorbed by vegetation canopy [FPAR<sub>canopy</sub>], and leaf phenology) have profound impacts on ecosystem fluxes of matter and energy, including carbon sinks and sources (Pielke et al., 1998; Fitzjarrald et al., 2001; Arora, 2002; Defries et al., 2002; Lawrence et al., 2004; Osborne et al., 2004; Zhang et al., 2004a; Linderman et al., 2005). While the National Oceanic and Atmospheric Administration (NOAA) Advanced Very High Resolution Radiometer (AVHRR), particularly Normalized Difference Vegetation Index (NDVI, Tucker, 1979) of AVHRR, has been widely used to monitor long-term and/or large-scale vegetation trends, its inherent data and sensor problems and other noises limited its utility in change analyses in detail for short-terms, for example, daily, monthly or seasonally (Goward et al., 1995; Prince et al., 1996; Lovell et al., 2001; Pettorelli et al., 2005).

---

<sup>2</sup> This chapter is under review by Remote Sensing of Environment

The Moderate Imaging Spectrometer (MODIS) onboard Terra and Aqua satellites provides unprecedented data to monitor and quantify seasonal changes of forest canopy and phenology at local, regional and global scales. The MODIS science team provides standard products of LAI and fraction of PAR absorbed by canopy ( $FPAR_{canopy}$ ) (Knyazikhin et al., 1998a; Knyazikhin et al., 1998b). The MODIS-based LAI and  $FPAR_{canopy}$  at 1-km spatial resolution were generated by inversion of a radiative transfer model that uses surface reflectance of red and near infrared bands or by an empirical model that describes the relationships among NDVI-LAI- $FPAR_{canopy}$  when there are not enough good-quality observations for inversion of the radiative transfer model. The retrieval algorithms are based on the assumption that leaf spectral properties for each biome type are constant (Myneni et al., 2002; Wang, 2002). Similarly, Gobron and colleagues assumed a single spectra profile for all leaves when they retrieved  $FPAR_{canopy}$  (Gobron et al., 2000b; Gobron et al., 2002; Taberner et al., 2002).

However, many experiments showed that leaf structure and chemistry vary seasonally, resulting in seasonal dynamics of spectral properties. For example, some experiments showed that the chlorophyll concentration of leaves changed during the plant growing season (Demarez et al., 1999; Kodani et al., 2002). Another experiment also showed the variations of leaf water thickness and dry matter during the plant growing season (Gond et al., 1999). Accordingly, some researchers reported that their spectral measurements of leaves changed over the plant growing season (e.g., Demarez et al., 1999; Gitelson et al., 2002a; Stylinski et al., 2002). Ustin, Duan and Hart documented the changes of the canopy reflectance of the grass vegetation, deciduous vegetation and evergreen vegetation over a plant growing season (Ustin et al., 1994). Kodani and

colleagues documented the seasonal reflectance variation of Japanese beech from spring to autumn (Kodani et al., 2002), whereas Remer, Wald and Kaufman demonstrated changes in reflectance spectra of various ground surface targets, including forests, across three seasons (Remer et al., 2001). Work by Richardson and coauthors demonstrates that leaf reflectance properties change along elevational and latitudinal gradients; presumably this variation is driven by physiological differences resulting from differences in climate and site quality (Richardson et al., 2002; Richardson et al., 2003). So the seasonal and geographic variations of observed MODIS reflectance can be possibly attributed to variations of both canopy-level and leaf level characteristics of vegetation.

The specific objectives of this study are threefold: (1) to develop an improved procedure that identifies snow-contaminated, atmosphere-contaminated or other poor quality observations in daily MODIS images; (2) to study the seasonal dynamics of surface reflectance and some widely used vegetation indices, using contamination-free-or-less MODIS time series data collection; and (3) to estimate LAI and the fractions of PAR absorbed by chlorophyll, leaf and canopy, i.e.,  $FAPAR_{canopy}$ ,  $FAPAR_{leaf}$  and  $FAPAR_{chl}$  with contamination-free multiple daily MODIS images. We used a coupled leaf-canopy radiative transfer model (PROSPECT model +SAIL-2 model; Zhang et al., 2005). Both the leaf-level PROSPECT model and canopy-level SAIL model have been discussed extensively in the published literature, both separately and in combination (Verhoef, 1984; Kuusk, 1985; Verhoef, 1985; Jacquemoud et al., 1990; Braswell et al., 1996; Jacquemoud et al., 1996; Baret et al., 1997; Gond et al., 1999; Jacquemoud et al., 2000; Weiss et al., 2000; Bacour et al., 2002a; Combal et al., 2002; Verhoef et al., 2003; Zarco-Tejada et al., 2003; Di Bella et al., 2004). Our coupled PROSPECT+SAIL-2

model (hereafter called PROSAIL-2 model) retrieves simultaneously both leaf-level variables and canopy-level variables (Zhang et al., 2005). As a case study, we selected a temperate deciduous broadleaf forest at the Bartlett Experimental Forest in the White Mountains of New Hampshire, USA, where field-based measurements of LAI, leaf dry matter, leaf chlorophyll content and  $FAPAR_{canopy}$  are available for evaluating the inverted model variables.

## **5.2 Brief description of the Bartlett Experimental Forest site**

The Bartlett Experimental Forest eddy flux tower site ( $44.06^{\circ}$  N,  $71.29^{\circ}$  W, 272 m elevation) is within the White Mountain National Forest in north central New Hampshire, USA. Established in 1932 as a USDA Forest Service research forest, the Bartlett Experimental Forest is a 1050 ha tract of secondary successional northern deciduous and mixed northern coniferous forest. The vegetation is primarily deciduous forest, dominated by American beech (*Fagus grandifolia*), yellow birch (*Betula alleghaniensis*), sugar maple (*Acer saccharum*), red maple (*Acer rubum*), paper birch (*Betula papyrifera*), white ash (*Fraxinus Americana*), and pin cherry (*Prunus pennsylvanica*). There are also some evergreen needleleaf species within the forest, for example, eastern hemlock (*Tsuga canadensis*), red spruce (*Picea rubens*), white pine (*Pinus strobus*) and balsam fir (*Abies balsamea*). Soils are mainly moist but well drained spodosols. The climate is warm in summer and cold in winter. Annual mean precipitation is about 127 cm, and the precipitation is distributed throughout the year. Winter snow can accumulate to the depths of 150 to 180 cm. Winter season covers from November to next May. Additional

information of the study site are available elsewhere (Ollinger et al., 2005;

<http://www.fs.fed.us/ne/durham/4155/bartlett.htm#MPC> ).

The area surrounding on the eddy flux tower site is relatively flat. Instruments to measure incident and canopy-reflected radiation (PPFD, LI-190 quantum sensor, Li-Cor Biosciences, Lincoln, NE; global radiation, CM-3 pyranometer, Kipp & Zonen, Delft, Netherlands) are located at the top of a 25 m eddy covariance flux tower. A below-canopy network of six quantum sensors is located in a circle (radius = 15 m) around the base of the tower. Instruments are sampled every 10 seconds, and half-hourly means are output to a data logger (CR-10, Campbell Scientific, Logan, UT).

### **5.3 Method to remove snow- or atmosphere-contaminated MODIS daily observations**

The MODIS daily surface reflectance (MOD09GHK and MYD09GHK, v004), MODIS daily observation viewing geometry (MODMGGAD and MYDMGGAD, v004), and MODIS daily observation pointers (MODPTHKM and MYDPPTHKM, v004) are used in this study. There are reflectance values of the seven spectral bands (500m spatial resolution) in the MODIS daily surface reflectance product: red (620-670 nm), blue (459 – 479 nm), green (545-565 nm), near infrared (NIR<sub>1</sub>, 841-875 nm, and NIR<sub>2</sub>, 1230 – 1250 nm), and short-wave infrared (SWIR<sub>1</sub>, 1628 – 1652 nm, and SWIR<sub>2</sub>, 2105-2155 nm). The MODIS daily observation viewing geometry product contains observation viewing geometry information (view zenith angle, view azimuth angle, sun zenith angle and sun azimuth angle) at a nominal 1-km scale. The MODIS daily observation pointers product provides a reference, at the 500 m scale, to observations that intersect each pixel of

MODIS daily surface reflectance product in MODIS daily observation viewing geometry product (Zhang et al., 2005). All the MODIS data products are freely available at USGS Earth Observing System Data Gateway (<http://edcimswww.cr.usgs.gov/pub/imswelcome/>).

We acquired daily MODIS data (tile H12V04) from the NASA data archive for an area containing the Bartlett Experimental Forest eddy flux tower site. Using the geo-location information of the eddy flux tower site, we extracted time series data of daily MODIS images for one MODIS pixel that centers on the flux tower site. All daily MODIS data in 2004 are used to study the seasonal dynamics of reflectance and phenology, and the daily MODIS data over date of year (DOY) of 184-201 in 2005 were used for inversion of the PROSAIL-2 model.

The MODIS daily surface reflectance product has product quality information. The quality control (QC) data layer of the reflectance product includes information about errors and missing data in the daily surface reflectance product, for each of the seven MODIS bands, as well as information about whether an atmospheric correction was performed, and information about whether an adjacency correction was performed. If the QC value indicated any quality problem, the observation was not used in our analysis.

Furthermore, we examined reflectance values of SWIR<sub>2</sub> and blue bands for additional quality inspection. If one observation has SWIR<sub>2</sub> reflectance greater than 0.15 or blue reflectance greater than 0.2, the observation is identified as a bad observation and excluded for analysis. Figure 5.1a-b shows the MODIS blue and SWIR<sub>2</sub> reflectance for those observations in 2004 with blue reflectance of  $\leq 0.2$  and SWIR<sub>2</sub> of  $\leq 0.15$ . Some observations having both blue band  $\leq 0.1$  and SWIR<sub>2</sub> band  $\leq 0.15$  appear as clusters in

Figure 5.1c-d, while the other observations are randomly scattered. Contaminated atmosphere (e.g., partial cloud cover or residual aerosols) is one likely source that contributed to the scattering, though there are possibly other sources. We continued to remove those scattering observations, and Figure 5.2 shows the reflectance of the MODIS seven bands for the remaining clustering observations or atmospheric-contamination-free observations.

We calculated NDVI, Enhanced Vegetation Index (EVI, Huete et al., 1997), Land Surface Water Index (LSWI, Xiao et al., 2004c), and snow cover fraction ( $f_{snow}$ , Kaufman et al., 2002) for those observations in Figure 5.2a – g. The vegetation indices and snow cover fraction are shown in Figure 5.2h and Figure 5.3.

$$NDVI = \frac{\rho_{NIR_1} - \rho_{red}}{\rho_{NIR_1} + \rho_{red}} \quad (1)$$

$$EVI = 2.5 \times \frac{\rho_{NIR_1} - \rho_{red}}{\rho_{NIR_1} + 6 \times \rho_{red} - 7.5 \times \rho_{blue} + 1} \quad (2)$$

$$LSWI = \frac{\rho_{NIR_1} - \rho_{SWIR_1}}{\rho_{NIR_1} + \rho_{SWIR_1}} \quad (3)$$

$$f_{snow} = \begin{cases} \frac{\rho_{red} - 0.5\rho_{SWIR_2}}{0.6} \\ 0.51 + 0.07 \times \frac{\rho_{red} - 0.5\rho_{SWIR_2}}{0.6} \end{cases}, \text{if } \rho_{red} > 0.5\rho_{SWIR_2} \text{ and } \rho_{SWIR_2} \leq 0.15 \quad (4)$$

$$0, \text{otherwise}$$

where  $\rho_{blue}$ ,  $\rho_{red}$ ,  $\rho_{NIR_1}$ ,  $\rho_{SWIR_1}$ , and  $\rho_{SWIR_2}$  are reflectance values of the blue, red, NIR<sub>1</sub>, SWIR<sub>1</sub> and SWIR<sub>2</sub> bands. Figure 5.4a – g showed the observations in Figure 5.2a – g except the LSWI affected observations. Figure 5.4h shows the NDVI, EVI and LSWI in Figure 5.2h except the snow affected observations.

## **5.4 Description of the radiative transfer model and the inversion algorithm**

### **5.4.1 Brief description of the PROSPECT+SAIL-2 model**

We used the same PROSPECT+SAIL-2 model as in our previous study (Zhang et al., 2005). The PROSPECT model we used has five variables - leaf internal structure variable ( $N$ ), leaf chlorophyll content ( $C_{ab}$ ), leaf dry matter content ( $C_m$ ), leaf water thickness ( $C_w$ ) and leaf brown pigment ( $C_{brown}$ ) (Baret et al., 1997; Verhoef et al., 2003; Di Bella et al., 2004). The brown pigment in the five-variable PROSPECT model is needed for light absorption by non-chlorophyll (or non-photosynthetic) pigments in leaf. The SAIL (Scattering from Arbitrarily Inclined Leaves) model is a canopy radiative transfer model. The SAIL model has evolved gradually over time with minor changes reflecting individual study objectives in earlier studies (e.g., Goel et al., 1984c; Verhoef, 1984; Badhwar et al., 1985; Goel et al., 1985; Kuusk, 1985; Verhoef, 1985; Major et al., 1992; Braswell et al., 1996; Andrieu et al., 1997; Jacquemoud et al., 2000). The version of SAIL model described by Braswell and others (SAIL-2; Braswell et al., 1996) was used in this study. The SAIL-2 model decomposes a vegetation canopy into stems and leaves. In a typical parameterization, stems have spectral properties that are more similar to soil and litter than leaves. Leaf and stem mean inclination angles, and the self-shading effect of both leaves and stems are also considered.

The five-variable PROSPECT model was coupled with the SAIL-2 model (hereafter called PROSAIL-2) through replacing the leaf reflectance component in the SAIL-2 model with the PROSPECT model. The coupled PROSAIL-2 model was used to describe optical characteristics (reflectance, absorption and transmittance) of the canopy



and its components. The search ranges of the sixteen biophysical/ biochemical variables of the PROSAIL-2 model, based on an extensive literature review, were listed in Table 1. The sixteen biophysical and biochemical variables are plant area index (PAI), stem fraction (SFRAC), cover fraction (CF), stem inclination angle (STINC), stem bidirectional reflectance distribution function (BRDF) effect variable (STHOT), leaf inclination angle (LFINC), leaf BRDF effect variable (LFHOT), five leaf variables that simulate leaf optical properties ( $N$ ,  $C_{ab}$ ,  $C_m$ ,  $C_w$ ,  $C_{brown}$ ), two soil/litter variables that simulate soil/litter optical properties ( $SOIL_A$ ,  $SOIL_B$ ), and two stem variables that simulate stem optical properties ( $STEM_A$ ,  $STEM_B$ ). Because the MODIS data used in the study were atmospherically corrected, we do not consider atmospheric effect when we do inversion of the PROSAIL-2 model.

#### 5.4.2 Description of inversion algorithm -- the Metropolis algorithm

A method based on the Metropolis algorithm (Metropolis et al., 1953; Hurtt et al., 1996; Braswell et al., 2005; Zhang et al., 2005) was employed for inversion of the MODIS data. Figure 4 (a) shows that the MODIS blue reflectance over the site under cloud-free condition is less than 0.05 during plant growing season in 2004. There are thirteen observations for the period (DOY 184 to 201 in 2005) after discarding the observations with MODIS blue reflectance greater than 0.05. The thirteen observations are used for inversion. All mathematical description of the method can be found in the previous paper (Zhang et al., 2005). The strength of the method is that it can estimate posterior probability distributions of the variables and thus the retrieved distributions can provide estimates of uncertainty (such as standard deviations and confidence intervals) of

individual variables, conditioned on both the model and the observed data. The retrieved distributions can also provide information about the variable sensitivity of the model. The Metropolis algorithm is relatively computationally intensive, owing to the need for simulation of a large number of samples required to obtain a reliable estimate of the variables' distributions.

The Metropolis algorithm (Metropolis et al., 1953), is a type of Markov Chain Monte Carlo (MCMC) estimation procedure. It arises within a Bayesian statistical estimation framework (Gelman et al., 2000) and reflects the remaining uncertainty after the model has been constrained (inverted) with data. The Bayesian framework also requires quantification of prior information about the variables as prior probability densities and the prior to posterior scheme of calculations following Bayes' theorem. The MCMC constructs a random walk (Markov chain) through two steps: first at the current iteration, generating a new randomly generated "proposal" value and secondly testing an acceptance as follows: if the posterior density increases, the proposed value is accepted, i.e. it becomes the new value of the random walk, if the posterior density decreases, the proposed value is only accepted with probability equals the ratio of the new value posterior density over current value posterior density. MODIS red, green, NIR<sub>1</sub>, NIR<sub>2</sub> and SWIR<sub>1</sub> reflectance are used to calculate likelihood function. We also employed the same adaptive annealing temperate algorithm as in our previous study (Zhang et al., 2005). All mathematical description can be found in the previous paper.

### 5.4.3 Calculation of $FAPAR_{canopy}$ , $FAPAR_{leaf}$ , and $FAPAR_{chl}$

We developed a two-step procedure to calculate  $FAPAR_{chl}$ ,  $FAPAR_{leaf}$  and  $FAPAR_{canopy}$  using the PROSAIL-2 model. The first step is to invert the biophysical and biochemical variables using the coupled PROSAIL-2 model with observed spectral reflectance data (reflectance plus relative observation geometry), and the second is to calculate  $FAPAR_{canopy}$  (Goward et al., 1992),  $FAPAR_{leaf}$  (Braswell et al., 1996), and  $FAPAR_{chl}$  (see equations 9 - 13 ) using forward simulations.

$$FAPAR_{canopy} = \frac{APAR_{canopy}}{PAR_0} \quad (9)$$

$$FAPAR_{leaf} = \frac{APAR_{leaf}}{PAR_0} \quad (10)$$

$$FAPAR_{chl} = \frac{APAR_{chl}}{PAR_0} \quad (11)$$

$$APAR_{canopy} = APAR_{leaf} + APAR_{stem} \quad (12)$$

$$APAR_{leaf} = APAR_{chl} + APAR_{dry\ matter} + APAR_{brown\ pigment} \quad (13)$$

where  $PAR_0$  is the incoming PAR at the top of the canopy, and APAR is the absorbed PAR.  $APAR_{canopy}$ ,  $APAR_{leaf}$ ,  $APAR_{stem}$ ,  $APAR_{chl}$ ,  $APAR_{dry\ matter}$ , and  $APAR_{brown\ pigment}$  are absorbed PAR by canopy, leaf, stem, chlorophyll in leaf, dry matter in leaf, and brown pigment in leaf, respectively.

## **5.5 Results**

### **5.5.1 Temporal analyses of MODIS daily reflectance data in 2004**

Figure 5.2 exhibits the time series of surface reflectance for the seven spectral bands among the clustering MODIS daily data that covered the Bartlett Experimental Forest flux tower site. The blue surface reflectance values for the period after DOY 122 are much lower than those for the period before DOY 122 (Figure 5.2a). Similar seasonal patterns are also observed for surface reflectance in the green and red bands (Figure 5.2c, e). In comparison, surface reflectance values of NIR<sub>1</sub>, NIR<sub>2</sub> and SWIR<sub>1</sub> bands have a strong seasonal dynamics with peaks values in mid summer (Figure 5.2d, f, g).

Higher surface reflectance values of the visible bands (blue, green and red) and lower surface reflectance values of the SWIR bands (SWIR<sub>1</sub> and SWIR<sub>2</sub>) in the early period of the year suggest that snow cover occurs over that period and thus affects surface reflectance. There exists fractional snow cover through much of winter and early spring (Figure 5.3). We further exclude those observations with a fractional snow cover and Figure 5.4 shows the surface reflectance values of those observations without snow cover. Among the three visible bands, surface reflectance of green band has a distinct seasonal dynamics with peak values in late-June to early July (Figure 5.4e).

The seasonal dynamics of surface reflectance of individual spectral bands provide rich information for interpreting vegetation indices from the MODIS data and understanding the impacts of snow cover on vegetation indices. Our analysis identifies those daily observations that were partially covered by snow (Figure 5.3). The snow-covered season in 2004 for the study site ended around DOY 110. Without knowing

information of both the fraction of snow cover and surface reflectance over a MODIS pixel, one will have some difficulties in accurately interpreting NDVI, EVI and LSWI during the winter/spring seasons. There is very little green vegetation for the periods of DOY 1-100 and DOY 300 - 365 (Figure 5.4d). However, many observations in the winter/spring seasons still have high NDVI values, for example, one MODIS observation on DOY 57 has NDVI value of 0.856 (Figure 5.2h). The high NDVI values in the winter/spring seasons are likely attributed to both the wetness of soil/canopy background and higher solar zenith angles in winter/spring seasons (than solar zenith angles in summer/autumn). Note that SWIR<sub>2</sub> reflectance was low during the winter/spring seasons, which clearly suggests a wet soil/canopy background in that period. Moderate LSWI values in that period also suggest a wet soil/canopy background. The NIR<sub>1</sub> reflectance was low during the period, which suggests that there is little green vegetation during the period. Observations of bare or sparse vegetation targets with higher solar zenith angles have higher NDVI values than observations of same targets with lower solar zenith angles (Goward et al., 1992; Huete et al., 1992). Although the NIR<sub>1</sub> reflectance was low during the same period, but reflectance values of blue, green, and red bands were much smaller than NIR<sub>1</sub> reflectance (Figure 5.4a, c, d, and e). As the result, the mathematic formulation of NDVI still gives high NDVI values for some observations in the winter/spring seasons. This is consistent with earlier studies that examined the impacts of soil background and solar-view geometry on NDVI (Huete et al., 1997). Caution should be taken when using only NDVI to monitor vegetation phenology because NDVI is very sensitive to soil/canopy background wetness and solar-view geometry when vegetation cover fraction is small.

### 5.5.2 Comparison between retrieved and observed reflectance values of MODIS daily data collection from DOY 184 to 201 in 2005

The mean values of the retrieved variable distributions for the data collection from DOY 184 to 201 in 2005 were utilized as inputs to calculate the reflectance with forward simulations of the PROSAIL-2 model. Figure 5.5 shows a comparison of PROSAIL-2 retrieved reflectance with observed reflectance of MODIS green, red, NIR<sub>1</sub>, NIR<sub>2</sub>, and SWIR<sub>1</sub> bands. The correlation coefficient between retrieved and observed MODIS visible reflectance is 0.92 for the green band and 0.93 for the red band, respectively. The root mean squared error (RMSE) between observed and retrieved MODIS visible reflectance is 0.0023 for the green band and 0.0040 for the red band. The correlation coefficient between retrieved and observed NIR/SWIR reflectance is 0.92, 0.89, and 0.90 for NIR<sub>1</sub>, NIR<sub>2</sub> and SWIR<sub>1</sub>, respectively. The RMSE between observed and retrieved NIR/SWIR reflectance is 0.025, 0.025, and 0.016 for NIR<sub>1</sub>, NIR<sub>2</sub> and SWIR<sub>1</sub>, respectively. Note that the data collection spanned eighteen days, and any variation of leaf and canopy during the period may have contributed to the discrepancies between the retrieved reflectance and MODIS observed reflectance though we would not expect large changes at either leaf or canopy level because the canopy was well fully developed during early July. Possible errors introduced during MODIS pre-processing may also contribute to the discrepancies (e.g. imperfect atmospheric correction). The comparison suggests that the PROSAIL-2 model with the retrieved mean values of individual variables reasonably reproduces the surface reflectance of the temperate deciduous broadleaf forest site.

### 5.5.3 Uncertainty of individual variables from inversion of the PROSAIL-2 model with MODIS daily data collection from DOY 184 to 201 in 2005

The Metropolis inversion algorithm estimated probability distributions for individual model variables for the data collection from DOY 184 to 201 in 2005. The posterior distributions offer a measure of uncertainty in the form of their standard deviations or other quantile intervals, and the shape of the distributions provide a measure of compatibility between model and data. We examined the histograms of the sixteen variables from inversion of PROSAIL-2 for the MODIS data collection, and simply ranked them into three categories: “well-constrained”, “poorly-constrained” and “edge-hitting” (Braswell et al., 2005; Zhang et al., 2005). The “well-constrained” variables usually have a well-defined distribution, with small standard deviations relative to their allowable ranges. The “poorly-constrained” variables have relatively flat distributions with large standard deviations relative to their allowable ranges. The “edge-hitting” variables are those for which the modes of their retrieved values occurred near one of the edges of their allowable ranges and most of the retrieved values were clustered near this edge. Figures 5.6 – 5.10 showed the histograms of the sixteen variables in the PROSAIL-2 model and the histogram of leaf area index (LAI). Eight variables belong to “well-constrained”: plant area index (Figure 5.6a), five leaf variables (leaf internal structure variable, leaf chlorophyll content, leaf brown pigment content, leaf dry matter and leaf equivalent water thickness, Figure 5.8), average leaf inclination angle and leaf BRDF effect variable (Figure 5.9a and c). Six variables belong to “poor-constrained”: average stem inclination angle, stem BRDF effect variable (Figure 5.9b and d), two soil variables and two stem variables in SAIL-2 model (Figure 5.10). Stem fraction and cover fraction

belong to “edge-hitting” (Figure 5.7). Because stem fraction was distributed near zero and cover fraction was distributed near one, stem and soil had little effect on the canopy optical characteristics and consequently little information about stem and soil could be retrieved from MODIS observations. We calculated LAI using the equation  $LAI = (1 - SFRAC) \times PAI$ . LAI is also a well-constrained variable (Figure 5.6b) with mean value of 3.99 and standard deviation of 0.66.

#### 5.5.4 Distribution of $FAPAR_{canopy}$ , $FAPAR_{leaf}$ , and $FAPAR_{chl}$ using MODIS daily data collection from DOY 184 to 201 in 2005

We estimated the distributions of  $FAPAR_{canopy}$ ,  $FAPAR_{leaf}$ , and  $FAPAR_{chl}$  for the data collection of MODIS daily data from DOY 184 to 201 in 2005 using the retrieved distributions of individual variables in PROSAIL-2, and extracted their mean and standard deviation values (Figure 5.11). The mean values of  $FAPAR_{canopy}$ ,  $FAPAR_{leaf}$ , and  $FAPAR_{chl}$  were 0.879, 0.858, and 0.707, respectively. The standard deviation values were 0.033, 0.035, and 0.026, respectively.  $FAPAR_{canopy}$ ,  $FAPAR_{leaf}$ , and  $FAPAR_{chl}$  were well-constrained variables.

The difference between  $FAPAR_{canopy}$  and  $FAPAR_{leaf}$  is attributed to light absorption by stem ( $APAR_{stem}$ ), i.e., the non-leaf part of the canopy. During DOY 184 to 201 in 2005, the vegetation canopy is dominated by leaves, and only a very small proportion of stems are observed by the MODIS sensor. This may explain why the mean  $FAPAR_{canopy}$  value is only slightly higher than the mean value of  $FAPAR_{leaf}$ . The difference between  $FAPAR_{leaf}$  and  $FAPAR_{chl}$  is attributed to light absorption by the non-



chlorophyll component of the leaf. The mean  $FAPAR_{chl}$  value is 15% lower than the mean value of  $FAPAR_{leaf}$  and 17% lower than the mean value of  $FAPAR_{canopy}$ .

NDVI has been widely used for estimation of  $FAPAR_{canopy}$  and GPP (Potter et al., 1993; Prince et al., 1995; Ruimy et al., 1996; Running et al., 2004). In recent years, EVI has been used frequently as well (Justice et al., 1998). We calculated the mean and standard deviation of NDVI and EVI using the same MODIS images for the data collection from DOY 184 to 201 in 2005. The mean values of NDVI and EVI were 0.853 and 0.578, respectively. The standard deviations of NDVI and EVI were 0.010 and 0.073, respectively. The mean NDVI values are very similar to  $FAPAR_{leaf}$ , which supports the earlier studies that used NDVI to approximate  $FAPAR_{canopy}$  (e.g., Goward et al., 1992), as  $FAPAR_{leaf}$  and  $FAPAR_{canopy}$  values are close to each other. The mean EVI value is close to the mean  $FAPAR_{chl}$  values. Note that reflectance values in daily MODIS images are not BRDF corrected reflectance; therefore, the observation viewing geometry has an effect on the ranges of NDVI and EVI.

## **5.6 Discussion**

The MODIS sensors on the Terra and Aqua platforms provide daily observations of the land surface at moderate spatial resolution (250m -1000m). MODIS has been used to monitor phenology (e.g., Zhang et al., 2003; Xiao et al., 2004c; Zhang et al., 2004a; Zhang et al., 2004b; Xiao et al., 2005c). However there is a snowy winter season over temperate forest areas like Harvard Forest in MA, Howland Forest in ME, and Bartlett Experimental Forest in NH, USA. Through better screening out of the observations contaminated by snow and atmosphere, one can construct high quality time series data for

identifying forest green-up and leaf-off more accurately (Figures 5.2, 5.3 and 5.4). The plant growing period at the study site was from around DOY 122 to 282 in 2004. EVI values during the growing period was greater than 0.3. Figure 5.4h shows that NDVI, EVI and LSWI had a rapid increase during DOY 122 to DOY 135, and also had a quick decrease after DOY 275 in 2004 over the Bartlett Experimental Forest site. The field measured daily  $FAPAR_{canopy}$  and NDVI over the Bartlett Experimental Forest flux tower site in 2004 (unpublished results and they will be reported in another paper) shows similar green-up increase and leaf-senescence tendencies during same periods. The MODIS measurements were consistent with field measurements.

Many radiative transfer models have been used to retrieve LAI and estimate  $FAPAR_{canopy}$  (e.g., Myneni et al., 1997; Asner et al., 1998b; Bicheron et al., 1999). The MODIS LAI/FPAR team has used MODIS red and  $NIR_1$  bands as inputs to a 3-dimensional radiative transfer model to provide standard products of  $FAPAR_{canopy}$  and LAI at 1-km spatial resolution (Justice et al., 1998; Knyazikhin et al., 1998b, and personal communication with Dr. Ranga Myneni). The PROSAIL-2 model we used in this study is relatively simple in structure (one dimension in space) and but complex in chemistry. The input data of PROSAIL-2 are from five MODIS spectral bands. We leave the combination of complex canopy radiative transfer models and PROSPECT for future studies.

Little independent *in situ* data for evaluation of biophysical/biochemical variables at moderate (250m to 1000m) spatial resolution, including both canopy variables and leaf variables, have been collected because of expensive financial and human resource cost (e.g., Cohen et al., 2003; Turner et al., 2003). Here we discuss four variables (LAI, leaf

dry matter, leaf chlorophyll content and  $FAPAR_{canopy}$ ) that are important for interpreting the results of inversion of PROSAIL-2 in this study. The inversion of the PROSAIL-2 model estimated LAI with a mean of  $3.99 \text{ m}^2 / \text{m}^2$  and a standard deviation of 0.66. The field measured LAI around the footprint of the Bartlett Experimental Forest flux tower site during the peak growing season in 2004 varied between 3.6 and  $5.1 \text{ m}^2/\text{m}^2$  (Smith et al. unpublished data). The model-based estimation of LAI overlapped with the range of field measured LAI. Leaf dry matter ( $C_m$ ,  $\text{g}/\text{cm}^2$ ), another widely used variable in biogeochemical models, had a mean of  $0.0105 \text{ g}/\text{cm}^2$  and standard deviation of  $0.0041 \text{ g}/\text{cm}^2$ . The top-canopy leaf specific weight used for the deciduous trees in the Bartlett Experimental Forest by Ollinger and Smith (2005) was  $0.01 \text{ g}/\text{cm}^2$ , which was very close to the model-based estimate of the mean value of leaf dry matter. The histogram of inverted leaf chlorophyll content has a mean of  $52.3 \mu\text{g}/\text{cm}^2$  and standard deviation of  $2.6 \mu\text{g}/\text{cm}^2$ . The field measured leaf chlorophyll content for the leaves of mid to upper canopy of the deciduous species in early July of 2005 has a range of 23.5 –  $52.6 \mu\text{g}/\text{cm}^2$ . The range of inverted leaf chlorophyll content overlapped with the range of field measurements. Field measured leaf chlorophyll content for top, middle and bottom leaves of forest canopy are proposed to conduct in future. We suspect MODIS observed leaf chlorophyll content is closer to top-leaf chlorophyll content than to middle-leaf and bottom-leaf contents. The model-based  $FAPAR_{canopy}$  (Figure 5.11) had a range from 0.72 to 0.95 (most in the range from 0.77 to 0.95). The  $FAPAR_{canopy}$  calculated from field measurements of radiation above- and below- canopy at the Bartlett Experimental Forest flux tower site, had a range from 0.798 to 0.930 during 11:00am to 1:00pm of DOY 184 to 201 in 2005. The range of field measured  $FAPAR_{canopy}$  falls within the inverted range

of  $FAPAR_{canopy}$ , although the field radius is 15m and the MODIS pixel has a spatial resolution of 500m.

The results of this study plus the results from our previous study (Zhang et al., 2005) highlight the substantial difference between  $FAPAR_{canopy}$  and  $FAPAR_{chl}$  for the two temperate deciduous broadleaf forests (the Harvard Forest and the Bartlett Experimental Forest). The results suggest that the Production Efficiency Models (e.g., Potter et al., 1993; Prince et al., 1995; Ruimy et al., 1996; Running et al., 2004) that use  $FAPAR_{canopy}$  to estimate the amount of PAR for photosynthesis may potentially overestimate light absorption for photosynthesis, hence GPP.

In summary, this study provides an improved procedure for selecting atmosphere-contamination and snow-contamination free MODIS observations. With a contamination-free (atmospheric-contamination-free and/or snow-contamination-free) time series of daily MODIS observations, the seasonal variations of NDVI, EVI, LSWI and snow cover fraction of a temperate deciduous broadleaf forest site is better interpreted through the seasonal dynamics of surface reflectance of MODIS seven spectral bands. This study retested an innovative methodology presented in our previous study (Zhang et al., 2005) that combined radiative transfer model with the Metropolis statistical method to estimate leaf- and canopy-level biophysical/biochemical properties of the forest utilizing real MODIS data. This study also enhances the suggestion that both measurements of canopy-level variables (e.g., LAI) and field measurements of leaf-level variables (e.g., chlorophyll, other pigments, leaf dry matter, and leaf water content) will be useful for remote sensing and ecological research.

Table 5.1 A list of variables in the PROSAIL-2 model and their search ranges

	Variable	Description	Unit	Search range
Biophysical /biochemical variables	PAI	plant area index, i.e., leaf +stem area index		1 – 7.5
	SFRAC	Stem fraction		0 – 1
	CF	Cover fraction: area of land covered by vegetation/ total area of land		0.5 – 1
	C <sub>ab</sub>	Leaf chlorophyll a+b content	µg/cm <sup>2</sup>	0 – 80
	N	Leaf structure variable: measure of the internal structure of the leaf		1.0 – 4.5
	C <sub>w</sub>	Leaf equivalent water thickness	cm	0.001 – 0.15
	C <sub>m</sub>	Leaf dry matter content	g/cm <sup>2</sup>	0.001 – 0.04
	C <sub>brown</sub>	Leaf brown pigment content		0.00001 – 8
	LFINC	Mean leaf inclination angle	degree	10 – 89
	STINC	Mean stem inclination angle	degree	10 – 89
	LFHOT	Leaf BRDF variable: length of leaf/ height of vegetation		0 – 0.9
	STHOT	Stem BRDF variable: length of stem / height of vegetation		0 – 0.9
	STEM <sub>A</sub>	Stem reflectance variable: maximum (for a fitted function)		0.2 – 20
	STEM <sub>B</sub>	Stem reflectance variable range (for same fitted function)		50 – 5000
	SOIL <sub>A</sub>	Soil reflectance variable: maximum (for a fitted function)		0.2 – 20
	SOIL <sub>B</sub>	Soil reflectance variable: range (for same fitted function)		50 – 5000

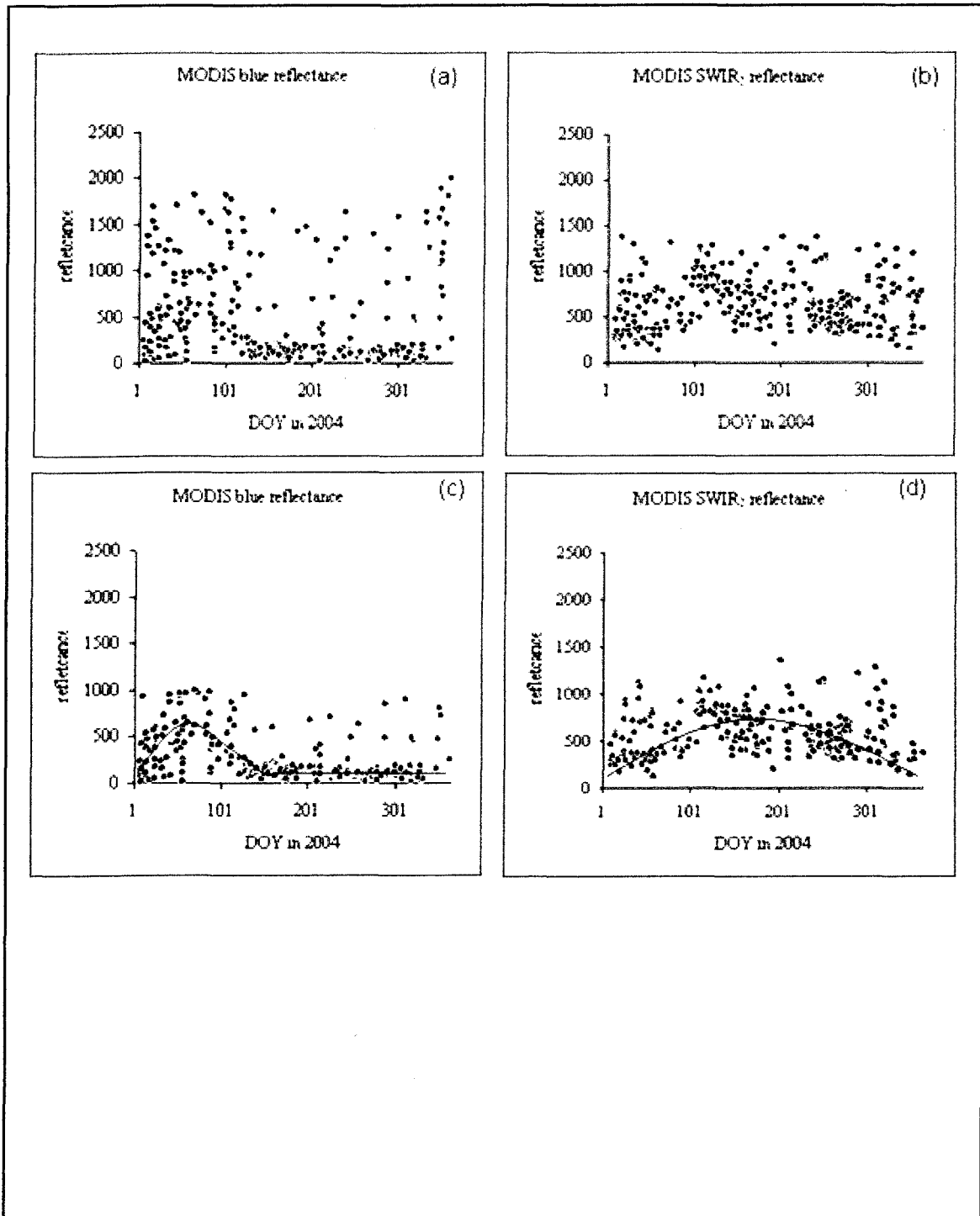


Figure 5.1 Reflectance of (a) blue and (b) SWIR<sub>2</sub> of MODIS daily observations of the Bartlett Experimental Forest tower site in 2004 (reflectance scale=0.0001) with blue less than 0.2 and SWIR<sub>2</sub> less than 0.15; reflectance of (c) blue and (d) SWIR<sub>2</sub> of MODIS daily observations in 2004 (reflectance scale=0.0001) with blue less than 0.1 and SWIR<sub>2</sub> less than 0.15

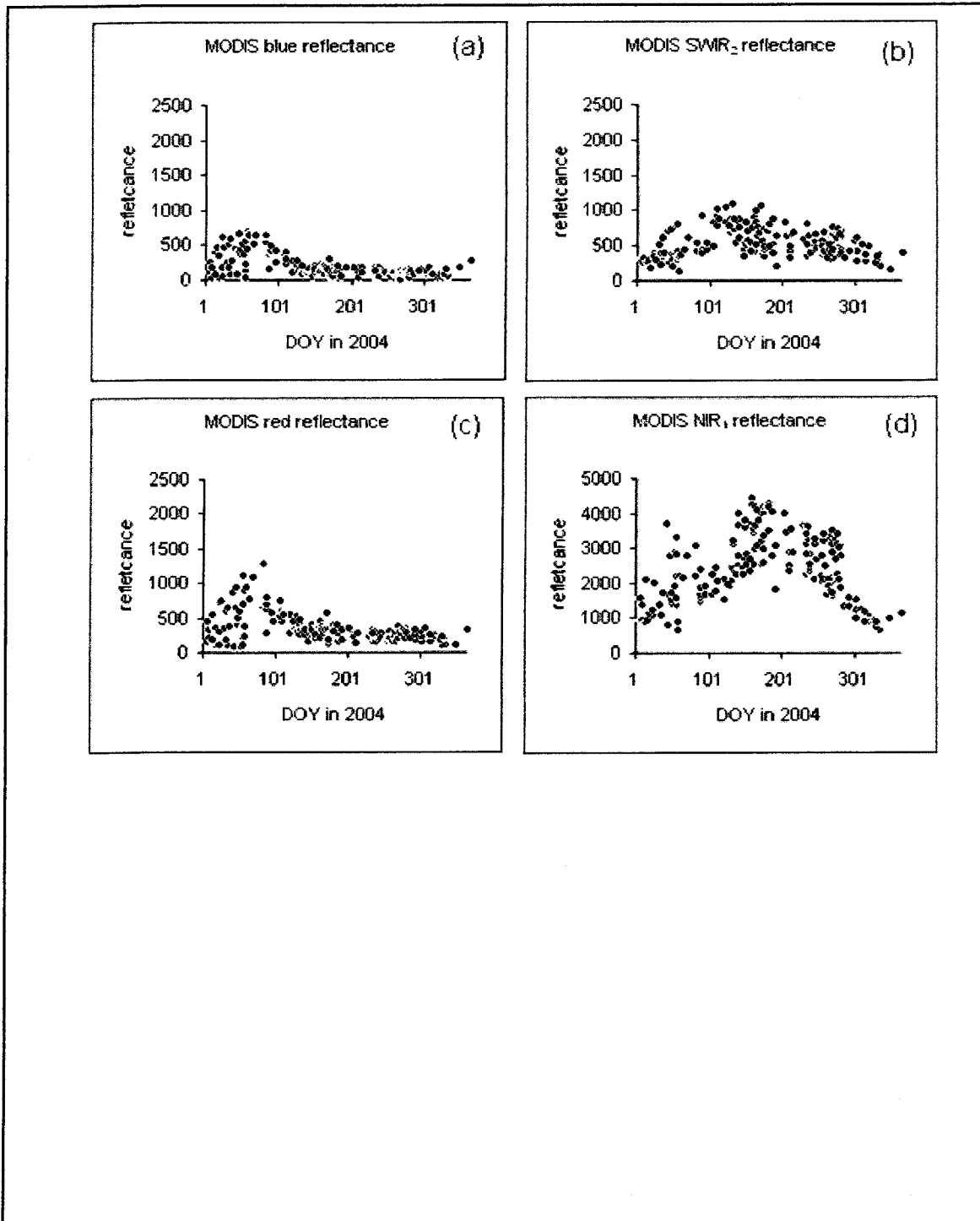


Figure 5.2 Clustering MODIS daily observations of the Bartlett Experimental Forest tower site in 2004 (reflectance scale=0.0001) and related NDVI, EVI and LSWI

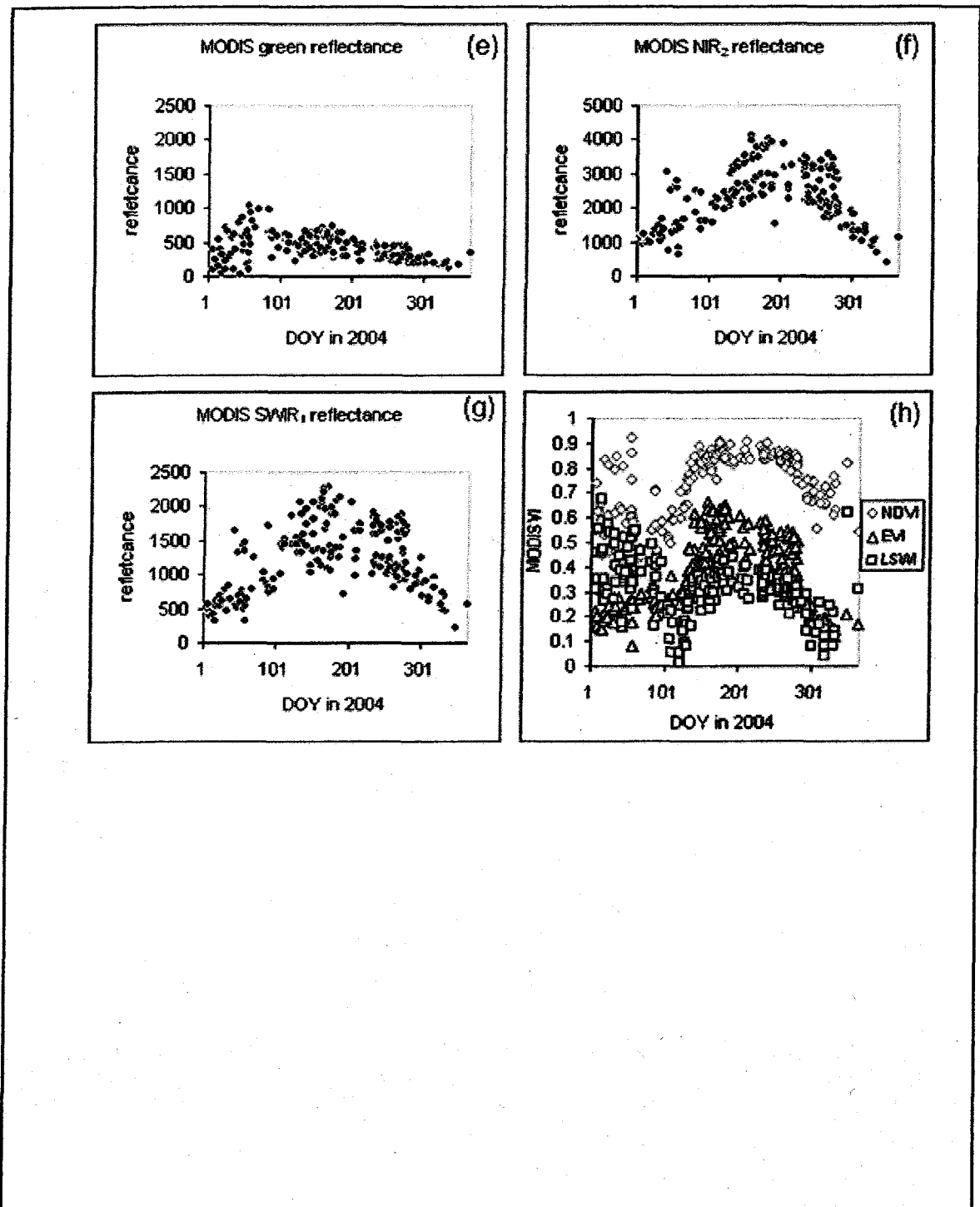


Figure 5.2 (continued) Clustering MODIS daily observations of the Bartlett Experimental Forest tower site in 2004 (reflectance scale=0.0001) and related NDVI, EVI and LSWI



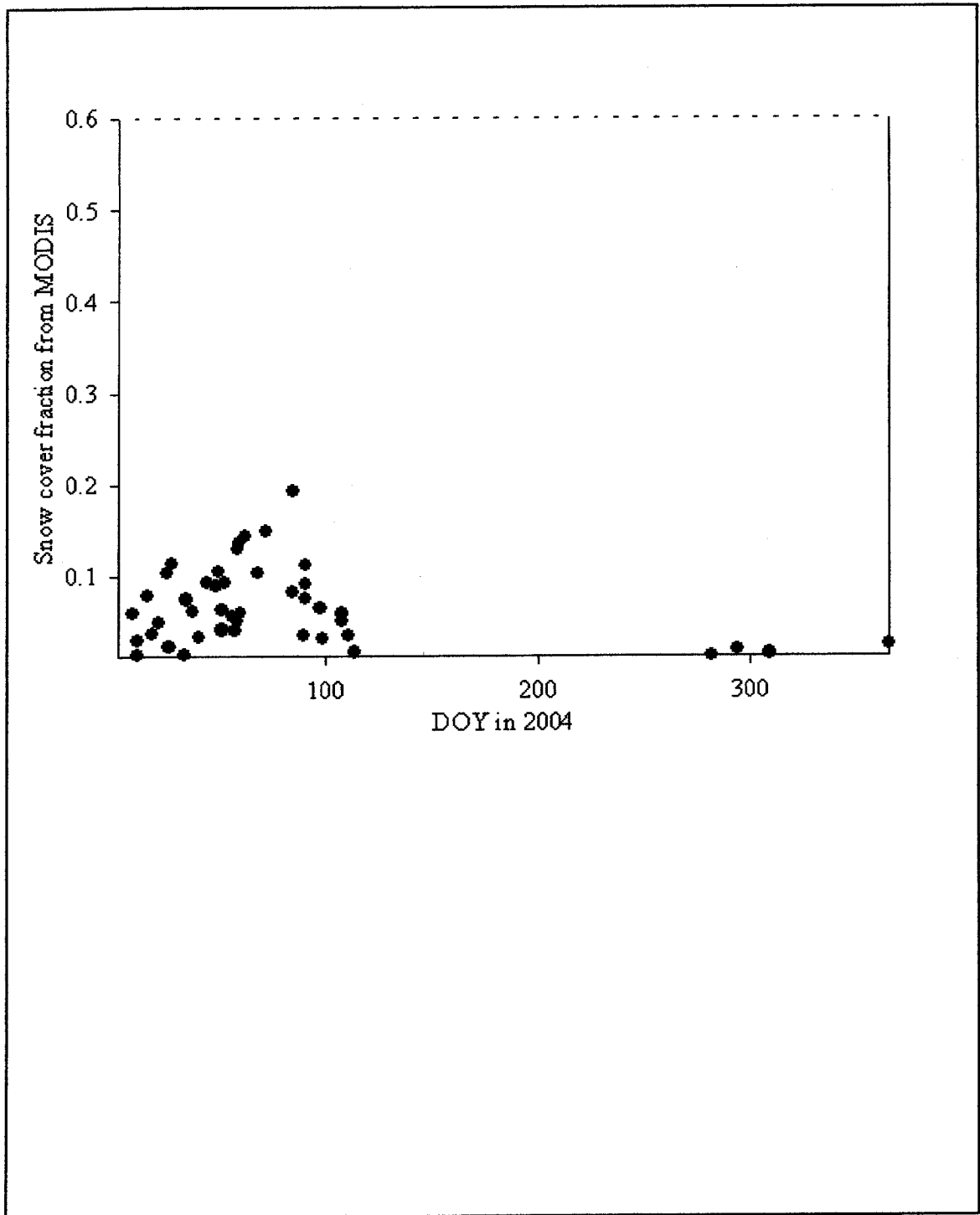


Figure 5.3 Snow cover fraction calculated with clustering MODIS daily observations of the Bartlett Experimental Forest tower site in 2004

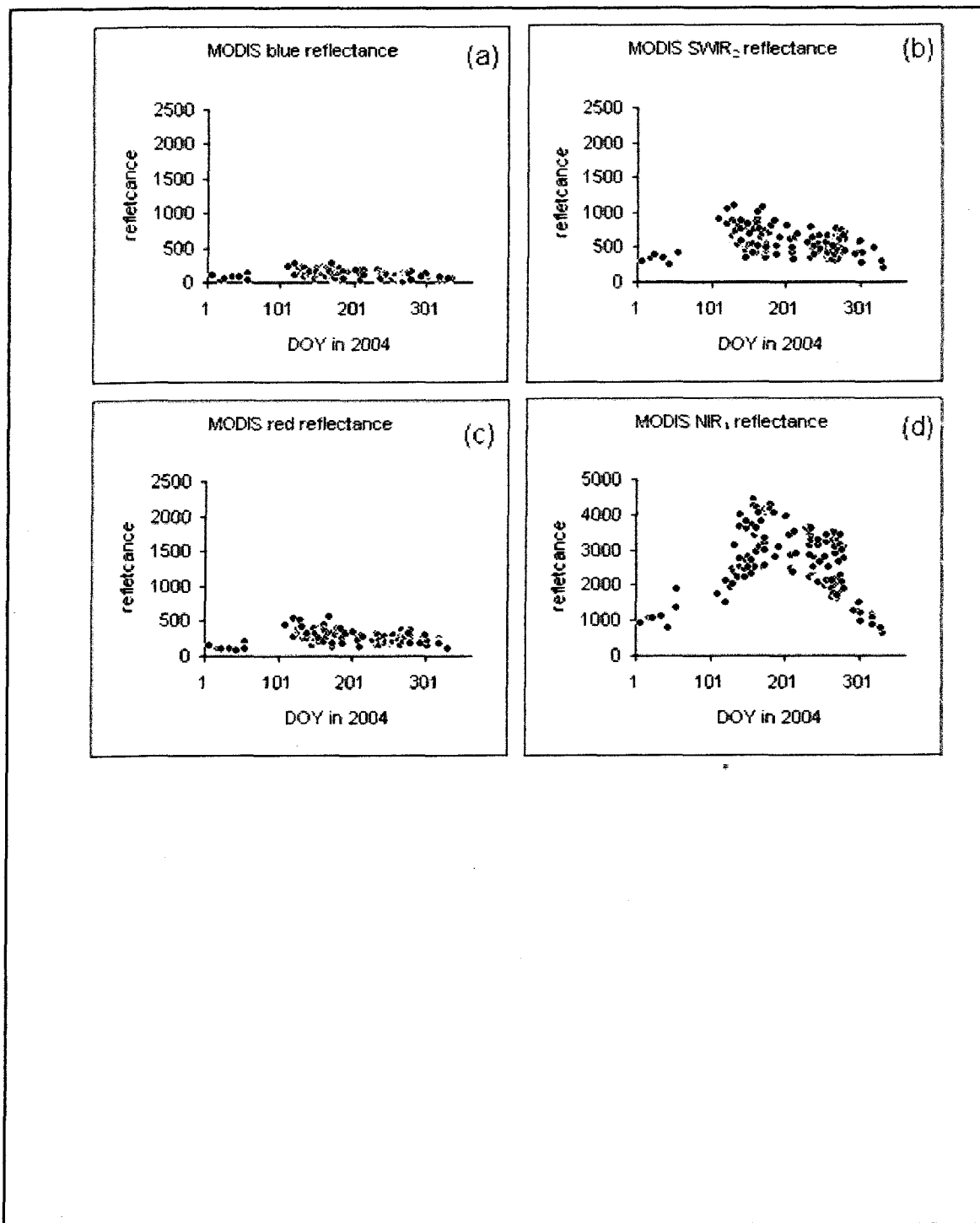


Figure 5.4 Contamination free MODIS daily observations of the Bartlett Experimental Forest tower site in 2004 (reflectance scale=0.0001) and related NDVI, EVI and LSWI

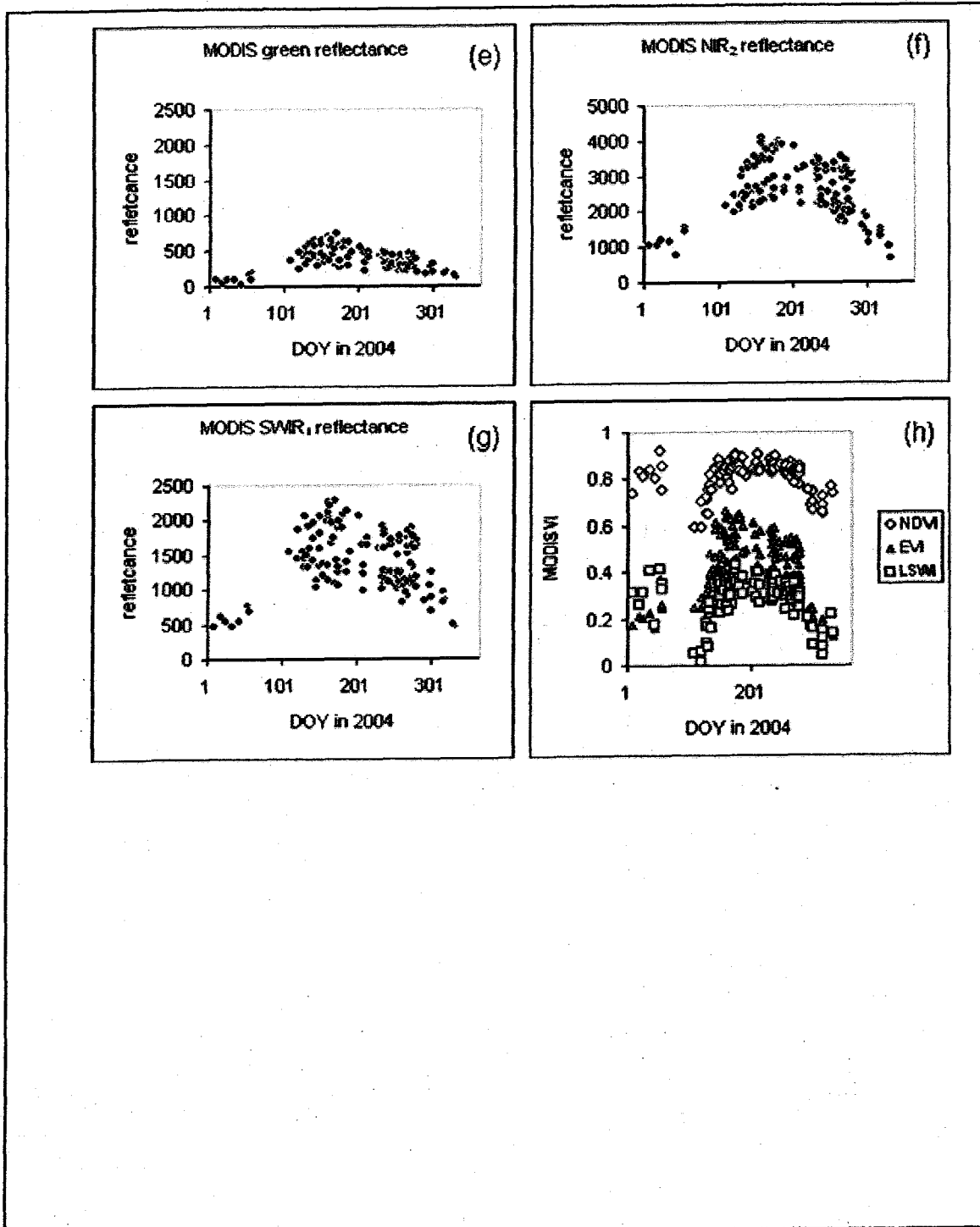


Figure 5.4 (continued) Contamination free MODIS daily observations of the Bartlett Experimental Forest tower site in 2004 (reflectance scale=0.0001) and related NDVI, EVI and LSWI

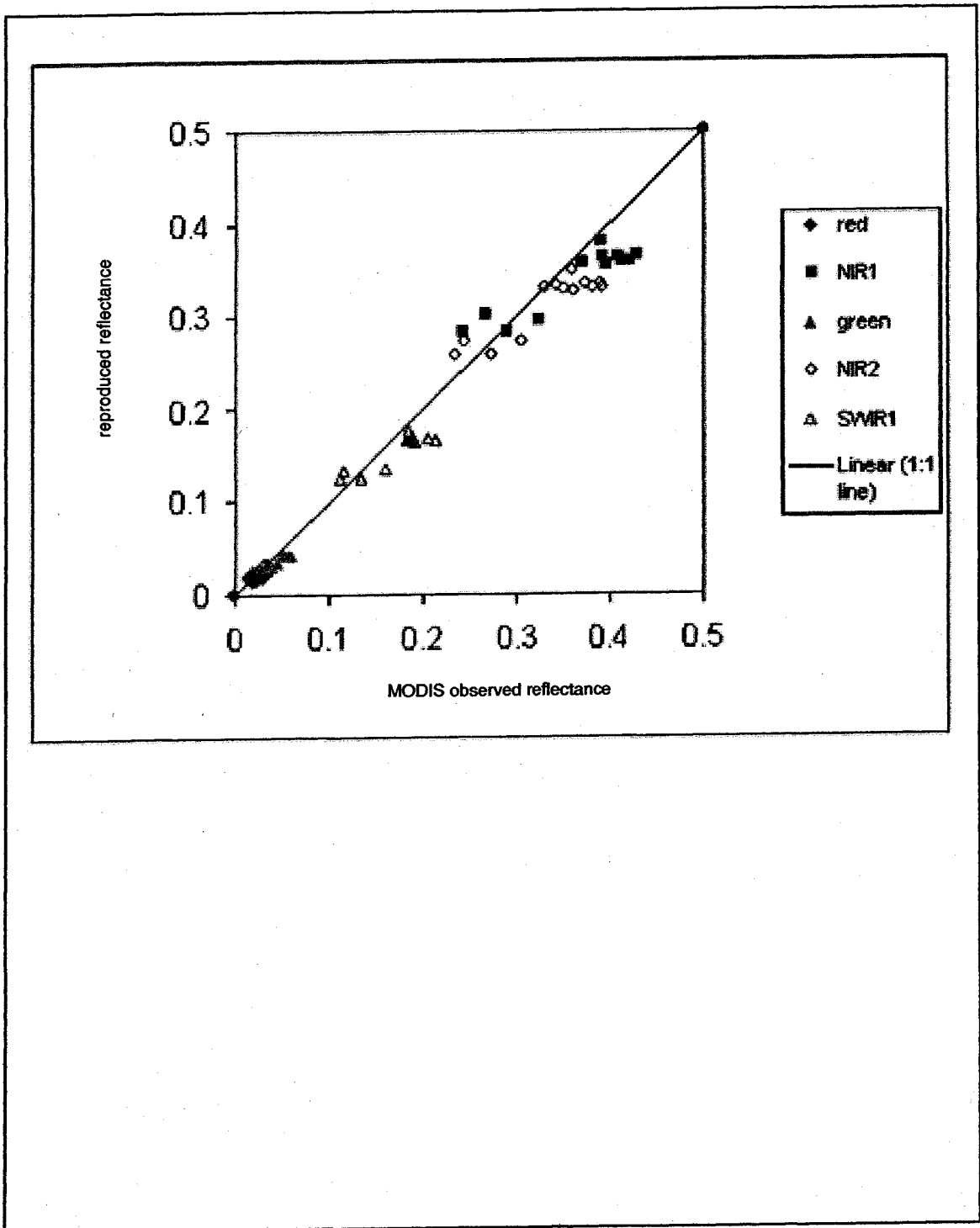


Figure 5.5 A comparison between the observed reflectance and PROSAIL-2-reproduced reflectance for five MODIS spectral bands (red, green, NIR<sub>1</sub>, NIR<sub>2</sub> and SWIR<sub>1</sub>). Surface reflectances were reproduced with the mean values of inverted variables from the PROSAIL-2 model using MODIS from DOY 184 to 201 in 2005.

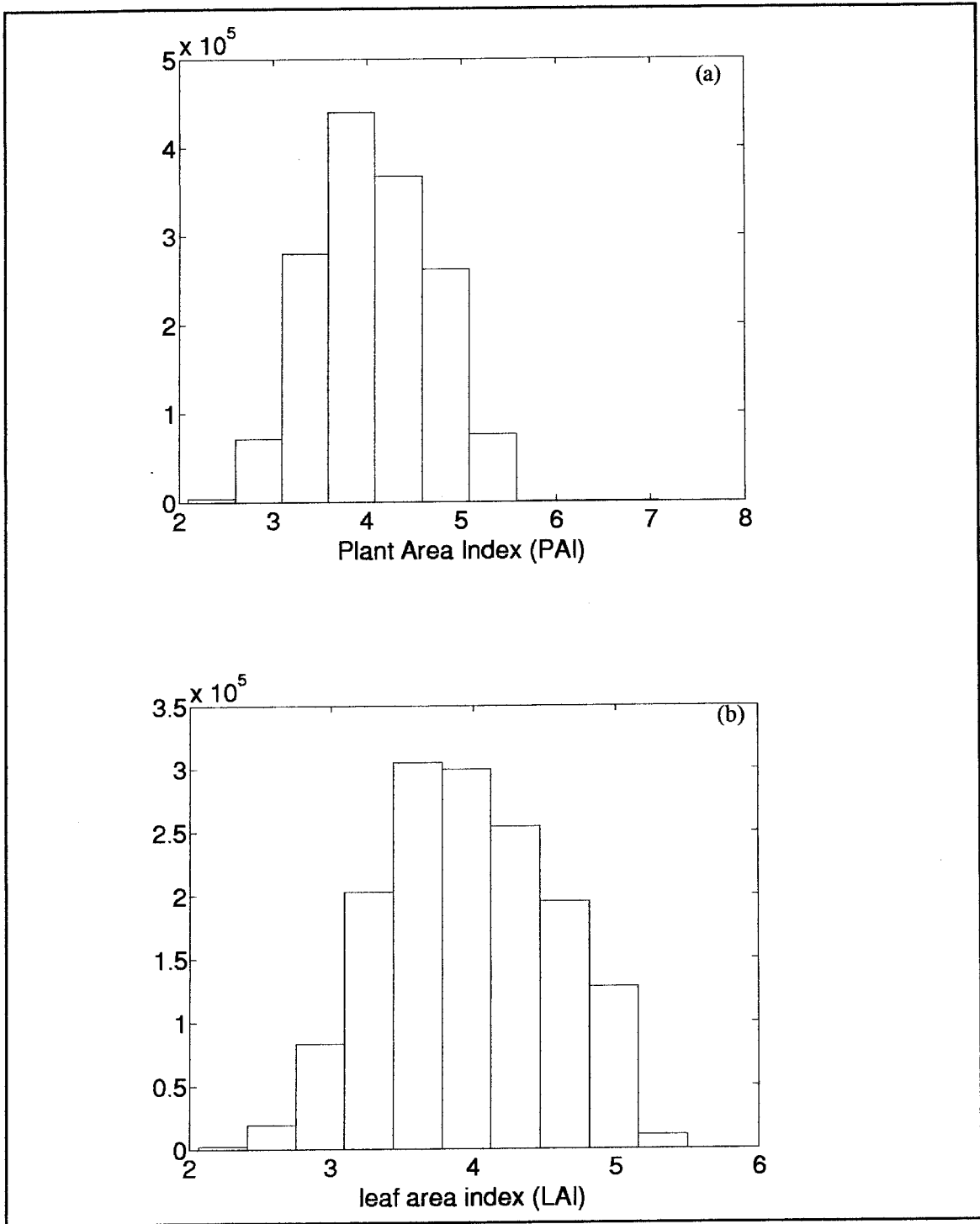


Figure 5.6 (a) Histogram of plant area index (PAI) for MODIS data collection of the Bartlett Experimental Forest tower site from DOY 184 to 201 in 2005; (b) Histogram of leaf area index (LAI) for MODIS data collection of the Bartlett Experimental Forest tower site from DOY 184 to 201 in 2005

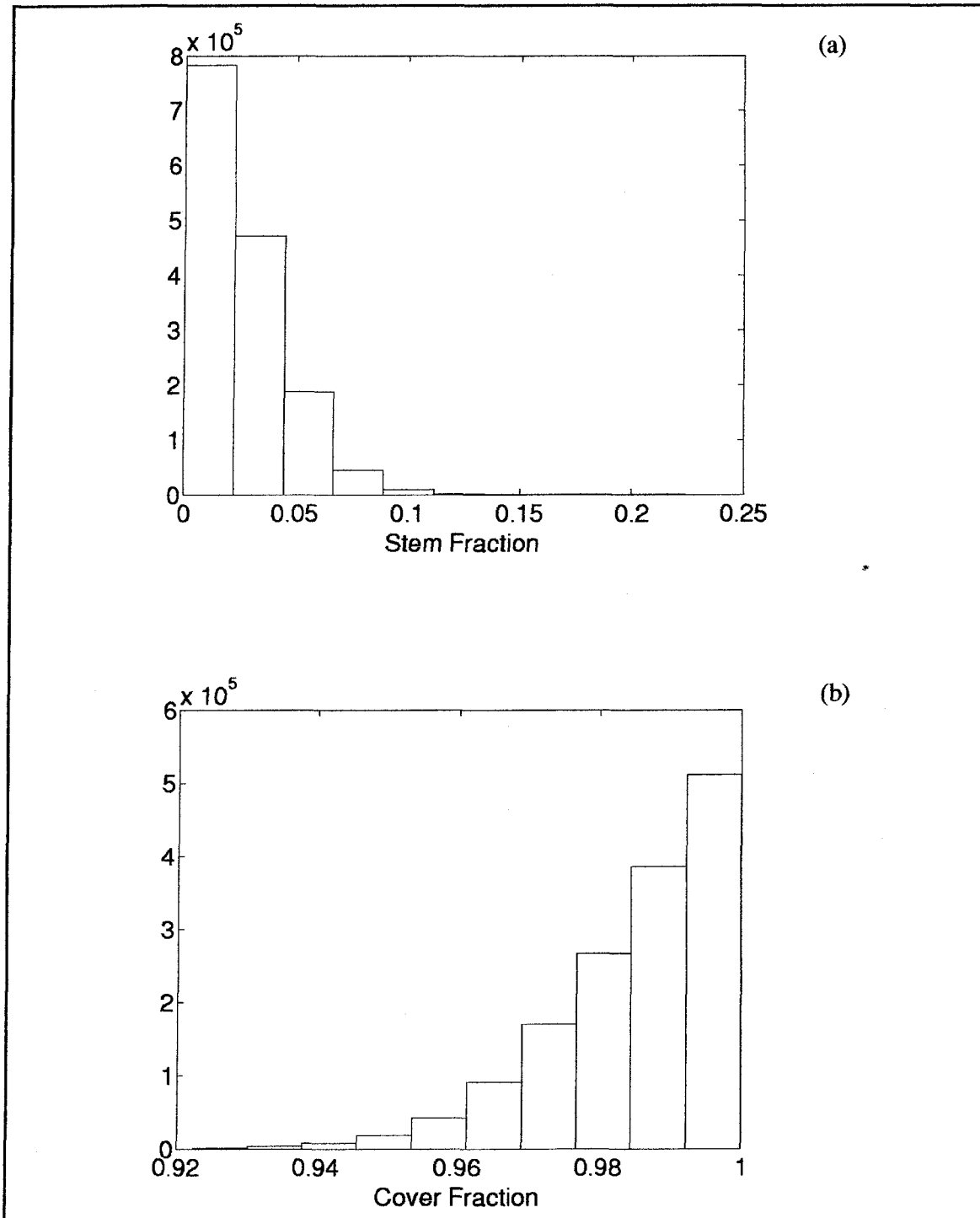


Figure 5.7 (a) Histogram of stem fraction for MODIS data collection of the Bartlett Experimental Forest tower site from DOY 184 to 201 in 2005; (b) Histogram of cover fraction for MODIS data collection of the Bartlett Experimental Forest tower site from DOY 184 to 201 in 2005

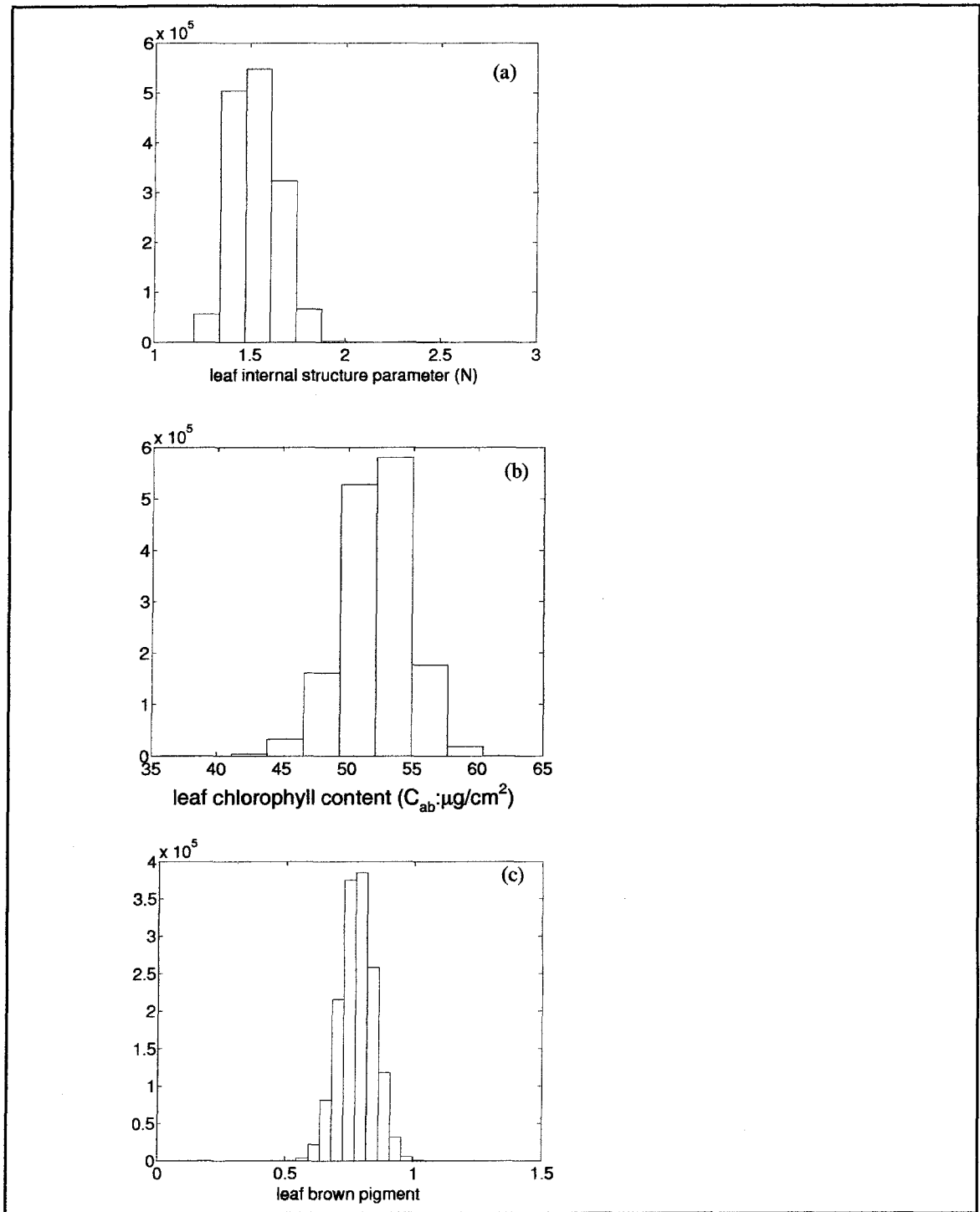


Figure 5.8 Histograms of leaf variables for MODIS data collection of the Bartlett Experimental Forest tower site from DOY 184 to 201 in 2005

Histograms of (a) leaf internal variable (N); (b) leaf chlorophyll content ( $C_{ab}$ ,  $\mu\text{g}/\text{cm}^2$ ); (c) leaf brown pigment ( $C_{brown}$ )

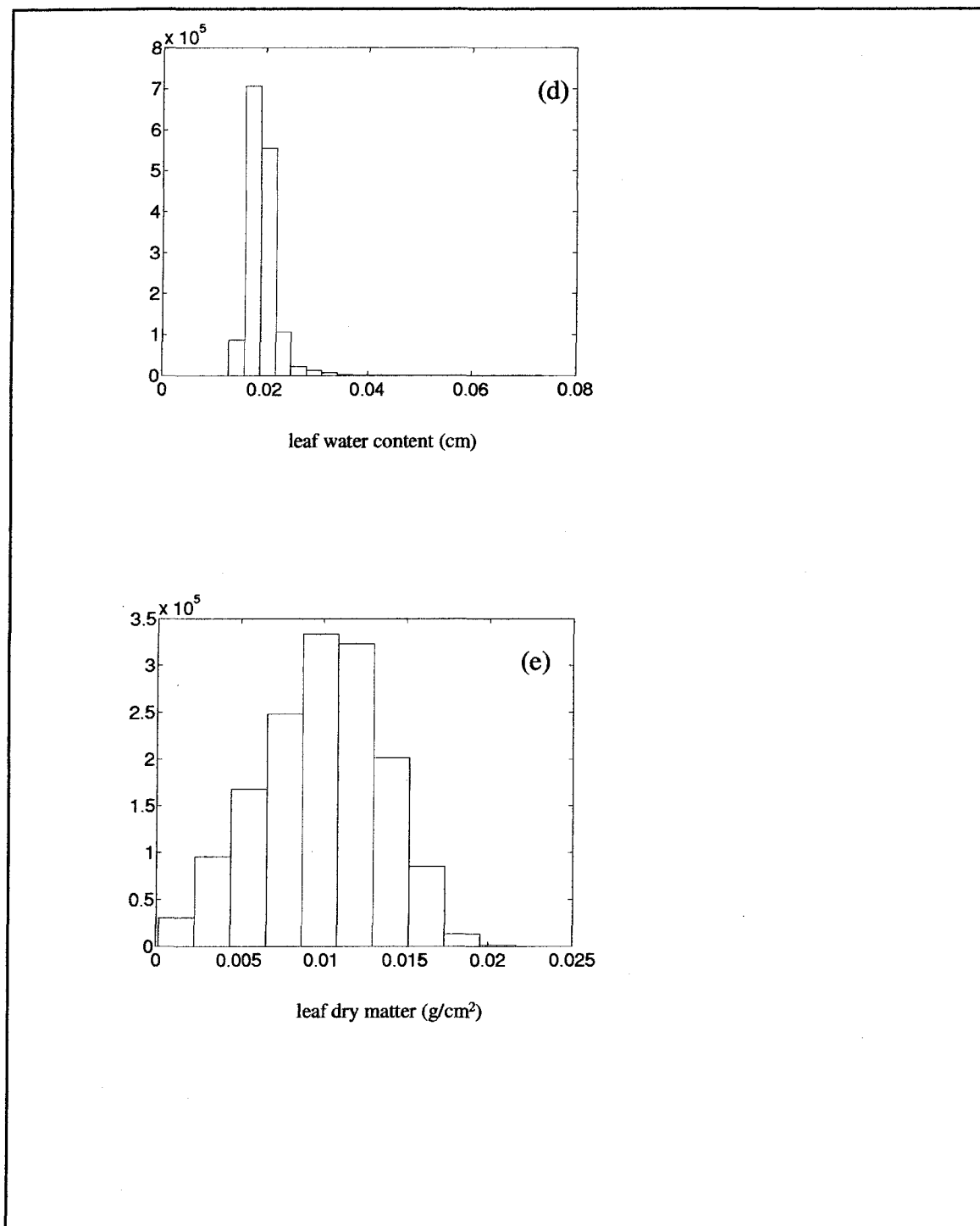


Figure 5.8 (continued) Histograms of (d) leaf equivalent water thickness ( $C_w$ , cm); and (e) leaf dry matter ( $C_m$ , g/cm<sup>2</sup>) for MODIS data collection of the Bartlett Experimental Forest tower site from DOY 184 to 201 in 2005



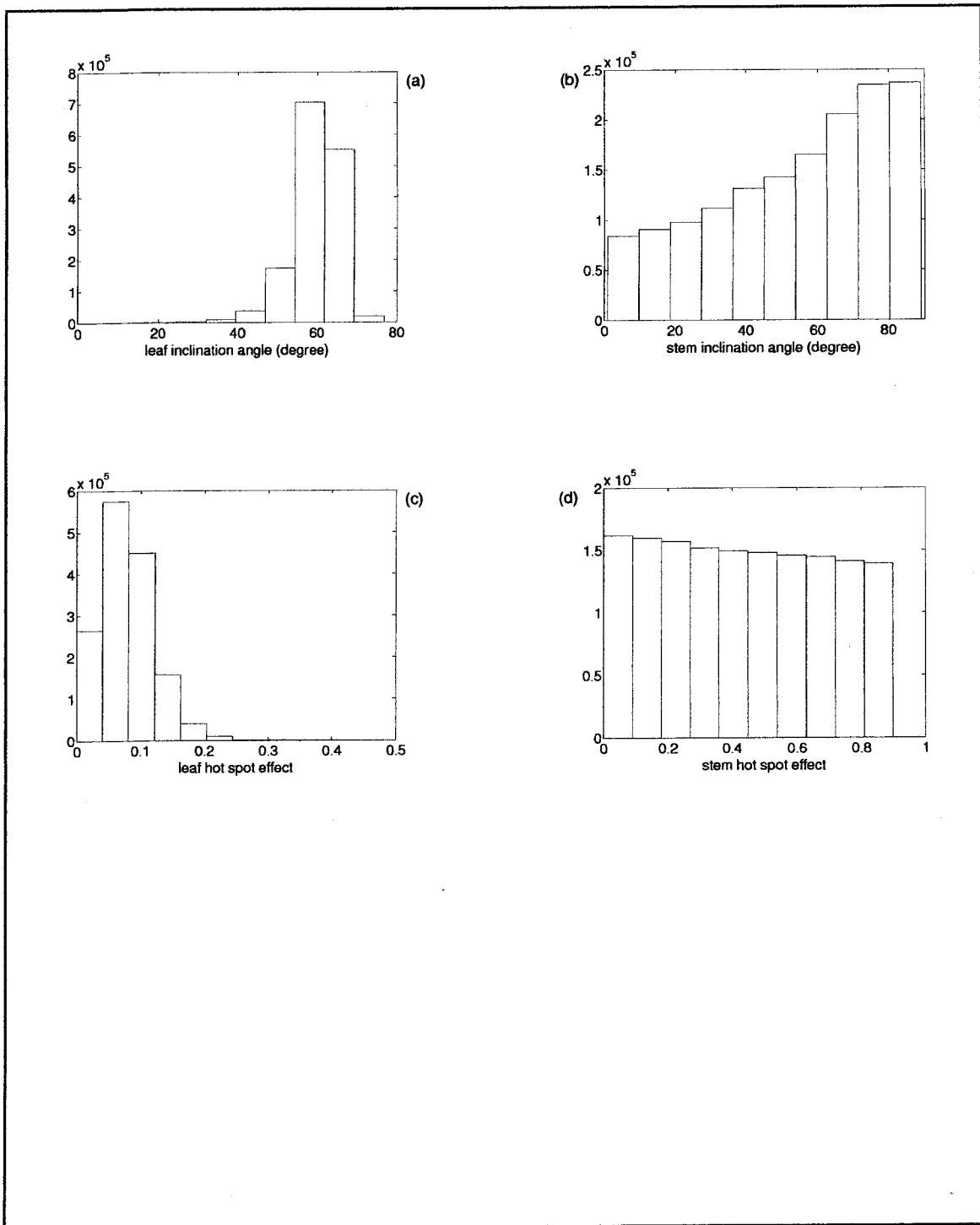


Figure 5.9 Histograms of (a) average leaf inclination angle (degree);(b) average stem inclination angle(degree); (c) leaf BRDF effect variable (d) stem BRDF effect variable for MODIS data collection of the Bartlett Experimental Forest tower site from DOY 184 to 201 in 2005

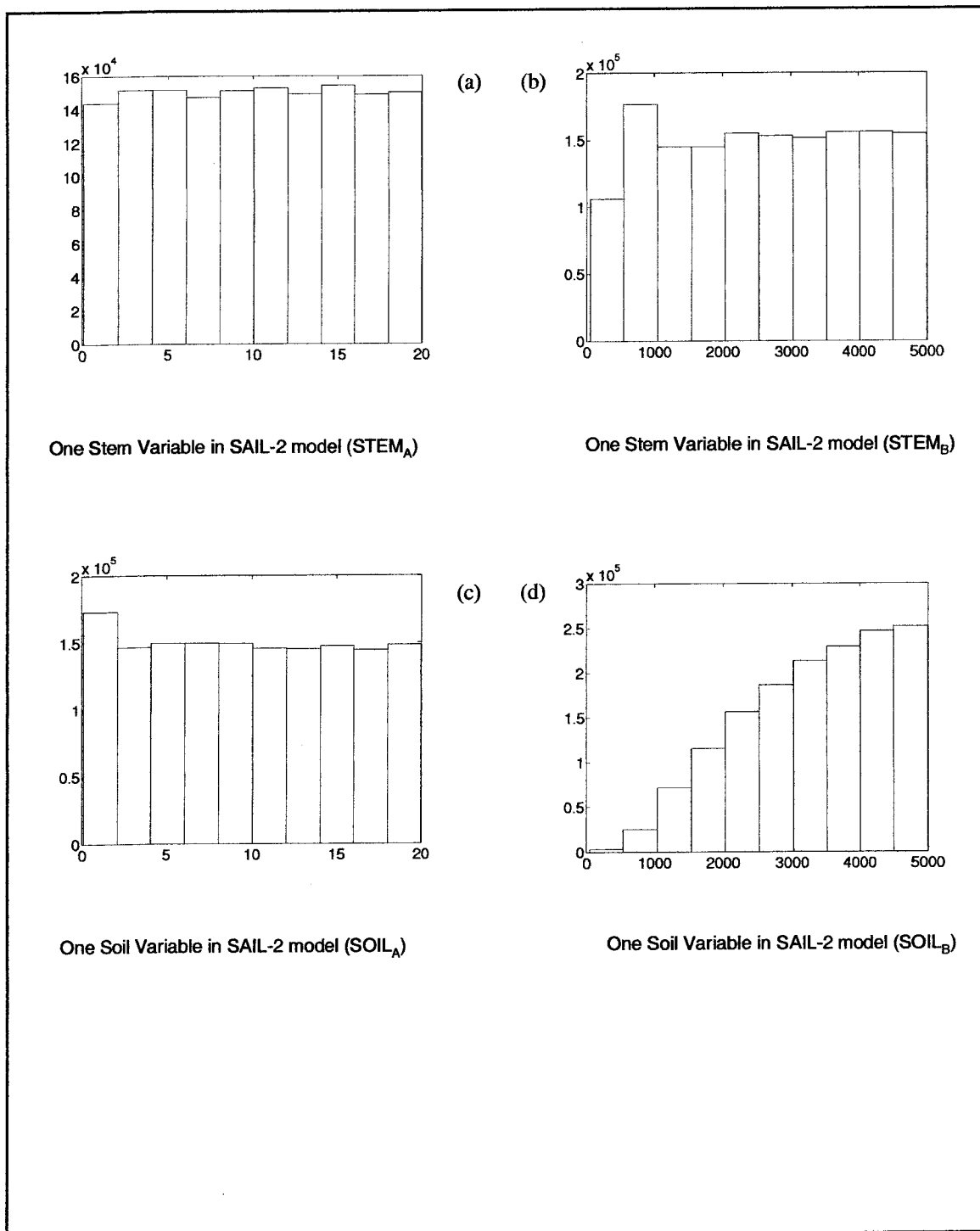


Figure 5.10 Histograms of (a) one stem variable in SAIL-2 ( $STEM_A$ ); (b) one stem variable in SAIL-2 ( $STEM_B$ ); (c) one soil variable in SAIL-2 ( $SOIL_A$ ); (d) one soil variable in SAIL-2 ( $SOIL_B$ ) for MODIS data collection of the Bartlett Experimental Forest tower site from DOY 184 to 201 in 2005

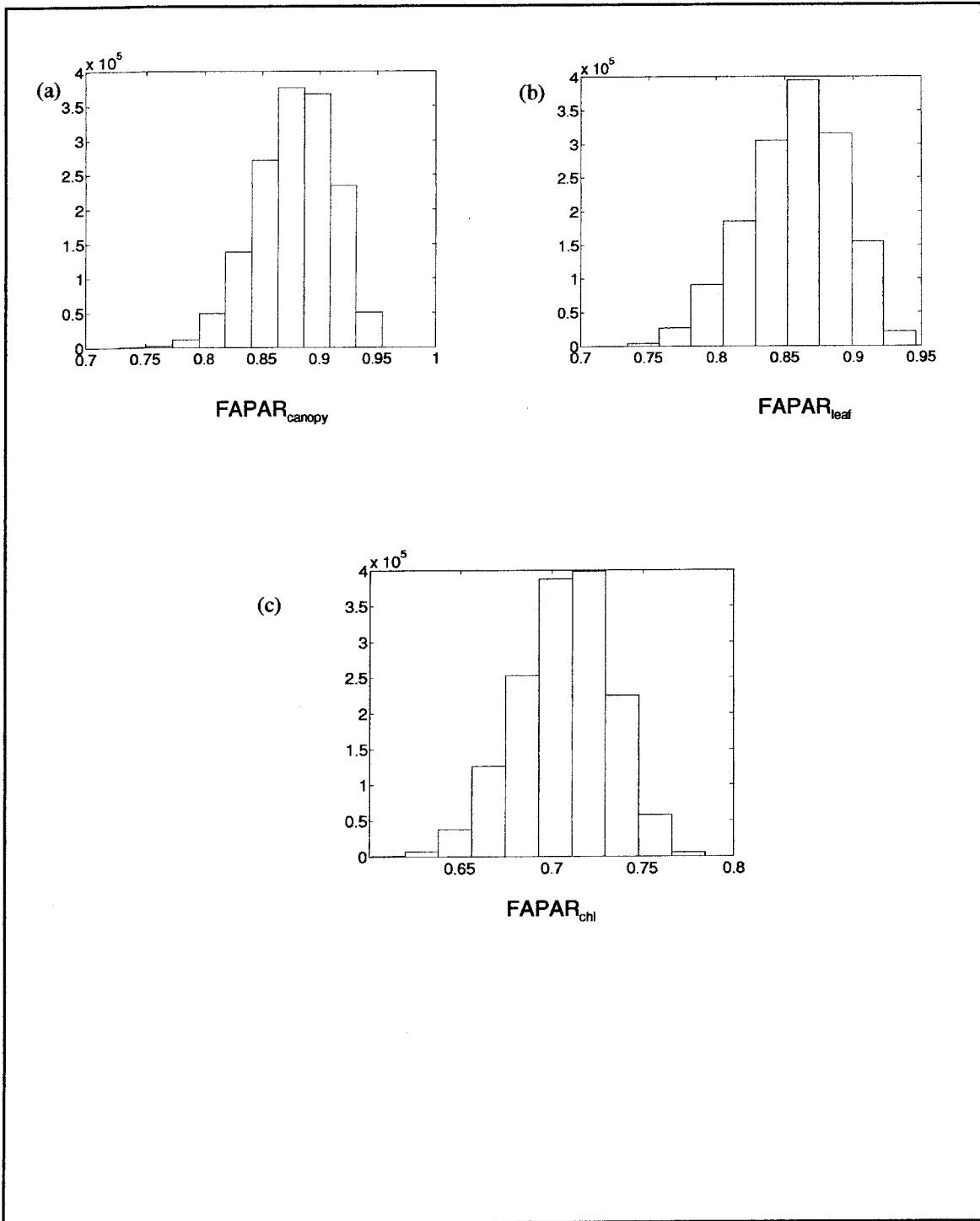


Figure 5.11 Histograms of fraction of photosynthetically active radiation absorbed by (a) canopy (FAPAR<sub>canopy</sub>); (b) by leaf (FAPAR<sub>leaf</sub>); (c) by chlorophyll (FAPAR<sub>chl</sub>) for MODIS data collection of the Bartlett Experimental Forest tower site from DOY 184 to 201 in 2005

## CHAPTER 6

# ARE SEASONAL MODIS SPECTRAL VARIATIONS OF TWO TEMPERATE DECIDUOUS BROADLEAF FOREST CANOPIES DURING PLANT GROWING SEASON ONLY DUE TO VEGETATION'S ANISOTROPIC NATURE?<sup>3</sup>

### 6.1 Introduction

Normalized Difference Vegetation Index (NDVI, Tucker, 1979) of the National Oceanic and Atmospheric Administration (NOAA) Advanced Very High Resolution Radiometer (AVHRR) has been widely used to monitor large-scale and/or long-term land cover studies (e.g., Sellers et al., 1995; Prince et al., 1996; Batista et al., 1997; Chen et al., 1999; Liu et al., 1999; Rodriguez-Yi et al., 2000; Shimabukuro et al., 2000; Dessay et al., 2004; Pettorelli et al., 2005). However, AVHRR NDVI has two kinds of limitations: one is related to the quality of the sensors and data pre-processing procedures (e.g., Cihlar et al., 1997; Cihlar, 2000); another one is related to the inherent problem of NDVI itself (Huete et al., 1994; Huete et al., 2002). The AVHRR NDVI is easy to be affected by atmosphere, canopy/soil background, and viewing geometry, and it is also easy to saturate (Cihlar et al., 1994a; Cihlar et al., 1994b; Cihlar et al., 1994c; Huete et al., 1997). Some experiemnts and radiative transfer model simulation studies studied the relationship between vegetation indices (e.g. NDVI) and sun-sensor-target or viewing geometry (e.g.,

---

<sup>3</sup> This chapter will be submitted to Remote Sensing of Environment soon

Goward et al., 1992; Huete et al., 1992; Cihlar et al., 1994c; Epiphanio et al., 1995; Chopping, 2001). Huete and colleagues proposed an 'enhanced vegetation index' (EVI) for sensors that have red, near infrared and blue bands to overcome the effect of atmosphere and canopy/soil background (Huete et al., 1997). Literature showed that many studies have contributed great efforts on the consideration of viewing geometry effect for different study objectives (e.g., Baret et al., 1991; Cihlar et al., 1994c; Roujean et al., 1995; Braswell et al., 1996; Asner et al., 1998a; Gobron et al., 2000b; White et al., 2002; Latifovic et al., 2003).

The Moderate Imaging Spectrometer (MODIS) has finer spatial, spectral resolution and better calibrated and atmospherically corrected observations than AVHRR and offer an unprecedented opportunity to monitor and quantify seasonal changes of vegetation canopy and phenology at local, regional and global scales for both short-term and long-term periods. Ever though many efforts have been contributed to the consideration of viewing geometry effect of land targets, it is still a question to debate that: is seasonal spectral variation of a land target only due to the viewing geometry effect after the well calibration and atmospheric correction data processing? Specially, are seasonal MODIS spectral variations of a temperate broadleaf deciduous forest during the plant growing season only due to the viewing geometry effect (i.e., the anisotropic nature of the forest)? Note that Myneni and others (Knyazikhin et al., 1998a; Knyazikhin et al., 1998b; Myneni et al., 2002; Wang, 2002), in order to derive leaf area index [LAI] and fraction of photosynthetically active radiation [PAR] absorbed by canopy [FPAR<sub>canopy</sub>] from bidirectional reflectance, assumed that leaf spectral properties for each biome type are constant; Gobron and colleagues assumed a single spectra profile for any

leaf to derive  $FPAR_{\text{canopy}}$  (Gobron et al., 2000b; Gobron et al., 2002; Taberner et al., 2002). The former efforts were based on the up-to-date exploration of AVHRR and were useful. When these assumptions are relaxed, we may be possible to see more details of canopy and leaf with MODIS.

Vegetation has anisotropic nature, i.e., the bidirectional reflectance distribution function (BRDF). The origins of BRDF of vegetation canopy are mainly microscopic shadow casting of the canopy and volume scattering in the vegetation canopy. The bidirectional reflectance provided by wide-swath satellite sensors (e.g., AVHRR/NOAA and MODIS) combines the BRDF effect and the information of the seasonal changes of canopy and leaf together. Some studies documented canopy reflectance changing during the plant growing season, or along elevational and latitudinal gradients (Ustin et al., 1994; Remer et al., 2001; Kodani et al., 2002; Richardson et al., 2002; Richardson et al., 2003). Leaf structure and chemistry was reported to vary seasonally, resulting in seasonal patterns of spectral variation (Demarez et al., 1999; Gond et al., 1999; Kodani et al., 2002; Gitelson et al., 2002a; Stylinski et al., 2002). So the seasonal variation of observed MODIS reflectance of vegetation, hence the seasonal change of retrieved LAI,  $FPAR_{\text{canopy}}$ , and vegetation indices (e.g., NDVI, EVI, and land surface water index [LSWI], Huete et al., 1997; Xiao et al., 2004c) can be possibly contributed from variations of canopy level characteristics, leaf level characteristics and/or BRDF effect. To uncouple BRDF effect from bidirectional reflectance for quantitative analysis of seasonal changes of the vegetation and its leaves is a challenging task (Chopping, 2000).

The objectives of this study are threefold: (1) to study the seasonal dynamics of surface reflectance and NDVI, EVI and LSWI, using contamination free MODIS time

series data collection; (2) to estimate LAI and the fractions of PAR absorbed by chlorophyll, leaf and canopy, i.e.,  $FAPAR_{canopy}$ ,  $FAPAR_{leaf}$  and  $FAPAR_{chl}$  with contamination-free multiple daily MODIS images; and (3) to evaluate if the seasonal variations of observed contamination free MODIS reflectance, NDVI, EVI and LSWI are only because of the BRDF effect. Selected seasonal reflectance dynamics from (1) and inverted variables from (2) are useful for our evaluation in (3). A coupled leaf-canopy radiative transfer model was utilized in the study (PROSPECT+SAIL-2 model; Zhang et al., 2005). Our coupled PROSPECT-SAIL-2 model estimates simultaneously both leaf-level variables and canopy-level variables (Zhang et al., 2005). As a case study, we selected two research sites of the Missouri Ozark Forest (MOF) in the southeastern Missouri, USA, where field-based observations leaf chlorophyll concentration and leaf dry matter are available for evaluating the inverted model variables.

## **6.2 Brief description of two research sites of the Missouri Ozark Forest (MOF)**

The two research sites in the Missouri Ozark Forest (MOF) locate in the southeastern Missouri Ozarks. One site ( $37^{\circ}11'53.12''N$ ,  $91^{\circ}0'29.75''W$ ; hereafter called site 1) has a 100m\*100m intermediate forest stand (~ 20 years old) surrounded by mature forest (~70 years old); and another site ( $37^{\circ}10'38.26''N$ ,  $91^{\circ}7'53.17''W$ ; hereafter called site 2) is occupied totally by mature forest (~70 years old). White oak (*Quercus alba*) and black oak (*Quercus velutina*), along with scarlet oak (*Quercus coccinea*) and hickory (*Carya* spp.), dominate the forest canopy of MOF. The oak species are little resilient to drought and fire. Mean annual temperature and mean annual precipitation is  $13.3^{\circ}C$  and

1120 mm, respectively. Soils were formed mostly in residuum. More than 90% of MOF has an elevation less than 300m (Xu et al., 2004).

### **6.3 Method to get contamination free MODIS daily observations**

The MODIS daily surface reflectance (MOD09GHK and MYD09GHK, v004), MODIS daily observation viewing geometry (MODMGGAD and MYDMGGAD, v004), and MODIS daily observation pointers (MODPTHKM and MYDPHMKM, v004) are used in this study. There are reflectance values of the seven spectral bands (500m spatial resolution) in the MODIS daily surface reflectance product: red (620-670 nm), blue (459 – 479 nm), green (545-565 nm), near infrared (NIR<sub>1</sub>, 841-875 nm, and NIR<sub>2</sub>, 1230 – 1250 nm), short-wave infrared (SWIR<sub>1</sub>, 1628 – 1652 nm, and SWIR<sub>2</sub>, 2105-2155 nm). The MODIS daily surface reflectance product has product quality information. The quality control (QC) data layer of the reflectance product includes information about errors and missing data in the daily surface reflectance product, for each of the seven MODIS bands, as well as information about whether an atmospheric correction was performed, and information about whether an adjacency correction was performed. If the QC value indicates any quality problem, the observation was excluded in our analysis. The MODIS daily observation viewing geometry product contains observation viewing geometry information (view zenith angle, view azimuth angle, sun zenith angle and sun azimuth angle) at a nominal 1-km scale. The MODIS daily observation pointers product provides a reference, at the 500 m scale, to observations that intersect each pixel of MODIS daily surface reflectance product in MODIS daily observation viewing geometry product



(Zhang et al., 2005). All the MODIS data products are freely available at USGS Earth Observing System Data Gateway (<http://edcimswww.cr.usgs.gov/pub/imswelcome/>).

We acquired daily MODIS data (year 2003) from the NASA data archive for one MODIS tile that covers both MOF site 1 and site 2. The blue reflectance of a pixel with vegetation and/or soil covered will increase if cloud or residual aerosol contaminates (King et al., 1999). Green vegetation, wet soil and snow have low SWIR<sub>2</sub> reflectance. If one observation has SWIR<sub>2</sub> reflectance greater than 0.15 or blue greater than 0.2, the observation is identified as a bad observation and excluded for analysis. Figure 6.1a-b showed the MODIS blue and SWIR<sub>2</sub> reflectance of the observations of site 1 for the whole year of 2003 with blue reflectance not greater than 0.2 and SWIR<sub>2</sub> not greater than 0.15. Some of observations in both blue band (less than 0.065) and SWIR<sub>2</sub> band (less than 0.15) are clustering in Figure 6.1c-d. Other observations are randomly scattering (Figure 6.1). Figure 6.9a-b showed the MODIS blue and SWIR<sub>2</sub> reflectance of the observations of site 2 for the whole year of 2003 with blue reflectance not greater than 0.2 and SWIR<sub>2</sub> not greater than 0.15. Some of observations in both blue band (less than 0.051) and SWIR<sub>2</sub> band (less than 0.15) are clustering in Figure 6.9c-d. Other observations are randomly scattering (Figure 6.9). Contaminated atmosphere (e.g., partial cloud cover or residual aerosols) is one likely source that contributed to the scattering of those scattering observations. There possibly are some other unknown sources. After removing the scattering observations, we got the clustering observations and calculated NDVI, EVI (Huete et al., 1997), LSWI, (Xiao et al., 2004c), and snow cover fraction ( $f_{snow}$ , Kaufman et al., 2002) with the clustering observations. There were a few observations of sites 1 and 2 that were affected by snow. The snow-affected observations

were discarded. Figure 6.2a–g showed the reflectance of MODIS seven bands for the remaining contamination-free observations of site 1. Figure 6.10a–g showed the reflectance of MODIS seven bands for the remaining contamination-free observations of site 2. The indices were shown in Figure 6.2h and Figure 6.10h.

$$NDVI = \frac{\rho_{NIR_1} - \rho_{red}}{\rho_{NIR_1} + \rho_{red}} \quad (1)$$

$$EVI = 2.5 \times \frac{\rho_{NIR_1} - \rho_{red}}{\rho_{NIR_1} + 6 \times \rho_{red} - 7.5 \times \rho_{blue} + 1} \quad (2)$$

$$LSWI = \frac{\rho_{NIR_1} - \rho_{SWIR_1}}{\rho_{NIR_1} + \rho_{SWIR_1}} \quad (3)$$

$$f_{snow} = \begin{cases} \frac{\rho_{red} - 0.5\rho_{SWIR_2}}{0.6} \\ 0.51 + 0.07 \times \frac{\rho_{red} - 0.5\rho_{SWIR_2}}{0.6}, & \text{if } \rho_{red} > 0.5\rho_{SWIR_2} \text{ and } \rho_{SWIR_2} \leq 0.25 \\ 0, & \text{otherwise} \end{cases} \quad (4)$$

where  $\rho_{blue}$ ,  $\rho_{red}$ ,  $\rho_{NIR_1}$ ,  $\rho_{SWIR_1}$ , and  $\rho_{SWIR_2}$  are reflectance values of the blue, red, NIR<sub>1</sub>, SWIR<sub>1</sub> and SWIR<sub>2</sub> bands.

## **6.4 Description of the radiative transfer model, the inversion algorithm and forward simulation**

### **6.4.1 Brief description of the coupled leaf-canopy radiative transfer model PROSPECT+SAIL-2**

This study used the PROSPECT+SAIL-2 model presented in our previous study (Zhang et al., 2005). We simply depict the model here. We used the PROSPECT model

with five variables - leaf internal structure variable ( $N$ ), leaf chlorophyll content ( $C_{ab}$ ), leaf dry matter content ( $C_m$ ), leaf water thickness ( $C_w$ ) and leaf brown pigment ( $C_{brown}$ ) (Baret et al., 1997; Verhoef et al., 2003; Di Bella et al., 2004). The version of SAIL (Scattering from Arbitrarily Inclined Leaves) model, a canopy radiative transfer model, described by Braswell and others (SAIL-2; Braswell et al., 1996) was utilized in this study. The PROSPECT model was coupled with the SAIL-2 model (hereafter called PROSAIL-2) through replacing the leaf reflectance component in the SAIL-2 model with the PROSPECT model. The sixteen biophysical/ biochemical variables of the PROSAIL-2 model and their search ranges, based on an extensive literature review, were listed in Table 6.1.

#### 6.4.2 Brief description of the Metropolis algorithm for inversion

The daily MODIS/Terra and MODIS/Aqua data from day of year (DOY) 193 to 216 in 2003 for MOF site 1 were extracted. Twelve contamination-free observations were collected for site 1. The daily MODIS data from DOY 201 to 216 in 2003 for MOF site 2 were also extracted. Twelve contamination-free observations were collected for site 2. The Metropolis algorithm in our previous study (Metropolis et al., 1953; Zhang et al., 2005), a type of Markov Chain Monte Carlo (MCMC) estimation procedure, was employed for inversion of the MODIS data. The strength of the method is that it can reflect the remaining uncertainty after the model has been constrained (inverted) with data and estimate posterior probability distributions of the variables conditioned on both the model and the observed data. The retrieved distributions will provide both estimates of uncertainty (such as standard deviations and confidence intervals) of individual

variables and the information about the variable sensitivity of the model. The Metropolis algorithm is relatively computationally intensive, owing to the need for simulation of a large number of samples required to obtain a reliable estimate of the variables' distributions. Reflectance of red, NIR<sub>1</sub>, green, NIR<sub>2</sub>, and SWIR<sub>1</sub> bands and relative viewing geometries of the MODIS observations are used as input to invert the PROSAIL-2 model. Details about the Metropolis algorithm for inversion can be found in Zhang et al. (2005).

With the estimates of the biophysical and biochemical variables by inverting PROSAIL-2 with observed spectral reflectance data (reflectance plus relative observation geometry) using the Metropolis algorithm, we calculate FAPAR<sub>canopy</sub> (Goward et al., 1992), FAPAR<sub>leaf</sub> (Braswell et al., 1996), and FAPAR<sub>chl</sub> (Zhang et al., 2005) using forward simulations.

#### 6.4.3 Reproducing bidirectional MODIS five band reflectance with seasonal MODIS observation geometry

We estimated the biophysical/ biochemical variables using the observed twelve daily MODIS observations from DOY 193 – 216 in 2003 (reflectance plus relative observation geometry) in section 6.4.2 for site 1. We also did the inversion with twelve daily MODIS data from DOY 201 – 216 in 2003 in section 6.4.2 for site 2. We collected all contamination free daily MODIS observations in the whole year of 2003 for both site 1 and site 2 (see Figures 6.2 and 6.10). We forwardly simulated the red, green, NIR<sub>1</sub>, NIR<sub>2</sub> and SWIR<sub>1</sub> reflectance of MODIS, for sites 1 and 2, with the mean values of the

inverted variables for sites 1 and 2 and observation geometries of the observations in Figures 6.2 and 6.10, respectively (see Figures 6.8 and 6.16).

## **6.5 Results**

### **6.5.1 Temporal analyses of MODIS daily reflectance data in 2003**

Figure 6.2 exhibited the time series of surface reflectance of the seven spectral bands among the clustering MODIS daily data that covered MOF site 1 in 2003. The blue reflectance values for the period from DOY 125 to 280 are much lower than those for the periods before DOY 125 or after DOY 280 (Figure 6.2a). Similar seasonal patterns were also observed for the SWIR<sub>1</sub> and red reflectance (Figure 6.2b, c). In comparison, the seasonal NIR<sub>1</sub> and NIR<sub>2</sub> reflectance values have a strong seasonal dynamics with peaks values in mid summer (Figure 6.2d, f). Figure 6.10 exhibited the time series of the seven MODIS spectral reflectance among the clustering MODIS daily data that covered MOF site 2 in 2003. The MODIS reflectance values of site 2 have similar seasonal patterns of the spectral reflectance values of site 1.

The seasonal reflectance dynamics of individual spectral bands provide rich information for interpreting vegetation indices from the MODIS data. There was very little green vegetation for the periods of DOY 1-100 and DOY 300 - 365 over sites 1 and 2 (Figure 6.2d and Figure 6.10d). MODIS observed less water content for the periods than the period from DOY 125 – 280 (Figure 6.2b and Figure 6.10b). However, one observation on DOY 19 over site 1 has blue, red, NIR<sub>1</sub> and SWIR<sub>2</sub> reflectance values as 0.0105, 0.0272, 0.2202 and 0.0771, and has NDVI, EVI and LSWI as 0.7801, 0.3698, and 0.2020. One observation on DOY 23 over site 2 has blue, red, NIR<sub>1</sub> and SWIR<sub>2</sub>

reflectance values as 0.0096, 0.0279, 0.2173 and 0.0840, and has NDVI, EVI and LSWI as 0.7724, 0.3607, and 0.1946. The two observations have high NDVI, relatively high EVI and LSWI in winter/spring season. Some other similar observations in winter/spring seasons were also exhibited in Figures 6.2 and 6.10. One should take caution when interpreting NDVI, EVI and LSWI of these observations.

#### 6.5.2 Comparison between retrieved and observed reflectance values of MODIS daily data collections from DOY 193-216 for site 1 and from DOY 201-216 for site 2 in 2003

The mean values from the retrieved variable distributions for the data collection from DOY 193 to 216 in 2003 for site 1 were utilized as inputs to calculate the reflectance with forward simulations of the PROSAIL-2 model. Figure 6.3 shows a comparison of the PROSAIL-2 retrieved reflectance with the observed reflectance of the MODIS green, red, NIR<sub>1</sub>, NIR<sub>2</sub>, and SWIR<sub>1</sub> bands. The correlation coefficient between the retrieved and observed MODIS visible reflectance is 0.90 for the green band and 0.84 for the red band, respectively. The root mean squared error (RMSE) between the observed and retrieved MODIS visible reflectance is 0.38% for the green band and 0.35% for the red band. The correlation coefficient between the retrieved and observed NIR/SWIR reflectance is 0.87, 0.92, and 0.93 for NIR<sub>1</sub>, NIR<sub>2</sub> and SWIR<sub>1</sub>, respectively. The RMSE between the observed and retrieved NIR/SWIR reflectance is 2.1%, 1.6%, and 1.0% for NIR<sub>1</sub>, NIR<sub>2</sub> and SWIR<sub>1</sub>, respectively. The mean values from the retrieved variable distributions for the data collection from DOY 201 to 216 in 2003 for site 2 were utilized as inputs to calculate the reflectance with forward simulations of PROSAIL-2. Figure 6.11 shows a comparison of the PROSAIL-2 retrieved reflectance with the

observed reflectance of the MODIS green, red, NIR<sub>1</sub>, NIR<sub>2</sub>, and SWIR<sub>1</sub> bands. The correlation coefficient between the retrieved and observed MODIS visible reflectance is 0.95 for both the green band and red band. The RMSE between the observed and retrieved MODIS visible reflectance is 0.29% for the green band and 0.18% for the red band. The correlation coefficient between retrieved and observed NIR/SWIR reflectance is 0.91, 0.90, and 0.94 for NIR<sub>1</sub>, NIR<sub>2</sub> and SWIR<sub>1</sub>, respectively. The RMSE between the observed and retrieved NIR/SWIR reflectance is 2.5%, 2.8%, and 1.3% for NIR<sub>1</sub>, NIR<sub>2</sub> and SWIR<sub>1</sub>, respectively. Note that the data collections spanned twenty-four days and sixteen days, respectively, and any variation of leaf and canopy during the periods may have contributed to the discrepancies between the retrieved reflectance and MODIS observed reflectance though we would not expect very large changes at either leaf or canopy level because the canopy was well fully developed during early July. Possible errors introduced during MODIS pre-processing may also contribute to the discrepancies (e.g. imperfect atmospheric correction). The comparison suggests that the PROSAIL-2 model with the retrieved mean values of individual variables reasonably reproduces the surface reflectance of the temperate deciduous broadleaf forest sites.

### 6.5.3 Uncertainty of individual variables from inversion of the PROSAIL-2 model with MODIS daily data collections from DOY 193-216 for site 1 and from DOY 201-216 for site 2 in 2003

The Metropolis algorithm retrieved posterior probability distributions for individual variables for the data collections from DOY 193 to 216 for site 1 and from DOY 201 to 216 for site 2 in 2003. The posterior distributions offer a measure of

uncertainty in the form of their standard deviations or other quantile intervals, and the shape of the distributions provide a measure of compatibility between model and data. We simply ranked the sixteen variables into three categories: “well-constrained”, “poorly-constrained” and “edge-hitting” through examining their histograms from inversion (Braswell et al., 2005; Zhang et al., 2005). The “well-constrained” variables usually have a well-defined distribution, with small standard deviations relative to their allowable ranges. The “poorly-constrained” variables have relatively flat distributions with large standard deviations relative to their allowable ranges. Edge-hitting variables are those for which the modes of their retrieved values occurred near one of the edges of their allowable ranges and most of the retrieved values were clustered near this edge. Figures 6.4 and 6.6 for site 1 and figures 6.12 and 6.14 for site 2 show that the histograms of plant area index (PAI), LAI, and five leaf variables (leaf internal structure variable, leaf chlorophyll concentration, leaf brown pigment concentration, leaf dry matter and leaf equivalent water thickness) are “well-constrained” variables. Cover fraction of both site 1 and site 2 is “edge-hitting” variable (Figures 6.5b and 6.13b). Stem fraction for site 1 is “well-constrained” while stem fraction for site 2 is “edge-hitting” (Figures 6.5a and 6.13a). Because stem fraction is distributed near 0.03 for site 1 and near 0.0 for site 2 and cover fraction is distributed near 1.0 for both sites 1 and 2, stem and soil have little effect on the canopy optical characteristics and consequently little information about stem and soil could be retrieved from the MODIS observations.



#### 6.5.4 Distribution of $FAPAR_{canopy}$ , $FAPAR_{leaf}$ , and $FAPAR_{chl}$ using MODIS daily data collections from DOY 193-216 for site 1 and from DOY 201-216 for site 2 in 2003

The histograms of fractions of absorbed PAR by canopy, leaf and chlorophyll are “well-constrained” variables (figure 6.7 for site 1 and Figure 6.15 for site 2). We estimated the distributions of  $FAPAR_{canopy}$ ,  $FAPAR_{leaf}$ , and  $FAPAR_{chl}$  for the data collections of the MODIS daily data from DOY 193 to 216 for site 1 and from DOY 201 to 216 for site 2 in 2003 using the retrieved distributions of individual variables in PROSAIL-2. We also extracted mean and standard deviation values of the fractions. The mean values of  $FAPAR_{canopy}$ ,  $FAPAR_{leaf}$ , and  $FAPAR_{chl}$  for the data collection of the MODIS daily data from DOY 193 to 216 in 2003 for site 1 were 0.915, 0.865, and 0.707, respectively. Their standard deviation values were 0.029, 0.042, and 0.028, respectively. The mean values of  $FAPAR_{canopy}$ ,  $FAPAR_{leaf}$ , and  $FAPAR_{chl}$  for the data collection of the MODIS daily data from DOY 201 to 216 in 2003 for site 2 were 0.912, 0.885, and 0.729, respectively. Their standard deviation values were 0.029, 0.035, and 0.025, respectively.

The  $FAPAR_{canopy}$  and  $FAPAR_{leaf}$  for site 1 from DOY 193 to 216 in 2003 have difference, and the  $FAPAR_{canopy}$  and  $FAPAR_{leaf}$  for site 2 from DOY 201 to 216 in 2003 have difference, too. The differences are attributed to light absorption by stem ( $APAR_{stem}$ ), i.e., the non-leaf part of the canopy. During DOY 193 to 216 in 2003, the vegetation canopies over the two sites are dominated by leaves, and only a very small proportion of stems are observed by the MODIS sensor. This may explain why the mean  $FAPAR_{canopy}$  values are only slightly higher than the mean values of  $FAPAR_{leaf}$ . The differences between  $FAPAR_{leaf}$  and  $FAPAR_{chl}$  are attributed to light absorption by the non-chlorophyll component of the leaf.

NDVI and EVI are two MODIS standard products that have been used frequently (Justice et al., 1998). We calculated the mean and standard deviation of NDVI and EVI using the same MODIS images for the two data collections. The mean values of NDVI and EVI for the data collection of the MODIS daily data from DOY 193 to 216 in 2003 for site 1 were 0.863 and 0.607, respectively. The standard deviations of NDVI and EVI were 0.020 and 0.041, respectively. The mean values of NDVI and EVI for the data collection of the MODIS daily data from DOY 201 to 216 in 2003 for site 2 were 0.881 and 0.591, respectively. The standard deviations of NDVI and EVI were 0.012 and 0.062, respectively. The mean NDVI values are very similar to  $FAPAR_{leaf}$ , which supports the earlier studies that used NDVI to approximate  $FAPAR_{canopy}$  (e.g., Goward et al., 1992), as  $FAPAR_{leaf}$  and  $FAPAR_{canopy}$  values are close to each other. The mean EVI values are lower than the mean  $FAPAR_{chl}$  values. Note that reflectance values in daily MODIS images are not BRDF corrected reflectance; therefore, the observation viewing geometry has an effect on the ranges of NDVI and EVI.

#### 6.5.5 Comparison of reflectance, related NDVI, EVI and LSWI in 2003 and reproduced reflectance and related NDVI, EVI and LSWI with the inverted mean variables in PROSAIL-2 and with the viewing geometries from MODIS daily data collection

Figures 6.8 and 6.16 show comparison of reflectance, related NDVI, EVI and LSWI and reproduced reflectance, related NDVI, EVI and LSWI using the inverted mean values of the variables in PROSAIL-2 and the viewing geometries for the data collection of the MODIS daily data from DOY 193 to 216 in 2003 for site 1 and the data collection of the MODIS daily data from DOY 201 to 216 in 2003 for site 2, respectively. During

the MODIS daily data collections' periods, canopies were fully developed. The reflectance difference for red and green bands because of viewing geometries can be 0.01 and the reflectance difference for NIR<sub>1</sub>, NIR<sub>2</sub> and SWIR<sub>1</sub> can be 0.1. For fully developed canopies, viewing geometry has the least effect on NDVI, medium effect on LSWI and the greatest effect on EVI. The difference between real reflectance, related NDVI, EVI and LSWI in 2003 and reproduced reflectance, related NDVI, EVI and LSWI during before DOY 116 and after DOY 258 could be explained by leaf-on and leaf-off-senescence processes. There is still significant difference between real reflectance, related NDVI, EVI and LSWI and reproduced reflectance, related NDVI, EVI and LSWI during DOY 116 - DOY 258 in 2003 that has not been studied widely.

## **6.6 Discussion**

MODIS observations during winter/spring season have higher solar zenith angles than during other seasons. Reproduced NDVI (Figures 6.8 and 6.16) shows weak variation between observations with high zenith angles and observations with low zenith angles. Our results about NDVI are consistent with Goward and Huemmrich (1992) that reported that NDVI of vegetation with high LAI changed little. Variation of solar zenith angles does not affect NDVI of dense vegetation very much. Similarly, variation of solar zenith angles does not affect LSWI of dense vegetation very much even though its variation is greater than the variation of NDVI. Because we did not reproduce blue band reflectance, we could not conclude completely that the variation of reproduced EVI is completely because of solar-earth-target geometry variation. We speculate that the viewing geometry has the greatest effect on EVI.

Forests are believed to have unchanged LAI during plant growing season (e.g., DOY 116 – 258 in 2003 for the MOF). If there is no variation in canopy or leaf during the plant growing season, what are the reasons that the real reflectance and reproduced reflectance are obviously different during the period? If the BRDF effect is the only reason, there should be no such significant difference. So some other factors should be also responsible for the difference. And the assumption that leaf optical variations can not be observed or leaf optical characteristics do not change during plant growing season need to be argued.

Even though there is a central 100m\*100m intermediate forest plot in the mature forests of site 1 while the whole site 2 is totally covered by mature forests, little difference of MODIS spectral range optics between the two sites was observed except that MODIS can observe around 3% stem in canopy for site 1 and 0% stem in canopy for site 2. MODIS has little capability to distinguish the two sites as there is only four percent of vegetation of the two sites having different ages. To detect the age difference of such small plots, we recommend use finer spatial and/or finer spectral resolution data.

Leaf dry matter and leaf chlorophyll content that are important for interpreting the results of inversion of the PROSAIL-2 model in this study are discussed here though it is hard to validate all variables at 500m scale. Leaf chlorophyll content is an important leaf-level biophysical variable. The inversion of the PROSAIL-2 model using the data collection from DOY 193 -216 in 2003 for site 1 has estimated leaf chlorophyll content with mean of  $69.17\mu\text{g}/\text{cm}^2$  and standard deviation of  $5.99\mu\text{g}/\text{cm}^2$ , and leaf dry matter with mean of  $0.00786\text{ g}/\text{cm}^2$  and standard deviation of  $0.00432\text{ g}/\text{cm}^2$ . The inversion of the PROSAIL-2 model using the data collection from DOY 201 - 216 in 2003 for site 2

has estimated leaf chlorophyll content with mean of  $70.955\mu\text{g}/\text{cm}^2$  and standard deviation of  $4.36\mu\text{g}/\text{cm}^2$ , and leaf dry matter with mean of  $0.00684\text{g}/\text{cm}^2$  and standard deviation of  $0.00361\text{g}/\text{cm}^2$ . We measured leaf chlorophyll content and leaf dry matter for major species in MOF in August 1 – 7 in 2003. The field measured ranges of top leaf chlorophyll content are as following: white oak 65.538 – 67.110, hickory 38.730 – 56.100, black oak 59.918 – 70.365, and scarlet oak 85.922 – 90.048 $\mu\text{g}/\text{cm}^2$ . The field measured ranges of top leaf dry matter are white oak 0.00516 – 0.00644, hickory 0.00888 – 0.01054, black oak 0.00226 – 0.01025, and scarlet oak 0.00507 – 0.01281  $\text{g}/\text{cm}^2$ . Our estimated leaf chlorophyll content and leaf dry matter ranges (mean  $\pm$  standard deviation) are overlapped by the field measurement ranges. In future when we have more sources to evaluate the area fractions of major forest species, we may evaluate our inversion algorithm in more details.

The results of this study highlight the substantial variations of the red, green, NIR<sub>1</sub>, NIR<sub>2</sub> and SWIR<sub>1</sub> bands except viewing geometry effect during the plant growing season. NDVI and LSWI do not provide much information about these variations. More study about the physiological basis of the variations in the future will be useful. The variations suggest that in addition to measurements of canopy-level variables (e.g., LAI), field measurements of leaf-level variables (e.g., chlorophyll, other pigments, leaf dry matter, and leaf water content) during the plant growing season will be useful for both remote sensing and ecological research.

Table 6.1 A list of variables in the PROSAIL-2 model and their search ranges

	Variable	Description	Unit	Search range
Biophysical /biochemical variables	PAI	plant area index, i.e., leaf +stem area index		1 – 7.5
	SFRAC	Stem fraction		0 – 1
	CF	Cover fraction: area of land covered by vegetation/ total area of land		0.5 – 1
	C <sub>ab</sub>	Leaf chlorophyll a+b content	µg/cm <sup>2</sup>	0 – 80
	N	Leaf structure variable: measure of the internal structure of the leaf		1.0 – 4.5
	C <sub>w</sub>	Leaf equivalent water thickness	cm	0.001 – 0.15
	C <sub>m</sub>	Leaf dry matter content	g/cm <sup>2</sup>	0.001 – 0.04
	C <sub>brown</sub>	Leaf brown pigment content		0.00001 – 8
	LFINC	Mean leaf inclination angle	degree	10 – 89
	STINC	Mean stem inclination angle	degree	10 – 89
	LFHOT	Leaf BRDF variable: length of leaf/ height of vegetation		0 – 0.9
	STHOT	Stem BRDF variable: length of stem / height of vegetation		0 – 0.9
	STEM <sub>A</sub>	Stem reflectance variable: maximum (for a fitted function)		0.2 – 20
	STEM <sub>B</sub>	Stem reflectance variable range (for same fitted function)		50 – 5000
	SOIL <sub>A</sub>	Soil reflectance variable: maximum (for a fitted function)		0.2 – 20
SOIL <sub>B</sub>	Soil reflectance variable: range (for same fitted function)		50 – 5000	
Atmospheric condition variable	VIS	Diffuse/ direct variable: scope of atmospheric clarity	km	50

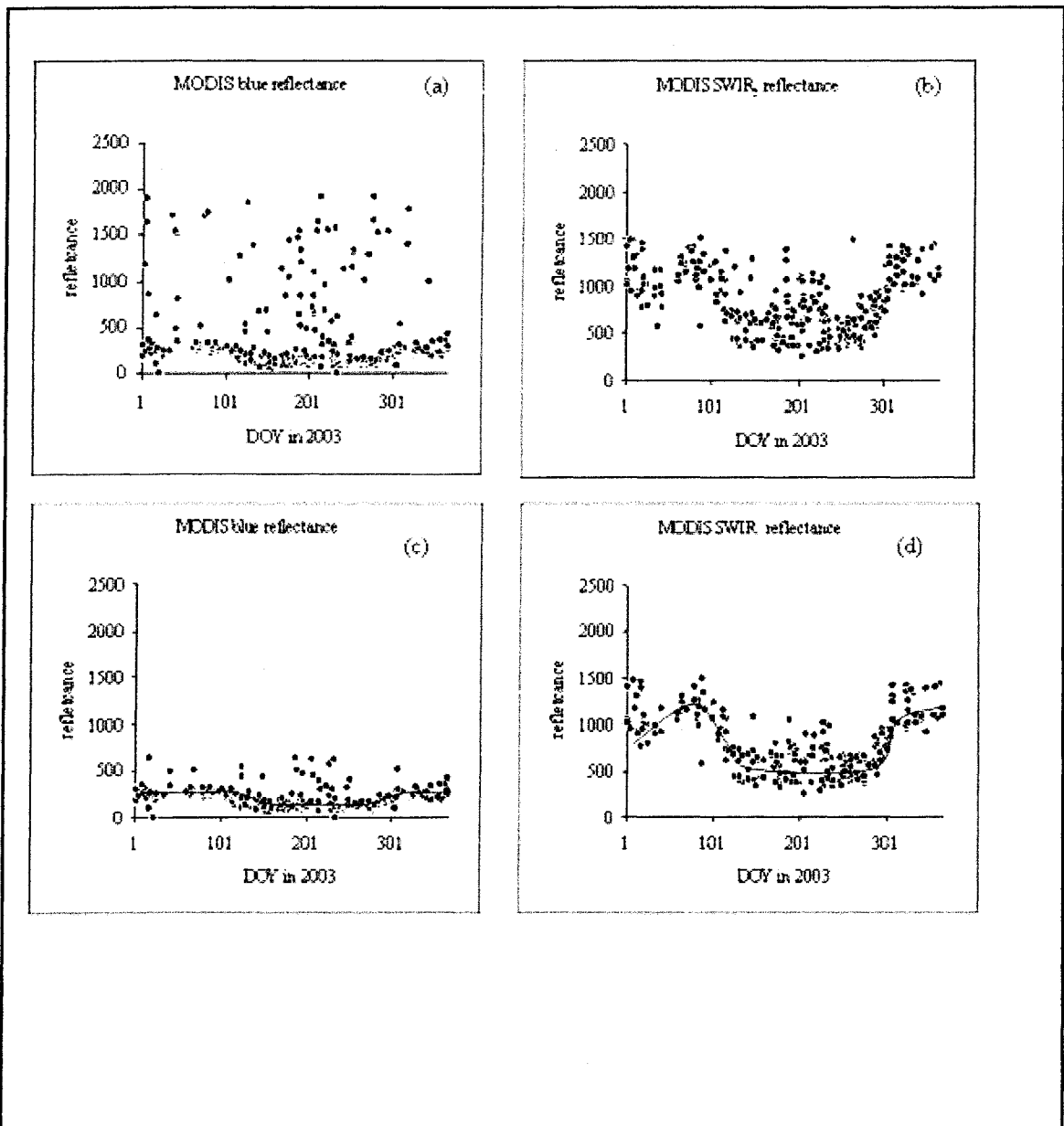


Figure 6.1 Reflectance of (a) blue and (b) SWIR<sub>2</sub> of MODIS daily observations of the Missouri Ozark Forest (MOF) site 1 in 2003 (reflectance scale=0.0001) with blue less than 0.2 and SWIR<sub>2</sub> less than 0.15; reflectance of (c) blue and (d) SWIR<sub>2</sub> of MODIS daily observations in 2003 with blue less than 0.065 and SWIR<sub>2</sub> less than 0.15

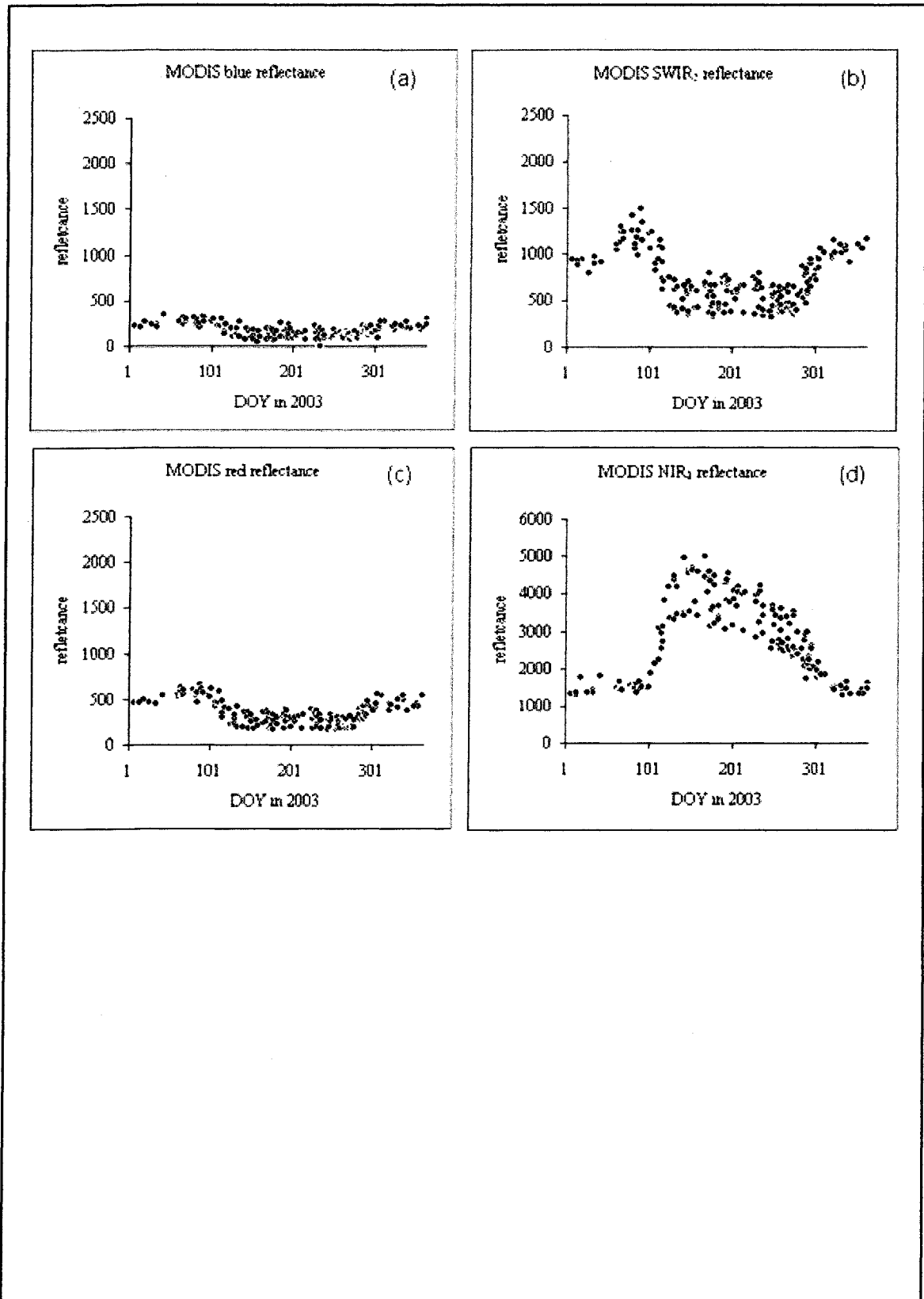


Figure 6.2 Reflectance of clustering MODIS daily observations of the MO Forest site 1 in 2003 (reflectance scale=0.0001) and related NDVI, EVI and LSWI



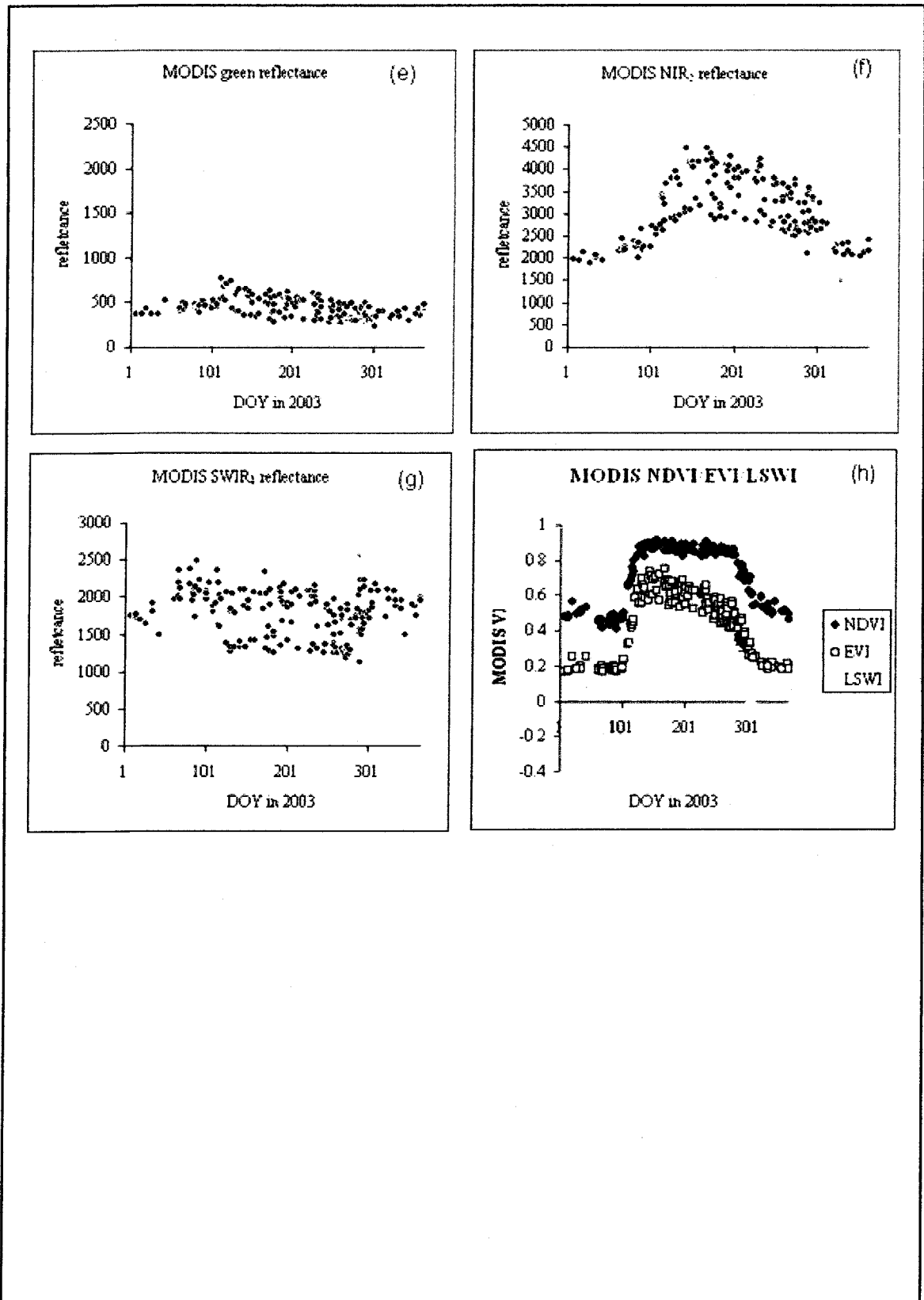


Figure 6.2 (continued) Reflectance of clustering MODIS daily observations of the MO Forest site 1 in 2003 (reflectance scale=0.0001) and related NDVI, EVI and LSWI

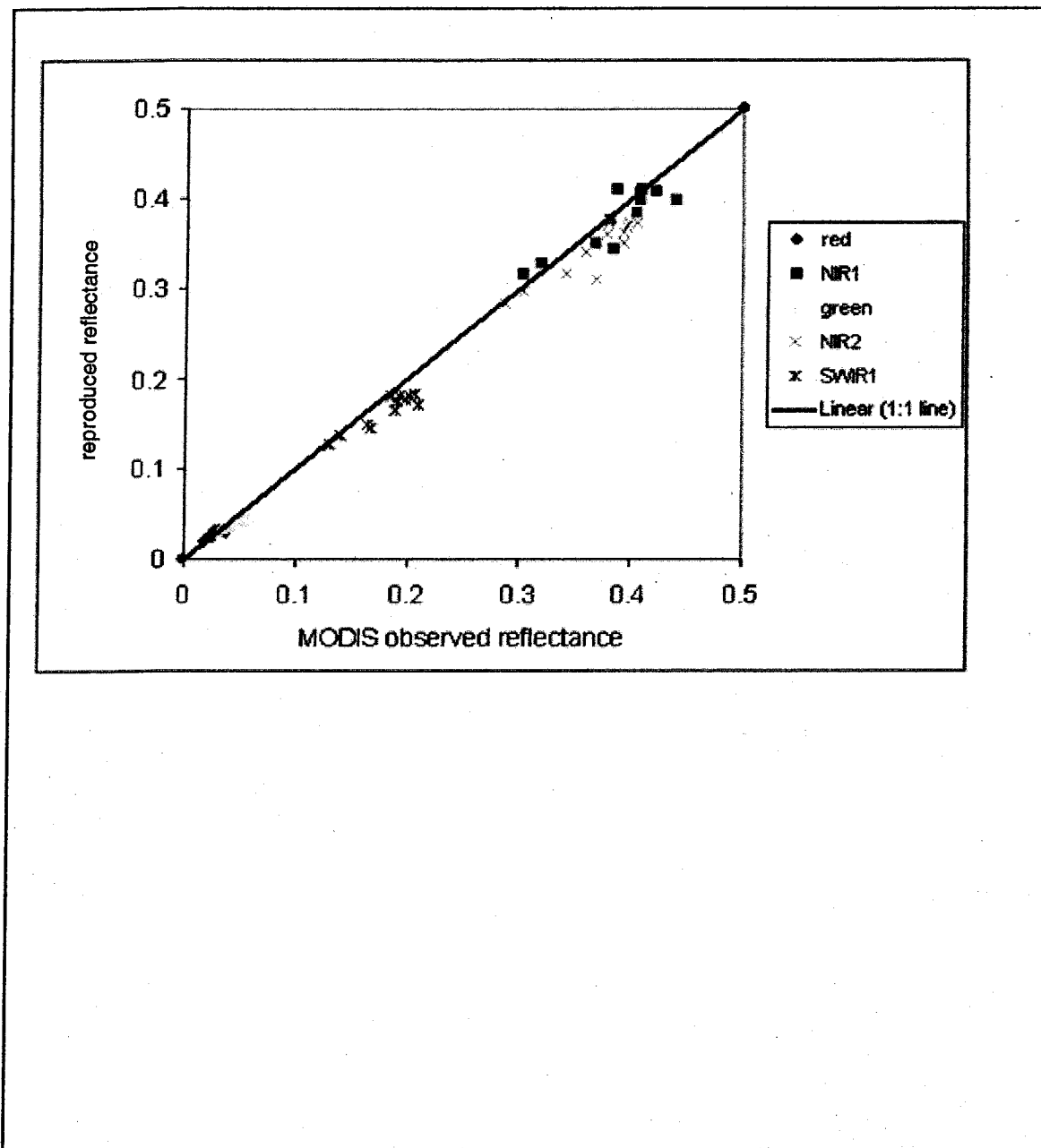


Figure 6.3 A comparison between the observed reflectance and PROSAIL-2 reproduced reflectance for five MODIS spectral bands (red, green, NIR<sub>1</sub>, NIR<sub>2</sub> and SWIR<sub>1</sub>). Surface reflectance were reproduced with the mean values of inverted variables from the PROSAIL-2 model using MODIS over the MO forest site 1 from DOY 193 to 216 in 2003.

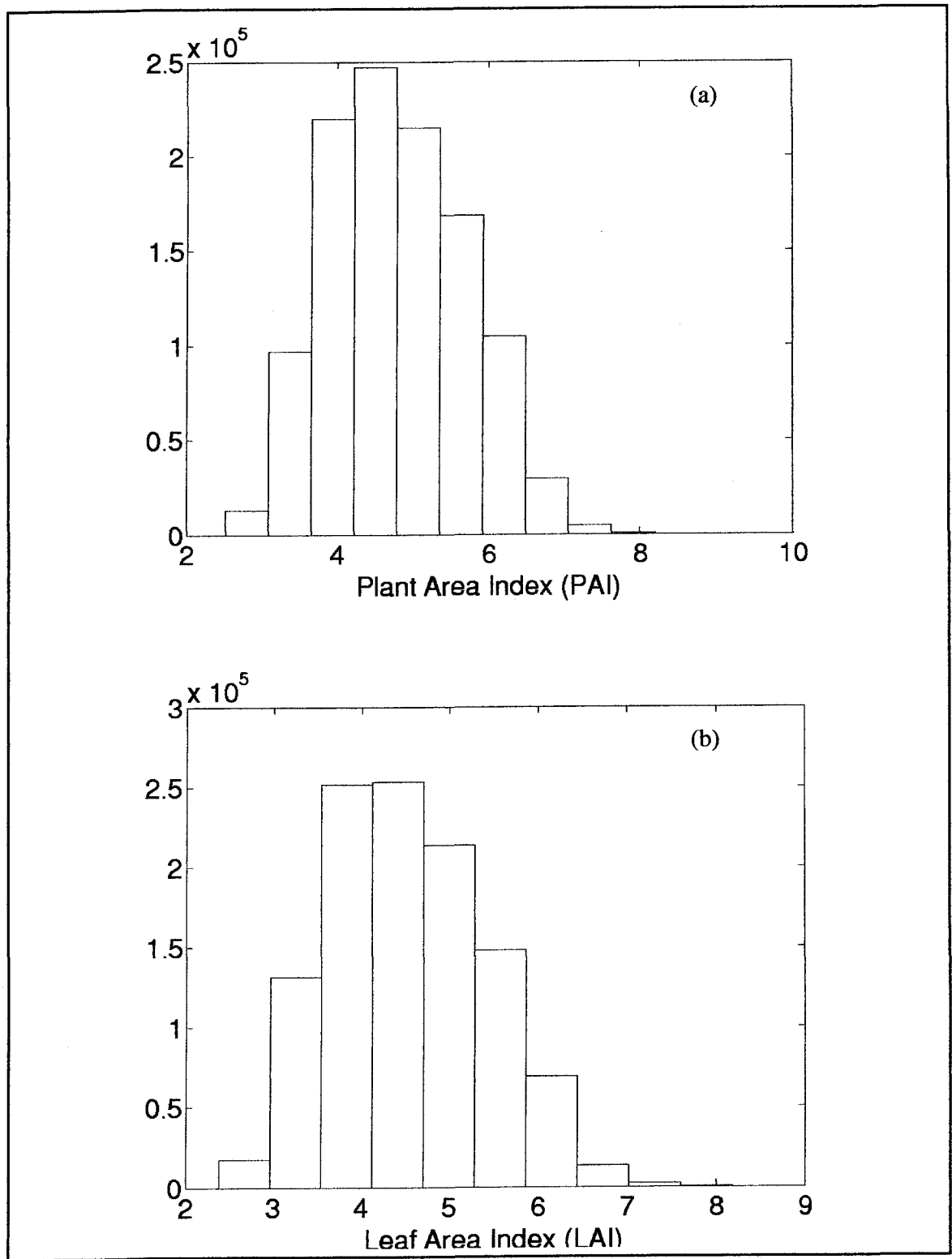


Figure 6.4 (a) Histogram of plant area index (PAI) for MODIS data collection of the MO forest site 1 from DOY 193 to 216 in 2003; (b) Histogram of leaf area index (LAI) for MODIS data collection of the MO forest site 1 from DOY 193 to 216 in 2003.

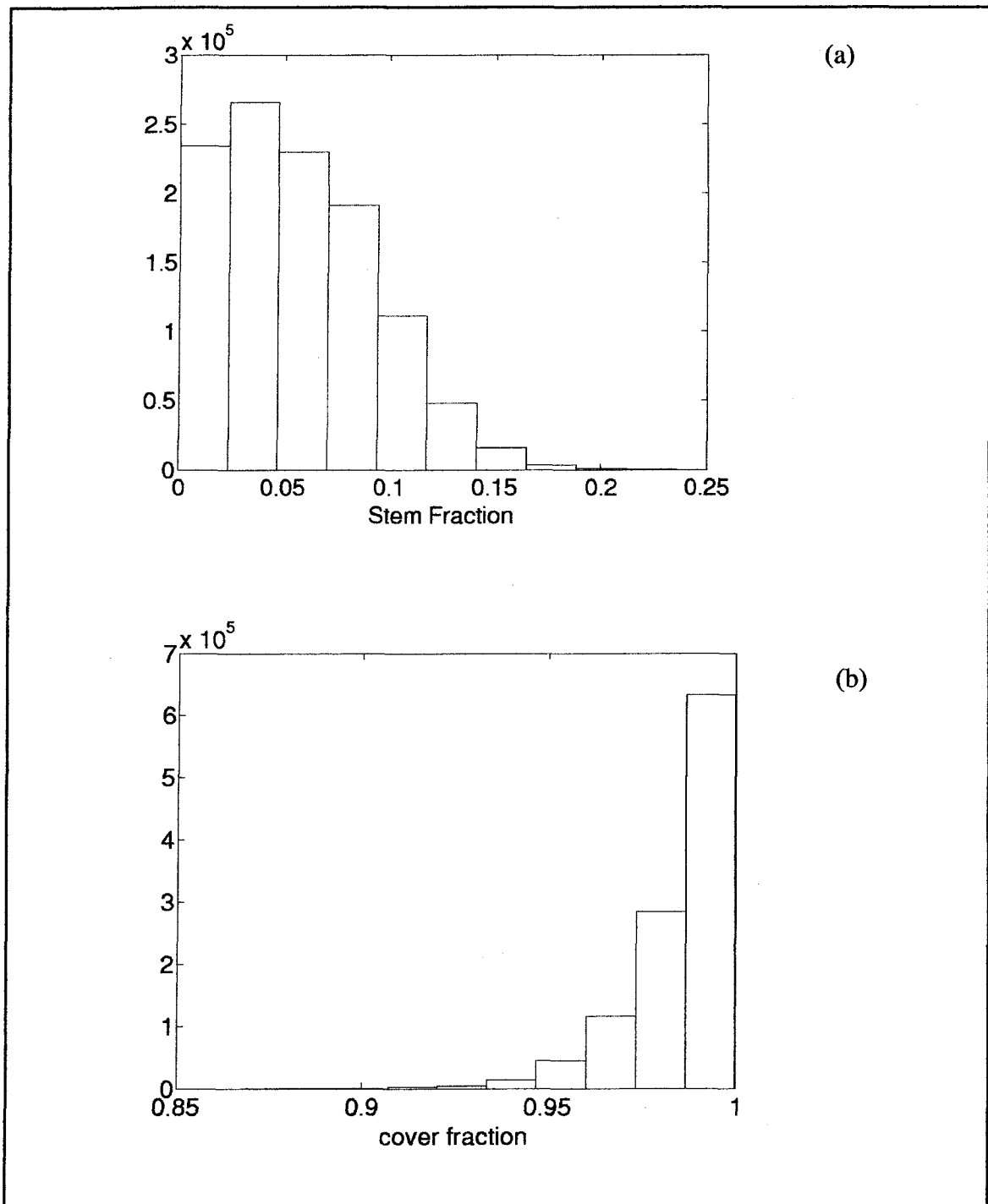


Figure 6.5 (a) Histogram of stem fraction for MODIS data collection of the MO forest site 1 from DOY 193 to 216 in 2003; (b) Histogram of cover fraction for MODIS data collection of the MO forest site 1 from DOY 193 to 216 in 2003

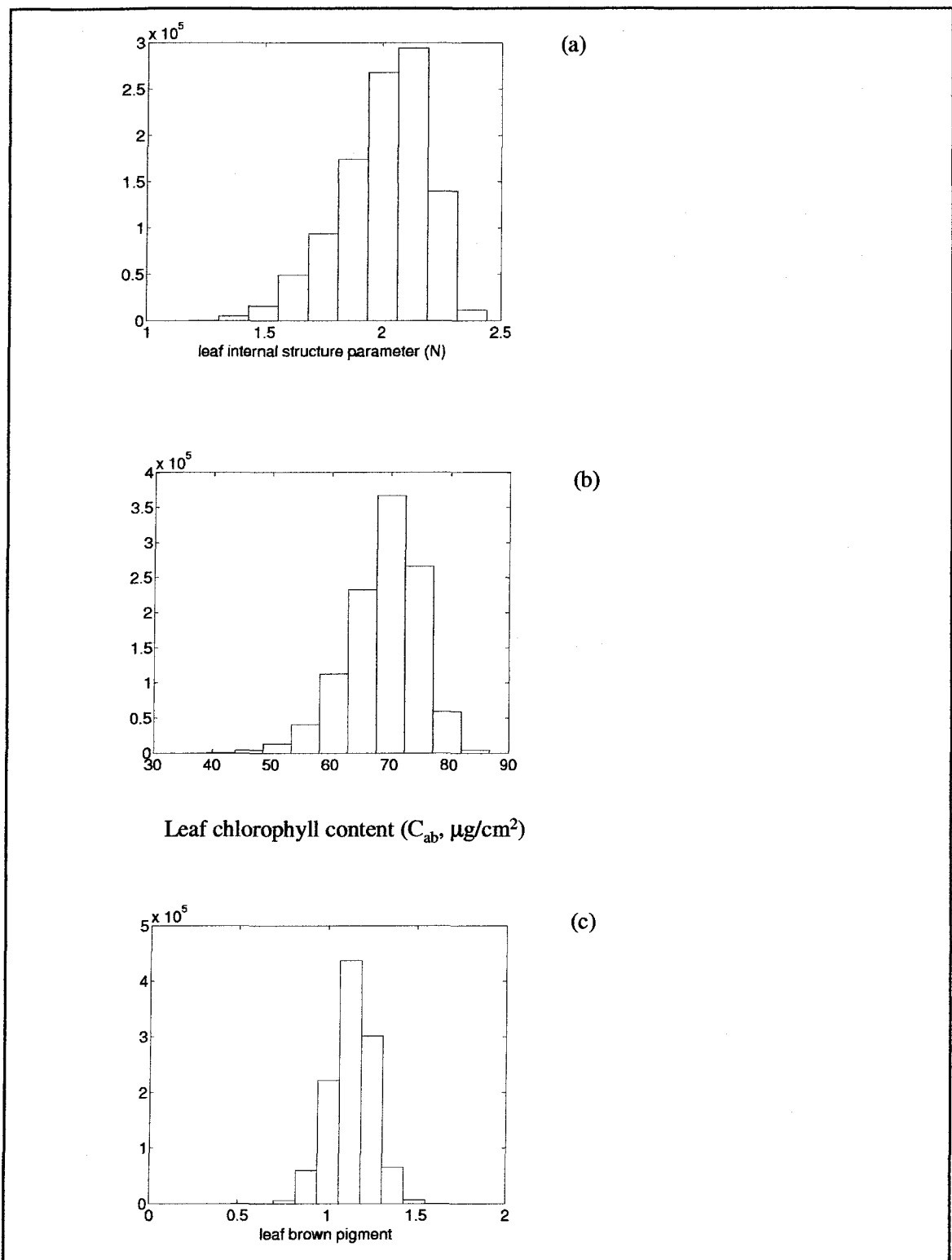


Figure 6.6 Histograms of leaf variables for MODIS data collection of the MO forest site 1 from DOY 193 to 216 in 2003

(a) leaf internal variable (N); (b) leaf chlorophyll content ( $C_{ab}$ ,  $\mu\text{g}/\text{cm}^2$ ); (c) leaf brown pigment ( $C_{brown}$ )

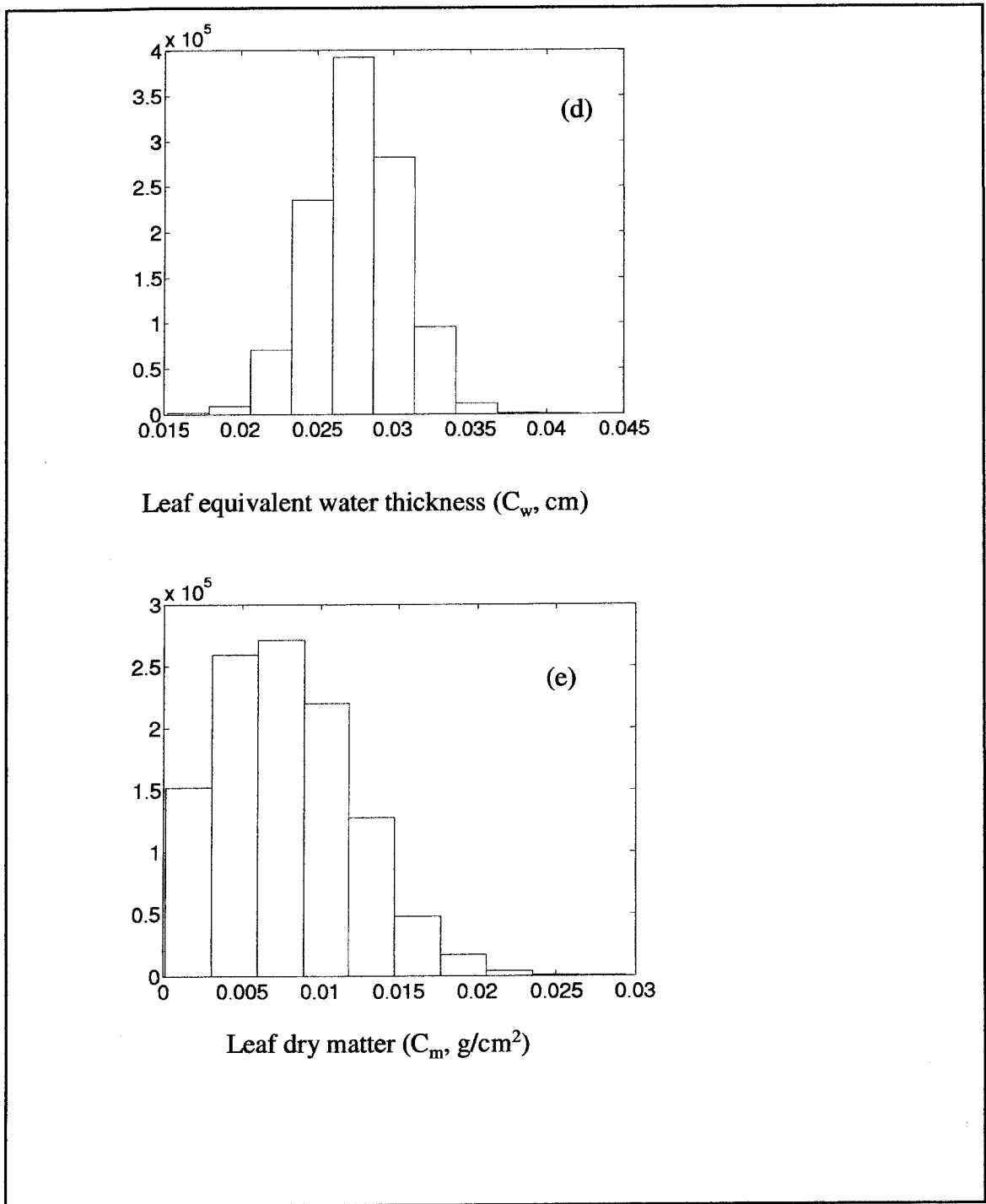


Figure 6.6 (continued) Histograms of (d) leaf equivalent water thickness ( $C_w$ , cm); and (e) leaf dry matter ( $C_m$ ,  $g/cm^2$ ) for MODIS data collection of the MO forest site 1 from DOY 193 to 216 in 2003

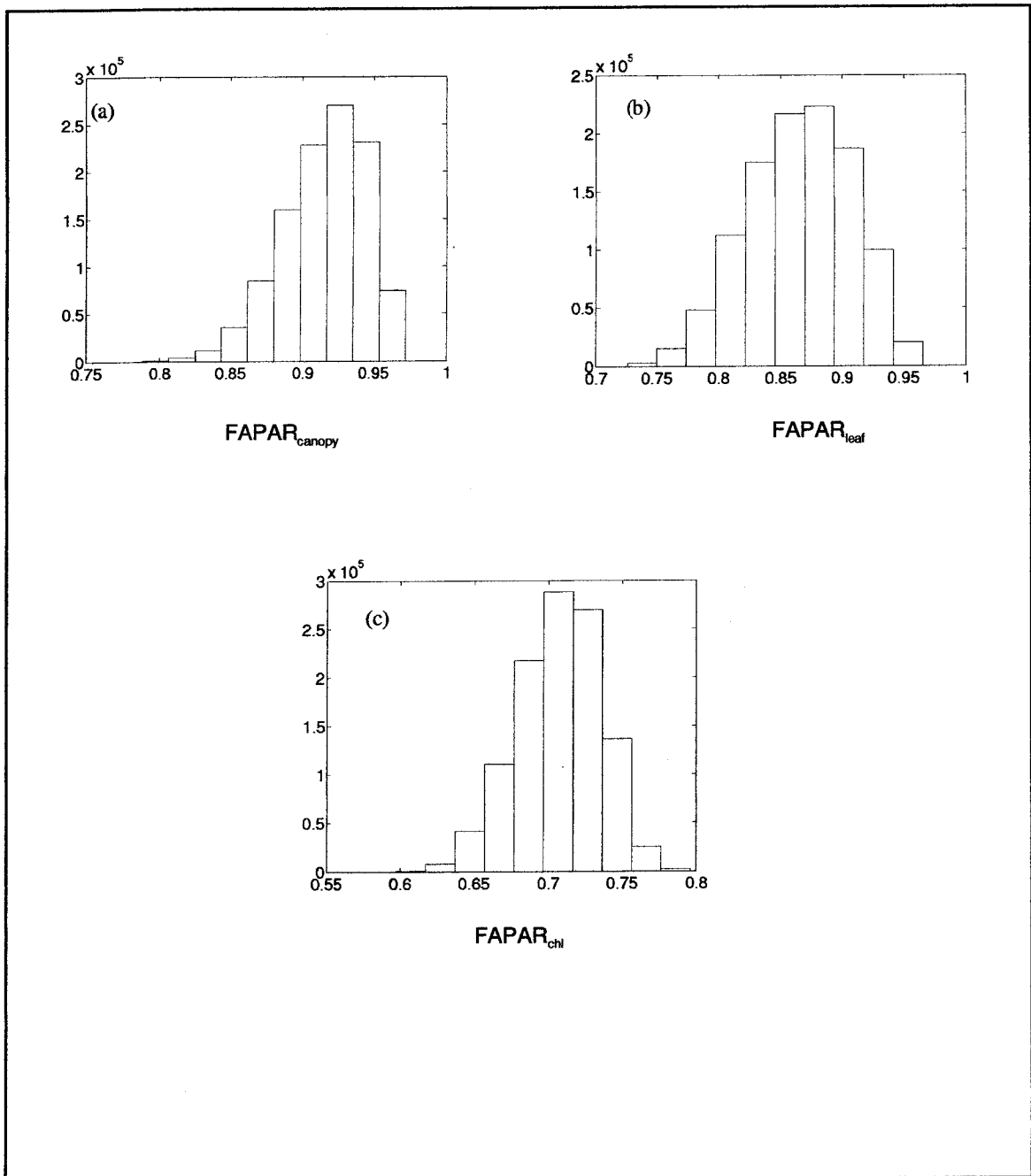


Figure 6.7 Histograms of fraction of photosynthetically active radiation absorbed by (a) canopy (FAPAR<sub>canopy</sub>); (b) by leaf (FAPAR<sub>leaf</sub>); (c) by chlorophyll (FAPAR<sub>chl</sub>) for MODIS data collection of the MO forest site 1 from DOY 193 to 216 in 2003

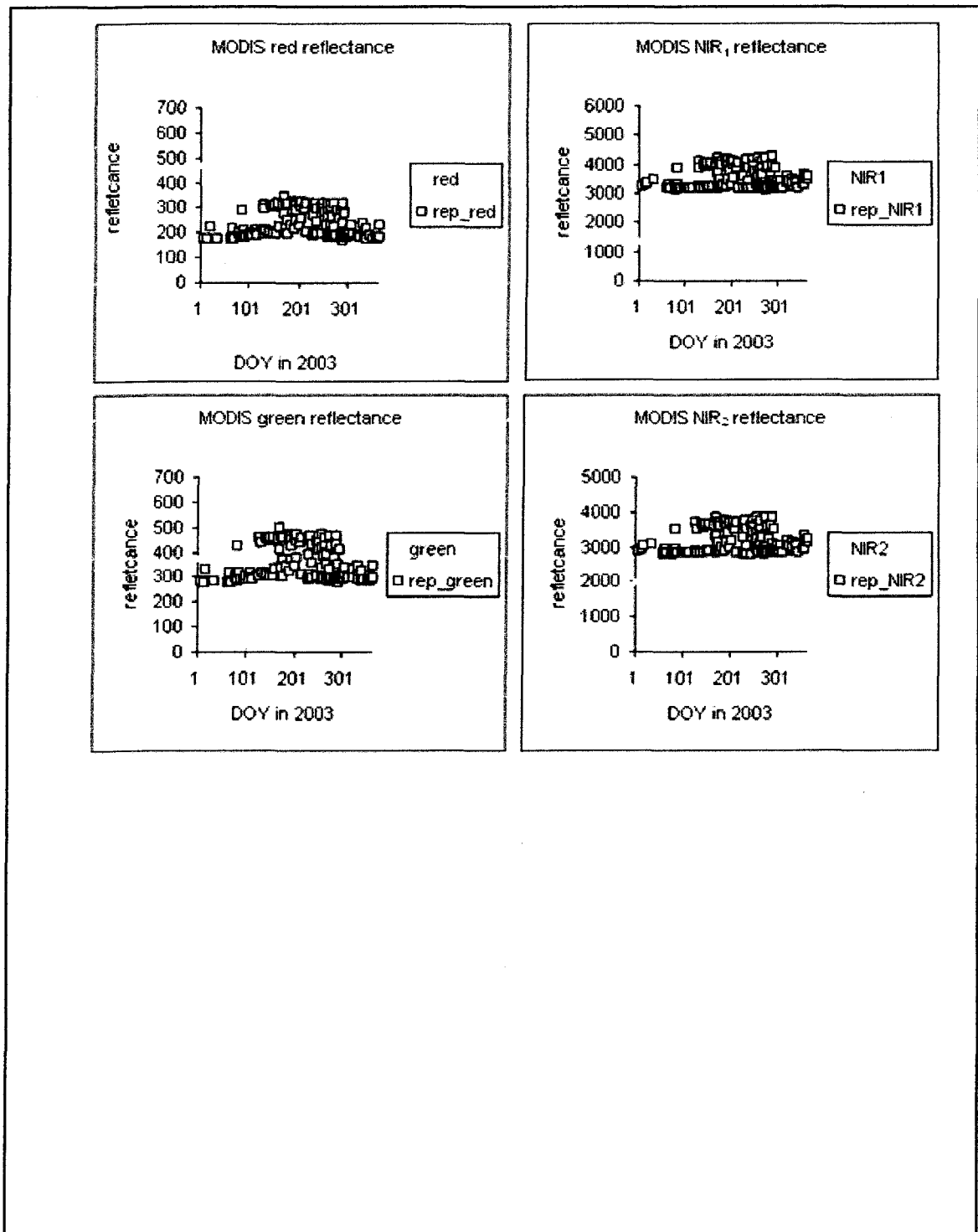


Figure 6.8 A comparison of reflectance, related NDVI, EVI and LSWI of MODIS clustering daily observations of the MO Forest site 1 in 2003 (reflectance scale=0.0001) and reproduced reflectance and related NDVI, EVI and LSWI with the inverted mean variables in PROSPECT-SAIL-2 of data collection from DOY 196 – 216 in 2003 and with the same viewing geometries.



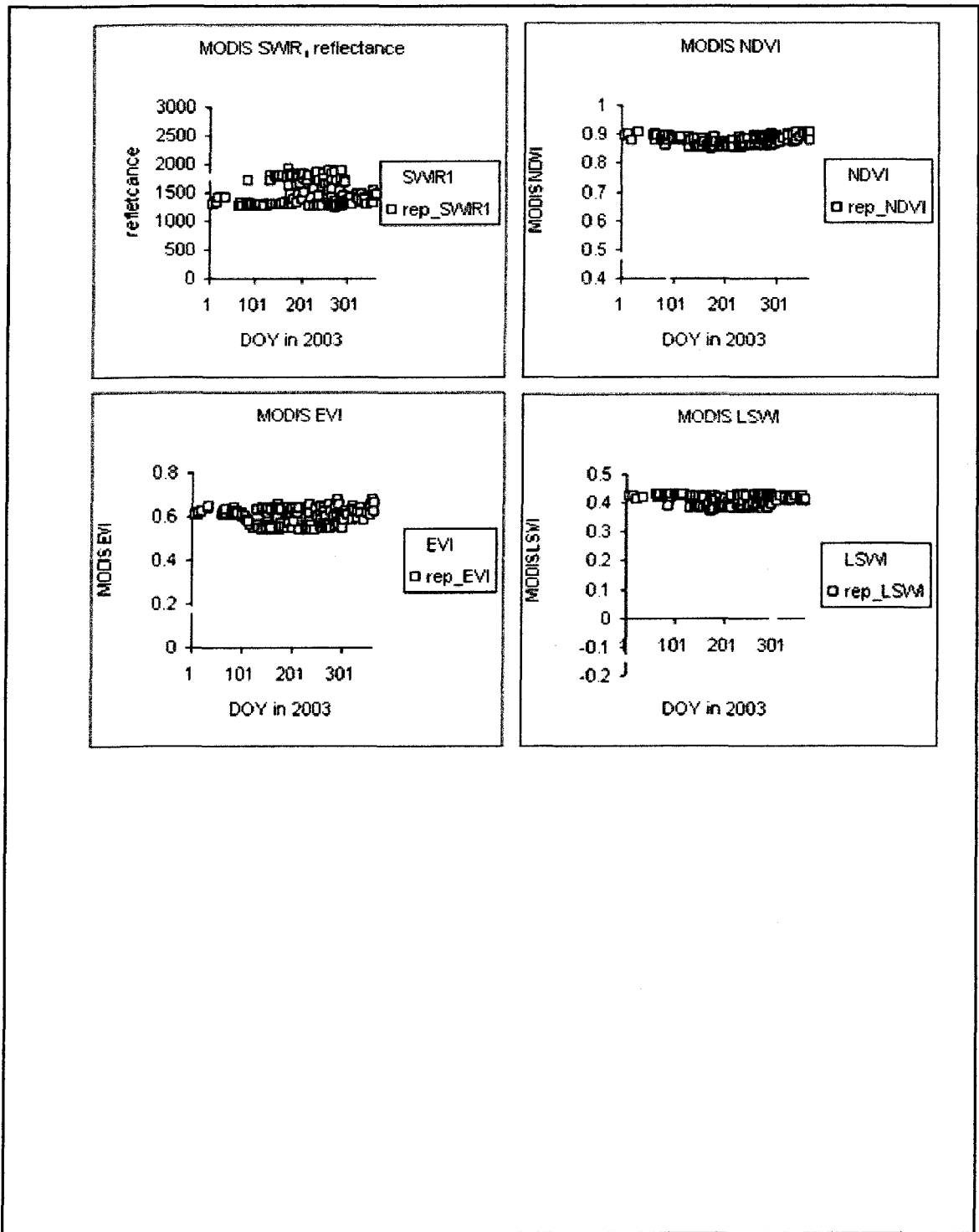


Figure 6.8 (continued) A comparison of reflectance, related NDVI, EVI and LSWI of MODIS clustering daily observations of the MO Forest site 1 in 2003 (reflectance scale=0.0001) and reproduced reflectance and related NDVI, EVI and LSWI with the inverted mean variables in PROSPECT-SAIL-2 of data collection from DOY 196 – 216 in 2003 and with the same viewing geometries.

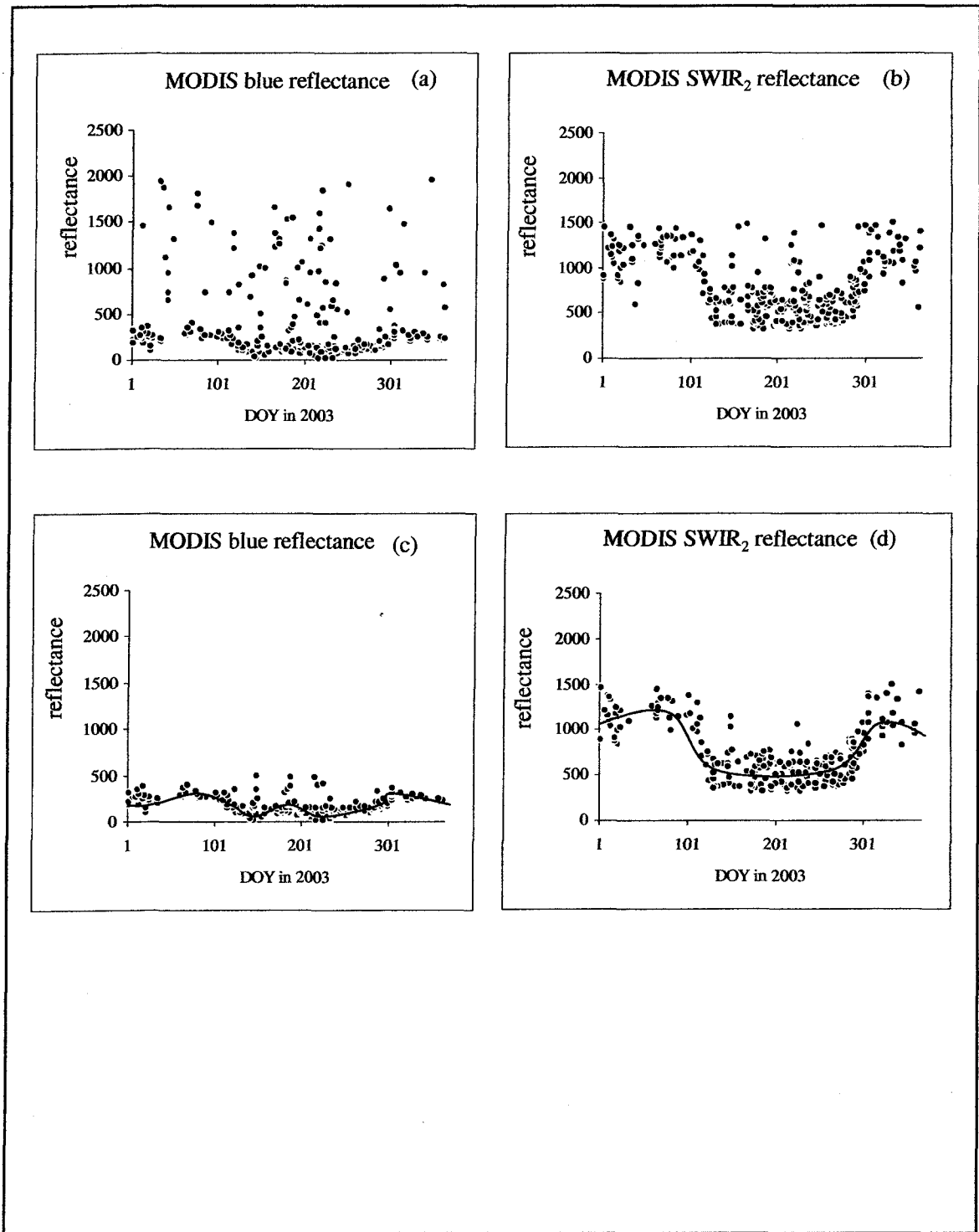


Figure 6.9 Reflectance of (a) blue and (b) SWIR<sub>2</sub> of MODIS daily observations of the Missouri Ozark Forest (MOF) site 2 in 2003 (reflectance scale=0.0001) with blue less than 0.2 and SWIR<sub>2</sub> less than 0.15; reflectance of (c) blue and (d) SWIR<sub>2</sub> of MODIS daily observations in 2003 with blue less than 0.051 and SWIR<sub>2</sub> less than 0.15

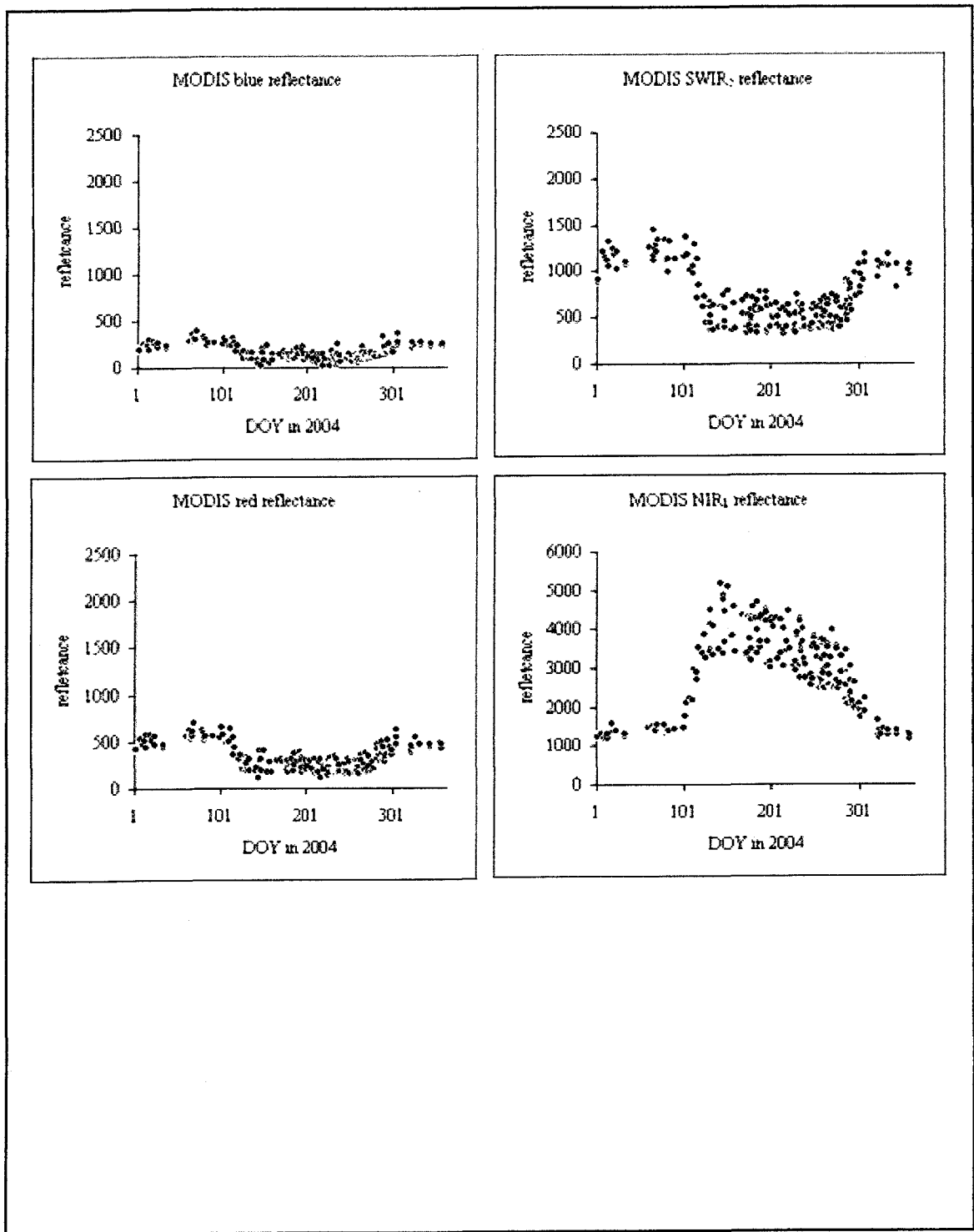


Figure 6.10 Reflectance of clustering MODIS daily observations of the MO Forest site 2 in 2003 (reflectance scale=0.0001) and related NDVI, EVI and LSWI

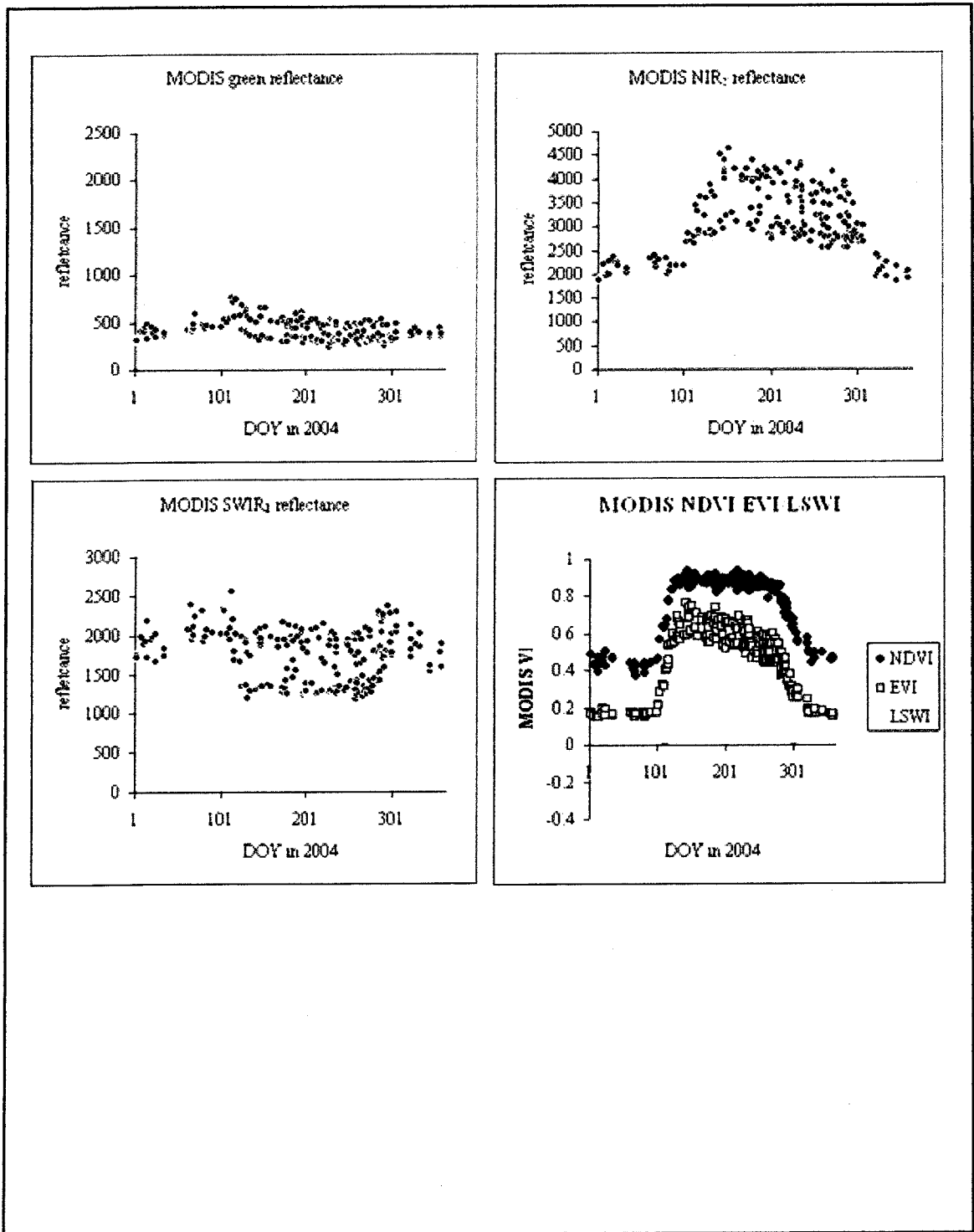


Figure 6.10 (continued) Reflectance of clustering MODIS daily observations of the MO Forest site 2 in 2003 (reflectance scale=0.0001) and related NDVI, EVI and LSWI

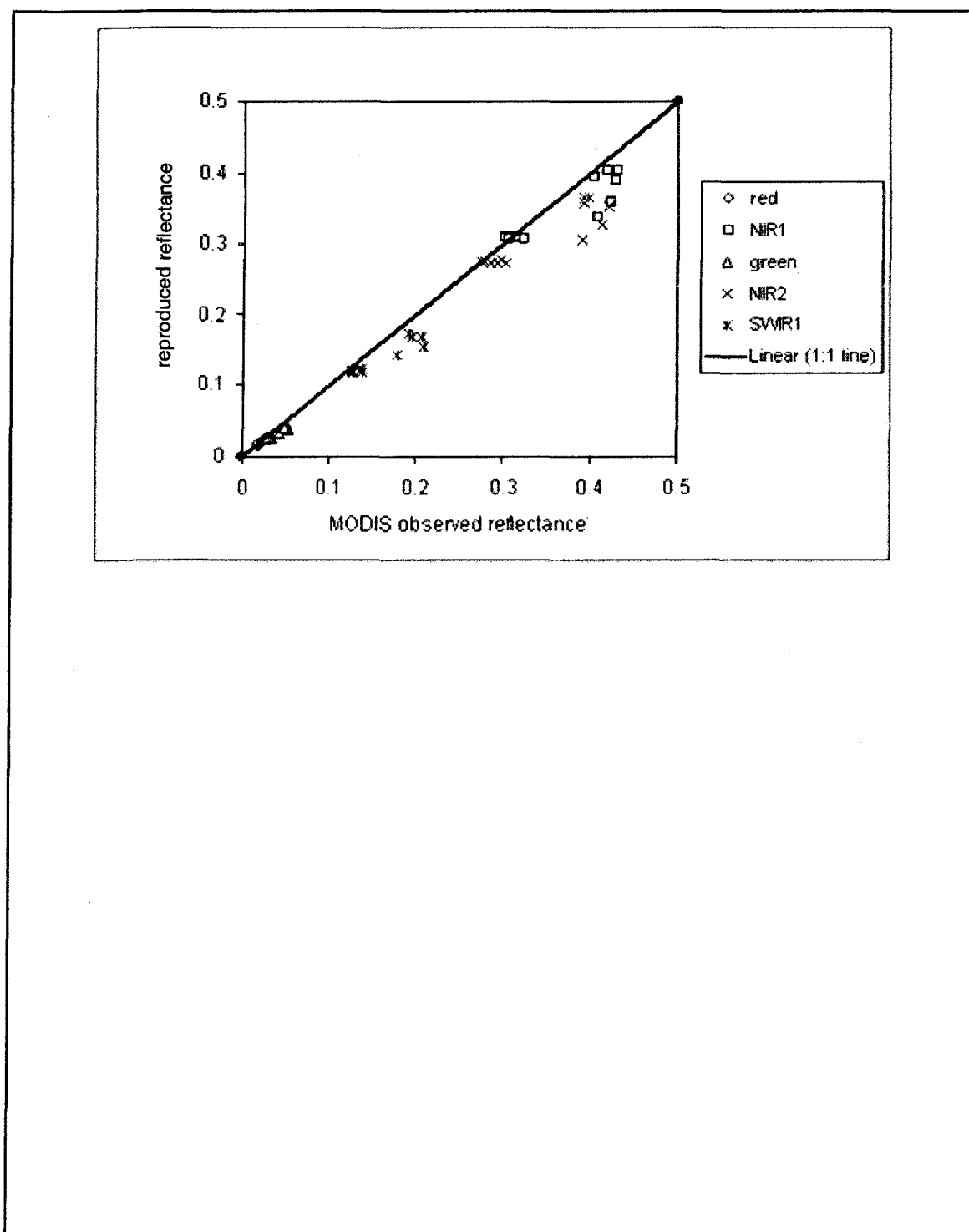


Figure 6.11 A comparison between the observed reflectance and PROSAIL-2 reproduced reflectance for five MODIS spectral bands (red, green, NIR<sub>1</sub>, NIR<sub>2</sub> and SWIR<sub>1</sub>). Surface reflectance were reproduced with the mean values of inverted variables from the PROSAIL-2 model using MODIS over the MO forest site 2 from DOY 201 to 216 in 2003.

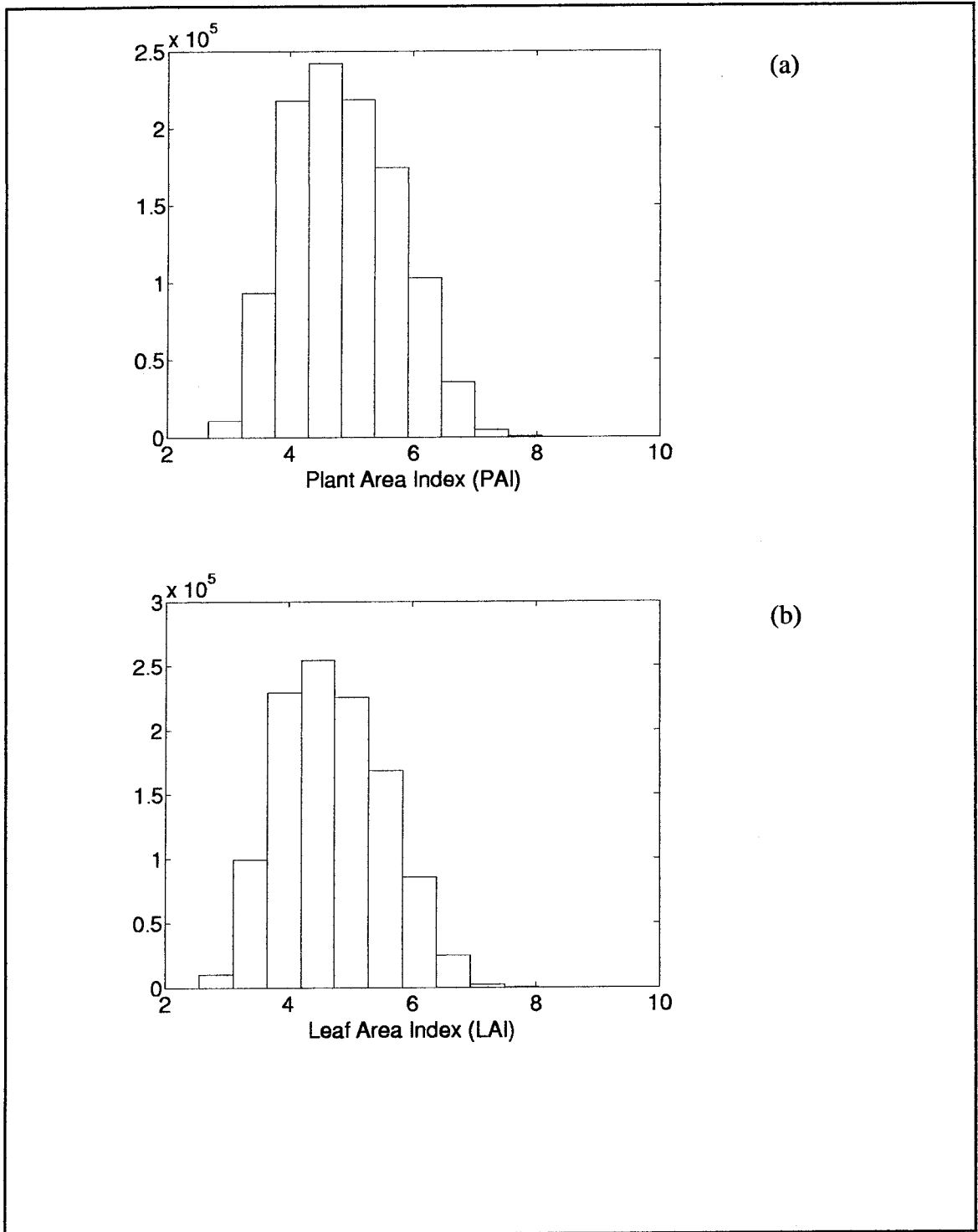


Figure 6.12 (a) Histogram of plant area index (PAI) for MODIS data collection of the MO forest site 2 from DOY 201 to 216 in 2003; (b) Histogram of leaf area index (LAI) for MODIS data collection of the MO forest site 2 from DOY 201 to 216 in 2003

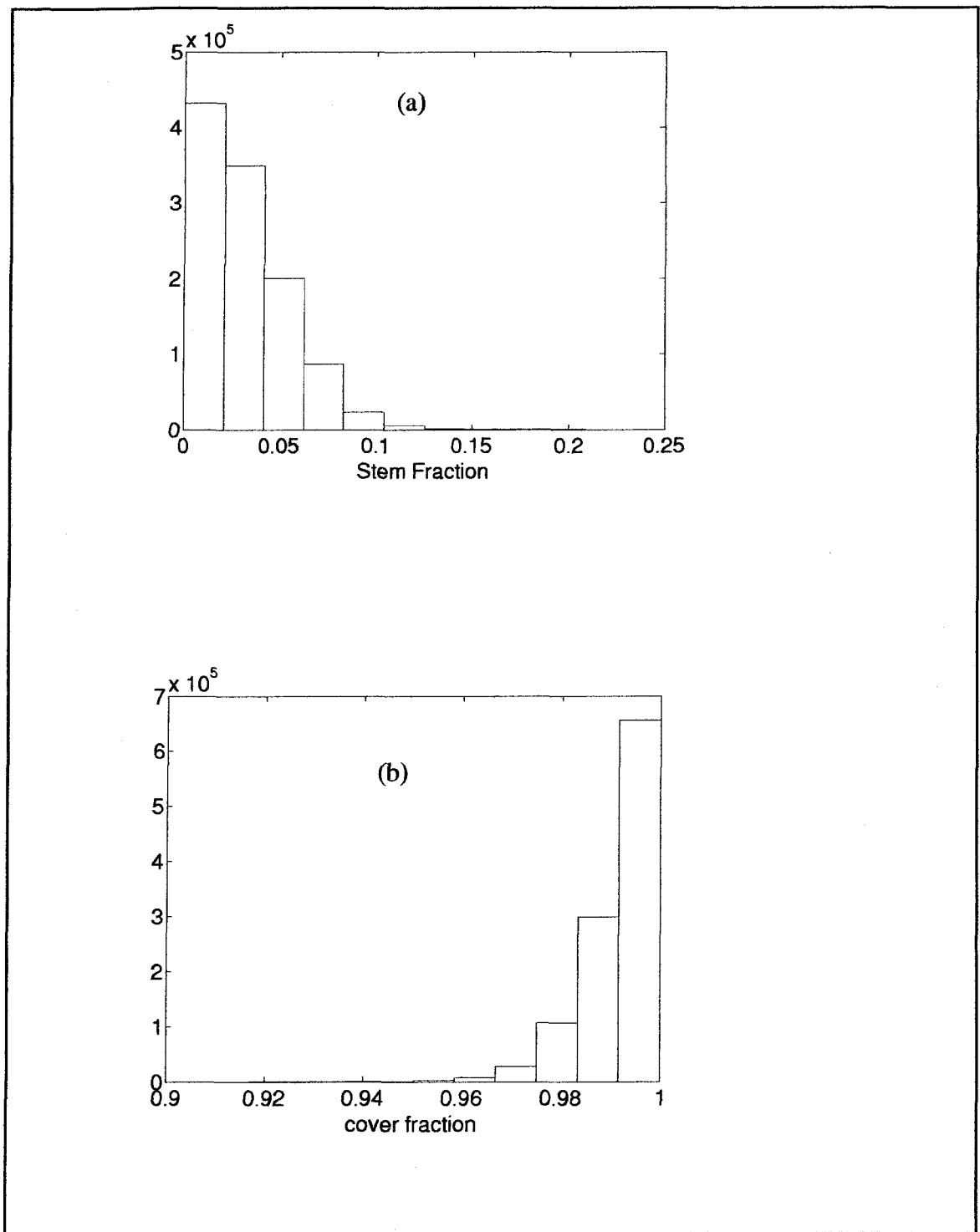


Figure 6.13 (a) Histogram of stem fraction for MODIS data collection of the MO forest site 2 from DOY 201 to 216 in 2003; (b) Histogram of cover fraction for MODIS data collection of the MO forest site 2 from DOY 201 to 216 in 2003

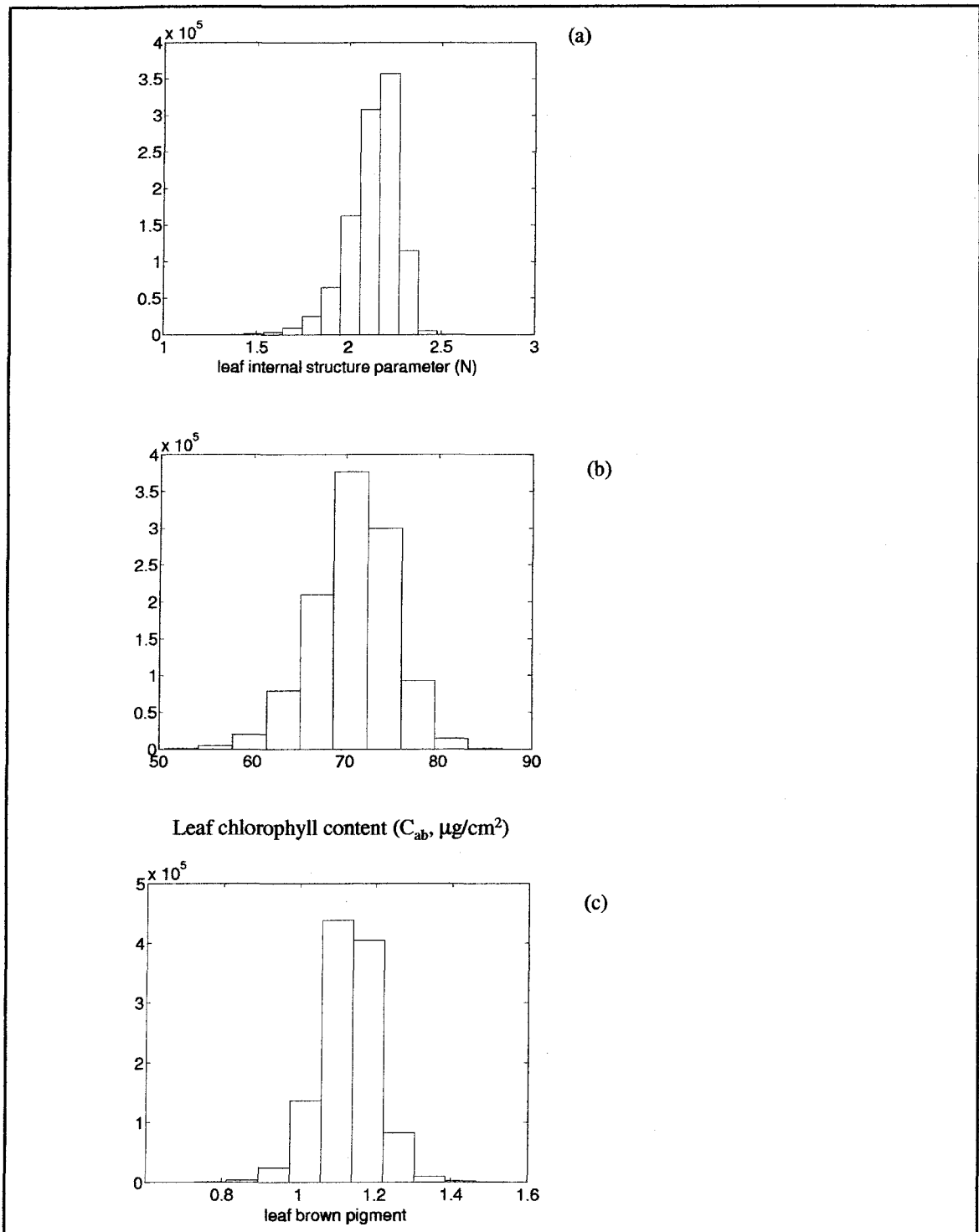


Figure 6.14 Histograms of leaf variables for MODIS data collection of the MO forest site 2 from DOY 201 to 216 in 2003

(a) leaf internal variable (N); (b) leaf chlorophyll content ( $C_{ab}$ ,  $\mu\text{g}/\text{cm}^2$ ); (c) leaf brown pigment ( $C_{brown}$ )



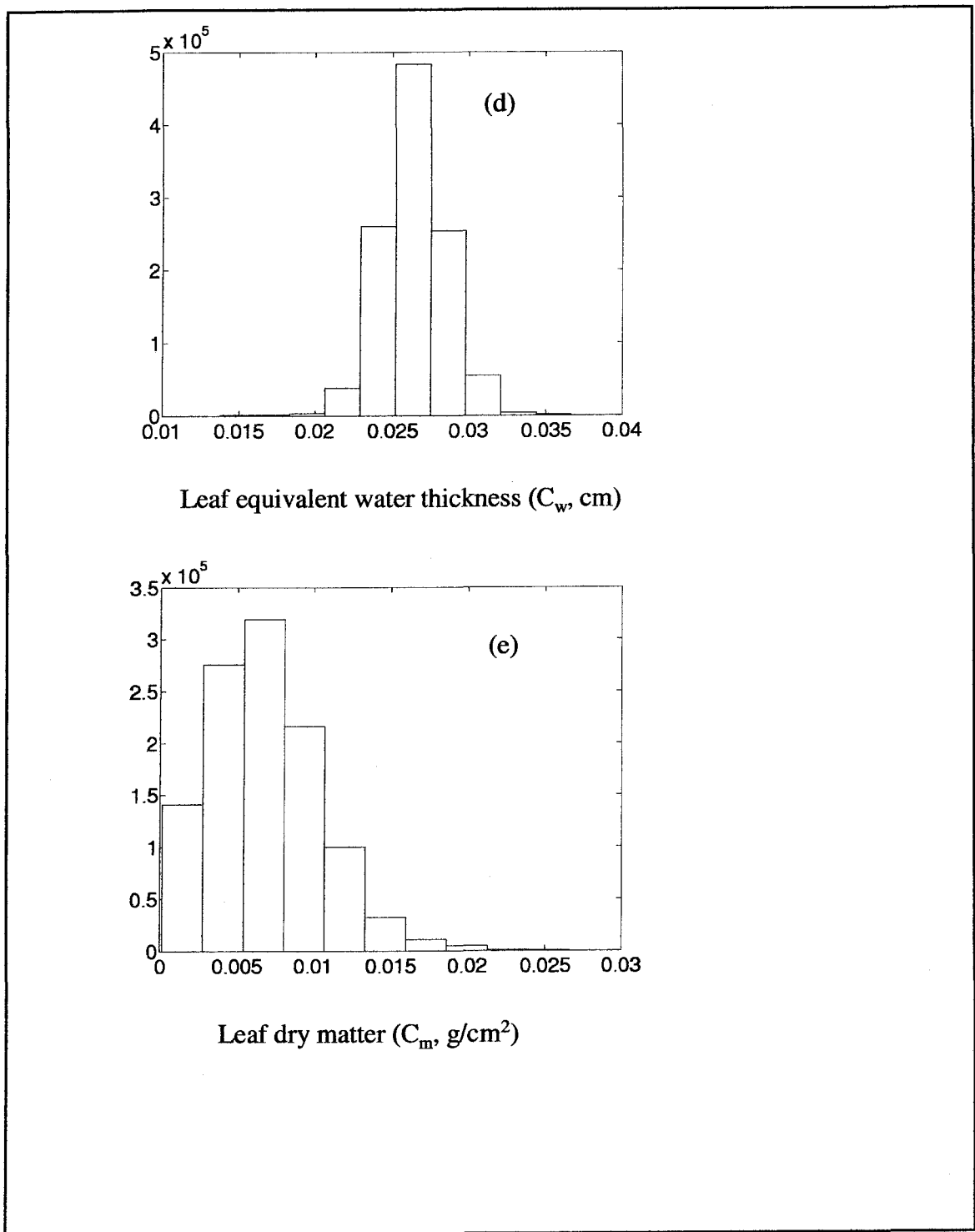


Figure 6.14 (continued) Histograms of (d) leaf equivalent water thickness ( $C_w$ , cm); and (e) leaf dry matter ( $C_m$ ,  $g/cm^2$ ) for MODIS data collection of the MO forest site 2 from DOY 201 to 216 in 2003

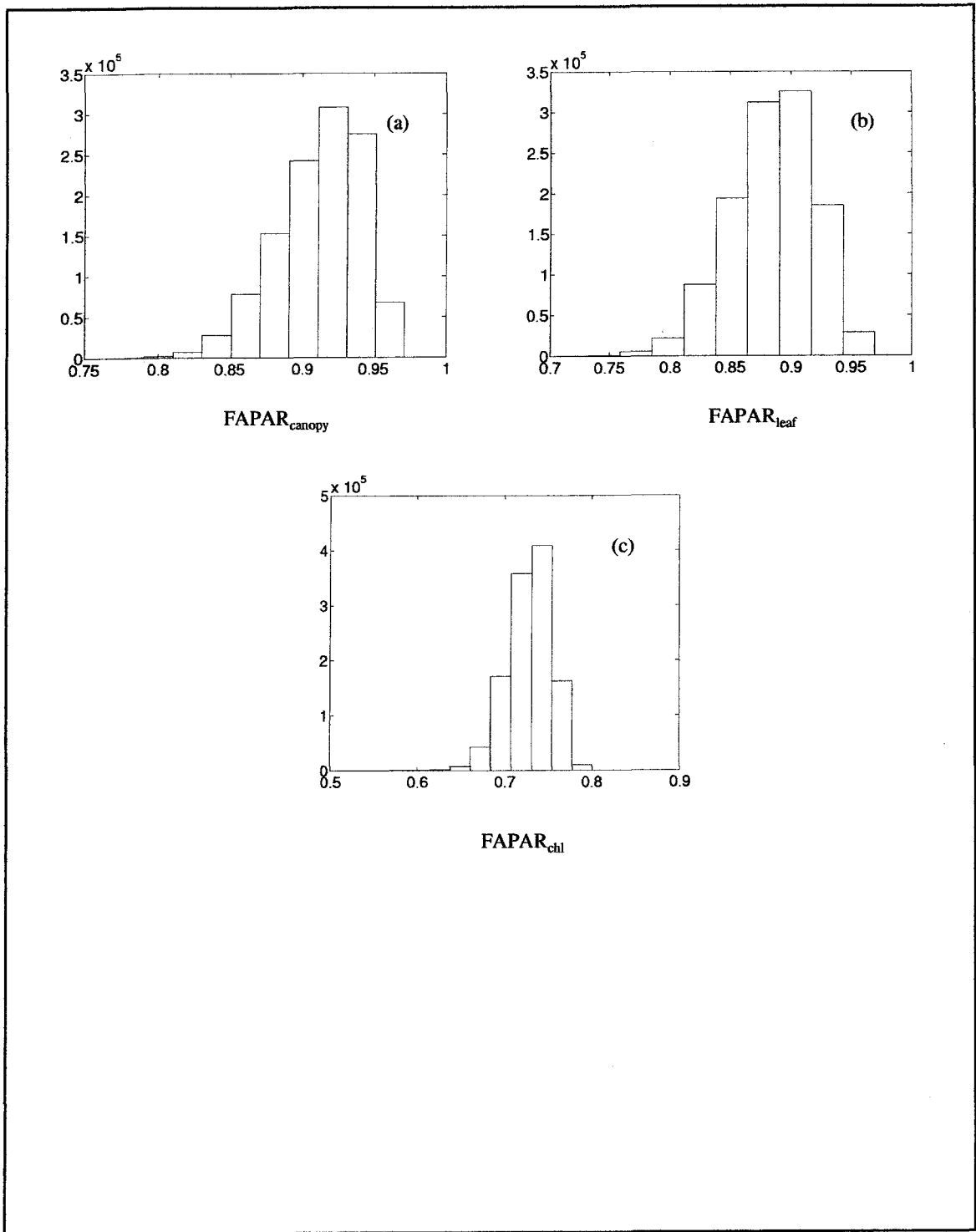


Figure 6.15 Histograms of fraction of photosynthetically active radiation absorbed by (a) canopy (FAPAR<sub>canopy</sub>); (b) by leaf (FAPAR<sub>leaf</sub>); (c) by chlorophyll (FAPAR<sub>chl</sub>) for MODIS data collection of the MO forest site 2 from DOY 201 to 216 in 2003

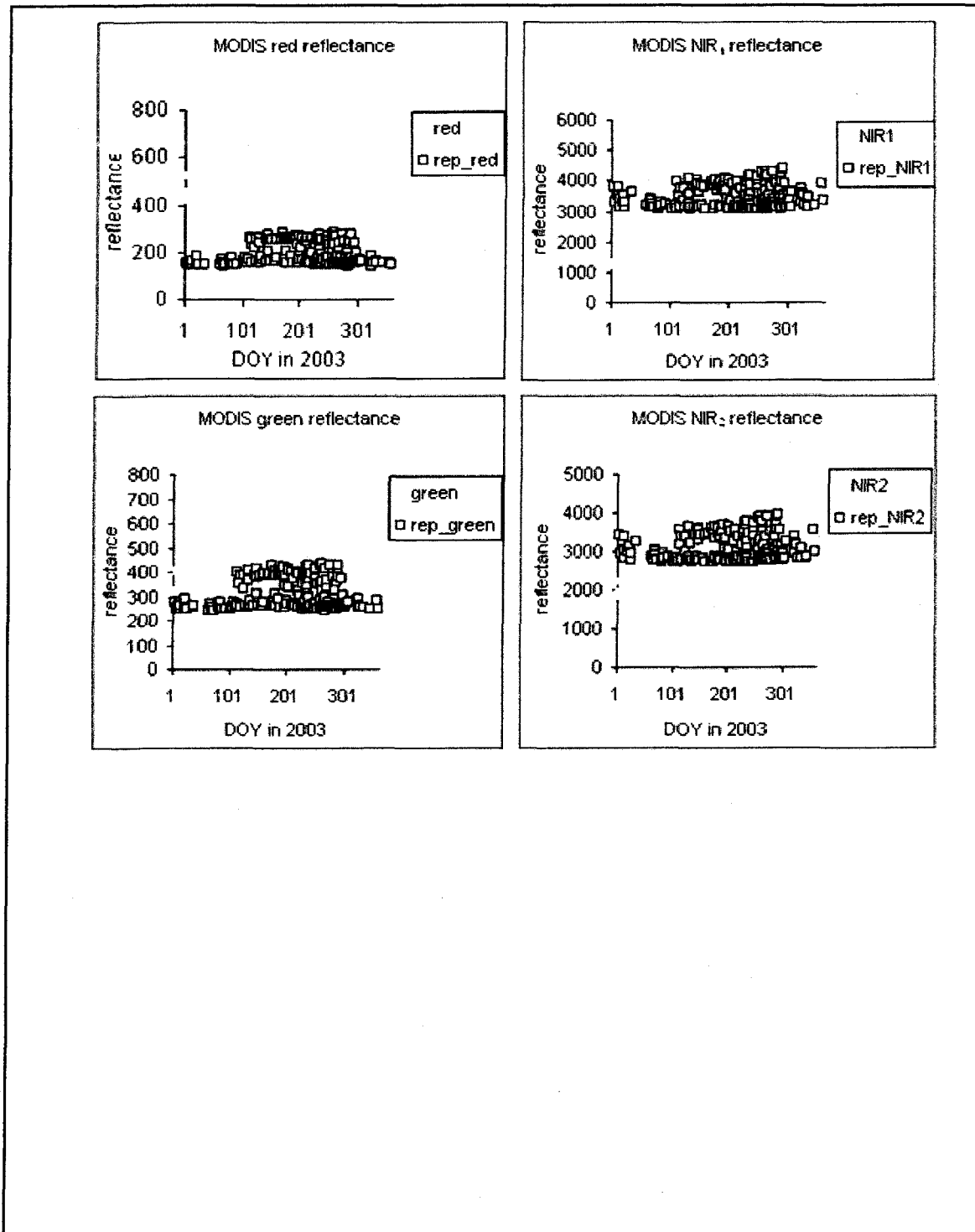


Figure 6.16 A comparison of reflectance, related NDVI, EVI and LSWI of MODIS clustering daily observations of the MO Forest site 2 in 2003 (reflectance scale=0.0001) and reproduced reflectance and related NDVI, EVI and LSWI with the inverted mean variables in PROSPECT-SAIL-2 of data collection from DOY 201 – 216 in 2003 and with the same viewing geometries.

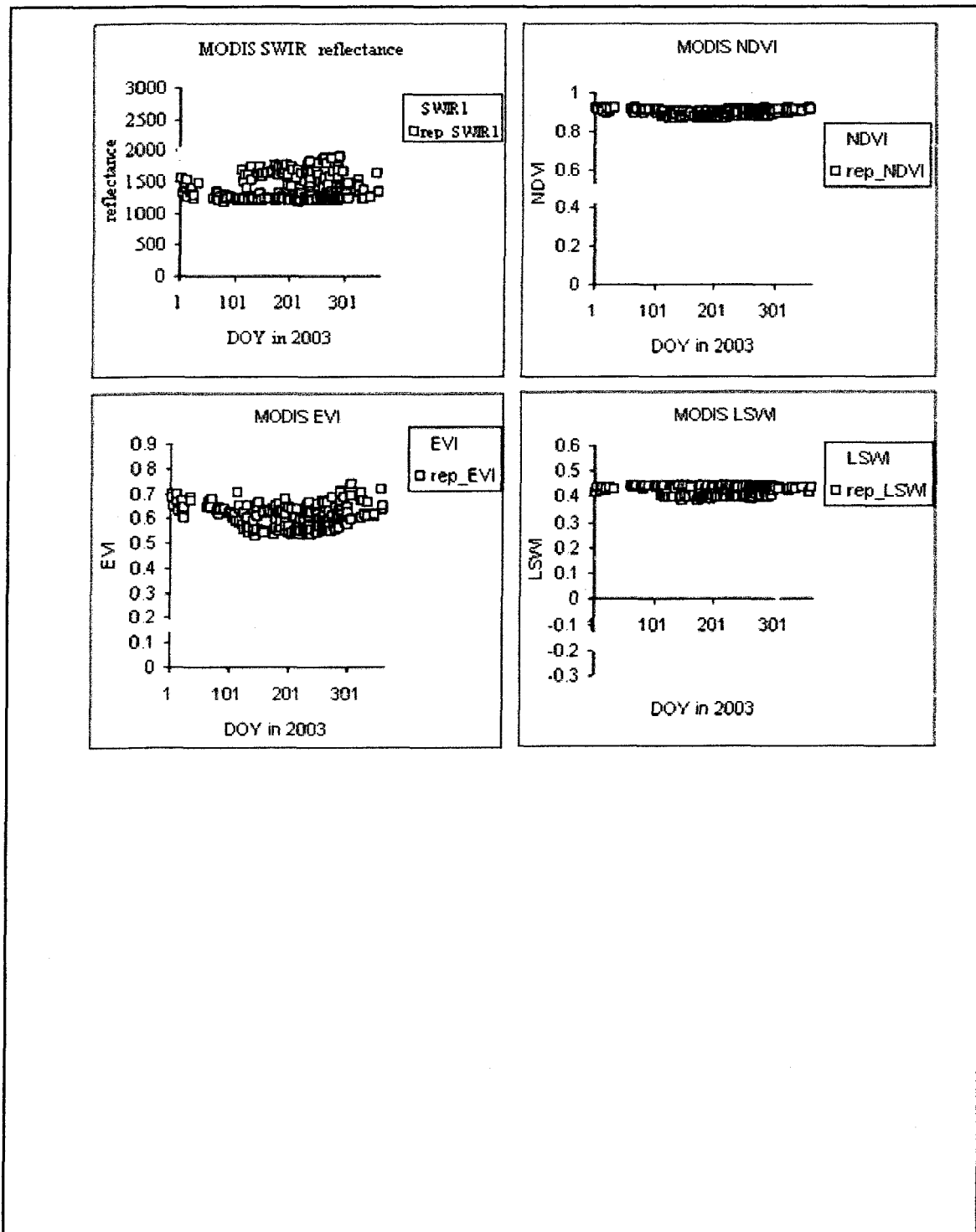


Figure 6.16 (continued) A comparison of reflectance, related NDVI, EVI and LSWI of MODIS clustering daily observations of the MO Forest site 2 in 2003 (reflectance scale=0.0001) and reproduced reflectance and related NDVI, EVI and LSWI with the inverted mean variables in PROSPECT-SAIL-2 of data collection from DOY 201 – 216 in 2003 and with the same viewing geometries

## CHAPTER 7

### SUMMARY AND CONCLUSIONS

This doctoral research is to provide new insight about physiology that is critical to better understanding of primary productivity and carbon dynamics on the land. The daily MODIS data and radiative transfer models are the major employed tools.

The first topic of this dissertation is how to get atmospheric-contamination and snow-contamination free daily MODIS observations. I developed a procedure using daily MODIS reflectance of blue and SWIR<sub>2</sub> bands to detect atmospheric-contaminated observations and using daily MODIS reflectance of red and SWIR<sub>2</sub> bands to detect snow-contaminated observations. MODIS SWIR<sub>2</sub> band is also used to track phenology in tropical vegetation areas where fire smoke often occurs and visible bands are severely contaminated by aerosol. Discussion on this topic is important because scientists have difficulties to distinguish contamination free observations and contaminated observations with only widely used vegetation indices, e.g. NDVI, EVI, and LSWI. This dissertation provides a procedure to distinguish them. The procedure can provide seasonal snow cover fraction for temperate forest areas. To check the MODIS spectral reflectance of all seven bands is a useful tool to distinguish contamination free observations and contaminated observations. I suspect it is also a potential tool to classify land cover types and monitor land use change.

The second topic of this dissertation is to monitor phenology using daily MODIS data. Seasonal MODIS observations after filtered with the procedure improve the

capability of phenology analysis in three perspectives: (1) providing daily MODIS seven spectral reflectance without atmospheric or snow contamination; (2) providing daily MODIS vegetation indices (e.g., NDVI, EVI and LSWI) without atmospheric or snow contamination; and (3) providing concise dates about leaf-on and leaf-off. Figures 2.11, 2.14, 2.16, 2.17, 2.19, 5.4, 6.2 and 6.10 showed concise phenology signals of the Xillingol grassland site, the Harvard Forest, the Howland Forest, the Walker Branch Watershed Forest, the Nebraska Soybean, the Bartlett Experimental Forest, and the two Missouri Ozark Forests, respectively. Through the summary statistical analysis using the procedure in Chapter 2, I also find it is possible to monitor seasonal phenology of tropical forest areas using the MODIS NIR<sub>1</sub> and SWIR<sub>2</sub> bands, at least for no rain days (Figure 2.26). This finding may be expanded to use in the Amazon area and other tropical vegetation areas. The contamination free phenology signals obtained by this method will not mix with the atmospheric and/or snow contaminated signals while AVHRR NDVI series cannot partition them. The contamination free phenology signals can be used in GPP models (e.g., Vegetation Photosynthesis Model) without worrying about easily confusing signals in spring/winter seasons. If fund is available, I would like to produce these contamination free products at various time scales (daily, 8-day composite, etc.) and spatial scales (local, regional, continental) in future.

The third topic is about a question: are seasonal MODIS spectral variations of forests during the plant growing season only due to vegetation's anisotropic nature? This is an open question since satellite remote sensing was available. Whether "yes" or "no", no direct or indirect evidences in literature was provided to support or argue. In Chapters 2, 5, and 6, obvious seasonal MODIS spectral dynamics are observed during the plant

growing season. The simulation study of this dissertation suggests that vegetation's BRDF effect does not completely cover the seasonal MODIS spectral dynamics during the plant growing seasons and there should be other factors except the BRDF effect that are due to the seasonal variations. LAI and  $FAPAR_{canopy}$  of forests generally don't change during the period from leaf full expansion to leaf senescence. Some factors related to leaf are hinted to be partly in charge of the variations. Seasonal NDVI series don't have the obvious seasonal dynamics during the plant growing season because NDVI is saturated during the period. Using only AVHRR NDVI has no way to detect this kind of seasonal variations. My suggestion is that seasonal BRDF field measurements and physiological study for the seasonal variations may start in future. I expect some interesting findings. Very few studies reported the findings of seasonal spectral variations of forests or other vegetations in literature; hence scientists do not know the reasons of the variations yet.

The fourth topic is  $FAPAR_{chl}$ , the central point of this dissertation. Partitioning  $FAPAR_{canopy}$  into  $FAPAR_{chl}$  and  $FAPAR_{NPV}$  has not really been explicitly discussed before. To calculate  $FAPAR_{chl}$  with MODIS observations, I did two major things in this dissertation: (1) improving PROSPECT model through including brown pigment and coupling the improved PROSPECT with the SAIL-2 code from Rob; (2) inverting the variables with the Metropolis algorithm that can provide distributions of individual variables. Studies in Chapters 4-6 illustrate that little stem and soil in the Harvard Forest, the Bartlett Experimental Forest and the two Missouri Ozark Forest sites is observed by MODIS during peak of the plant growing season and there is little difference between  $FAPAR_{canopy}$  and  $FAPAR_{leaf}$  during the peak. The SAIL-2 model can be simplified next time by assuming no stem or soil is observed over forests like the Bartlett Experimental

Forest during summer peaks. However, there is significant difference between  $FAPAR_{leaf}$  and  $FAPAR_{chl}$ . This finding suggests that the amount of absorbed PAR for photosynthesis estimated using  $FAPAR_{canopy}$  may be overestimated. This finding can reduce some uncertainty/error in the estimating of GPP. LAI of the Harvard Forest estimated through the Metropolis algorithm (in Chapter 4) is less than LAI from the MODIS standard product of LAI and is much closer to field measurement. LAI of the Bartlett Experimental Forest estimated through the Metropolis algorithm is covered by field measurement range (Chapter 5). Leaf chlorophyll concentration and leaf dry matter (leaf specific weight) estimated through the Metropolis algorithm are in the same order of literature reporting and field measurements. The Metropolis algorithm has potential to be applied in local scale to regional scale in the future.

In the future, this research could continue along the following directions: to implement the procedure of getting atmospheric-contamination and snow-contamination free MODIS (daily) observations for whole MODIS tiles; to produce an alternative phenology datasets from contamination free observations; to measure leaf biophysical and biochemical variables to study which would contribute to the seasonal spectral variations; to continue to improve the radiative transfer models; to conduct more evaluation for the inversion of PROSAIL-2; to invent new instruments to measure  $FAPAR_{chl}$  in the field; and to expand the above methodology to USA and the globe.



## REFERENCES

- Aber, J. D., Reich, P. B., &Goulden, M. L. (1996). Extrapolating leaf CO<sub>2</sub> exchange to the canopy: A generalized model of forest photosynthesis compared with measurements by eddy correlation. *Oecologia*, *106*, 257-265.
- Allen, W. A.&Richardson, A. J. (1968). Interaction of light with a plant canopy. *Journal of the Optical Society of America*, *58*, 1023-1028.
- Allen, W. A., Gausman, H. W., Richardson, A. J., Thomas, J. R., &. (1969). Interaction of isotropic light with compact plan leaf. *J Optic Soc Amer*, *59*, 1376-1379.
- Allen, W. A., Gayle, A. J., &Richardson, A. J. (1970). Plant canopy irradiance specified by the Duntley equations. *J Opt Soc Am*, *60*, 372-376.
- Andrieu, B., Baret, F., Jacquemoud, S., Malthus, T., &Steven, M. (1997). Evaluation of an improved version of SAIL model for simulating bidirectional reflectance of sugar beet canopies. *Remote Sensing of Environment*, *60*, 247-257.
- Arora, V. K. (2002). Modeling vegetation as a dynamic component in soil-vegetation-atmosphere transfer schemes and hydrological models. *Reviews of Geophysics*, *40*.
- Asner, G. P., Braşwell, B. H., Schimel, D. S., &Wessman, C. A. (1998a). Ecological research needs from multiangle remote sensing data. *Remote Sensing of Environment*, *63*, 155-165.
- Asner, G. P., Wessman, C. A., &Archer, S. (1998b). Scale dependence of absorption of photosynthetically active radiation in terrestrial ecosystems. *Ecological Applications*, *8*, 1003-1021.
- Bacour, C.&Jacquemoud, S. (2001). Coupling spectral and bidirectional information to estimate biophysical parameters by model inversion. *Proc International Workshop on Spectroscopy Application in Precision Farming (IWSAPF), Germany*, 74-77.
- Bacour, C., Jacquemoud, S., Leroy, M., Hautecoeur, O., Weiss, M., Prevot, L., Bruguier, N., &Chauki, H. (2002a). Reliability of the estimation of vegetation characteristics by inversion of three canopy reflectance models on airborne POLDER data. *Agronomie*, *22*, 555-565.
- Bacour, C., Jacquemoud, S., Tourbier, Y., Dechambre, M., &Frangi, J. P. (2002b). Design and analysis of numerical experiments to compare four canopy reflectance models. *Remote Sensing of Environment*, *79*, 72-83.
- Badhwar, G. D., Verhoef, W., &Bunnik, N. J. J. (1985). Comparative-Study of SUITS and SAIL Canopy Reflectance Models. *Remote Sensing of Environment*, *17*, 179-195.
- Baldocchi, D.&Wilson, K. (2001). Modeling CO<sub>2</sub> and water vapor exchange of a temperate broadleaved forest across hourly to decadal time scales. *ECOLOGICAL MODELLING*, *142*, 155-184.
- Baret, F.&Guyot, G. (1991). Potentials and Limits of Vegetation Indexes for Lai and Apar Assessment. *Remote Sensing of Environment*, *35*, 161-173.

- Baret, F., Clevers, J., & Steven, M. (1995). THE ROBUSTNESS OF CANOPY GAP FRACTION ESTIMATES FROM RED AND NEAR-INFRARED REFLECTANCES - A COMPARISON OF APPROACHES. *REMOTE SENSING OF ENVIRONMENT*, 54, 141-151.
- Baret, F. & Fourty, T., 1997: Radiometric estimates of nitrogen status in leaves and canopies. In Lemaire, G. (ed.), *Diagnosis of the Nitrogen Status in Crops*. Berlin: Springer, 201-227.
- Barford, C. C., Wofsy, S. C., Goulden, M. L., Munger, J. W., Pyle, E. H., Urbanski, S. P., Hutyra, L., Saleska, S. R., Fitzjarrald, D., & Moore, K. (2001). Factors controlling long- and short-term sequestration of atmospheric CO<sub>2</sub> in a mid-latitude forest. *Science*, 294, 1688-1691.
- Bassow, S. L. & Bazzaz, F. A. (1998). How environmental conditions affect canopy leaf-level photosynthesis in four deciduous tree species. *Ecology*, 79, 2660-2675.
- Batista, G. T., Shimabukuro, Y. E., & Lawrence, W. T. (1997). The long-term monitoring of vegetation cover in the Amazonian region of northern Brazil using NOAA-AVHRR data. *International Journal of Remote Sensing*, 18, 3195-3210.
- Bicheron, P. & Leroy, M. (1999). A method of biophysical parameter retrieval at global scale by inversion of a vegetation reflectance model. *Remote Sensing of Environment*, 67, 251-266.
- Bishop, C. (1995). Neural networks for pattern recognition. New York: Oxford University Press.
- Bousquet, L., Lacherade, S., Jacquemoud, S., & Moya, I. (2005). Leaf BRDF measurements and model for specular and diffuse components differentiation. *Remote Sensing of Environment*, 98, 201-211.
- Braswell, B. H., Schimel, D. S., Privette, J. L., Moore, B., Emery, W. J., Sulzman, E. W., & Hudak, A. T. (1996). Extracting ecological and biophysical information from AVHRR optical data: An integrated algorithm based on inverse modeling. *Journal of Geophysical Research-Atmospheres*, 101, 23335-23348.
- Braswell, B. H., Sacks, W. J., Linder, E., & Schimel, D. S. (2005). Estimating Diurnal to Annual Ecosystem Parameters by Synthesis of a Carbon Flux Model with Eddy Covariance Net Ecosystem Exchange Observations. *Global Change Biology*, 11, 335-355.
- Breece, H. T. & Holmes, R. A. (1971). Bidirectional Scattering Characteristics of Healthy Green Soybean and Corn Leaves Vivo. *Appl Opt*, 10, 119-127.
- Cavender-Bares, J., Potts, M., Zacharias, E., & Bazzaz, F. A. (2000). Consequences of CO<sub>2</sub> and light interactions for leaf phenology, growth, and senescence in *Quercus rubra*. *Global Change Biology*, 6, 877-887.
- Ceccato, P., Flasse, S., Tarantola, S., Jacquemoud, S., & Gregoire, J. M. (2001). Detecting vegetation leaf water content using reflectance in the optical domain. *Remote Sensing of Environment*, 77, 22-33.
- Chandrasekhar, S. (1960). radiative transfer. New York: Dover Publications, pp 393.
- Chelle, M. & Andrieu, B. (1999). Radiative models for architectural modeling. *Agronomie*, 19, 225-240.
- Chen, J. M., Liu, J., Cihlar, J., & Goulden, M. L. (1999). Daily canopy photosynthesis model through temporal and spatial scaling for remote sensing applications. *Ecological Modelling*, 124, 99-119.

- Chopping, M. J. (2000). Testing a LiSK BRDF model with in situ bidirectional reflectance factor measurements over semiarid grasslands. *Remote Sensing of Environment*, 74, 287-312.
- Chopping, M. J. (2001). Testing LiSKBRDF models over a semi-arid grassland region with visible and near-infrared ATSR-2 and AVHRR data. *International Journal of Remote Sensing*, 22, 3533-3552.
- Cihlar, J. & Howarth, J. (1994a). Detection and Removal of Cloud Contamination from Avhrr Images. *Ieee Transactions on Geoscience and Remote Sensing*, 32, 583-589.
- Cihlar, J., Manak, D., & Diorio, M. (1994b). Evaluation of Compositing Algorithms for Avhrr Data over Land. *Ieee Transactions on Geoscience and Remote Sensing*, 32, 427-437.
- Cihlar, J., Manak, D., & Voisin, N. (1994c). Avhrr Bidirectional Reflectance Effects and Compositing. *Remote Sensing of Environment*, 48, 77-88.
- Cihlar, J., Ly, H., Li, Z. Q., Chen, J., Pokrant, H., & Huang, F. T. (1997). Multitemporal, multichannel AVHRR data sets for land biosphere studies - Artifacts and corrections. *Remote Sensing of Environment*, 60, 35-57.
- Cihlar, J. (2000). Land cover mapping of large areas from satellites: status and research priorities. *International Journal of Remote Sensing*, 21, 1093-1114.
- Cohen, W. B., Maiersperger, T. K., Yang, Z. Q., Gower, S. T., Turner, D. P., Ritts, W. D., Berterretche, M., & Running, S. W. (2003). Comparisons of land cover and LAI estimates derived from ETM plus and MODIS for four sites in North America: a quality assessment of 2000/2001 provisional MODIS products. *Remote Sensing of Environment*, 88, 233-255.
- Combal, B., Baret, F., & Weiss, M. (2002). Improving canopy variables estimation from remote sensing data by exploiting ancillary information. Case study on sugar beet canopies. *Agronomie*, 22, 205-215.
- Dawson, T. P., Curran, P. J., & Plummer, S. E. (1998). LIBERTY - Modeling the effects of leaf biochemical concentration on reflectance spectra. *Remote Sensing of Environment*, 65, 50-60.
- Defries, R. S., Houghton, R. A., Hansen, M. C., Field, C. B., Skole, D., & Townshend, J. (2002). Carbon emissions from tropical deforestation and regrowth based on satellite observations for the 1980s and 1990s. *Proceedings of the National Academy of Sciences of the United States of America*, 99, 14256-14261.
- Demarez, V., Gastellu-Etchegorry, J. P., Mougou, E., Marty, G., Proisy, C., Dufrene, E., & Le Dantec, V. (1999). Seasonal variation of leaf chlorophyll content of a temperate forest. Inversion of the PROSPECT model. *International Journal of Remote Sensing*, 20, 879-894.
- Depury, D. G. G. & Farquhar, G. D. (1997). Simple scaling of photosynthesis from leaves to canopies without the errors of big-leaf models. *Plant Cell and Environment*, 20, 537-557.
- Dessay, N., Laurent, H., Machado, L. A. T., Shimabukuro, Y. E., Batista, G. T., Diedhiou, A., & Ronchail, J. (2004). Comparative study of the 1982-1983 and 1997-1998 El Nino events over different types of vegetation in South America. *International Journal of Remote Sensing*, 25, 4063-4077.

- Di Bella, C. M., Paruelo, J. M., Becerra, J. E., Bacour, C., & Baret, F. (2004). Effect of senescent leaves on NDVI-based estimates of f APAR: experimental and modelling evidences. *International Journal of Remote Sensing*, 25, 5415-5427.
- Diner, D. J., Martonchik, J. V., Borel, C., Gerstl, S. A. W., Gordon, H. R., Knyazikhin, Y., Myneni, R., Pinty, B., & Verstraete, M. (1999). MISR Level 2 Surface Retrieval Algorithm Theoretical Basis.
- Epiphanio, J. C. N. & Huete, A. R. (1995). Dependence of Ndvi and Savi on Sun Sensor Geometry and Its Effect on Fapar Relationships in Alfalfa. *Remote Sensing of Environment*, 51, 351-360.
- Fang, H. L. & Liang, S. L. (2003). Retrieving leaf area index with a neural network method: Simulation and validation. *Ieee Transactions on Geoscience and Remote Sensing*, 41, 2052-2062.
- Field, C. (1987). Leaf-age effects on stomatal conductance. Stanford: Stanford University Press, pp 367- 384.
- Field, C. B., Randerson, J. T., & Malmstrom, C. M. (1995). Global Net Primary Production - Combining Ecology and Remote-Sensing. *Remote Sensing of Environment*, 51, 74-88.
- Fitzjarrald, D. R., Acevedo, O. C., & Moore, K. E. (2001). Climatic consequences of leaf presence in the eastern United States. *Journal of Climate*, 14, 598-614.
- Gamon, J., Serrano, L., & Surfus, J. (1997). The photochemical reflectance index: an optical indicator of photosynthetic radiation use efficiency across species, functional types, and nutrient levels. *OECOLOGIA*, 112, 492-501.
- Gamon, J. & Surfus, J. (1999). Assessing leaf pigment content and activity with a reflectometer. *NEW PHYTOLOGIST*, 143, 105-117.
- Ganapol, B. D., Johnson, L. F., Hammer, P. D., Hlavka, C. A., & Peterson, D. L. (1998). LEAFMOD: A new within-leaf radiative transfer model. *Remote Sensing of Environment*, 63, 182-193.
- Ganapol, B. D., Johnson, L. F., Hlavka, C. A., Peterson, D. L., & Bond, B. (1999). LCM2: A coupled leaf/canopy radiative transfer model. *Remote Sensing of Environment*, 70, 153-166.
- Gao, B. C. (1996). NDWI - A normalized difference water index for remote sensing of vegetation liquid water from space. *Remote Sensing of Environment*, 58, 257-266.
- Garcia-Haro, F. J., Gilabert, M. A., & Melia, J. (1999). A radiosity model for heterogeneous canopies in remote sensing. *Journal of Geophysical Research- Atmospheres*, 104, 12159-12175.
- Garcia-Haro, F. J. & Sommer, S. (2002). A fast canopy reflectance model to simulate realistic remote sensing scenarios. *Remote Sensing of Environment*, 81, 205-227.
- Gausman, H. W., Allen, W. A., Cardenas, R., & Richardson, A. J. (1970). Relation of light reflectance to histological and physical evaluations of cotton leaf maturity. *Appl Optic*, 9, 545-552.
- Gelman, A., Carlin, J. B., Stern, H. S., & Rubin, D. B. (2000). Markov chain simulation (chapter 11) in *Bayesian Data Analysis*. New York: Chapman & Hall /CRC.
- Gitelson, A., Stark, R., Grits, U., Rundquist, D., Kaufman, Y., & Derry, D. (2002a). Vegetation and soil lines in visible spectral space: a concept and technique for remote estimation of vegetation fraction. *INTERNATIONAL JOURNAL OF REMOTE SENSING*, 23, 2537-2562.

- Gitelson, A. A. & Merzlyak, M. N. (1996). Signature analysis of leaf reflectance spectra: Algorithm development for remote sensing of chlorophyll. *Journal of Plant Physiology*, *148*, 494-500.
- Gitelson, A. A. & Merzlyak, M. N. (1997). Remote estimation of chlorophyll content in higher plant leaves. *International Journal of Remote Sensing*, *18*, 2691-2697.
- Gitelson, A. A., Zur, Y., Chivkunova, O. B., & Merzlyak, M. N. (2002b). Assessing carotenoid content in plant leaves with reflectance spectroscopy. *Photochemistry and Photobiology*, *75*, 272-281.
- Gobron, N., Pinty, B., Verstraete, M. M., & Govaerts, Y. (1997). A semidiscrete model for the scattering of light by vegetation. *Journal of Geophysical Research-Atmospheres*, *102*, 9431-9446.
- Gobron, N., Pinty, B., Verstraete, M. M., Martonchik, J. V., Knyazikhin, Y., & Diner, D. J. (2000a). Potential of multiangular spectral measurements to characterize land surfaces: Conceptual approach and exploratory application. *Journal of Geophysical Research-Atmospheres*, *105*, 17539-17549.
- Gobron, N., Pinty, B., Verstraete, M. M., & Widlowski, J. L. (2000b). Advanced vegetation indices optimized for up-coming sensors: Design, performance, and applications. *Ieee Transactions on Geoscience and Remote Sensing*, *38*, 2489-2505.
- Gobron, N., Pinty, B., Verstraete, M. M., Widlowski, J. L., & Diner, D. J. (2002). Uniqueness of multiangular measurements - Part II: Joint retrieval of vegetation structure and photosynthetic activity from MISR. *Ieee Transactions on Geoscience and Remote Sensing*, *40*, 1574-1592.
- Goel, N. (1988). Models of vegetation canopy reflectance and their use in estimation of biophysical parameters from reflectance data. *Remote Sensing Reviews*, *4*, 1-212.
- Goel, N. S., Strelbel, D. E., & Thompson, R. L. (1984a). Inversion of Vegetation Canopy Reflectance Models for Estimating Agronomic Variables. 2. Use of Angle Transforms and Error Analysis as Illustrated by Suits Model. *Remote Sensing of Environment*, *14*, 77-111.
- Goel, N. S. & Thompson, R. L. (1984b). Inversion of Vegetation Canopy Reflectance Models for Estimating Agronomic Variables. 3. Estimation Using Only Canopy Reflectance Data as Illustrated by the Suits Model. *Remote Sensing of Environment*, *15*, 223-236.
- Goel, N. S. & Thompson, R. L. (1984c). Inversion of Vegetation Canopy Reflectance Models for Estimating Agronomic Variables. 5. Estimation of Leaf-Area Index and Average Leaf Angle Using Measured Canopy Reflectances. *Remote Sensing of Environment*, *16*, 69-85.
- Goel, N. S. & Thompson, R. L. (1984d). Inversion of Vegetation Canopy Reflectance Models for Estimating Agronomic Variables. 4. Total Inversion of the Suits Model. *Remote Sensing of Environment*, *15*, 237-253.
- Goel, N. S. & Deering, D. W. (1985). Evaluation of a Canopy Reflectance Model for LAI Estimation through Its Inversion. *IEEE Transactions on Geoscience and Remote Sensing*, *23*, 674-684.
- Gond, V., De Pury, D. G. G., Veroustraete, F., & Ceulemans, R. (1999). Seasonal variations in leaf area index, leaf chlorophyll, and water content; scaling-up to

- estimate fAPAR and carbon balance in a multilayer, multispecies temperate forest. *Tree Physiology*, 19, 673-679.
- Goulden, M. L., Munger, J. W., Fan, S. M., Daube, B. C., & Wofsy, S. C. (1996). Exchange of carbon dioxide by a deciduous forest: Response to interannual climate variability. *Science*, 271, 1576-1578.
- Govaerts, Y. M., Jacquemoud, S., Verstraete, M. M., & Ustin, S. L. (1996). Three-dimensional radiation transfer modeling in a dicotyledon leaf. *Applied Optics*, 35, 6585-6598.
- Govaerts, Y. M. & Verstraete, M. M. (1998). Raytran: A Monte Carlo ray-tracing model to compute light scattering in three-dimensional heterogeneous media. *Ieee Transactions on Geoscience and Remote Sensing*, 36, 493-505.
- Goward, S. N. & Huemmrich, K. F. (1992). Vegetation Canopy PAR Absorptance and the Normalized Difference Vegetation Index - an Assessment Using the SAIL Model. *Remote Sensing of Environment*, 39, 119-140.
- Goward, S. N. & Prince, S. D. (1995). Transient effects of climate on vegetation dynamics: Satellite observations. *Journal of Biogeography*, 22, 549-564.
- Hanan, N. P., Kabat, P., Dolman, A. J., & Elbers, J. A. (1998). Photosynthesis and carbon balance of a Sahelian fallow savanna. *Global Change Biology*, 4, 523-538.
- Hanan, N. P., Burba, G., Verma, S. B., Berry, J. A., Suyker, A., & Walter-Shea, E. A. (2002). Inversion of net ecosystem CO<sub>2</sub> flux measurements for estimation of canopy PAR absorption. *Global Change Biology*, 8, 563-574.
- Hollinger, D. Y., Goltz, S. M., Davidson, E. A., Lee, J. T., Tu, K., & Valentine, H. T. (1999). Seasonal patterns and environmental control of carbon dioxide and water vapour exchange in an ecotonal boreal forest. *Global Change Biology*, 5, 891-902.
- Hosgood, B., Jacquemoud, S., Andreoli, G., Verdebout, J., Pedrini, G., & Schmuck, G. (1995). Leaf Optical Properties EXperiment 93 (LOPEX93). *European Commission, Joint Research Center, Institute for Remote Sensing Applications, Report EUR 16095 EN*.
- Huete, A., Justice, C., & Liu, H. (1994). Development of Vegetation and Soil Indexes for Modis-Eos. *Remote Sensing of Environment*, 49, 224-234.
- Huete, A., Didan, K., Miura, T., Rodriguez, E. P., Gao, X., & Ferreira, L. G. (2002). Overview of the radiometric and biophysical performance of the MODIS vegetation indices. *Remote Sensing of Environment*, 83, 195-213.
- Huete, A. R., Hua, G., Qi, J., Chehbouni, A., & Vanleeuwen, W. J. D. (1992). Normalization of Multidirectional Red and NIR Reflectances with the SAVI. *Remote Sensing of Environment*, 41, 143-154.
- Huete, A. R., Liu, H. Q., Batchily, K., & Vanleeuwen, W. (1997). A comparison of vegetation indices global set of TM images for EOS-MODIS. *Remote Sensing of Environment*, 59, 440-451.
- Hurt, G. C. & Armstrong, R. A. (1996). A pelagic ecosystem model calibrated with BATS data. *Deep-Sea Research Part Ii-Topical Studies in Oceanography*, 43, 653-683.
- Ishimaru, A. (1978a). Wave Propagation and scattering in Random Media. *Single Scattering and Transport Theory*, 1.
- Ishimaru, A. (1978b). Wave Propagation and scattering in Random Media. *Multiple Scattering, Turbulence, Rough Surfaces, and Remote Sensing*, 2.

- Jackson, R. D., Reginato, R. T., Printer, P. J., & Idso, S. B. (1979). Plant Canopy Information Extraction from Composite Scene Reflectance of Row Crops. *Appl Opt*, 18, 3775-3782.
- Jacquemoud, S. & Baret, F. (1990). PROSPECT - a Model of Leaf Optical-Properties Spectra. *Remote Sensing of Environment*, 34, 75-91.
- Jacquemoud, S. (1993). Inversion of the Prospect + Sail Canopy Reflectance Model from Aviris Equivalent Spectra - Theoretical-Study. *Remote Sensing of Environment*, 44, 281-292.
- Jacquemoud, S., Baret, F., Andrieu, B., Danson, F. M., & Jaggard, K. (1995). Extraction of Vegetation Biophysical Parameters by Inversion of the Prospect Plus Sail Models on Sugar-Beet Canopy Reflectance Data - Application to Tm and Aviris Sensors. *Remote Sensing of Environment*, 52, 163-172.
- Jacquemoud, S., Ustin, S. L., Verdebout, J., Schmuck, G., Andreoli, G., & Hosgood, B. (1996). Estimating leaf biochemistry using the PROSPECT leaf optical properties model. *Remote Sensing of Environment*, 56, 194-202.
- Jacquemoud, S., Bacour, C., Poilve, H., & Frangi, J. P. (2000). Comparison of four radiative transfer models to simulate plant canopies reflectance: Direct and inverse mode. *Remote Sensing of Environment*, 74, 471-481.
- Jahnke, L. S. & Lawrence, D. B. (1965). Influence of Photosynthetic Crown Structure on Potential Productivity of Vegetation Based Primarily on Mathematical Models. *Ecology*, 46, 319-326.
- Justice, C. O., Vermote, E., Townshend, J. R. G., Defries, R., Roy, D. P., Hall, D. K., Salomonson, V. V., Privette, J. L., Riggs, G., Strahler, A., Lucht, W., Myneni, R. B., Knyazikhin, Y., Running, S. W., Nemani, R. R., Wan, Z. M., Huete, A. R., Van Leeuwen, W., Wolfe, R. E., Giglio, L., Muller, J. P., Lewis, P., & Barnsley, M. J. (1998). The Moderate Resolution Imaging Spectroradiometer (MODIS): Land remote sensing for global change research. *IEEE Transactions on Geoscience and Remote Sensing*, 36, 1228-1249.
- Karnieli, A., Kaufman, Y., Remer, L., & Wald, A. (2001). AFRI - aerosol free vegetation index. *REMOTE SENSING OF ENVIRONMENT*, 77, 10-21.
- Kaufman, Y., Wald, A., Remer, L., Gao, B., Li, R., & Flynn, L. (1997). The MODIS 2.1- $\mu\text{m}$  channel - Correlation with visible reflectance for use in remote sensing of aerosol. *IEEE TRANSACTIONS ON GEOSCIENCE AND REMOTE SENSING*, 35, 1286-1298.
- Kaufman, Y., Kleidman, R., Hall, D., Martins, J., & Barton, J. (2002). Remote sensing of subpixel snow cover using 0.66 and 2.1  $\mu\text{m}$  channels. *GEOPHYSICAL RESEARCH LETTERS*, 29, -.
- King, M. D., Kaufman, Y. J., Tanre, D., & Nakajima, T. (1999). Remote sensing of tropospheric aerosols from space: Past, present, and future. *Bulletin of the American Meteorological Society*, 80, 2229-2259.
- Knyazikhin, Y., Martonchik, J. V., Diner, D. J., Myneni, R. B., Verstraete, M., Pinty, B., & Gobron, N. (1998a). Estimation of vegetation canopy leaf area index and fraction of absorbed photosynthetically active radiation from atmosphere-corrected MISR data. *Journal of Geophysical Research-Atmospheres*, 103, 32239-32256.

- Knyazikhin, Y., Martonchik, J. V., Myneni, R. B., Diner, D. J., & Running, S. W. (1998b). Synergistic algorithm for estimating vegetation canopy leaf area index and fraction of absorbed photosynthetically active radiation from MODIS and MISR data. *Journal of Geophysical Research-Atmospheres*, *103*, 32257-32275.
- Kodani, E., Awaya, Y., Tanaka, K., & Matsumura, N. (2002). Seasonal patterns of canopy structure, biochemistry and spectral reflectance in a broad-leaved deciduous *Fagus crenata* canopy. *FOREST ECOLOGY AND MANAGEMENT*, *167*, 233-249.
- Kubelka, P. & Munk, F. (1931). Ein Beitrag zur optik der Farbanstriche. *Ann Tech Phys*, *11*, 593-610.
- Kussk, A. (1985). The hotspot effect of a uniform vegetative cover. *Sov J Remote Sensing*, *3*, 645-658.
- Kuusk, A. (1985). The hotspot effect of a uniform vegetative cover. *Soviet Journal of Remote Sensing*, *3*, 645-658.
- Lacaze, R. & Roujean, J. L. (2001). G-function and HOt SpoT (GHOST) reflectance model - Application to multi-scale airborne POLDER measurements. *Remote Sensing of Environment*, *76*, 67-80.
- Lambers, H., Chapin, F. S., & Pons, T. L. (1998). *Plant physiological ecology*. New York: Springer - Verlag.
- Latifovic, R., Cihlar, J., & Chen, J. (2003). A comparison of BRDF models for the normalization of satellite optical data to a standard sun-target-sensor geometry. *Ieee Transactions on Geoscience and Remote Sensing*, *41*, 1889-1898.
- Lawrence, D. M. & Slingo, J. M. (2004). An annual cycle of vegetation in a GCM. Part II: global impacts on climate and hydrology. *Climate Dynamics*, *22*, 107-122.
- Li, X. & Strahler, A. H. (1986). Geometrical-Optical Bidirectional Reflectance Modeling of a Conifer Forest Canopy. *IEEE Trans Geosci Remote Sensing*, *24*, 906-919.
- Li, X. & Strahler, A. H. (1992). Geometric-optical bidirectional Reflectance modeling of the Discrete-Crown Vegetation Canopy: Effect of Crown Shape and Mutual Shadowing. *IEEE Trans Geosci Remote Sensing*, *30*, 276-292.
- Li, X., Strahler, A. H., & Woodcock, C. E. (1995). A hybrid geometric optical-radiative transfer approach for modeling albedo and directional reflectance of discontinuous canopies. *IEEE Trans Geosci Remote Sens*, *33*, 466-480.
- Linderman, M., Rowhani, P., Benz, D., Serneels, S., & Lambin, E. F. (2005). Land-cover change and vegetation dynamics across Africa. *Journal of Geophysical Research-Atmospheres*, *110*, -.
- Liu, J., Chen, J. M., Cihlar, J., & Chen, W. (1999). Net primary productivity distribution in the BOREAS region from a process model using satellite and surface data. *Journal of Geophysical Research-Atmospheres*, *104*, 27735-27754.
- Lovell, J. L. & Graetz, R. D. (2001). Filtering pathfinder AVHRR land NDVI data for Australia. *International Journal of Remote Sensing*, *22*, 2649-2654.
- Major, D. J., Schaalje, G. B., Wiegand, C., & Blad, B. L. (1992). Accuracy and Sensitivity Analyses of SAIL Model-Predicted Reflectance of Maize. *Remote Sensing of Environment*, *41*, 61-70.
- Merzlyak, M. N., Gitelson, A. A., Pogosyan, S. I., Chivkunova, O. B., Lehimena, L., Garson, M., Buzulukova, N. P., Shevyreva, V. V., & Rumyantseva, V. B. (1997). Reflectance spectra of leaves and fruits during their development and senescence and under stress. *Russian Journal of Plant Physiology*, *44*, 614-622.



- Metropolis, N., Rosenbluth, A. W., Rosenbluth, M. N., Teller, A. H., & Teller, E. (1953). Equations of state calculations by fast computing machines. *Journal of Chemical Physics*, 21, 1087-1092.
- Myneni, R. B., Asrar, G., Tanre, D., & Choudhury, B. J. (1992). Remote-Sensing of Solar-Radiation Absorbed and Reflected by Vegetated Land Surfaces. *Ieee Transactions on Geoscience and Remote Sensing*, 30, 302-314.
- Myneni, R. B., Nemani, R. R., & Running, S. W. (1997). Estimation of global leaf area index and absorbed PAR using radiative transfer models. *IEEE Transactions on Geoscience and Remote Sensing*, 35, 1380-1393.
- Myneni, R. B., Hoffman, S., Knyazikhin, Y., Privette, J. L., Glassy, J., Tian, Y., Wang, Y., Song, X., Zhang, Y., Smith, G. R., Lotsch, A., Friedl, M., Morisette, J. T., Votava, P., Nemani, R. R., & Running, S. W. (2002). Global products of vegetation leaf area and fraction absorbed PAR from year one of MODIS data. *Remote Sensing of Environment*, 83, 214-231.
- Newnham, G. J. & Burt, T. (2001). Validation of a Leaf Reflectance and Transmittance Model for Three Agricultural Crop Species. *International Geoscience and Remote Sensing Symposium*, 7, 2976-2978.
- North, P. R. J. (1996). Three-dimensional forest light interaction model using a Monte Carlo method. *Ieee Transactions on Geoscience and Remote Sensing*, 34, 946-956.
- Ollinger, S. & Smith, M. L. (2005). Net Primary Production and Canopy Nitrogen in a Temperate Forest Landscape: an Analysis Using Imaging Spectroscopy, Modeling and Field Data. *Ecosystems*, in press.
- Osborne, T. M., Lawrence, D. M., Slingo, J. M., Challinor, A. J., & Wheeler, T. R. (2004). Influence of vegetation on the local climate and hydrology in the tropics: sensitivity to soil parameters. *Climate Dynamics*, 23, 45-61.
- Pettorelli, N., Vik, J. O., Mysterud, A., Gaillard, J.-M., Tucker, C. J., & Stenseth (2005). Using the satellite-derived NDVI to assess ecological responses to environmental change. *TRENDS in Ecology and Evolution*, 20, 503-510.
- Pielke, R. A., Avissar, R., Raupach, M., Dolman, A. J., Zeng, X. B., & Denning, A. S. (1998). Interactions between the atmosphere and terrestrial ecosystems: influence on weather and climate. *Global Change Biology*, 4, 461-475.
- Potter, C. S., Randerson, J. T., Field, C. B., Matson, P. A., Vitousek, P. M., Mooney, H. A., & Klooster, S. A. (1993). Terrestrial Ecosystem Production - a Process Model-Based on Global Satellite and Surface Data. *Global Biogeochemical Cycles*, 7, 811-841.
- Prince, S. D. & Goward, S. N. (1995). Global primary production: A remote sensing approach. *Journal of Biogeography*, 22, 815-835.
- Prince, S. D. & Goward, S. N. (1996). Evaluation of the NOAA/NASA Pathfinder AVHRR Land Data Set for global primary production modelling. *International Journal of Remote Sensing*, 17, 217-221.
- Rahman, H., Pinty, B., & Verstraete, M. M. (1993a). Coupled Surface-Atmosphere Reflectance (Csar) Model.2. Semiempirical Surface Model Usable with Noaa Advanced Very High-Resolution Radiometer Data. *Journal of Geophysical Research-Atmospheres*, 98, 20791-20801.

- Rahman, H., Verstraete, M. M., & Pinty, B. (1993b). Coupled Surface-Atmosphere Reflectance (Csar) Model. 1. Model Description and Inversion on Synthetic Data. *Journal of Geophysical Research-Atmospheres*, 98, 20779-20789.
- Remer, L., Wald, A., & Kaufman, Y. (2001). Angular and seasonal variation of spectral surface reflectance ratios: Implications for the remote sensing of aerosol over land. *IEEE TRANSACTIONS ON GEOSCIENCE AND REMOTE SENSING*, 39, 275-283.
- Rice, A., Pyle, E., Saleska, S., Hutyrá, L., Palace, M., Keller, M., De Camargo, P., Portilho, K., Marques, D., & Wofsy, S. (2004). Carbon balance and vegetation dynamics in an old-growth Amazonian forest. *ECOLOGICAL APPLICATIONS*, 14, S55-S71.
- Richardson, A. D. & Berlyn, G. P. (2002). Spectral reflectance and photosynthetic properties of *Betula papyrifera* (Betulaceae) leaves along an elevational gradient on Mt. Mansfield, Vermont, USA. *AMERICAN JOURNAL OF BOTANY*, 89, 88-94.
- Richardson, A. D., Berlyn, G. P., & Duigan, S. P. (2003). Reflectance of Alaskan black spruce and white spruce foliage in relation to elevation and latitude. *Tree Physiology*, 23, 537-544.
- Roberts, D. A., Nelson, B. W., Adams, J. B., & Palmer, F. (1998). Spectral changes with leaf aging in Amazon caatinga. *Trees-Structure and Function*, 12, 315-325.
- Rodriguez-Yi, J. L., Shimabukuro, Y. E., & Rudorff, B. F. T. (2000). Image segmentation for classification of vegetation using NOAA AVHRR data. *International Journal of Remote Sensing*, 21, 167-172.
- Roujean, J. L. & Breon, F. M. (1995). Estimating Par Absorbed by Vegetation from Bidirectional Reflectance Measurements. *Remote Sensing of Environment*, 51, 375-384.
- Ruimy, A., Dedieu, G., & Saugier, B. (1996). TURC: A diagnostic model of continental gross primary productivity and net primary productivity. *Global Biogeochemical Cycles*, 10, 269-285.
- Ruimy, A., Kergoat, L., & Bondeau, A. (1999). Comparing global models of terrestrial net primary productivity (NPP): analysis of differences in light absorption and light-use efficiency. *Global Change Biology*, 5, 56-64.
- Running, S., Nemani, R., Heinsch, F., Zhao, M., Reeves, M., & Hashimoto, H. (2004). A continuous satellite-derived measure of global terrestrial primary production. *BIOSCIENCE*, 54, 547-560.
- Saleska, S. R., Miller, S. D., Matross, D. M., Goulden, M. L., Wofsy, S. C., Da Rocha, H. R., De Camargo, P. B., Crill, P., Daube, B. C., De Freitas, H. C., Hutyrá, L., Keller, M., Kirchhoff, V., Menton, M., Munger, J. W., Pyle, E. H., Rice, A. H., & Silva, H. (2003). Carbon in amazon forests: Unexpected seasonal fluxes and disturbance-induced losses. *Science*, 302, 1554-1557.
- Sellers, P., Hall, F., Margolis, H., Kelly, B., Baldocchi, D., Denhartog, G., Cihlar, J., Ryan, M. G., Goodison, B., Crill, P., Ranson, K. J., Lettenmaier, D., & Wickland, D. E. (1995). The Boreal Ecosystem-Atmosphere Study (Boreas) - an Overview and Early Results from the 1994 Field Year. *Bulletin of the American Meteorological Society*, 76, 1549-1577.

- Shimabukuro, Y. E. & Rudorff, B. F. T. (2000). Fraction images derived from NOAA AVHRR data for global studies. *International Journal of Remote Sensing*, 21, 3191-3194.
- Silver, W., Neff, J., McGroddy, M., Veldkamp, E., Keller, M., & Cosme, R. (2000). Effects of soil texture on belowground carbon and nutrient storage in a lowland Amazonian forest ecosystem. *ECOSYSTEMS*, 3, 193-209.
- Strahler, A. H. & Jupp, D. L. B. (1990). Modeling bidirectional reflectance of forest and woodlands using Boolean models and geometric optics. *Remote Sens Environ*, 34, 153-160.
- Strahler, A. H., Et Al. (1999). MODIS BRDF/Albedo Product: Algorithm Theoretical Basis Document, Version 5.0.
- Styliniski, C. D., Gamon, J. A., & Oechel, W. C. (2002). Seasonal patterns of reflectance indices, carotenoid pigments and photosynthesis of evergreen chaparral species. *Oecologia*, 131, 366-374.
- Taberner, M., Gobron, N., Melin, F., Pinty, B., & Verstraete, M. (2002). The STARS FAPAR algorithm: A consolidated and generalized software package. *EUR Report No 20145 EN, Joint Research Center, Italy*.
- Terjung, W. H. & Louie, S. S. F. (1972). Potential Solar Radiation on Plant Shapes. *Int J Biometeor*, 16, 25-43.
- Tucker, C. J. (1979). Red and Photographic Infrared Linear Combinations for Monitoring Vegetation. *Remote Sensing of Environment*, 8, 127-150.
- Tucker, C. J. (1980). Remote-Sensing of Leaf Water-Content in the near-Infrared. *Remote Sensing of Environment*, 10, 23-32.
- Turner, D. P., Ritts, W. D., Cohen, W. B., Gower, S. T., Zhao, M. S., Running, S. W., Wofsy, S. C., Urbanski, S., Dunn, A. L., & Munger, J. W. (2003). Scaling Gross Primary Production (GPP) over boreal and deciduous forest landscapes in support of MODIS GPP product validation. *Remote Sensing of Environment*, 88, 256-270.
- Ustin, S. L., Duan, L., & Hart, Q. J., 1994: Seasonal changes observed in AVIRIS images of Jasper Ridge, California. in *Proceedings International Geoscience and Remote Sensing Symposium IGARSS '94*.
- Ustin, S. L., Jacquemoud, S., & Govaerts, Y. (2001). Simulation of photon transport in a three-dimensional leaf: implications for photosynthesis. *Plant Cell and Environment*, 24, 1095-1103.
- Van Schaik, C. P., Terborgh, J. W., & Wright, S. J. (1993). The phenology of tropical forests-adaptive significance and consequences for primary consumers. *Annual Review of Ecology and Systematics*, 24, 353- 377.
- Verhoef, W. (1984). Light-Scattering by Leaf Layers with Application to Canopy Reflectance Modeling - the SAIL Model. *Remote Sensing of Environment*, 16, 125-141.
- Verhoef, W. (1985). Earth Observation Modeling Based on Layer Scattering Matrices. *Remote Sensing of Environment*, 17, 165-178.
- Verhoef, W., (1998). Theory of radiative transfer models applied in optical remote sensing of vegetation canopies. Ph.D, Remote Sensing Department, National Aerospace Lab, NLR, Wageningen.

- Verhoef, W. & Bach, H. (2003). Simulation of hyperspectral and directional radiance images using coupled biophysical and atmospheric radiative transfer models. *Remote Sensing of Environment*, 87, 23-41.
- Vina, A., Gitelson, A., Rundquist, D., Keydan, G., Leavitt, B., & Schepers, J. (2004). Remote sensing - Monitoring maize (*Zea mays* L.) phenology with remote sensing. *AGRONOMY JOURNAL*, 96, 1139-1147.
- Wang, Y., (2002). Assessment of the MODIS LAI and FPAR algorithm: Retrieval quality, theoretical basis and validation. Ph.D., Geography, Boston University, Boston.
- Waring, R. H., Law, B. E., Goulden, M. L., Bassow, S. L., McCreight, R. W., Wofsy, S. C., & Bazzaz, F. A. (1995). Scaling Gross Ecosystem Production at Harvard Forest with Remote-Sensing - a Comparison of Estimates from a Constrained Quantum-Use Efficiency Model and Eddy-Correlation. *Plant Cell and Environment*, 18, 1201-1213.
- Weiss, M. & Baret, F. (1999). Evaluation of canopy biophysical variable retrieval performances from the accumulation of large swath satellite data. *Remote Sensing of Environment*, 70, 293-306.
- Weiss, M., Baret, F., Myneni, R. B., Pragnere, A., & Knyazikhin, Y. (2000). Investigation of a model inversion technique to estimate canopy biophysical variables from spectral and directional reflectance data. *Agronomie*, 20, 3-22.
- White, H. P., Miller, J. R., & Chen, J. M. (2002). Four-Scale Linear Model for Anisotropic Reflectance (FLAIR) for plant canopies - Part II: Validation and inversion with CASI, POLDER, and PARABOLA data at BOREAS. *Ieee Transactions on Geoscience and Remote Sensing*, 40, 1038-1046.
- Willstatter, R. & Stoll, A. (1913). *Untersuchungen über die Assimilation der Kohlensäure*. Berlin: Springer.
- Wofsy, S. C., Goulden, M. L., Munger, J. W., Fan, S. M., Bakwin, P. S., Daube, B. C., Bassow, S. L., & Bazzaz, F. A. (1993). Net Exchange of CO<sub>2</sub> in a Midlatitude Forest. *Science*, 260, 1314-1317.
- Wright, S. J. & Van Schaik, C. P. (1994). Light and the phenology of tropical trees. *The American Naturalist*, 143, 192-199.
- Xiao, X., Ojima, D., Parton, W., Chen, Z., & Chen, D. (1995). Sensitivity of Inner Mongolia grasslands to climate change. *JOURNAL OF BIOGEOGRAPHY*, 22, 643-648.
- Xiao, X., Boles, S., Frohling, S., Salas, W., Moore, B., Li, C., He, L., & Zhao, R. (2002a). Observation of flooding and rice transplanting of paddy rice fields at the site to landscape scales in China using VEGETATION sensor data. *International Journal of Remote Sensing*, 23, 3009-3022.
- Xiao, X., Boles, S., Frohling, S., Salas, W., Moore, B., Li, C., He, L., & Zhao, R. (2002b). Landscape-scale characterization of cropland in China using Vegetation and Landsat TM images. *International Journal of Remote Sensing*, 23, 3579-3594.
- Xiao, X., Zhang, Q., Boles, S., Rawlins, M., & Moore, B. (2004a). Mapping snow cover in the pan-Arctic zone, using multi-year (1998-2001) images from optical VEGETATION sensor. *INTERNATIONAL JOURNAL OF REMOTE SENSING*, 25, 5731-5744.
- Xiao, X. M., Braswell, B., Zhang, Q. Y., Boles, S., Frohling, S., & Moore, B. (2003). Sensitivity of vegetation indices to atmospheric aerosols: continental-scale observations in Northern Asia. *Remote Sensing of Environment*, 84, 385-392.

- Xiao, X. M., Hollinger, D., Aber, J., Goltz, M., Davidson, E. A., Zhang, Q. Y., & Moore, B. (2004b). Satellite-based modeling of gross primary production in an evergreen needleleaf forest. *Remote Sensing of Environment*, *89*, 519-534.
- Xiao, X. M., Zhang, Q. Y., Braswell, B., Urbanski, S., Boles, S., Wofsy, S., Moore, B., & Ojima, D. (2004c). Modeling gross primary production of temperate deciduous broadleaf forest using satellite images and climate data. *Remote Sensing of Environment*, *91*, 256-270.
- Xiao, X. M., Zhang, Q. Y., Hollinger, D., Aber, J., & Moore, B. (2005a). Modeling seasonal dynamics of gross primary production of an evergreen needleleaf forest using MODIS images and climate data. *Ecological Applications*, *in press*.
- Xiao, X. M., Zhang, Q. Y., Hollinger, D., Aber, J., & Moore, B. (2005b). Modeling gross primary production of an evergreen needleleaf forest using modis and climate data. *Ecological Applications*, *15*, 954-969.
- Xiao, X. M., Zhang, Q. Y., Saleska, S., Hutyrá, L., Camargo, P. D., Wofsy, S., Frohling, S., Boles, S., Keller, M., & B., M. (2005c). Satellite-based modeling of gross primary production in a seasonally moist tropical evergreen forest. *Remote Sensing of Environment*, *94*, 105 -122.
- Xu, M., Qi, Y., Chen, J. Q., & Song, B. (2004). Scale-dependent relationships between landscape structure and microclimate. *Plant Ecology*, *173*, 39-57.
- Yamada, N. & Fujimura, S., 1988: A mathematical model of reflectance and transmittance of plant leaves as a function of chlorophyll pigment content. *Proceedings of the International Geoscience and Remote Sensing Symposiums*: 8330-8334.
- Young, A., Phillip, D., Ruban, A., Horton, P., & Frank, H. (1997). The xanthophyll cycle and carotenoid-mediated dissipation of excess excitation energy in photosynthesis. *PURE AND APPLIED CHEMISTRY*, *69*, 2125-2130.
- Zarco-Tejada, P. J., Miller, J. R., Mohammed, G. H., & Noland, T. L. (2000a). Chlorophyll fluorescence effects on vegetation apparent reflectance: I. Leaf-level measurements and model simulation. *Remote Sensing of Environment*, *74*, 582-595.
- Zarco-Tejada, P. J., Miller, J. R., Mohammed, G. H., Noland, T. L., & Sampson, P. H. (2000b). Chlorophyll fluorescence effects on vegetation apparent reflectance: II. Laboratory and airborne canopy-level measurements with hyperspectral data. *Remote Sensing of Environment*, *74*, 596-608.
- Zarco-Tejada, P. J., Rueda, C. A., & Ustin, S. L. (2003). Water content estimation in vegetation with MODIS reflectance data and model inversion methods. *Remote Sensing of Environment*, *85*, 109-124.
- Zarco-Tejada, P. J., Miller, J. R., Harron, J., Hu, B. X., Noland, T. L., Goel, N., Mohammed, G. H., & Sampson, P. (2004). Needle chlorophyll content estimation through model inversion using hyperspectral data from boreal conifer forest canopies. *Remote Sensing of Environment*, *89*, 189-199.
- Zhang, Q. Y., Xiao, X. M., Braswell, B., Linder, E., Baret, F., & Moore, B. (2005). Estimating light absorption by chlorophyll, leaf and canopy in a deciduous broadleaf forest using MODIS data and a radiative transfer model. *Remote Sens Environ*, *99*, 357-371.

- Zhang, X. Y., Friedl, M. A., Schaaf, C. B., Strahler, A. H., Hodges, J. C. F., Gao, F., Reed, B. C., & Huete, A. (2003). Monitoring vegetation phenology using MODIS. *Remote Sensing of Environment*, *84*, 471-475.
- Zhang, X. Y., Friedl, M. A., Schaaf, C. B., & Strahler, A. H. (2004a). Climate controls on vegetation phenological patterns in northern mid- and high latitudes inferred from MODIS data. *Global Change Biology*, *10*, 1133-1145.
- Zhang, X. Y., Friedl, M. A., Schaaf, C. B., Strahler, A. H., & Schneider, A. (2004b). The footprint of urban climates on vegetation phenology. *Geophysical Research Letters*, *31*, -.